

Size Effect in Micromachining

A thesis submitted to

THE UNIVERSITY OF MANCHESTER

for the degree of

DOCTOR OF PHILOSOPHY

In the Faculty of Engineering and Physical Sciences

2011

AAMER JALIL MIAN

School of Mechanical, Aerospace and Civil Engineering

(Intentionally left blank)

Table of Contents

List of Figures	8
List of Tables	12
List of Nomenclature	13
List of Abbreviations	14
Abstract	15
List of Publications	16
Declaration	17
Copyright Statement	18
Dedication	19
Acknowledgements	20
CHAPTER ONE	21
Introduction	21
1.1 Background	21
1.2 Aim and objectives	23
1.3 Thesis outline	24
CHAPTER TWO	27
Literature Review	27
2.1 Introduction	27
2.2 Size effect in micro machining	29
2.2.1 Specific cutting energy	30
2.2.1.1 Material strengthening effect	31
2.2.1.2 Subsurface plastic deformation	34
2.2.1.3 Tool edge radius effect	34
2.2.1.4 Ductile fracture	35
2.2.2 Material heterogeneity	37
2.2.3 Minimum chip thickness effect	37
2.2.4 Elastic plastic deformation	41
2.2.5 Chip formation	42
2.2.6 Surface generation	46
2.2.7 Burr formation	51
2.2.8 Micro tool	52
2.2.9 Cutting forces	53

2.3	Machinability of ductile materials	54
2.3.1	Overview of micro mechanical machining from a material perspective	56
2.4	Machining process monitoring	59
2.4.1	Acoustic emission during metal cutting	60
2.4.1.1	AE sensitivity to machining parameters	63
2.4.1.2	AE signal processing	64
2.5	Summary	66
 CHAPTER THREE		 68
Experimental Procedure		68
3.1	State of the art equipment	68
3.1.1	Machine tool	68
3.1.2	Hitachi Scanning electron microscope (SEM)	69
3.1.3	WYKO [®] NT-1100 white light interferometer	70
3.1.4	MTS Nano Indenter [®] XP	70
3.1.5	Acoustic emission sensing system	71
3.2	Measurement methods	72
3.2.1	Tool edge radius measurement	72
3.2.2	Surface roughness measurement	73
3.2.3	Burr size measurement	74
3.2.4	Tool wear measurement	75
3.2.5	Subsurface microstructure measurement	76
3.2.6	Micro chips characterisation	76
3.3	Experimental setup	77
3.4	Experimental procedure	78
3.5	Acoustic emission signal processing	79
 CHAPTER FOUR		 80
A Comparative Study of Material Phase Effects on Micro-Machinability of Multiphase Materials		80
Abstract		80
4.1	Introduction	81
4.1.1	Micro machining	81
4.1.2	Material microstructure effect on surface generation in micro machining	81
4.1.3	Burrs in micromachining	82

4.1.4 Research motivation	83
4.2 Experimental details and evaluations	84
4.2.1 Material metallographic grain size measurement	84
4.2.2 Material characterisation using instrumented indentation testing	84
4.2.3 Experimental details and cutting parameters	86
4.3 Micro milling results and discussions	87
4.3.1 Surface roughness	87
4.3.2 Subsurface microstructure modification	91
4.3.3 Burr formation	96
4.3.4 Tool wear	97
4.4 Conclusions	99
CHAPTER FIVE	101
Identification of Factors that Dominates “Size Effect” in Micro Machining	101
Abstract	101
5.1 Introduction	102
5.1.1 Size effect in micromachining	102
5.1.2 Machinability of nickel alloys	102
5.1.3 Acoustic emission signal in micro milling process	103
5.1.4 Research motivation	106
5.2 Experimental details	106
5.2.1 Experimental setup	106
5.2.2 Workpiece material characterisation	107
5.2.3 Micro end mill	107
5.2.4 Acoustic emission measurement	108
5.2.5 Surface roughness and burr size measurements	108
5.3 Experimental methodology	108
5.3.1 Signal processing technique	108
5.3.2 Taguchi method	110
5.4 Results and discussions	111
5.4.1 AE signal spectral analysis	111
5.4.1.1 Energy analysis	115
5.4.2 Statistical analysis of factor dominance	117
5.4.2.1 Specific acoustic emission energy	118
5.4.2.2 Surface roughness	118

5.4.2.3 Burr formation	119
5.4.2.4 Energy bands and micro milling mechanism	121
5.5 Optimum process parameters and confirmation tests	123
5.6 Conclusions	124
CHAPTER SIX	126
Chip Formation in Micro-Scale Milling and Correlation with Acoustic Emission Signal	126
Abstract	126
6.1 Introduction	126
6.2 Research methodology	128
6.3 Micro milling experiments	129
6.4 Results and discussions	132
6.4.1 Chip morphology	132
6.4.1.1 Chip morphology below tool edge radius	132
6.4.1.2 Chip morphology above tool edge radius	137
6.4.2 Acoustic emission in micro cutting	143
6.4.2.1 AE and chip formation	143
6.4.2.2 Specific AE energy	148
6.5 Conclusions	150
CHAPTER SEVEN	152
Estimation of Minimum Chip Thickness in Micro Milling using Acoustic Emission	152
Abstract	152
7.1 Introduction	153
7.2 Experimental plan	155
7.2.1 Micro milling tests	155
7.2.2 AE signal acquisition	158
7.3 Research methodology	159
7.4 Results and discussions	161
7.4.1 AE signal in rubbing dominated region	161
7.4.2 AE signal in shearing dominated region	168
7.5 Boundary conditions for successful implementation of this methodology	178
7.6 Conclusions	181

CHAPTER EIGHT	183
Conclusions and Recommendations for Future Research	183
8.1 Conclusions	183
8.2 Recommendations	185
REFERENCES	187
APPENDIX A Sample MatLab commands	202
APPENDIX B Wavelet transformation technique	204
APPENDIX C Evaluation of key process variables	205

List of Figures

Figure 2.1	Variation in specific cutting energy for three major machining processes	31
Figure 2.2	Importance of incorporating strain gradient in explaining size effect	32
Figure 2.3	Specific energies for average in-plane forces R	33
Figure 2.4	Stack of plates cut with tool having finite radius of curvature at its tip	36
Figure 2.5	Flow of material on the tool face with a high effective negative rake angle	38
Figure 2.6	Cross sectional profile of scratch groove	41
Figure 2.7	Chip formation with different rake angles. Cutting conditions: workpiece, 0.45%C carbon steel (S45C); tool, cutting speed, 10m/s; (a) 70 μm feed/tooth, -20° rake angle (b) 40 μm feed/tooth, -30° rake angle [84]	43
Figure 2.8	Classification of chip (adapted from [89])	44
Figure 2.9	Effects of minimum chip thickness and burr formation on multiphase surface roughness	47
Figure 2.10	SEM image of slot floor for (a) pearlite, (b) ferrite, (c) ferritic DI, and (d) pearlitic DI	47
Figure 2.11	SEM images of chips for (a) pearlite, (b) ferrite,(c) ferritic DI, and (d) pearlitic DI	48
Figure 2.12	Deterministic and stochastic components influencing machined surface	50
Figure 2.13	Categorization of burr types	51
Figure 2.14	Stress strain curves of some ferrous and non ferrous materials	55
Figure 2.15	AE generation in metal cutting	61
Figure 2.16	AE source mechanisms	62
Figure 2.17	Micro-mechanisms of fracture in metals	63
Figure 3.1	MIKRON HSM 400 high speed milling machine	69
Figure 3.2	Hitachi S-3400N SEM at the University of Manchester	69
Figure 3.3	Wyko NT1100 at Laser Processing Research Centre (LPRC)	70
Figure 3.4	Nano-indenter XP at the University of Manchester Material Science Centre	71
Figure 3.5	Acoustic emission sensing system	72
Figure 3.6	Micro and meso scale tool bottom views (a) Fraisa (800 μm) (b) Dixi (500 μm) (c) Dixi (2mm) in diameters	72
Figure 3.7	Measurement of tool edge radius	73
Figure 3.8	Surface roughness measurement	74

Figure 3.9	Wyko scans to estimate burr width of ferrous workpieces	74
Figure 3.10	Down milled side burr root thickness measurement	75
Figure 3.11	Micrographs showing maximum flank wear	75
Figure 3.12	Slot down-milled side (a) AISI 1005 (b) AISI 1045	76
Figure 3.13	Experimental setup for (a) Ferrous workpieces (b) Inconel 718	77
Figure 4.1	Workpiece microstructure (a) AISI 1005 steel (b) AISI 1045 steel	84
Figure 4.2	Comparison of (a) elastic modulus/hardness ratio (b) percentage elastic recovery for workpiece specimens	86
Figure 4.3	Surface roughness	88
Figure 4.4	Micro milled slot base for AISI 1045 steel generated at 0.02 $\mu\text{m}/\text{tooth}$	89
Figure 4.5	Magnified area of AISI 1045 slot floor machined at 2 $\mu\text{m}/\text{tooth}$	90
Figure 4.6	Surface generated at different feedrates	91
Figure 4.7	Subsurface micro-structural modification and material side flow	92
Figure 4.8	Slot floor subsurface layer properties (a) Nano-hardness (b) Elastic modulus	93
Figure 4.9	Slot down-milled side (a) AISI 1005 (b) AISI 1045	94
Figure 4.10	AISI 1045 steel nano-hardness in-depth profiles generated at (a) up-mill side wall (b) down-mill side wall	95
Figure 4.11	AISI 1005 steel nano-hardness in-depth profiles generated at (a) up-mill side wall (b) down-mill side wall	95
Figure 4.12	Burr size in down-milling	97
Figure 4.13	Burr size in up-milling	97
Figure 4.14	Material deformation effects on the tool cutting edges	98
Figure 4.15	Flank wear comparison	99
Figure 5.1	AE signal source mechanisms	104
Figure 5.2	Micro-mechanisms of fracture in metals	105
Figure 5.3	AE signal trends at $V_c = 10 \text{ m/min}$; $f_z/r_e = 0.4$; $a_p = 30\mu\text{m}$; coated	113
Figure 5.4	AE signal trends at $V_c = 25\text{m/min}$; $f_z/r_e = 0.4$; $a_p = 60\mu\text{m}$; uncoated	114
Figure 5.5	AE signal trends at $V_c = 40 \text{ m/min}$, $f_z/r_e = 0.4$, $a_p = 90 \mu\text{m}$, coated	115
Figure 5.6	Wavelet decomposition at $V_c = 40 \text{ m/min}$, $f_z/r_e = 0.4$, $a_p = 90 \mu\text{m}$, uncoated	116
Figure 5.7	Energy distribution in AE signal	117
Figure 5.8	(a) Topographical surface profile maps for $f_z/r_e = 0.4$ at cutting speeds of 10, 25 and 40m/min (b) Sectional profile	119

	across slot width for 40 m/min sample.	
Figure 5.9	Micro slots root subsurface microstructure and nano hardness (G Pa) variation	121
Figure 6.1	AE source mechanisms	129
Figure 6.2	Experimental set up	130
Figure 6.3	Workpieces microstructure	131
Figure 6.4	Material dependent chip morphologies at 0.02 μm feed/tooth	133
Figure 6.5	Rewelding of titanium alloy chip at 0.02 μm feed/tooth	134
Figure 6.6	Distribution of elements across line A-A (chip flow direction) on the free surface of Ti-6Al-4V generated at 0.02 μm feed/tooth (a) scanning line A-A on chip (b) Normalised element population	135
Figure 6.7	Material dependent chip morphologies at 0.5 μm feed/tooth	136
Figure 6.8	Typical chip side views at 0.5 μm maximum undeformed chip thickness	137
Figure 6.9	Material dependent chip morphologies at 2 μm feed/tooth	138
Figure 6.10	Material dependent chip morphologies at 10 μm feed/tooth	139
Figure 6.11	Material dependent chip types at 10 μm maximum undeformed chip thickness	140
Figure 6.12	Nano hardness (H_{chip} in G Pa) distribution in chip cross section of (a) Cu (OFHC) (b) Al 6082-t6 (c) AISI 1005 steel (d) AISI 1045 steel (e) Ti-6Al-4V (f) Inconel 718	141
Figure 6.13	Work hardening severity for different materials	142
Figure 6.14	AE Energy distribution for different workpiece material	143
Figure 6.15	D3 and D4 frequency bandwidths percent energy contribution at different maximum undeformed chip thickness for (a) Non ferrous materials and titanium alloy (b) Ferrous materials and nickel alloy	145
Figure 6.16	Typical lamellae on the free surface of micro chips produced at different undeformed chip thickness in row (top to bottom) (a) Cu (OFHC) (b) Al 6082-T6 (c) AISI 1005 steel (d) AISI 1045 steel (e) Inconel 718 (f) Ti-6Al-4V	146
Figure 6.17	Stick-slip tracks on underside of chip at 10 μm maximum undeformed chip thickness	147
Figure 6.18	Variation in stick-slip interface at different uncut chip thickness	147
Figure 6.19	Relationship between specific AE energy and maximum undeformed chip thickness (a) for a 1 mm and (b) 3 mm width of cut	149
Figure 7.1	Mechanics of micro-scale cutting	153
Figure 7.2	Workpieces microstructure	156
Figure 7.3	Single tooth tool	156
Figure 7.4	Experimental set up	158

Figure 7.5	Signal measurement chain	159
Figure 7.6	Data handling in Extracting $AE_{r.m.s}$ signal characteristics	161
Figure 7.7	$AE_{r.m.s}$ and chip morphology generated at 0.02 $\mu\text{m}/\text{tooth}$	164
Figure 7.8	AE STFT plots generated at 0.02 $\mu\text{m}/\text{tooth}$	167
Figure 7.9	Variations in residual stresses	168
Figure 7.10	$AE_{r.m.s}$ generated at 0.5 $\mu\text{m}/\text{tooth}$	171
Figure 7.11	Machined wall surface generated at 0.5 $\mu\text{m}/\text{tooth}$ of (a) Al 6082-T6 (b) Cu (OFHC) (c) Inconel 718	171
Figure 7.12	$AE_{r.m.s}$ generated at 2 $\mu\text{m}/\text{tooth}$	173
Figure 7.13	Typical chip thickness variation at 2 μm feed/tooth	174
Figure 7.14	$AE_{r.m.s}$ generated at 10 $\mu\text{m}/\text{tooth}$	176
Figure 7.15	Typical chip thickness variation at 10 μm feed/ tooth in micro milling of (a) AISI 1005 steel (b) AISI 1045 steel (c) Ti-6Al-4V alloy	177
Figure 7.16	Material microstructure damping effect on $AE_{r.m.s}$ signature at 0.02 μm chip load in micro milling of (a) AISI 1005 steel (b) AISI 1045 steel	179
Figure 7.17	Material microstructure damping effect on $AE_{r.m.s}$ signature at 10 μm chip load in micro milling of (a) Al 6082-T6 (b) Cu (OFHC)	180
Figure B1	Wavelet decomposition of a signal	204
Figure C1	Factor effect on specific AE energy	206
Figure C2	Factor effect on surface finish	206
Figure C3	Factor effect on down-milled burr root thickness	207
Figure C4	Factor effect on D1 energy band	207
Figure C5	Factor effect on D3 energy band	207
Figure C6	Factor effect on D5 energy band	208

List of Tables

Table 2.1	Proposed definition for micro machining	28
Table 2.2	Reported research on size effect	30
Table 2.3	Micro milling investigation using carbide tools	57
Table 2.4	Acoustic emission parameters and information about the source event	65
Table 4.1	Mechanical properties variation as a function of nano-indentation depth	85
Table 4.2	Process parameters	87
Table 5.1	Chemical properties of Inconel 718 alloy in percent	107
Table 5.2	Factors and their levels	110
Table 5.3	Dummy-level technique on the L9 (3^4) array and measured outputs	111
Table 5.4	ANOVA for specific AE energy	118
Table 5.5	ANOVA for surface finish	118
Table 5.6	ANOVA for down-milled burr root thickness	120
Table 5.7	ANOVA for D1 energy band	122
Table 5.8	ANOVA for D3 energy band	122
Table 5.9	ANOVA for D5 energy band	123
Table 5.10	Experimental results at optimal points	124
Table 6.1	Cutting parameters	130
Table 6.2	Workpiece material characterisation	131
Table 7.1	Previous research on minimum chip thickness effect	154
Table 7.2	Cutting parameters	156
Table 7.3	Acoustic emission sampling	159
Table 7.4	Proto-IXRD settings	168
Table 7.5	Estimated minimum chip thicknesses from AE signals	178

List of Nomenclature

Notation	Description	Units
a_e	Width of cut	μm
a_p	Axial depth of cut	μm
$b.c.c$	Body centered cubic	
Al	Symbol for Aluminum	
C	Symbol for Carbon	
Co	Symbol for Cobalt	
Cu	Symbol for Copper	
f_z	Chip load or feed per tooth	$\mu\text{m}/\text{tooth}$
$f.c.c$	Face centered cubic	
$F\text{-ratio}$	Fisher ratio	
Fe	Symbol for Iron	
h	Chip thickness	μm
h_m	Minimum chip thickness	μm
N	Symbol for Nitrogen	
O	Symbol for Oxygen	
rpm	revolutions per minute	r/min
Ra	Average surface roughness	μm
r_e	Tool edge radius	μm
Ti	Symbol for Titanium	
t_c	Effective cutting time	μm
V_c	Cutting velocity	m/min
v_f	Feed velocity	mm/min
W	Symbol for Tungsten	
α	Effective rake angle	deg
ϕ_s	Shear angle	deg
ϕ	Swept angle of cut	deg
ρ	Density	kg/m^3
θ	Cutting temperature	$^{\circ}\text{C}$

List of Abbreviations

Notation	Description
AE	Acoustic emission
AlTiN	Aluminium Titanium Nitride
ANOVA	Analysis of Variance
AISI	American Iron and Steel Institute
BUE	Built-up Edge
BSE	Back scatter electron microscopy
CNC	Computer Numerical Controlled
df	Degree of Freedom
DWT	Discrete wavelet transformation
EDX	Energy Dispersive X-Ray spectroscopy
FFT	Fast Fourier transformation
HRC	Rockwell Hardness (C scale)
HSM	High Speed Machining
KPVs	Key Process Variables
MQL	Minimum Quantity Lubricant
RMS	Root Mean Square
rpm	Rotations per minute
SEM	Scanning Electron Microscope
STFT	Short time Fourier transformation
TiAlN	Titanium Aluminium Nitride
Ti _x Al	Titanium Aluminide
WT	Wavelet transformation

Abstract

The world is experiencing a growing demand for miniaturised products. Micro-milling, using carbide micro tools has the potential for direct, economical manufacture of micro parts from a wide range of workpiece materials. However, in previous studies several critical issues have been identified that preclude the direct application of macro machining knowledge in the micro domain through simple dimensional analysis. The research presented in this thesis focused on some of the areas that require development of the scientific knowledge base to enable determining improved microscale cutting performance.

In the mechanical micro machining of coarse grained materials, the programmed undeformed chip thickness can be lower than the length scale of the workpiece grains. Moreover, when the microstructure of such materials is composed of more than one phase, the micro cutting process can be undertaken at a length scale where this heterogeneity has to be considered. Driven by this challenge, the material microstructure “size effect” on micro-machinability of coarse grain steel materials was investigated in this PhD. In this regard, a predominantly single phase ferritic workpiece steel material and another workpiece material with near balanced ferrite/pearlite volume fractions was studied over a range of feedrates. The results suggested that for micro machined parts, differential elastic recovery between phases leads to higher surface roughness when the surface quality of micro machined multiphase material is compared to that of single phase material. On the other hand, for single phase predominantly ferritic materials, reducing burr size and tool wear are major challenges.

In micro machining the so called “size effect” has been identified as critical in defining the process performance. However, an extensive literature search had indicated that there was no clear reported evidence on the effect of process variables on driving this size effect phenomenon. It is often assumed in literature that the un-deformed chip thickness was the main factor driving the size effect. This limit manufactures to only altering the feedrate to try and influence size effect. To explore the significance of a range of inputs variables and specifically, cutting variables on the size effect, micro cutting tests were conducted on Inconel 718 nickel alloy. Taguchi methodology along with signal processing techniques were applied to micro milling acoustic emission signals to identify frequency/energy bands and hence size effect specific process mechanism. The dominant cutting parameters for size effect characteristics were determined by analysis of variance. These findings show that despite most literature focussing on chip thickness as the dominant parameter on size effect, the cutting velocity is a dominant factor on size effect related process performance. This suggests that manipulating the cutting speed can also be a very effective strategy in optimising surface finish in micro machining and in breaking the lower limit of micro machining.

In micro machining the lower limit of the process window is set by the minimum chip thickness. Identifying this limit is thus important for establishing the process window. Process windows are valuable guidelines for industrial selection of cutting conditions. Additionally, understanding factors that influence the value of minimum chip thickness is even more important for progressing micro machining capability to the nano-scale machining regime. For this reason, in this PhD study, acoustic emission signatures emanating from microscale milling of six different workpiece materials were characterised to identify the rubbing mode and this enabled the identification of the threshold conditions for occurrence of minimum chip thickness. The minimum chip thickness predicted by this novel approach compares reasonably well to the values that exist in published literature. Additionally, the decomposition of raw acoustic signal allowed the determination of energy levels corresponding to deformation mechanisms.

The PhD work provides significant and new knowledge on the utility and importance of acoustic emission signals in characterising chip formation in micro machining. A novel method for determining the minimum chip thickness was developed, micro machining chip formation mechanisms were identified and the machinability of coarse grained multiphase material is presented.

List of Publications

1. **Mian A.J., Driver N., and Mativenga P.T.**, “Micromachining of coarse-grained multi-phase material”, Proceedings of the Institution of Mechanical engineers, Part B: Journal of Engineering Manufacture (2009) **223** (4), 377-385 (Professional Engineering Publishing). (This paper is based on the PhD literature review and the cutting tests results of the author’s University of Manchester MSc Thesis. The paper was prepared in the first year of the PhD).
2. **Mian A.J., Driver N., Mativenga P. T.**, “A comparative study of material phase effects on micro-machinability of multiphase materials”, The International Journal of Advanced Manufacturing Technology (2010) **50** (1):163-174 (Springer).
3. **Mian A.J., Driver N., and Mativenga P.T.**, “Estimation of minimum chip thickness for multi-phase steel using acoustic emission”, 36th International MATADOR Conference, Manchester, 14– 16 July, 2010.
4. **Mian A.J., Driver N., and Mativenga P.T.**, “Identification of factors that dominate “size effect” in micro machining”, The International Journal of Machine Tools and Manufacture. (2011) **51**:383-394 (Elsevier).
5. **Mian A.J., Driver N., and Mativenga P.T.**, “Chip formation in micro-scale milling and correlation with acoustic emission signal”, **In press** in The International Journal of Advanced Manufacturing Technology, DOI (**10.1007/s00170-011-3185-x**).
6. **Mian A.J., Driver N., and Mativenga P.T.**, “Estimation of minimum chip thickness in micro milling using acoustic emission”, **In press** in special issue of Proceedings of the Institution of Mechanical engineers, Part B: Journal of Engineering Manufacture. Accepted for publication

Declaration

No portion of the work referred to in this thesis has been submitted in support of an application for another degree or qualification of this or any other university or another institute of learning.

Copyright Statement

- i. The author of this thesis (including any appendices and/or schedules to this thesis) owns certain copyright or related rights in it (the “Copyright”) and s/he has given The University of Manchester certain rights to use such Copyright, including for administrative purposes.
- ii. Copies of this thesis, either in full or in extracts and whether in hard or electronic copy, may be made only in accordance with the Copyright, Designs and Patents Act 1988 (as amended) and regulations issued under it or, where appropriate, in accordance with licensing agreements which the University has from time to time. This page must form part of any such copies made.
- iii. The ownership of certain Copyright, patents, designs, trade marks and other intellectual property (the “Intellectual Property”) and any reproductions of copyright works in the thesis, for example graphs and tables (“Reproductions”), which may be described in this thesis, may not be owned by the author and may be owned by third parties. Such Intellectual Property and Reproductions cannot and must not be made available for use without the prior written permission of the owner(s) of the relevant Intellectual Property and/or Reproductions.
- iv. Further information on the conditions under which disclosure, publication and commercialisation of this thesis, the Copyright and any Intellectual Property and/or Reproductions described in it may take place is available in the University IP Policy (see <http://documents.manchester.ac.uk/DocuInfo.aspx?DocID=487>), in any relevant Thesis restriction declarations deposited in the University Library, The University Library’s regulations (see <http://www.manchester.ac.uk/library/aboutus/regulations>) and in The University’s policy on Presentation of Theses

Dedication

To my family

Acknowledgements

I would like to thank my supervisor Dr P T Mativenga for his valuable guidance and support extended during the course of this research. I would also like to express my thanks to Government of Pakistan and The University of Manchester for the financial support extended for this research.

My thanks are also extended to all my friend and colleagues at The University of Manchester, especially at the School of Mechanical, Aerospace and Civil Engineering for the valuable discussions I had with them, and support and encouragement they offered during the course of this research. I must also mention my friend and colleague Dr Nicholas Driver for the discussions we had that proved highly useful during this research.

Finally, my special thanks are for my family, especially my parents, wife, daughter and siblings for their love, care and support that was a source of motivation for all I have achieved in my life.

Chapter 1

INTRODUCTION

1.1 Background

Mechanical micromachining is an emerging field that has shown potential to produce intricate three dimensional features with acceptable dimensional accuracy, cost effectiveness and in-process quality control [1, 2]. These attributes command an ever-increasing attention to the process driven by megatrends in miniaturisation of components, features and devices [1, 3-6]. It also enables manufacture of individual components in a rapid and cost effective manner [7]. Recently, a comparative study of different micro manufacturing process was carried out, which includes assessment based not only on geometrical features but also on process cost [8]. The technical-economic analysis shows that quality of micro end-milling process is closer to that obtained by lithography, in comparison with the other micromechanical processes. In addition to that, it has potential to overcome the challenges posed to lithographic processes at the micron and sub-micron scale.

Mechanical cutting, according to Chae et al [1] is important in bridging the macro and nano/micro domains for functional components, especially for complex micro systems. The main challenge concerning mechanical micromachining is the material removal mechanism whereby well established laws from the macro-machining domain may not be directly translated into the micro domain [9-11]. The differences are due to changes in the underlying physical phenomenon of “size effect” associated with tool edge radius,

workpiece non-homogeneity with respect to the tool/cut size, negative rake angles and workpiece material minimum chip thickness effects. These affect chip-formation process, cutting forces, vibrations and process stability, and the generation and subsequent quality of the resulting machined surface.

The role of workpiece grain sizes is imperative in micro machining. Simoneau et al suggested that the cutting domain could be moved between macro-, meso- and micro-scale by altering grain sizes of the workpiece material [12]. Interfacial interaction at the grain level affects the machined surface topography. The information provided in the literature suggested that surface roughness varies between the grains of material and is influenced by the tool edge radius, microstructure phases, minimum chip thickness effects [11], crystallographic orientation [13], material elastic recovery and phase dependent elastic-plastic anisotropy [14]. Weule et al reported by utilising different heat treated AISI 1045 steel that variation in material property from one grain to the next influenced the resulting surface finish [15]. In another study researcher asserted that plastic strain mismatch, grain orientation relative to cutting edge and large energy absorption in harder phases cause surface defects on multiphase steel [16, 17]. For stable micro cutting, hard, homogenous and small grain sizes are the prerequisite [18]. However, if the workpiece material cannot be freely changed, it is essential to formulate conditions that will enable micro machining to be commercially viable.

The low ratio of undeformed chip thickness to tool edge radius leads to ploughing, poor edge definition and burrs [10, 15, 19-22], this impedes the attainment of good finishing surface and hinders functional compliance. Post processing of micro components is extremely difficult or on higher cost [23, 24]. The application of conventional deburring techniques may introduce dimensional error and residual stresses in the components. Therefore, suppression of burr development commands special research interest in correlation with cutting conditions and material properties.

Size effects in materials involved in aerospace and biomedical applications are of particular interest since both these fields rely heavily on the use of micro-features. Mechanical micro machining of such difficult to cut materials, Inconel 718 an example, is recognised as a major challenge to manufacturing [2]. However, micro milling has the potential to create required surfaces on nickel based micro components [22, 25].

Minimum chip thickness phenomenon involved in chip formation process significantly differentiates micro machining from of its macro counterpart. The major limiting factor on achievable accuracy in micro machining is primarily attributable to the ploughing process. The chip formation during micro machining is retarded when the process operates below the minimum chip thickness. The minimum chip thickness of each grain is critical to determine its chip forming condition [26]. The most favourable undeformed chip thickness relative to tool edge radius that can result in best surface finish usually occurs at minimum chip thickness [27]. Therefore it can be an indicator of transitions in the cutting mechanisms (from rubbing to shearing mode) and to monitor the cutting process.

In micro cutting, acoustic signals are generated mainly through the micro structural features of the workpiece material, such as grain boundaries, micro cracks and inclusions [28]. The review of literature indicates that there are no applications of acoustic emission (AE) technique in micro machining process for detection of chip formation mechanisms.

1.2 Aim and Objectives

The aim of this research was to investigate and characterise the size effect phenomenon in micro milling process. The specific objectives set for this PhD were as follows:

- To critical review published literature and establish the body of existing knowledge and knowledge gaps in relation to size effect in micro machining.
- To investigate the influence of workpiece microstructure and hence properties by studying the machinability of single and multi phase material.
- To investigate and define the dominance of key process variables on size effect in micro machining.
- To investigate and exploit acoustic emission signals for
 - i. Detection of micro machining chip formation mechanisms
 - ii. Evaluating the minimum chip thickness and chip formation angle in micro milling process.

1.3 Thesis Outline

This thesis is organised into eight chapters based on the research carried out during the course of this PhD. The thesis is based on the alternate PhD format which appends research papers to a literature review and then supplements this with conclusions.

Chapter 1 Introduction

This chapter introduces the background and scope of this research, presents a critical overview of knowledge and identifies the research gaps. Based on these, it lays down the aim and objectives of the PhD.

Chapter 2 Literature Review

This chapter aims to provide a synopsis of past and on-going research relating to micro mechanical machining. The literature review is particularly focused on size effect related issues of tool edge radius as well as workpiece material microstructure effects in micro mechanical machining. Furthermore, the use of acoustic emission and signal processing techniques employed by other researchers is also discussed in this chapter.

Chapter 3 Experimental Procedure

This chapter presents a brief description of the equipment, workpiece materials and cutting tools used in this study. A concise step by step procedure of how the cutting tests were planned and executed, along with acoustic emission signals post processing technique applied to monitor deformation modes involved in micro machining. In addition, methodology used to measure tool edge radius, surface roughness, sub surface damage, burr formation and tool wear are also documented.

Chapter 4 A Comparative Study of Material Phase Effects on Micro-Machinability of Multiphase Materials

The focus of the research presented in this chapter is to study the machinability of two different kind of steel materials that would enable the elucidation of the effect of phase property variability on the mechanics and performance of the micro milling process. Therefore, pilot experimental investigation of micro-machinability of nearly single-phase (AISI 1005 steel) and multi-phase (AISI 1045 steel) microstructure materials were undertaken using tungsten carbide micro-end mills. From the resulting data the effects of

workpiece microstructure, undeformed chip thickness and tool edge radius on the resulting workpiece quality (burr formation and surface roughness) and tool wear was established.

Chapter 5 Identification of Factors that Dominates “Size Effect” in Micro Machining

Despite formidable challenges as far as machining of nickel base alloy is concerned, the superior thermo mechanical properties makes them attractive for aerospace applications. This was done to expand the scope of micromachining to include Inconel 718 alloy particularly useful for industrial and research usage. This work was important to underpin industrial prospects at Manchester. This chapter presents the use of Taguchi’s methodology alongside acoustic signals to evaluate the contributions of the different process parameters towards size effect. This study therefore quantified the effects of machining parameters namely, cutting velocity, undeformed chip thickness to tool edge radius ratio, depth of cut on acoustic emissions, surface finish and burr formation. Acoustic emission signals produced during these trials were also analysed with different signal processing techniques. It showed the limitations posed by Fourier transformation and proposes the way forward to use wavelet transformation techniques. Finally, decomposed frequency bands obtained from wavelet transformation was analysed statistically. From the resulting data new evidence in support of mechanisms responsible for the size effect was discovered based on their energy contribution in the AE signals.

Chapter 6 Chip Formation in Micro-Scale Milling and Correlation with Acoustic Emission Signal

In this chapter the effects of different workpiece materials on chip formation and associated mechanisms in micro cutting were investigated. The Wavelet Transformation technique was used to decompose acoustic emission (AE) signals generated from orthogonal micro milling of different workpiece materials. The analysis of frequency bands originating from various microstructure activities and their link with deformation mechanisms is one novel contribution of this chapter.

Chapter 7 Estimation of Minimum Chip Thickness in Micro Milling using Acoustic Emission

In this chapter an indirect technique to estimate the minimum chip thickness value is presented. The acoustic emission generated from the orthogonal micro milling process was employed to estimate the threshold conditions. Since milling operation is by default an intermittent cutting process, the minimum chip thickness effects involved in here tend to

have a greater variability in the process as compared to continuous cutting process. The repeated loading and unloading of the cutting edge serves to identify rubbing signature due to interactions taking place between the workpiece and tool contact zone in the initial arc of contact. This inherent characteristic was exploited to identify $AE_{r.m.s}$ rubbing signature in successive tool rotations. The minimum chip thickness predicted by this new and novel approach compares reasonably well with values that exist in published literature.

Chapter 8 Conclusions and Recommendations for Future Work

This chapter summarises the major conclusions made during the course of this research. It also makes suggestions regarding future research that can be undertaken based on the findings reported in this thesis.

Chapter 2

LITERATURE REVIEW

2.1 Introduction

The high demand of miniaturised components coupled with geometric and material range limitation of traditional lithographic techniques has generated strong interest in mechanical micro machining. In this respect, the capabilities of downscaled versions of traditional machining processes have gained momentum to achieve requirements of aerospace, automotive, biomedical, communications, electronics, environmental, optical and military industries [1, 3]. With the maturity of these high-tech processes, it was expected to develop micro systems that would enhance health care, quality of life and economic growth in applications like micro channels for lab-on-chips, shape memory alloys, medical devices, micro actuators, sensors and fluidic graphite channels for fuel cells. Due to the complex nature of machining process, previous researchers have come to the conclusion that it is often not possible to scale down processes, and these limitations lead to the so called size effect.

Micro engineering can be defined as the branch of engineering that deals with development and manufacture of products, whose functional features or at least one dimension is in the order of microns [3]. However, there is no universally agreed distinction between macro and micro-scale machining. Masuzawa suggested in the international academy of production engineering (CIRP) review paper that the range of micro machining varied according to contemporary level of conventional technologies, person perspective,

machining method, type of product or material [29]. Table 2.1 provides summary of the proposed definition available in the reviewed literature.

Table 2.1 Proposed definition for micro machining

Researcher(s)	Year	Definition
Masuzawa and Tonshoff [30]	1997	Undeformed chip thickness ranges from 0.1 to 200 μm
T. Masuzawa [29]	2000	Range of micro cutting varied according to era, person view point, machining method, type of product and material
Liu et al [31]	2004	Undeformed chip thickness is comparable to tool edge radius
Chae et al [1]	2006	A creation of miniature components and devices with features size varied from tens of microns to a few millimetres
Dornfeld et al [2]	2006	Mechanical cutting with geometrically defined cutting edges and tool engagement less than 1 mm in feed
Simoneau et al [32]	2006	Undeformed chip thickness is less than the average grain size of the smallest grain type in the material microstructure
Aramcharoen et al [33]	2008	Tool diameter falls in range of 1 to 999 μm or if undeformed chip thickness is comparable to tool edge radius or material grain size

Masuzawa and Tonshoff acknowledged that the word micro machining literary means the cutting of dimensions between 1 to 999 μm [30]. Other researchers also proposed that creation of features or material removal in sub millimetre range falls within micro cutting domain [1, 2] while the meso domain was in the 1 to 10 mm range [34]. Another aspect that has to be considered is the importance of tool edge radius. The assumption of perfectly sharp cutting edge is not valid in micromachining. The radius of cutting edge becomes significant compared to the thickness of the material to be removed. In such a situation the effective rake angle is negative and the material can be removed through extrusion.

When grain size is comparable to the undeformed chip thickness, the cutting edge tries to fracture a single grain of a workpiece material. This influences cutting forces, chip formation and quality of machined surface. Furthermore, when undeformed chip thickness is less than grain size of the smallest phase, it is important to consider material heterogeneity because elastic and plastic deformation of each material phase present in the material microstructure becomes more critical. Simoneau et al introduced this idea in

micro-scale machining [32]. However, the effect of tool edge radius was not considered. Aromcharoen et al definition covers the fragile nature of micro tools and the size effect in material removal [33].

2.2 Size effect in micro machining

Size effect in manufacturing of metallic components are deviations from extrapolated values of process characteristics which occur, when reducing or increasing all relevant length dimensions of the workpiece, tool and/ or process parameter(s) [35]. The size effect occurs as the ratio of decisive features which cannot be kept constant according to process requirements. It is also emphasised in the definition that size effects are of somewhat surprising in nature at the first glance, as they occur despite the fact that length relationship between all geometric features are held constant.

In machining, size effect is mainly related to the effects of small ratio of the undeformed chip thickness to the tool edge radius for which the assumptions of tool edge sharpness as well as workpiece material homogeneity and isotropic nature cannot be valid. Previous authors [1, 2, 31, 36, 37] reviewed the research carried out for mechanical micro machining and identified areas that could aid in process improvement. Several critical factors associated with micro domain cutting were highlighted which requires paradigm shift from macro machining. Some of these factors include:

- Specific cutting energy increases in a non-linear fashion when machining is performed at undeformed chip thickness smaller than the tool edge radius. Moreover, microstructure of the workpiece material has also been declared for the size effect phenomenon observed in the specific cutting energy.
- A minimum chip thickness effect sets the lower limit of feasible process window for a given workpiece and tool combination.
- Noticeable discrepancy between theoretical and measured surface roughness produced at low feeds typical in micro cutting process.
- Detrimental effects of ploughing process on component quality factors in terms of surface finish and burr size.
- Inherent fragility of micro tools and effects of noise factors like variations in temperature, vibrations, pressure, humidity and other environmental variables.

2.2.1 Specific cutting energy

The size effect is typically characterised in machining as a non-linear increase in specific cutting energy (or specific cutting force) with decrease in undeformed chip thickness. The specific cutting energy is used to measure the amount of effort needed to remove a unit amount of material. The higher consumption of specific cutting energy means that machinability of the material should be more difficult than expected in removing smaller amounts of material. Experimental observations associated with this phenomenon for different materials under different cutting conditions have been reported in literature. Most of the drivers/ mechanisms offered for the extra energy requirement are presented in table 2.2.

Table 2.2 Reported research on size effect

<i>Researchers</i>	<i>Process, Workpiece material</i>	<i>Cutting Speed (m/min)</i>	<i>Uncut chip thickness (μm)</i>	<i>Tool edge radius (μm)</i>	<i>Potential cause of size effect</i>
<i>Backer et al [38]</i>	Turning, SAE 1112	137	50 to 300	-	Strain hardening, decreasing the number of defects in microstructure
	Milling, SAE 1112	1630	5 to 13	-	
<i>Nakayama and Tamura [39]</i>	Milling, Brass	0.1	2 to 42	3 to 4	Subsurface plastic flow
<i>Larsen-Basse & Oxley [40]</i>	-, Low carbon steel	6.1 to 249	25 to 2500	-	Strain rate increases at the primary shear zone
<i>Kopalinsky and Oxley [41]</i>	-, Steel	420	10 to 200	-	Reduced thermal softening effect
<i>Furukawa and Moronuki [42]</i>	Planning, PMMA/ CaF ₂ / Germanium	6	0.5 to 10	-	Initiation point is influenced by combination of material property, tool edge sharpness and chip aspect ratio
<i>Lucca et al [43]</i>	Plunge cutting, OFHC Cu	6-108	0.025 to 20	0.10 to 0.30	Tool edge radius
<i>Lucca and Seo [44]</i>	Fly cutting, Te-Cu	7.6	0.01 to 20	0.25	Negative effective rake angle
<i>Ng et al [45]</i>	Turning, Al-7075	10,150	0.01 to 2	0.065 to 0.100	
<i>Liu and Melkote [46]</i>	Orthogonal Cutting, Al-5083	10,200	0.5 to 10	0.065 to 0.100	Strain gradient plasticity effects at low undeformed chip thickness
<i>Filiz et al [10]</i>	Milling, OFHC Cu	40,80, 120	0.75,1.5, 3,6	~2	Material softening is less dominant than strain rate hardening at higher speeds
<i>Subbiah et al [47]</i>	Orthogonal Cutting, Al2024-T3	150	15 to 105	12.5 to 75	Ductile tearing
<i>Wu and Liu [48]</i>	Orthogonal Cutting, AISI 1045 steel	15.7 to 141.3	1 to 10	16	Flow stress increases as uncut chip thickness decreases. The flow stresses are sensitive to strain rate.
- Means no data provided in the publication					

It can be seen from the table that the reported research work was undertaken over a limited cutting velocity range and the material thickness removed was in the sub-micron length scale. With respect to investigated workpiece materials, difficult to cut materials (Ni, Ti based alloys) have not been reported.

2.2.1.1 Material strengthening effect

Becker et al [38] were concerned with the apparent material strengthening when material removal took place below $0.7 \mu\text{m}$. They attributed this phenomenon to reduction in the availability of movable dislocations and the cutting force has to overcome the large atomic bonding force within crystals. Fig. 2.1 shows the relationship between the specific cutting energy consumption of SAE 1112 steel for three major machining processes along with Taniguchi [49], a more comprehensive trend which includes tensile test data. These trends suggest that decreasing undeformed chip thickness causes work-hardening of material surface. Shaw [50] described size effects as originating from the short range inhomogeneities present in all commercial engineering metals.

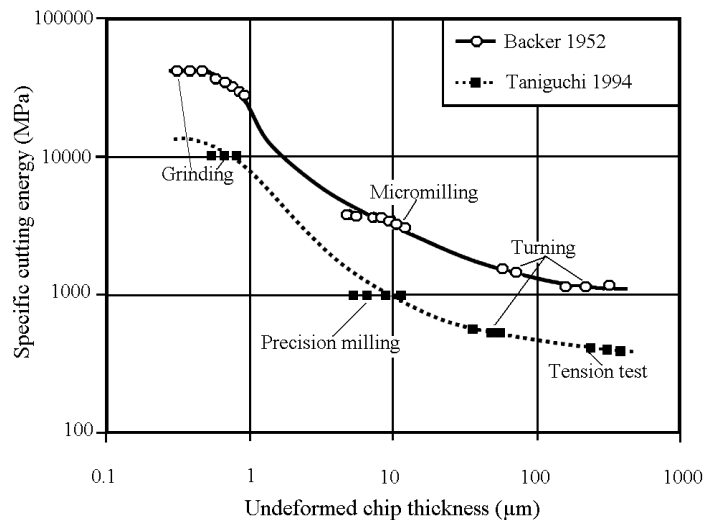


Fig. 2.1 Variation in specific cutting energy for three major machining processes ([38] [49])

Larsen-Basse and Oxley [40] explained the cause of size effect in machining in terms of the strain rate sensitivity of the workpiece material. Their reasoning was based on empirical data drawn from the experiments on plain carbon steel. The cutting velocity was varied from 6.1 to 249 m/min over a range of undeformed chip thickness (25-2500 μm). They concluded that the maximum shear strain rate within the primary shear zone is

inversely proportional to the uncut chip thickness. For most metals an increase in strain rate increases the flow stress with the strain-rate sensitivity of flow stress increasing rapidly in the range applicable to machining process ($>10^4/s$). Thus, this could be the reason for the increase in specific cutting energy with reduction in uncut chip thickness.

In later work, Kopalinsky and Oxley [41] found a decrease in the shear plane angle due to decrease in the tool-chip temperature. This, they stated, leads to increase in shear strength of the workpiece material which can be responsible for increase in specific cutting force. However, they acknowledged that the temperature effect does not explain size effect observed at undeformed chip thickness less than $50\mu\text{m}$. Fang attributed the size effect phenomenon to the material constitutive behaviour of varying shear flow stress with uncut chip thickness inline with a slip line model [51].

Liu and Melkote [46] incorporated strain gradient concept into the flow stress equations to simulate orthogonal micro-machining process in their finite element model. Strain-gradient plasticity suggests that when deformation is large and is constrained spatially to a narrow region, the stress not only depends on strain at a point but also on the strains in the region surrounding that point. The model was able to capture the size effect in specific cutting energy for Al5083-H116 aluminium alloy as shown in Fig.2.2. The study concluded that strain gradient strengthening contributes significantly to the size effect at low cutting speed and small uncut chip thickness ($<10\ \mu\text{m}$). Additionally, they found that temperature dependence of flow stress plays a dominant role in causing size effect at relatively high cutting speeds ($>200\ \text{m/min}$) and large uncut chip thickness ($>20\ \mu\text{m}$). This latter size effect is caused by material strengthening due to a drop in the secondary shear zone temperature with decrease in undeformed chip thickness.

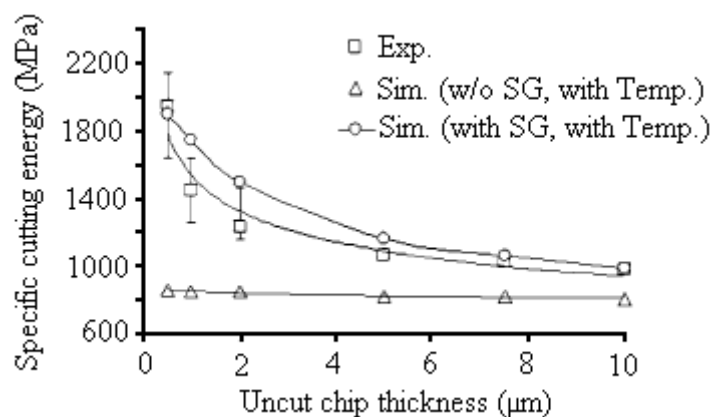


Fig. 2.2 Importance of incorporating strain gradient in explaining size effect (adapted from [46])

In later work [52], the researchers analysed the data available in literature and suggested that, for a given speed, the occurrence of nonlinear increase in the specific cutting energy at an uncut chip thickness comparable to tool edge radius is not often the case. However, the criticism one would make is the validity of comparing experimental data from different cutting conditions. Furthermore, they asserted that under conditions where the strain gradient effect is dominant, the nonlinear increase in specific cutting energy occurs at microstructural length scale of the material. Likewise, analysis of the data also suggested that increasing the cutting speed produces a noticeable change in the uncut chip thickness value at which the increase in nonlinearity of specific cutting energy begins.

Lai et al [53] developed a model to predict cutting forces and minimum undeformed chip thickness in micro milling, which incorporates size effect considering the effects of strain gradient, micro cutter edge radius and minimum chip thickness. The proposed model was reported to account for material strengthening behaviour which is regarded as main factors for the occurrence of size effect. Also, ploughing effects causes increase in specific shear energy when machining was undertaken at undeformed chip thickness smaller than the minimum chip thickness.

Filiz et al [10] showed specific energy dependence on cutting speed with decrease in the undeformed chip thickness (Fig. 2.3). Hence, suggested that at micro scale cutting, the effect of thermal softening of the workpiece is less dominant than the effect of strain rate hardening. Thus the apparent strength of the material increases.

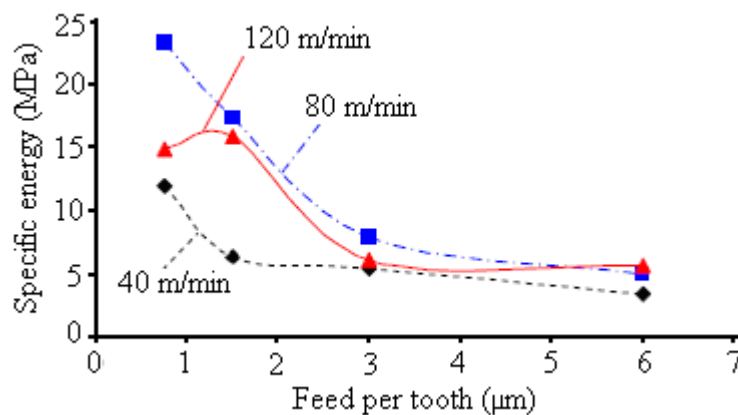


Fig. 2.3 Specific energies for average in-plane forces R (adapted from [10])

Furukawa and Moronuki [42] observed the initiation of size effect in the cutting force at the undeformed chip thickness of 3 microns. The point of nonlinearity is influenced by a combination of factors such as work material property, cutting edge sharpness and aspect ratio of the chip.

2.2.1.2 Subsurface plastic deformation

Nakayama and Tamura [39] carried out investigations at very low cutting velocity to avoid temperature and strain rate effects. They suggested that the energy expended in plastic flow in subsurface layer is not proportional to change in uncut chip thickness. The blunting of the cutting edge and decrease in shear angle due to highly negative effective rake angle could increase the specific cutting energy which contributes to the size effect phenomenon. The main cause of the subsurface plastic flow was recognised as an extension of shear zone below the machined surface at small undeformed chip thickness. Shimada et al also offered similar explanation based on molecular dynamics simulations [54]. They showed that depth of the deformed layer around the cutting edge radius is difficult to reduce to the level less than the size of tool edge radius. Moriwaki et al [55] asserted that depth of the damaged layer beneath a surface finished by diamond cutting becomes about 10 times the edge radius of the tool. These results indicate that the effect of previous pass in the newly generated surface layer influences the specific cutting energy when micro cutting is performed at very small undeformed chip thicknesses or with multiple passes.

2.2.1.3 Tool edge radius effect

The specific energy and fraction of energy going into the work are useful concepts relative to the energy considerations in cutting and grinding [56]. In cutting and coarse grinding (large chips) 90 percent of energy is carried away by the chips while in dry fine grinding (small chips) 80 percent of the energy is shifted to the workpiece. The extra plastic flow linked with a finite edge radius accounted for the decrease in the thermal flux into the chip at very small undeformed chip thickness. The presence of edge radius is said to cause ploughing ahead of the tool tip. Albrecht was among the earliest investigators to suggest the pushing of the material in front of the edge radius predominantly into the chip and some into the workpiece [57]. Kim and Kim showed analytically that in macro-machining,

shear takes place along the shear plane, and in micromachining, the shear takes place around the cutting edge [58].

Lucca et al [43] reported the effect of tool edge radius on force and energies consumed. They noticed that the specific cutting energy required to machine at very low chip thickness could not be explained by the energy required for shearing and for overcoming friction on the rake face of the tool. The dominance of ploughing under these conditions was used to explain the increase in specific cutting energy. Lucca et al experimentally studied the role of the effective rake angle. It was found that the thrust force is a dominant component below certain undeformed chip thickness and cutting is mainly due to ploughing process [44]. In another study, Lucca and co workers suggested that the tool edge condition has a significant effect on the resulting forces at small ratio of the undeformed chip thickness to the tool edge radius [59].

Komanduri et al [60] carried out molecular dynamics simulation studies by varying the tool edge radius (3.62-21.72 nm) and depths of cut (0.362-2.172 nm) maintaining the depth of cut to tool edge ratio constant (0.1, 0.2, and 0.3). Variations of the cutting and thrust forces, the force ratio, the specific energy, and the sub-surface deformation with the tool geometry and depths of cut were investigated and found significant. Another study reported that in nano scale cutting of copper, approximately 43 percent of the total energy was dissipated under a tool during plastic deformation process which was significantly larger than macro scale machining [61].

2.2.1.4 Ductile fracture

Evidence from multiple experiments showed that fracture initiates chip formation and further growth depends on the combination of the mechanical properties of workpiece material, tool geometry and cutting regime used [62]. However, the energy required to create these new surfaces was calculated to be negligible compared to shearing and friction in earlier studies [63]. The argument for occurrence of the fracture at the tool tip in continuous cutting and a possible mechanism is discussed in the literature which is as follows.

There will always be a finite radius of curvature no matter how carefully a tool may be ground. If a metal cut consists of a number of plates then shear the surface might be expected as shown in Fig. 2.4. The rake angle associated with plate 1 is very small and

hence the corresponding shear angle is also expected to be small. The chip from plate 1 would bend toward the tool by plate 2. The shear angle would increase for subsequent plates inasmuch as the rake angles associated with them increase. This variation in shear angle would occur up to point A beyond which the rake angle should remain constant. As a consequence, chips 1, 2, 3 and 4 would be of different lengths. In practice, the metal cut does not consist of separate plate and chips cannot be different lengths. Hence, the chip in the vicinity of the tool face must deform plastically in tension. The region subjected to tension will extend to tension up to point A. The tensile field of stress that is developed as a result of the curvature of the tool point can thus produce the crack necessary in the development of the new surface. The material beyond point A is subjected to large compressive stresses, and the crack will be quenched upon reaching this region in case of continuous cutting.

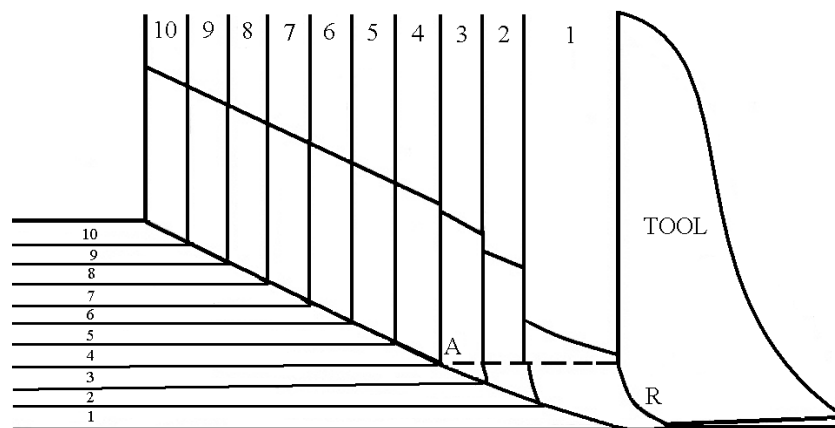


Fig.2.4 Stack of plates cut with tool having finite radius of curvature at its tip
(adapted from [63])

The concept of material separation via ductile fracture for the generation of new machined surface has its roots mainly from observing cross-sectional areas of the chip formed. Subbiah and Melkote [47] showed fracture zones in the chip roots during micro machining of aluminium alloy (Al 2024-T3) with finite edge radius tool. Atkins [64] theory suggests that the energy associated with chip separation is nearly corresponding to the material fracture toughness value. Based upon this observation, it was suggested that the energy expended during the creation of a new surface can not be neglected. This implies that its contribution in the specific energy increases at low undeformed chip thickness. Therefore,

energy consumed in new surface initiation by means of ductile fracture can be attributed to the probable cause of size effect.

2.2.2 Material heterogeneity

In micro-scale machining, material grain size for tool and workpiece comes into play, rendering each tool-workpiece combination unique. The average grain size of generally used engineering materials is between 100 nm to 100 μm . In addition to that, at present the achievable cutting radius (1~2 μm) is limited by tool grinding technology and carbide grain size (0.4-0.7 μm). The feature size of the micro-machined component is normally of a similar order, thus the role of material microstructure is ingrained in the micro-cutting process.

Bissacco et al stated that limited scalability of material grain size and tool edge radius manifest size effect at the micro-scale [9]. Moronuki et al suggested that polycrystalline material must be treated as discrete and heterogeneous at this level [65]. This is due to the undeformed chip thickness commonly employed in mechanical micro machining lies within the grain size of the material microstructure. The material microstructure regions (phases) with very different hardness and ductility have dimensions of the relevant tool sizes or unit of material being removed and hence causes inconsistency in machining conditions.

2.2.3 Minimum chip thickness effect

The first step in establishing a lower limit of mechanical micro machining is the prior knowledge of minimum chip thickness for a given tool and workpiece material. The minimum chip thickness is defined as a minimum undeformed chip thickness that can be removed stably from a work surface for a given cutting edge radius [66]. Thus, it can be seen as a measure of extreme accuracy attainable for a given set of parameters.

From the understanding of minimum chip thickness concept, it can be stated that when undeformed chip thickness is less than the minimum chip thickness, no material removal in the form of chip occurs and either rubbing or burnishing takes place [67]. The chip starts to form through ploughing coupled with an elastic deformation when material accumulated from non cutting passes exceeds the value of minimum chip thickness. Material is removed

completely in the form of a chip when the undeformed chip thickness is considerably greater than the minimum chip thickness. Thus, the less rigid the tool, the higher is the ratio of cutting edge radius to feed per tooth and the more is the accumulation of workpiece material as the tool advances.

Weule et al emphasised a strong contribution of material properties on the minimum chip thickness [15]. Previous researchers have also suggested knowledge of minimum chip thickness while selecting suitable machining parameters can help to reduce surface roughness [11, 15], subsurface microstructure modification and tool wear while reducing burr size [68]. It also proves useful to reduce fluctuations in cutting forces [69] and therefore improves process stability.

Even in macro scale machining, research was directed to investigate factors that affect or retard chip formation process. Komanduri [70] experimentally determined the transition from ploughing regime to cutting regime in turning of mild steel. When cutting is performed with negative rake angle tool, the flow of material on the tool face was said to be in two directions, some under the flank face and some up the rake face to form a chip, with a stagnation point, as shown in Fig.2.5. Based on the rake angle of cutting tools, no chips were reported to be formed at -55° rake angle while they were shown to have formed at -75° rake angle. Abdelmoneim and Scrutton reported that in milling of free-cutting brass and fine-grained zinc with very dull tool whose rake angle was more than -76° retarded the chip formation process [71].

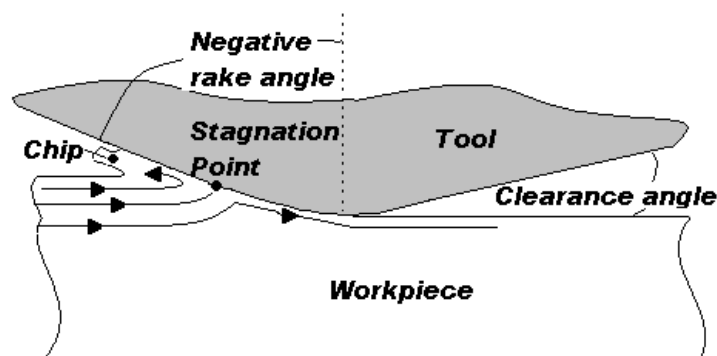


Fig. 2.5 Flow of material on the tool face with a high effective negative rake angle (adapted from [70])

L'vov evaluated the minimum chip thickness, by considering the theory of metal rolling, to be 29.3% of the tool edge radius [72]. Basuray et al [73] analytically and experimentally evaluated that minimum undeformed chip thickness is dependent on the sharpness of the tool edge radius. The experimental results showed that the minimum chip thickness ranges from 11 to 17 percent of the tool edge radius when cutting lead, aluminium and mild steel with high speed steel tools having exaggerated tool edge radii varying from 0.6 to 1.5 mm.

Shimada et al [54] used molecular dynamic simulations to predict the ultimate achievable accuracy using 5 to 10 nm edge radii diamond tools. In their study, the estimated minimum chip thickness obtained with 5 nm tool edge radius was at the same for both copper and aluminium workpieces. However, with larger cutting edge radius, the ratio of minimum chip thickness to edge radius was twice large for aluminium as that in copper cutting. The tool-work interface friction and / or resistivity to plastic deformation of work materials were the possible factors influencing the difference in minimum chip thickness. The analysis showed that minimum chip thickness in micro cutting can be expected to be about 5 to 10 percent of the radius of practical fine cutting edge.

Yuan et al [74] found that the frictional characteristics at chip-tool interface play an important role on the ratio of the minimum chip thickness to tool edge radius. The theoretical analysis supported the previously reported research where the ratio ranges from 25 to 38 percent when cutting steel with high speed steel or carbide tools. Furthermore, the authors suggested that tool sharpness strongly influence the machined surface integrity in terms of surface roughness, micro hardness, residual stress and the dislocation density.

Volger et al [11] used a customised finite element code to determine the minimum chip thickness of hard and soft phases of the steel. The reported values are in range of 14 to 25 percent and 29 to 43 percent of edge radius for pearlite and ferrite phases, respectively. The softer ferrite phase exhibit relatively higher value that indicates ploughing is more predominant when machining ferrite than pearlite owing to increased ductility.

Kim et al reported that unlike macro milling, effective feed/ tooth is not equal to the indented value in case of micro milling [67]. The deviation was due to the relatively small bending stiffness of the micro tool causing it to deflect easily and material accumulation in the non cutting passes when the feed per tooth was less than minimum chip thickness. In another study [75] an indirect technique to estimate minimum chip thickness by using

cutting force measurement was developed. The cutting was performed on brass workpiece material with carbide tool. The value was found about 22 to 25 percent of tool edge radius.

Son et al [27] considered the influence of friction between the workpiece materials (Aluminium, Brass and Copper) and the diamond tool. They developed an analytical expression of the minimum chip thickness (h_m), depending on the tool edge radius (r_e) and friction angle (β i.e. tangential force/normal force between the tool and uncut workpiece).

$$h_m = r_e \left[1 - \cos \left(\frac{\pi}{4} - \frac{\beta}{2} \right) \right] \quad (2.1)$$

The experimental validation of the model was done on a shaper machine and the minimum chip thickness values were reported between 18 to 24 percent of the tool edge radius.

Liu et al [76] presented an analytical slip line model to estimate minimum chip thickness based on thermo mechanical states of the machined material (cutting temperature, strain, strain rate). The transition criterion in the model from ploughing domain to shearing domain was analogous to that of scratch test. In experimental validations, minimum chip thickness to tool edge radius was about 38 to 40 percent for Al 6084-T6 and 24 to 35 percent for AISI 1040 steel. Furthermore, model simulations were performed for two types of carbon steels (AISI 1018 and AISI 1040) and Al6082-T6. They pointed out that cutting velocity, thermal softening, strain hardening and tool edge radius had compounded influence on the minimum chip thickness. For AISI 1040 steel, increase in cutting speed and tool edge radius led to an increase in the minimum chip thickness. An increase in the carbon composition also had the same result. This was attributed to the predominance of softening on strain hardening effects. Steel being then more ductile due to rise in cutting temperature, chips were formed less easily. This result suggests that relatively low cutting speed is preferable for carbon steels to avoid intermittent chip formation at low chip loads. However, in the case of Al6082-T6 the minimum chip thickness remained the same with variations in cutting speed and tool edge radius. This they put down to softening and strain hardening effects counteracting each other.

The knowledge gained from the previous work can be summarised as most of the researchers have used cutting forces as an elementary characteristic to estimate minimum chip thickness. The value of minimum chip thickness typically ranges from 5 to 43 percent of the tool edge radius. The variation in these values was found to be predominantly driven by workpiece material and tool combination as well as tool rigidity. The relative sharpness

of tool edge radius to magnitude of material being removed is crucial in determining the minimum chip thickness. Cutting operations can be scaled down (lower minimum chip thickness) when sharper cutting edge tool such as diamond are used. It suggests that advances in tool manufacturing that leads towards sharper tool edges and less fragility can improve the lower limit of mechanical micro machining. Furthermore, workpiece thermo mechanical properties, tool-work interface friction and cutting speed effects are also important to consider for the minimum chip thickness phenomenon.

2.2.4 Elastic plastic deformation

When cutting is performed below minimum chip thickness, large forces are produced between the tool and workpiece leading to tool deflection and machining of sloped walls that are intended to be vertical. Additionally due to elastic recovery, the machined surface may be several micrometers above the location where cutting edge of the tool passed [5]. Therefore, knowledge of material properties will be useful to select the appropriate cutting conditions to produce micro machined parts with greater dimensional accuracy.

In this regard, Jardret et al claimed that the proportion of the plastic deformation increases with Young's modulus to hardness ratio [77]. In a related study, Nakayama [78] stated that high value of the hardness to elastic modulus ratio means larger elastic recovery of the material. It was also suggested that 0.45 percent carbon steel will elastically recover more in its hardened state as compared to annealed state. Taniyama et al [79] carried out a scratch test on JIS S25C steel (Fig 2.6), in order to investigate the influence of heterogeneity of the workpiece material in the micro deformation process. The scratch grooves obtained on different phases were observed and compared under a field emission scanning electron microscope.

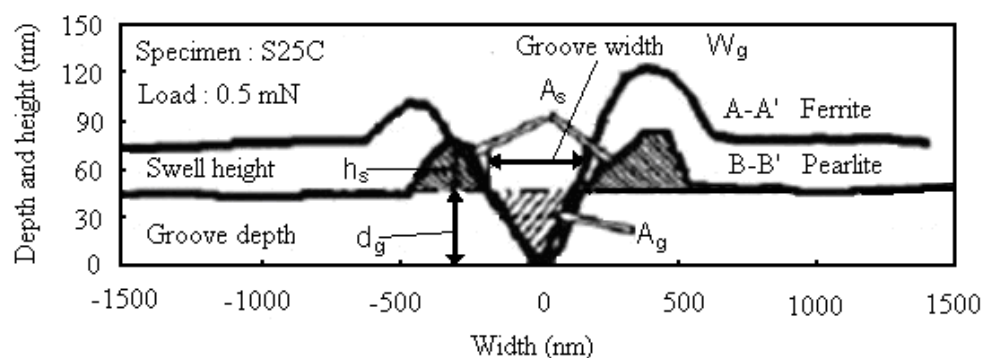


Fig. 2.6 Cross sectional profile of scratch groove (adapted from [79])

The work clearly showed that the scratch groove on pearlite was smaller than on ferrite. This implies that pearlite had experienced a higher elastic recovery than ferrite. The authors credited this occurrence to the presence of lamellar cementite in pearlite, which is ten times harder than ferrite. Moreover, they discovered that when scratching pearlite, plastic flow was concentrated in the lamellar ferrite rather than lamellar cementite.

2.2.5 Chip formation

The fundamental understanding of micro cutting and its response to process variables can be realised by studying the deformation mechanisms and how it can be manipulated and eventually controlled [80]. Workpiece material state, purity, crystallographic orientation, temperature and atmospheric conditions, cutting geometry and machining parameters and surface conditions of the materials were reported as the primary variables influencing plastic deformation.

In the case of polycrystalline materials, the micro cutting process was characterised by lamellae formation that are separated by shear fronts [81]. The lamellae are aligned perpendicular to chip flow direction and slide up on the rake face of the tool as the cutting action proceeds, irrespective of grain orientation. The thickness of the chip differs depending on the crystallographic orientation due to change in shear angle. The thickness also changes when the cutting tool passes through the grain boundary. Ueda et al found similar chip structure when micro cutting an amorphous metal. They found the chip lamellae occurred due to periodic localisation of shear bands [82].

In micro chip formation where uncut chip thickness approaches the edge radius, the effective rake angle becomes highly negative, leading to a change in the chip flow angle and shear angle [83]. Ohbuchi and Obikawa [84] observed a stable built-up edge for tools with high negative rake angle. The size of the dead metal under the tool depends on the chip thickness and effective rake angle as shown in Fig. 2.7. The cutting ratio becomes small as the ratio of tool edge radius to undeformed chip thickness increases [85]. It means that relative thickness of the deformed chip to the actual chip increases with a decrease in uncut chip thickness when the tool edge radius remains unchanged.

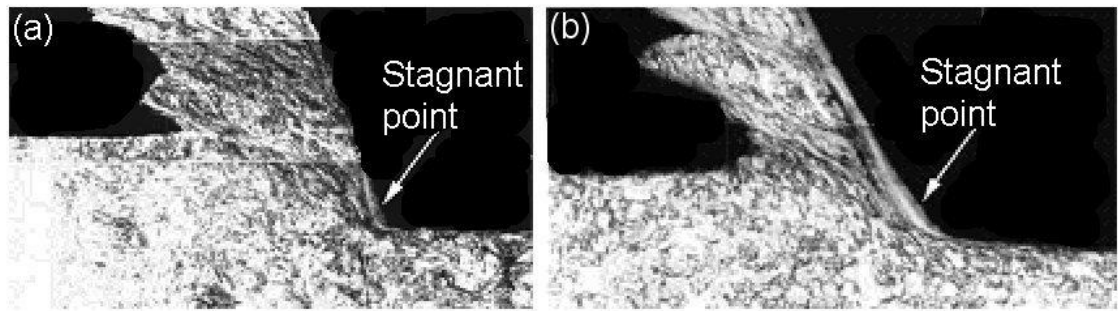


Fig. 2.7 Chip formation with different rake angles. Cutting conditions: workpiece, 0.45% C carbon steel (S45C); tool, cutting speed, 10m/s; (a) 70 μm feed/tooth, -20° rake angle (b) 40 μm feed/tooth, -30° rake angle [84].

Moriwaki et al [55] reported that the crystallographic orientation affects the chip formation process at undeformed chip thickness in the order of microns. However, it was not influential when undeformed chip thickness was reduced to submicron level. This was attributed to the presence of a damaged layer beneath the machined surface leading to a constant shear angle and which plays a dominant role as compared to crystallographic orientation. It is this damaged layer that is being machined when the depth of cut is kept to sub micron levels.

Simoneau et al [32] simulated chip formation process of normalised AISI 1045 steel. They assigned different hardness values to phases present in the microstructure of the steel and explained the chip formation and surface defects in micro-scale cutting. The results from the analysis and verified by experimental observation showed that microstructure phases alter the plastic deformation process. The chip morphology changed from continuous to a quasi-shear-extrusion type, when undeformed chip thickness moved below the smallest grain phase of material microstructure. Additionally, softer ferrite phase was ejected as a large plume at the chip free surface. In a latter work [12], they demonstrated a link between material microstructure and chip formation at macro, meso and micro-scale cutting of AISI 1045 steel. It was found that plastic strain increases as the scale of the cutting decreases.

The contact length between the chip and rake face is an important parameter that influences frictional force and cutting temperature. In the ultra precision diamond cutting of copper at 3 μm undeformed chip thickness, it was found that the contact length reaches about 50 times the undeformed chip thickness and further increases with smaller chip loads [55]. This peculiar increase in contact length complicates micro chip formation process. On the other hand, the nominal shear angle decreases. The chips bend and buckle as they pass

over the rake face. Lack of the chip control often led to coarse machined surface, poor machining accuracy and problems coupled with chip removal from the machining zone [86].

Some of the studies on chip formation suggest that due to small chip loads the cutting zone temperature at micro scale is lower as compared to the conventional cutting. Moriwaki and co-workers [85, 87] cited previous studies and reported that cutting temperature in the ultra precision diamond cutting of copper reached to a level of 150 to 350 °C. In the case of extreme machining accuracy requirements, they suggested that the effect of cutting heat cannot be neglected. Thermal expansion of the tool and workpiece were identified as responsible for tolerance deviations up to 0.5 to 1 µm for new and worn tools, respectively. Dhanorker and Özol [34] numerically simulated the cutting zone temperatures to be around 60 °C for Al 2024-T6 and around 150 °C for AISI 4340 steel in micro milling. The FEM simulations were carried out for the cutting condition of 80 m/min cutting speed and 10 µm feed/ tooth using 635 µm tool diameter having tool edge radius of 3 µm. However, a contrasting observation was reported by Komanduri [70] whereby signs of recrystallisation was shown in medium carbon steel chip obtained at -75 ° rake angle, 10 µm depth of cut and 182 m/min cutting velocity. This suggests high temperature in the region of plastic deformation with high negative rake angle.

Komaduri and Brown compiled different types of chips produced in non homogeneous cutting namely wavy, segmented and discontinuous chips [88]. The wavy chip is generated by a cyclic variation of the chip thickness due to an oscillation of the shear angle. The segments of the discontinuous chip are completely separated by fractured surfaces. Meanwhile, a distinction between the segmented chip and the shear chip is difficult to draw and normally they are both classified as segmented chips [89].

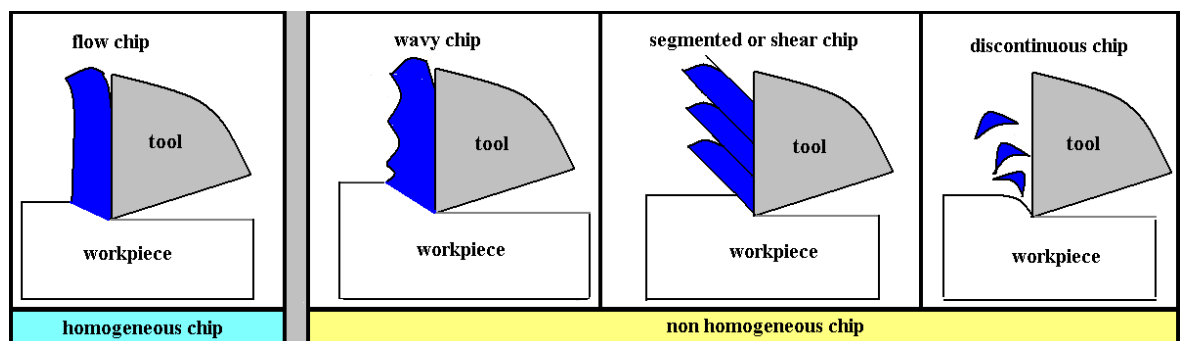


Fig. 2.8 Classification of chip (adapted from [89])

Tönshoff et al [89] summarised different theories and observations for chip formation in hardened steel. Generally, flow chips were observed when chip thickness was less than 20 μm , due to high compressive stress and high temperatures near the tool edge radius leading to plastic deformation of the material. When the chip thickness exceeds 20 μm , a portion of chip thickness above the workpiece free subsurface is not plastically deformed and instead transition from flow chip to segmented chip occurs. It was due to periodic fracture initiated at free surface of the workpiece where minimal compressive stresses exists [90] or thermoplastic instability occurs along a line, extending from the tool tip and propagates upwards to the free surface [91] favourably at high strain rates. Increasing feedrate and cutting speed were reported to have identical effect on the shear localised chip [92]. In practice cutting speed tends to have a greater influence on chip morphology for a given workpiece material. Cutting speed can be varied over a much larger range than undeformed chip thickness (working range of feedrate is sometime limited by the requirements of machined surface quality, machine tools and other factors). Barry et al [93] reported that the formation of saw-tooth is a fundamental characteristic of the machining of titanium alloys under conventional cutting conditions. However, lowering the cutting speed and/or undeformed chip thickness (less than 20 μm) results in transition from periodic to aperiodic saw-tooth chip formation. On further reduction in undeformed chip thickness to few microns (for 15 to 180 m/min cutting speeds range) continuous chips were observed.

Komanduri and Von Turkovich reported the formation of segmented chips in machining of titanium alloys at very low cutting speed (3.84 m/min) [94]. It was observed that plastic deformation in the primary zone is not uniform and intense thin shear occurs between chip segments due to poor heat dissipation properties of titanium alloys. Komanduri and Schroeder noted a thermoplastic instability leading to adiabatic shear in the chip formation process of Inconel 718 which was very similar to the mechanisms reported for titanium as well as hardened AISI 4340 steels, when machining at higher cutting speeds [95]. Barry et al [93] elaborated on this and presented two distinct mechanisms for catastrophic shear failure when machining Ti-6Al-4V at 80 μm undeformed chip thickness. Under high cutting velocity (180 m/min), material failure was attributed to ductile fracture due to increase in ductility as a result of thermal softening. However, it was also noted that the upper region of primary shear zone (segment tip) was sheared off due to cleavage. Under low cutting velocity (15 m/min), failure was said to have occurred due to cleavage.

2.2.6 Surface generation

The objective to create ultra-smooth functional surfaces with exponential accuracy and quality for micro components is the motivating factor behind research into surface generation in micro-scale machining. Moreover, because ratio of surface area to volume increases as devices and their features are miniaturized; more attention should be given to surface generation and phenomena that influence the surface character [31]. In this respect, better understanding of the effect of individual grains of a material microstructure and mechanisms that govern surface making in micro-scale aids in development of the broadly applicable micro-features/parts.

Several researchers reported dominant influence of chip thickness on surface roughness in micro machining [11, 15]. Bissacco et al [9] strengthened this observation by analysing SEM images at the last part of tool engagement arc in a downscaled milling process. They found formation of waves of plastically deformed material in the feed direction below a critical ratio of the chip thickness to cutting edge radius which supported the occurrence of size effect. These results indicate that the scaling of undeformed chip thickness to the tool diameter triggers the cutting edge radius influence on the process.

Vogler et al. [11] investigated the surface generation process in the micro-end milling of both single-phase and multiphase workpiece materials and found that “size effect” influences the surface generation process in several ways. The surface roughness values for the slots micro-milled in multiphase ductile iron workpieces were larger than that for the single phase material over the examined range of cutting conditions. For single-phase materials, edge radius of the cutting tool plays an important role in the surface generation process through the minimum chip thickness. For multiphase materials, the surface roughness was Fig 2.9 a combination of three separate factors i.e. a geometric effect, a minimum chip thickness effect, and a burr formation at the grain boundaries effect. In addition, to that it was found that large tool edge radius produces rougher surfaces.

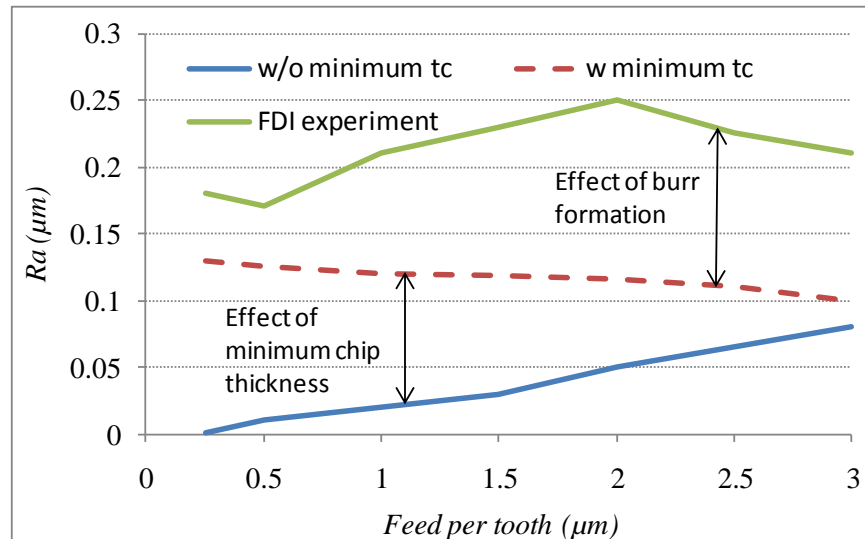


Fig. 2.9 Effects of minimum chip thickness and burr formation on multiphase surface roughness (adapted from [11])

The authors also studied the role of the phase boundaries by examining the slot floor using SEM as shown in Fig. 2.10. The surfaces in the case of single phase materials (Fig. 2.10(a, b)) were relatively smooth, with no indication of any grain size effects. However, for multiphase materials, SEM images (Fig. 2.10(c,d)) clearly signified some miniature burrs formed at distances that were comparable to the spacing between grain boundaries (white lines in the Figure 2.10(c,d)). One possible explanation for this behaviour as given was that the chip-formation process becomes interrupted as a cutting tool exits a phase at the grain boundary and subsequently a burr forms.

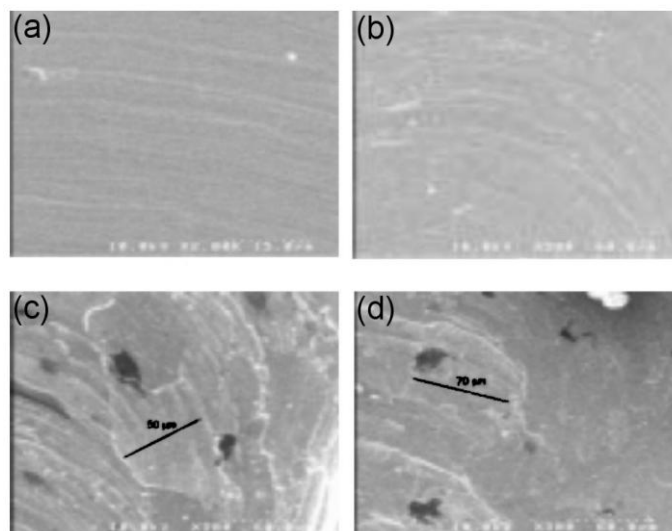


Fig. 2.10 SEM image of slot floor for (a) pearlite, (b) ferrite, (c) ferritic DI, and (d) pearlitic DI [11]

In order to test this hypothesis, chips were collected and examined using an SEM as shown in Fig. 2.11. The single phase material chips (Fig. 2.11(a, b)) appeared continuous, while the multiphase ductile iron chips (Fig. 2.11(c, d)) were highly fragmented, indicating the discontinuous/interrupted nature of the chip formation process.

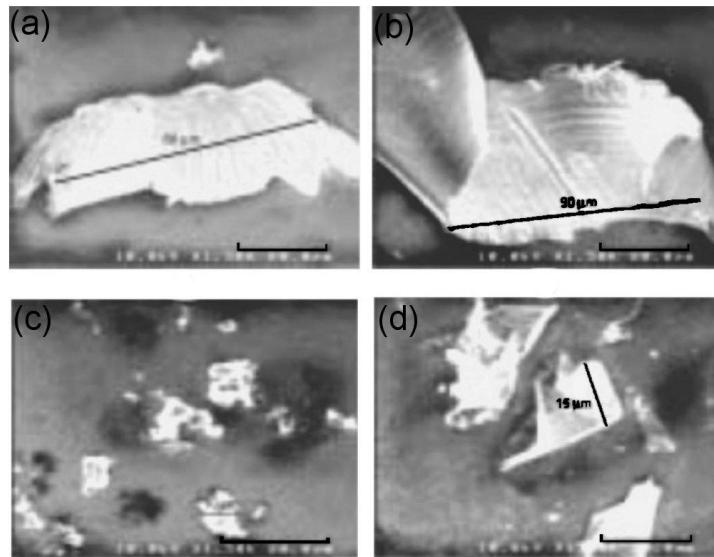


Fig. 2.11 SEM images of chips for (a) pearlite, (b) ferrite, (c) ferritic DI, and (d) pearlitic DI [11]

Weule et al [15] performed micro fly cutting/ end milling tests on different heat treated steel materials with a carbide tool. The experimental results revealed that variation in material property from one grain to another influences the resulting surface finish. Moreover, a saw tooth surface profile was detected with laser-based topography measuring device. Therefore, they stated that minimum chip thickness is probably responsible for determining achievable surface quality. They further highlighted that higher cutting velocities leads to better surface finish.

Son et al reported that the best surface finish and minimum residual stresses occurred at minimum chip thickness for aluminium, brass and copper workpiece materials and observed that this was associated with continuous chips when cutting with 1 mm width diamond square grooving tool [27].

Nakayama [78] recommended that improvements in the surface quality at this level can be achieved by usage of high precision machines and designing of more rigid setup as well as avoidance of built-up edge formation. In addition they proposed that the latter can be

avoided by (i) selecting non-adhesive materials for the tool and work material, (ii) maintaining a sharp cutting edge, (iii) machining at very high cutting speeds, (iv) using a high rake angle ($>30^\circ$) and (v) machining at cutting temperature above the re-crystallisation temperature of the work material.

The cutting mode is another important factor found to have influence the machined surface finish. Takács et al [19] and Min et al [96] in their experimental investigations established that up-milling exhibits much worse surface quality than down milling. Moreover, Schmidt and Tritschler [20] described similar findings in machining heat treated AISI H11 tool steel having different hardness values (42 and 52 HRC). They further showed that surface roughness depends on the workpiece material hardness, feedrate and measurement location within the area of machined surface.

Simoneau et al [17] considered the plastic dissipation energy in material microstructure using a heterogeneous FE cutting model. They suggested that plastic strain mismatch in multiphase microstructure AISI 1045 steel inflicts dimples on machined surface. Furthermore, in their later work, researchers suggested that reduction in the dimple size is possibly by grain refinement as well as appropriate grain orientation during machining (normal to shear plane) and more specifically by proper selection of undeformed chip thickness relative to material microstructure grain size [16].

Dornfeld et al stated that a single material may produce a ductile-like cutting mode in one grain and brittle-like cutting in another. [2]. To and co-workers reported that machining single crystal aluminium workpiece material along (100) plane yields best surface finish compared to cutting along (110) and (111) planes [97]. Zhou and Ngoi showed that for single crystal f.c.c. materials, intrinsic plastic behaviour of individual crystals had more dominant effect on surface roughness compared to crystallographic cutting direction [13].

Moriwaki et al [55] found that surface roughness is not affected by crystallographic orientation below cutting depth of 0.1 micrometers in machining of polycrystalline copper as the surface is not generated at the grain boundaries. Furthermore, decrease in surface roughness was also attributed to the formation of amorphous-like damaged layer due to burnishing effect induced by cutting edge at the $0.1\mu\text{m}$ undeformed chip thickness. It was also suggested that the effect of crystallographic orientation could be alleviated by selecting chip load ten times larger than the grain size of the material [42].

Liu et al [98] developed surface generation models to describe the sidewall and floor surface topography generated from the deterministic and stochastic components identified as influencing the machined surface roughness in micro-endmilling. These are grouped together in Fig. 2.12.

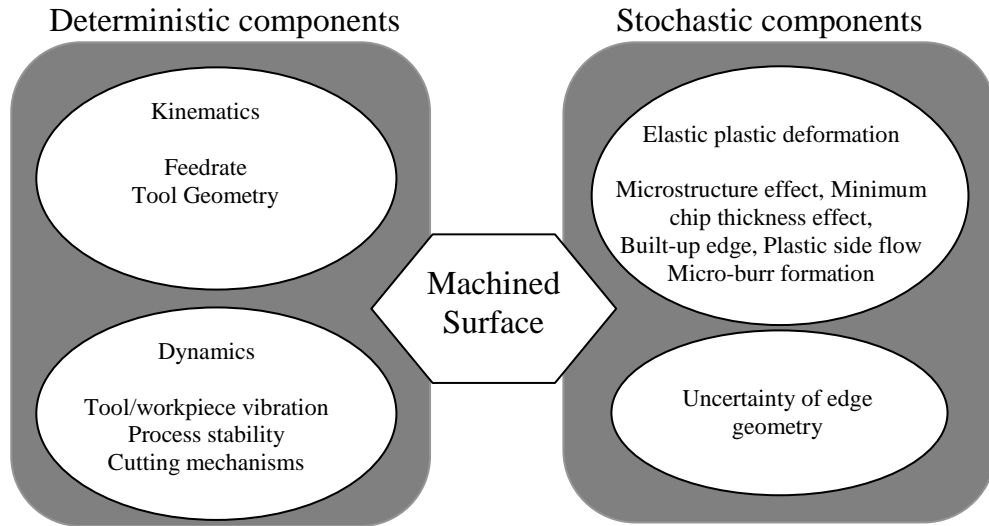


Fig. 2.12 Deterministic and stochastic components influencing machined surface

The surface-generation models for sidewall and floor surfaces consist of deterministic and stochastic elements. In the sidewall surface-generation model, the deterministic model characterises the surface topography generated from the relative motion between the major cutting edge and the workpiece material. The model incorporates the effects of process kinematics, dynamics, tool edge serration, and process faults (e.g., tool tip runout). The stochastic model predicts the increased surface roughness generated from ploughing due to the significant tool edge radius effect. In the floor surface-generation model, the deterministic model characterises the three-dimensional surface topography over the entire floor surface and considers the effects of the minimum chip thickness, the elastic recovery, and the transverse vibration. The variation of the ploughing amount across swept arc of the cutter due to the varying chip load conditions is considered in the stochastic model. These models were experimentally validated in micro milling (partial & full immersion tests) of aluminium Al 6061-T6 [99].

2.2.7 Burr formation

Burr formation and eradication is one of the biggest challenges in micro milling. Nano range surface finish is important and achievable but the challenge is how to reduce burr size. Burrs can be described as plastically deformed material beyond the edge of the workpiece. They can produce detrimental effect in handling machined micro-parts and can interfere with subsequent assembly operations.

Gillespie highlighted that suppression of burr development is most desirable in micro machining because conventional post processing could cause dimensional discrepancies and residual stresses in miniature precision parts. Moreover, edge finishing could often constitute 30 percent of the cost to produce a part [23]. Generally, there are three burr formation mechanisms namely; lateral deformation, chip bending and chip tearing. Four basic types of burrs were defined as Poisson, tear, rollover and cut-off burrs [100]. The formation of burrs progress through stages of initiation, initial development, pivoting point, and final development [101]. Lee and Dornfeld [102] categorised different burr types along the length of a slot as shown in Fig. 2.13. Lateral bulging and plastic deformation facilitates the formation of top burrs [100].

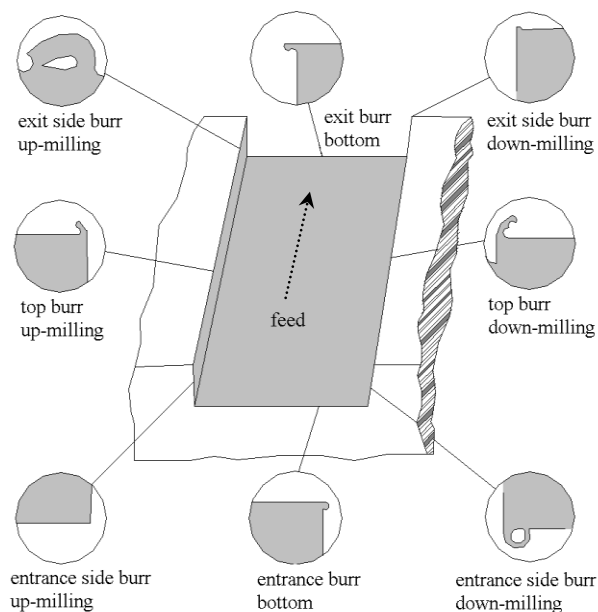


Fig. 2.13 Categorization of burr types [102]

Burr formation depends mainly on the workpiece material ductility, cutter geometry, cutting parameters (mainly chip load), tool wear and shape of workpiece [103]. In terms of burr control Nakayama and Arai [104] proposed that in macro-scale machining the size of the sideward burr could be minimised by decreasing the undeformed chip thickness and reducing shear strain of the chip. It is noted here that in micromachining, decreasing chip thickness only helps reduce burr size when machining at undeformed chip thickness greater than the tool edge radius. Otherwise ploughing effects would promote relatively larger burr size. Turning the direction of cutting force towards the workpiece and strengthening the workpiece edge was proposed to be useful in this regard [104]. Material properties also influence burr formation. In general, it was suggested that the workpiece materials with a higher ductility produce larger burr size [105].

Burr formation is driven by the size effect, with a larger tool edge radius leading to larger burrs [10, 102, 105]. The enlargement in the tool edge radius which occurs due to tool wear decreases the ratio of undeformed chip thickness to cutting edge radius; this means that effective rake angle becomes more negative. Material ahead of the tool is pushed /compressed and deformed plastically into a burr. Cutting modes in slot milling also generates different burr size. Filiz et al reported larger size of burr in down milling as compared to up milling [10]. Fang and Liu suggested that once the workpiece material and other process parameter are specified, the undeformed chip thickness will determine burr size [21].

2.2.8 Micro tool

An important factor in micro machining processes is the cutting tool. A decreasing tool diameter leads to increasing deviation in tool geometry like tool edge radius, rake angle and clearance angle from the tool design due to difficulty in controlling dimensional tolerance. The imprecise control and irregularity in micro tools manufacturing often downplay the advantages of ultra precision process control, state of the art machine tools and fine tuning of process parameters [2]. The performance of miniature end mills was reported to be greatly influenced by minor vibrations and excessive forces, which can be detrimental to the life of tools and control of component tolerances [1]. Another size effect was reported as the tool deflection [35]. It is also necessary to gain an understanding of the mechanism of wear considering the micro tool, dimensions and their consequent influence on micro machining process. Changes at the cutting edges of micro tools can create large

increase in the stress at the shaft and cause tool breakage. Moreover, increased cutting forces due to tool wear create tool deflections and geometrical inaccuracy in micro parts.

Chae et al [1] stated that very little work has been done on micro machining with carbide tools and its wear on the micro level. Despite their extensive use in ultra precision machining, diamond tools are of limited use as far as ferrous materials are concerned due to their high chemical affinity between the materials and excessive wear. Micro tools are consequently usually made of tungsten carbide. In order to improve wear resistance, very small grain size WC (<600nm) is used. For this purpose cobalt is used as a binder; lower cobalt content increases the hardness of the tool but also its brittleness.

Filiz et al [10] stated that the WC grains at the cutting edges are held by only a few facets, resulting in a weaker attachment. Therefore, at uncut chip thicknesses smaller than the WC grain size (0.4–0.7 μm) these weakly attached grains individually support the stresses due to the cutting and/or ploughing action. This causes individual grains of WC to dislodge from the softer Co binder. As a result, the dominant wear mechanism is the attrition wear in its most basic form. In addition, they encountered higher specific energy and high-negative effective rake angles during the indentation and suggested that this could be responsible for rapid wear at low undeformed chip thickness.

Aramcharoen et al recommended to use TiN, TiAlN, TiCN, CrN and CrTiAlN coated tools which assist in reducing cutting edge chipping and edge radius enlargement of ultra-fine grain carbide end mills as compared to uncoated tools [33]. Essentially coated tools have larger cutting radius when compared with the uncoated tools. However, coated tools slow down the wear rate and maintain a favourable feed to edge radius ratio compared to uncoated tools.

2.2.9 Cutting forces

It has been reported that in micromachining the use of cutting force models developed for macro scale cutting do not enable accurate predictions owing to their inability to account for the tool edge radius effects, negative rake angle ploughing and springback phenomenon [31, 58, 106]. Additionally, multiphase material microstructure effects account for 35 percent of the energy observed in the cutting force signal [107] and sub-harmonic response of the tooth passing frequency below minimum chip thickness also influences cutting forces [31]. Furukawa and Moronuki noted that the cutting forces varied as the tool passes

through microstructure grain boundaries of the workpiece material [42]. Due to these factors performance of micro milling is unstable, which in turn affects tool life and component quality.

During the transition from ploughing region to shearing region in the micro milling of brass, a key finding from the study by Kim et al was the identification of a local maximum in the radial thrust force in the vicinity of minimum chip thickness [75]. Volger et al. [69] developed a cutting force model for the micro-end milling process which catered for the minimum chip thickness concept. The model predicted that the forces were more sensitive when machining ferrite than pearlite. The increased ductility of the ferrite phase increases the ploughing forces.

2.3 Machinability of ductile materials

The term machinability is used to rate ease of machining with which a material can be cut. Common criteria for comparison include [108]:

- i. Surface finish: The surface achieved under specified conditions.
- ii. Limiting rate of removal: The maximum rate at which the material can be machined for a standard tool life.
- iii. Tool life: The amount of material removed by the tool under standardised cutting conditions, before the tool performance becomes unacceptable or the tool is worn by standard amount.
- iv. Cutting force: The force acting on the tool or power consumed.
- v. Chip shape: The chip shape as it influenced the clearance of the chips from the tool under standardised conditions.

The basic machinability of a material depends on its chemical and physical properties, grain structure and compatibility with tool material [63]. Machined materials may be grouped as

- i. Easy-machining materials (aluminium and copper alloys)
- ii. Ordinary wrought steels and cast irons
- iii. Difficult to machine materials

Fig 2.14 presents the true stress-strain characteristic of some ferrous and non ferrous alloys. It shows that heat treatment and alloy elements appreciably altered the physical properties and fracture characteristic of the materials. As far as steels are concerned, carbon content greatly affects its machinability. For high carbon steel (0.8 percent C or higher), carbides anchored in the material microstructure lead to excessive, abrasive tool wear. On the other end of the spectrum, a low carbon steel ($C < 0.3$ percent), should be machined as hard as possible to avoid excessive plastic deformation. Furthermore, steel has a relatively strong tendency to form BUE below 31 m/min cutting velocity which restricts achievable surface finish and frequently leads to tool edge chipping.

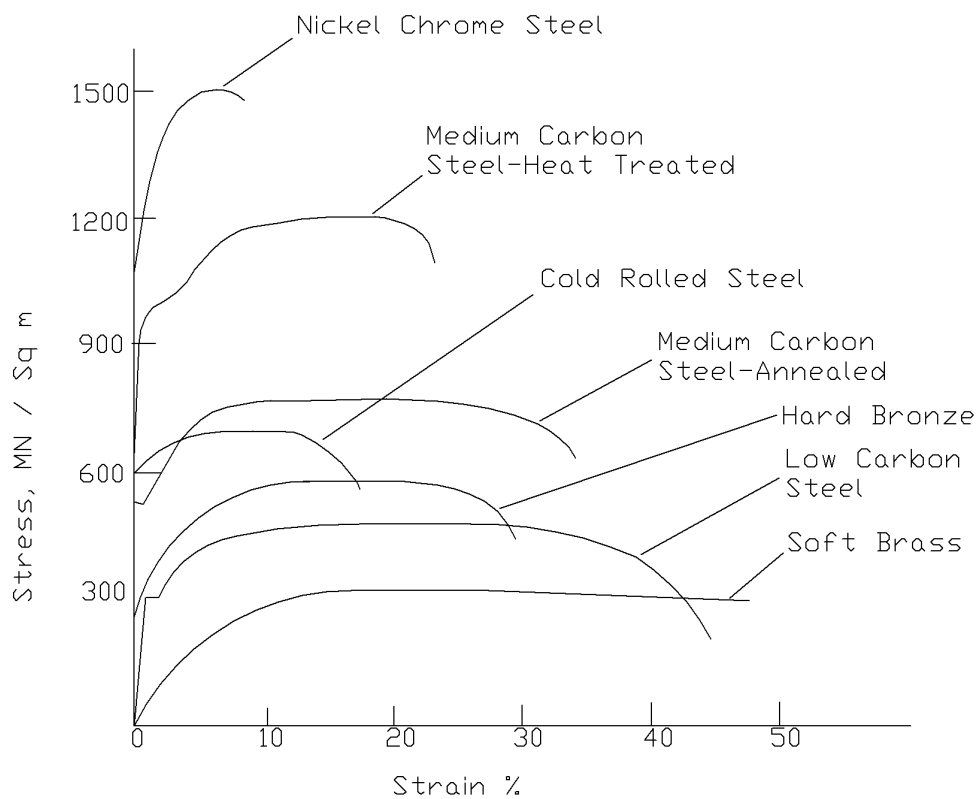


Fig. 2.14 Stress strain curves of some ferrous and non ferrous materials (adapted from [109])

Titanium and other aerospace alloys are regarded as not economical to machine at cutting speed higher than 60 m/min with carbide tools, owing to high chemical reactivity of titanium with most materials and hence rapid tool wear [94]. Besides that low thermal conductivity and low modulus of elasticity of titanium alloys are other main reasons of their poor machinability. The cutting edge abrades early due to accumulated heat near the cutting edge of the tool due to its low thermal conductivity [110]. Likewise, the low

modulus of elasticity was described as the main cause of chatter especially in finish machining, as titanium defects nearly twice compared to carbon steel. The greater springback behind the cutting edge resulted in premature flank wear, vibration and high cutting temperature. In conjunction with aforementioned properties, high strength at elevated temperatures resists plastic deformation of metal in the shear zone. Thin serrated chips create high stresses at tool edges. Moreover, its reactivity with tool materials during machining leads to adhesion and chemical reaction thus promoting tool degradation and poor surface finish.

The relationship between cutting velocity and thermal load for a given workpiece material takes the form (from Shaw [63]):

$$V_c \sim \frac{k\rho c}{u^2} \quad (2.2)$$

Where V_c is the cutting velocity, k is the thermal conductivity, ρ is the density, c is the specific heat and u is the specific energy of the workpiece material. In light of the aforementioned equation, the difference in the cutting temperatures between stainless steel and AISI 1113 steel was attributed to their specific energies. However, the still greater cutting temperatures for titanium alloys can not be explained in terms of specific energy alone. In fact the higher cutting temperatures for titanium alloys were attributed to the very low $k\rho c$ value.

Machining of nickel base alloys is also described as difficult to machine in order to meet production and quality requirements. They exhibit high temperature strength, tendency to work harden and potential reactivity with tool material. Moreover, presence of hard abrasive particles in the microstructure during machining poses serious challenges for the industry [111, 112]. The normal stresses on the cutting tool were measured to be twice as high for nickel alloy compared to machining steel at the same cutting speed. The combined effect of these factors affects the tool life and surface integrity of the machined components.

2.3.1 Overview of micro mechanical machining from a material perspective

The past decade has also witnessed a marked shift in the research quest, nonferrous materials that are more easily machined with diamond tools being replaced by those with enhanced material properties. Therefore, a lot of work was focused on the micro

machinability of comparatively hard and difficult to cut materials. These investigations suggested that micro milling offers good potential for manufacturing complex micro components [4, 15, 19, 20]. It is well known that hard, homogeneity and small grain size are the basic characteristics of workpiece materials with respect to achieve a good surface finish in micro machining. In another view, Popov et al demonstrated that mechanically modified grain structures are preferred over conventionally processed materials because of grain refinement and reduction in material structural anisotropy [113]. Beside grain refinement, mode of cutting, uncut chip thickness and minimum chip thickness effects are other critical factors influencing the capability to meet desirable surface finish and geometric shape in micromachining [10, 19, 20, 96].

The carbide tools are preferred choice to mill ferrous materials as carbide end mills provide good fracture toughness especially when ultra fine grain carbides are used for tool shanks. Most of the research in micro milling of non ferrous, ferrous and difficult to cut materials using carbide tools have been summarised in table 2.3. The tool diameters varied from 150 μm to 1000 μm . The cutting speeds used in these investigations are typically very low (<1 m/s). Moreover, the maximum undeformed chip thickness is less than 20 μm due to limited strength of micro tools.

Table 2.3 Micro milling investigation using carbide tools

<i>Researchers</i>	<i>Cutting velocity (m/min)</i>	<i>Chip load ($\mu\text{m}/\text{tooth}$)</i>	<i>Tool edge radius (μm)</i>	<i>Carbide Tool diameter (μm)</i>	<i>Workpeice material</i>	<i>Major findings</i>
<i>Rehman et al, [114]</i>	25-75	13.7	-	1000	Copper	Tool life increases with larger depth of cut.
<i>Popov et al, [113]</i>	15	7	-	150	Aluminum 5083	Metallurgical and mechanical grain structure modifications provided means for improving surface integrity and quality of the micro machined parts.
<i>Filiz et al, [10]</i>	40, 80, 120	0.75, 1.5, 3.0,6.0	~ 2	254	Copper (OFHC)	Tools were more prone to wear at low feedrates. Cutting modes in slotting generates different burr size. Down milling produced larger wavy type burrs while up milling formed smaller ragged type burrs.

(a) Non ferrous materials

<i>Researchers</i>	<i>Cutting velocity (m/min)</i>	<i>Chip load ($\mu\text{m}/\text{tooth}$)</i>	<i>Tool edge radius (μm)</i>	<i>Carbide Tool diameter (μm)</i>	<i>Workpeice material</i>	<i>Major findings</i>
<i>Weule et al, [15]</i>	5 - 420 (Fly cutting)	100	5	300	SAE 1045 (25 to 62HRC), SAE H13 (Milling only)	For stable machining, hard, homogeneous and no internal stress materials are the prerequisites. Low undeformed chip thickness produced rougher surfaces.
	15 (micro milling)	1				
<i>Takács et al, [19]</i>	30	0.1- 8	1- 2	150, 300, 400, 600	Tempered grade steel(42CrMo4), Carbon steel (Ck45)Up to 2h tempered (30,40,51,59 HRC), With out tempered(62HRC)	CK45 steel tempered at 450°C produced optimum surface quality. Higher burr formed at down milling side where as up-milling generated rougher surface.
<i>Vogler et al, [11]</i>	191.5	0.25, 0.5, 1, 2, 3	2, 5	508	Pearlite, Ferrite, Ferrite Ductile Iron, Pearlitic Ductile Iron	The effect of minimum chip thickness on machined surface roughness for micro milling is due to a combination of the cutting edge radius, workpiece microstructure/phase and feed per tooth. Miniature burrs formed along the grain boundaries of multiphase phase material contribute to rougher surface.
<i>Schmidt and Tritschler, [20]</i>	30,60, 75,90	1.5, 3, 6, 7, 10	-	100,500	AISI H11 (42, 56 HRC)	Finest and equidistantly distributed carbon steels or harder materials are preferred choice for micro machining. Strong tendency of producing large burrs in down milling was observed in the entire cutting range. Higher cutting velocity was advantageous to minimise burrs.
<i>Bissacco et al, [4]</i>	30	1, 3, 6, 15	1-4	200	Hardened steel (58 HRC)	Highly homogenous and small grain size material is preferred.
<i>Min et al, [96]</i>	20	0.25, 0.5, 1, 1.5, 2, 3	0.5- 1	254	304 stainless steel, Al 6061-T6511	Down milling showed better surface quality and dimensional accuracy than up milling. The error form size of vertical wall

						from deflecting of cutting tool increased with higher depth of cut.
<i>Aramcharoen et al, [33]</i>	47	5	2- 2.5	500	Hardened H13 tool steel (45 HRC)	TiN, TiCN, TiAlN, CrN and CrTiAlN coatings induced less edge chipping and edge radius wear as compared to uncoated ultra-fine grain carbide end mills.
<i>Aramcharoen and Mativenga [115]</i>	85	0.28- 2.8	1.4	900	Hardened H13 tool steel (45 HRC)	Burr formation appeared inevitable in micromachining. Micromilling with undefromed chip thickness equal to the edge radius gave best surface finish and reasonably low burr size.

(b) Ferrous materials

<i>Researchers</i>	<i>Cutting velocity (m/min)</i>	<i>Chip load ($\mu\text{m}/\text{tooth}$)</i>	<i>Tool edge radius (μm)</i>	<i>Carbide Tool diameter (μm)</i>	<i>Workpeice material</i>	<i>Major findings</i>
<i>Weinert and Petzoldt [22]</i>	33	12, 20	-	400	NiTi shape memory alloy	The high ductility of NiTi in combination with the strong adhesion tendency made micro material removal very difficult. Usage of minimum quantity lubricant is essential to attain acceptable micromachining results.
<i>Klocke et al, [25]</i>	50	15	-	800	Single crystal nickel based alloy Rene N5	An adequate tool life and surface quality was achieved with minimum quantity lubrication as compared to an emulsion cooling system.

(c) Difficult to cut materials

Note: “-“ means value is not reported in literature.

2.4 Machining process monitoring

Several techniques have been used for monitoring machining process to improve accuracy and productivity. These approaches depend on various signals, such as cutting force signals, vibration signals, spindle motor current signals, acoustic emission signals. Among those techniques, the uses of force sensors and accelerometers have more potential for macro scale machining processes. However, they are inadequate for monitoring micro

machining processes due to their low signal to noise ratio. The sensitivity and ratio of signal to noise of AE sensors are relatively superior when compared to the other sensing techniques. Since AE signals propagate at high frequencies, the environmental noise in the audible range can easily be eliminated. Hence, acoustic sensing techniques are particularly well suited to monitor and control micro scale machining with a high degree of confidence.

2.4.1 Acoustic emission during metal cutting

Acoustic emission (AE) is a sound and ultrasound phenomenon of low amplitude and high frequency arising from elastic wave radiations in materials undergoing deformation and fracture processes [116]. The emission spectra are load and materials depended with deforming load. The rapid release of strain energy from localised source within a material generates a spectrum over a frequency range 0 Hz to several MHz. These waves or frequencies are infrasonic, sonic and ultrasonic and transient in nature. The human ear can detect sonic frequency bandwidth (20 Hz to 20 kHz). An experienced machine tool operator can easily distinguish between a sharp, a semi-dull and a dull tool by simply listening to the sound generated during the machining process. The frequencies over 20 kHz falls in ultrasonic range which are triggered by internal rearrangement of microstructural activities [28]. This range has shorter wavelengths which in turn provide reliable and detectable information to characterise the material deformation mode. On the other end of the spectrum, the lowest frequencies are known as the infrasonic range. These frequencies normally employed to observe geological phenomena such as earthquakes.

In metal cutting, elastic and plastic deformations, internal and external friction in contact zones, chip fracture and tool wear are taking place simultaneously. Thus, when material is subjected to compression, stresses build up while material is within its elastic limit. Beyond its strength limit, the stored strain energy is released in the form of an acoustic emission event. AE signals can take two distinctive types of forms depending upon the mechanism that resulted in the elastic waves during machining process. If the signal consists of pulses that can be distinguishable in time domain, then the emission is called burst emission, which is usually associated with the chip breakage during or after formation or tool fracture. If resolution of individual pulses is not detectable, then the emission is of continuous type, which is related to plastic deformation of workpiece material in the three deformation zones [117, 118], as

- Plastic deformation of the workpiece material in the primary deformation zone,

- Plastic deformation and sliding friction in the secondary deformation zone,
- Sliding friction in the tertiary zone, and
- Collision, entanglement and breakage of chips

However, in the case of milling, periodic interruption of cutting process due to tool entrance and exit from the workpiece material acts as an additional AE source. During precision metal cutting operations at very low depth of cuts, it is well accepted that workpiece microstructure features are the main AE source [28]. Since these sources incorporate the basic mechanisms of the micro cutting process (see Fig. 2.15), AE phenomenon appears to be an ideal for process analysis and monitoring. Additionally, AE frequencies are significantly higher than those corresponding to machine tool vibration and ambient noise, which can be easily removed by using a high-pass filter.

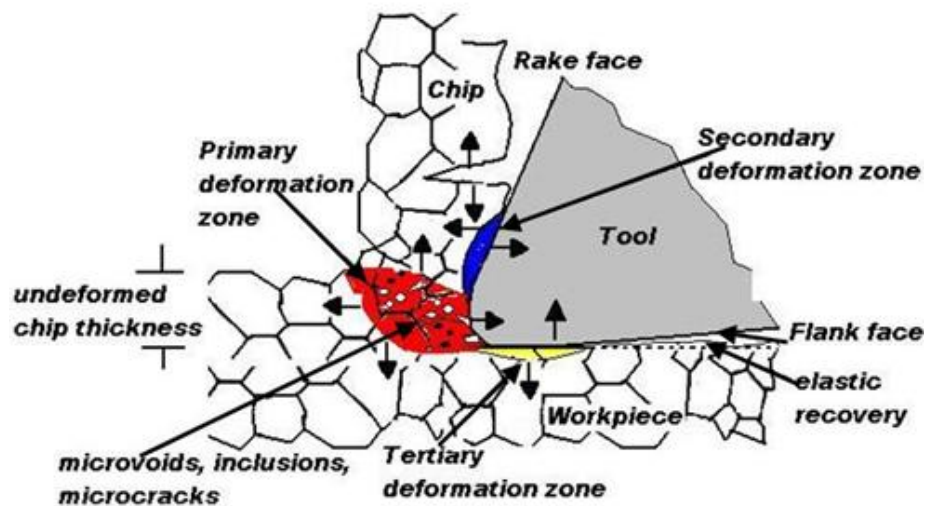


Fig. 2.15 AE generation in metal cutting

Uehara [119] reported that the amplitude of AE signals from the cutting tool is reduced during AE transfer from the tool to the workpiece possibly by damping or reflection at the primary interface. As a result, by monitoring the AE signal from workpiece side, the primary and tertiary deformation zones can be regarded as most accessible sources of AE generation in micro milling. In ultra precision cutting, Carpenter et al [120] suggested that the tertiary deformation zone becomes more significant source of AE due to the increased energy spent on sliding friction between the tool flank face and newly machined surface.

In literature it is suggested that, dynamic AE signal collected at the sensor contains many frequencies due to the several AE producing sources being active at the cutting zones [28]. Thus, the intensity of these different frequency bands can be used for inferring the

dominant sources of AE in the micro machining process. Fig. 2.16 shows dominant frequency range according to the material removal length scale and signal source mechanisms. It is clear from Fig. 2.16 that AE signals are better suited to characterising machining at very low length scales typically in the nm range as encountered in micro/nano scale machining. Again one could postulate from the graph that decomposing the AE signal into the frequency domain will enable identification of dislocation mechanics, inter-granular micro fracture, cleavage and shearing material machining modes.

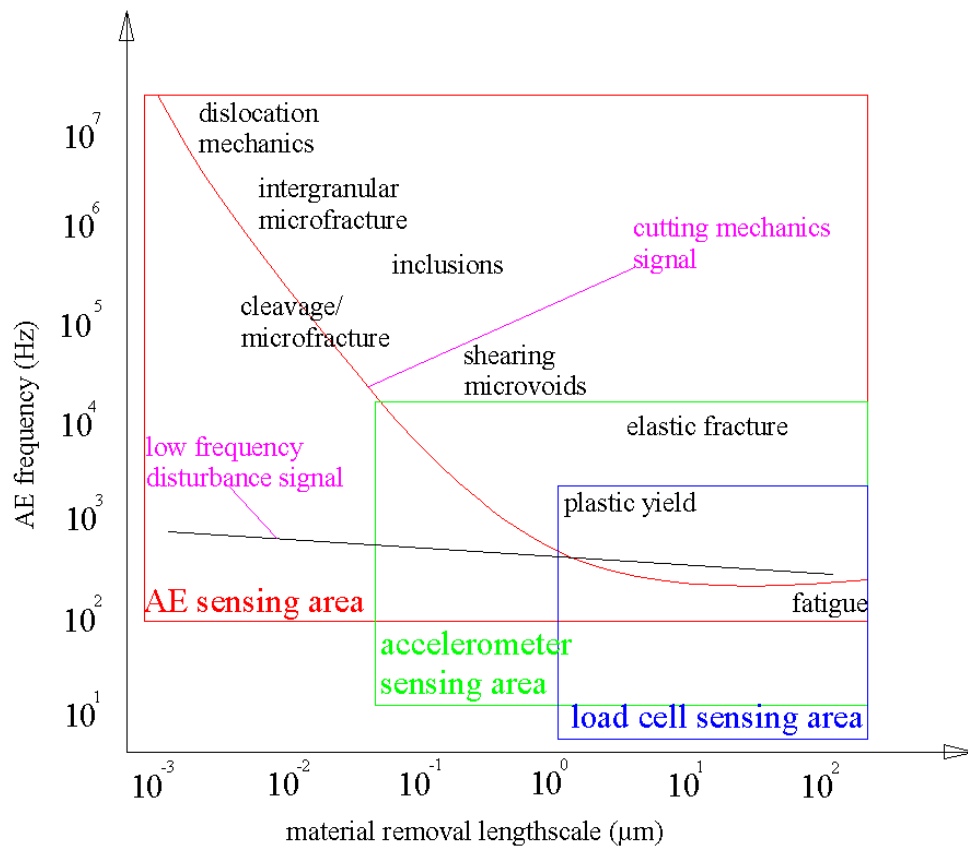


Fig. 2.16 AE source mechanisms (adapted from [28])

In relation to the cutting zones, the primary deformation zone is the largest AE source and generates in excess of 75 percent of the total AE signal [121]. Brittle and ductile fracture (as shown in Fig. 2.16) may occur in the deformation of ductile materials that can emit AE from the primary shear zone depending on the type of material to be machined and operating conditions. In metal cutting, Shaw proposed that ductile materials deformed as a result of nucleation, growth and coalescence of microscopic voids (micro crack initiation) that originated at inclusions and second phase particles separation [122]. However, due to

compressive plastic deformation, the micro cracks experience closure effectively postponing crack propagation until conditions are reached where plastic deformation does not occur. The cleavage (transgranular) often called brittle fracture, may occur in deformation of ductile materials such as mild steel [62]. The propagating crack in the carbide phase can initiate cleavage fracture in the adjacent ferrite phase subjected to high intensity of local stress and insufficient time available for stress relaxation. The ductile fracture can take place in intergranular manner, where the grain boundaries are the fracture path within the material. Most of the metals undergo the transition from transgranular fracture to intergranular fracture at temperatures greater than 0.5 to 0.7 times of the melting temperature. The application of AE signal can be useful to establish quantitative relationship between spectra of AE signal and the physical processes which cause emissions to occur, such as plastic deformation, void generation and collapse, crushing of inclusions, crack propagation and fracture.

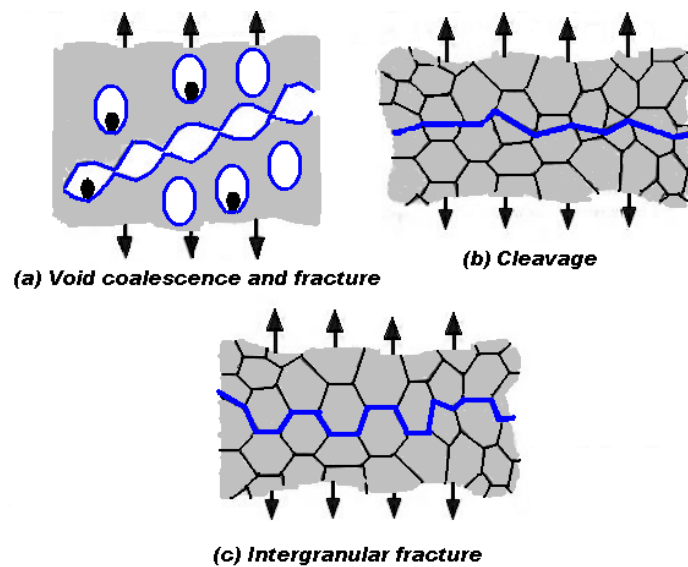


Fig. 2.17 Micro-mechanisms of fracture in metals ([123])

2.4.1.1 AE sensitivity to machining parameters

Previous work established the relationship between the primary machining parameters and the level of acoustic emission emitted. The power of the AE signal was reported to be proportional to the cutting power [116, 121, 124]. Some studies suggested that AE signal should increase with material shear strength, cutting velocity, feedrate, width of cut and rake angle [121, 124]. Lan and Dornfeld showed that $AE_{r.m.s}$ is less sensitive to the width of

cut [125]. Regarding dependence of AE signal on feedrate, some experimental results showed that AE signal decreases with increase in feedrate [118], whereas, other investigators have observed that it remains more or less unaffected by variation in the feedrate [118, 125]. All published experimental results led to the conclusion that AE signal is strongly dependent on the strain rate [116, 118], and since strain rate is directly dependent on cutting velocity, a strong relationship was observed between AE signal and cutting velocity [118, 121, 124]. However, in micro-domain cutting the issues related to size effect limit the direct application of these investigations (the effect of tertiary deformation zone was not considered).

The sliding friction between tool flank face and machined surface is a significant aspect to consider especially in precision machining. This effect on AE generation has been incorporated in the models developed for diamond turning [126] and peripheral milling [127] operations. The predicted $AE_{r.m.s}$ level from the diamond turning model matched reasonably with experimental data except below $3\mu\text{m}$ depths of cut [126]. The experimental results of peripheral milling on Al 7075 showed linear positive sensitivity to spindle speed, feedrate, axial depth of cut and radial depth of cut, however, the dominant effect on AE signal of the considered process parameters were masked due to interrelated effects on the effective shear angle and mean frictional angle [127].

2.4.1.2 AE signal processing

Acoustic emissions occur over a wide frequency range but typically from 100 kHz to 1 MHz [128]. However, due to complex and multiple originating AE sources in cutting process, signals experience changes through multiple reflections at interfaces and scattering by micro-structural defects and refraction when there is a medium change along the travel path from the source to the sensor. Moreover, contribution of the sensor sensitivity (AE activity whose frequency content is closer to the resonance of the sensor will have increased amplification) and measuring system (waves whose frequency is outside of the range of a band-pass filter will not be detected) may also be taken into account. All these factors significantly alter the waveform by phase change, amplitude attenuation and wave repetitions [129]. Thus, AE signals are intricate and random in their final waveform and using them to characterise a source could be difficult. Despite these difficulties, acoustic signals carry insight of the source event. Teti et al [130] provided an up-to-date comprehensive survey of sensor technologies, signal processing, and decision

making strategies for process monitoring. They reported that AE signal analysed in frequency and time domain was successfully employed to monitor tool wear, chip form, process state, surface integrity and white layer formation as well as smearing and plucking. Some of the important AE parameters are listed in table 2.4 which are used in data processing for extracting features.

Table 2.4 Acoustic emission parameters and information about the source event

<i>Feature extraction</i>	<i>Parameter</i>	<i>Interpretation</i>
Time domain	average value, amplitude, effective value (RMS)	Intensity of source event
	ring down count or pulse rate	number of times AE_{raw} signal crosses the threshold level
	pulse width	percentage of times AE_{raw} signal remains above the threshold level
	burst rate	number of times AE_{rms} signal exceeds preset thresholds per second
	burst width	percentage of time AE_{rms} signal remains above each threshold
Frequency domain	Frequency spectrum	Nature of source event
Time-frequency domain	Spectrogram	Energy distribution of source event as function of time
	wavelet spectrum	The intensities of source frequency bands

The most useful information about the process was extracted by analysing power spectral density in conventional machining process [131, 132]. The frequency spectrum shows the dominance and contribution of each frequency to the total power. In these investigations, the power spectral density of AE signals was computed using Fourier transform-based methods. However, the Fourier transform-based methods are good for analysing long periodic signals but not for AE signals which have both continuous and transient components [133]. Moreover, it fails to retain the information related to their occurrence in time. Chen et al [134] demonstrated a wavelet transformation technique, a more sophisticated approach to monitoring ultra-precision machining process by analysing the time-frequency spectrum of the AE signal for patterns corresponding to the process characteristics of interest. The distribution of frequencies in the time-frequency domain provides valuable insight of the process.

2.5 Summary

It is suggested from the literature survey that:

- For multi-phase material, it was suggested that plastic strain mismatch and higher absorption of energy at harder phase influences surface dimple formation. Solutions proposed were (i) grain refinement (ii) appropriate grain orientation (iii) selection of undeformed chip thickness relative to material grain structure. Other than few works in the reviewed literature, there is a lack of systematic approach to select undeformed chip thickness in view of the established importance of material grain size and microstructure phases in micro cutting process. Additional scientific examinations are needed in this regard to ascertain and embrace the material related size effects on surface generation process especially for multiphase and large grained microstructures.
- There is a suggestion in literature that when multi-phase materials are micro machined, “burrs” are formed at the grain boundaries. Consequently discontinuous chips are formed. These features (burrs) compromise surface roughness. Hence a new concept for burr is introduced.
- It is proposed that for single crystal materials machining along some crystallographic orientation direction yield better surface finish. The issue to be identified here is whether these crystals are not disturbed by previous cutting passes. If not, how to identify them accurately in industrial machining of multiphase materials. Other authors reported no influence of crystallographic direction below certain depths of cut.
- There is need to expand the knowledge of minimum chip thickness of the materials used in manufacturing of micro components as it determines the achievable surface finish. Moreover, subsurface damage is also a vital research issue due to increased ploughing in micro domain cutting.
- The minimum chip thickness is encountered in micro milling operations owing to the variation in chip load as predicted by the chip density function. The strong dependency of the minimum chip thickness on the workpiece material and tool geometry complicates this evaluation. Simple edge radius measurement for a tool would not be sufficient to determine the minimum chip thickness. Molecular dynamics simulation is more appropriate to nano-scale cutting as it gives only a

local representation of the material characteristics. The microstructure-level finite element simulation needs an experimentally characterised constitutive model of the material. Therefore, it is not suitable to be applied for a wide range of material. Moreover, accurate measurement of sudden change in thrust force is by itself a challenge due to bandwidth limitation of force sensors. Thus, it would be interesting to exploit relatively superior in process acoustic emission signal, to evaluate the minimum chip thickness phenomenon.

- During the course of survey, surprisingly almost negligible work has been found with regards to the micromachining of titanium and nickel based materials despite the fact that these materials are widely used in bio-medical and aerospace applications. New studies dealing with such materials would widen the scope of micro mechanical cutting applications and further enhance understanding and ability to tackle the complicated governing cutting mechanism present at the micro-scale.

Chapter 3

EXPERIMENTAL PROCEDURE

3.1 State of the Art Equipment

In the field of micro machining, portable micro-factories are considered superior when compared to high speed machining centres due to their better performance benefits like positional accuracy and resolution. Some researchers cautioned that micro-factories may not be able to produce micro-features on conventional workpieces.

3.1.1 Machine tool

The cutting tests for this study were performed on the Agie Charmilles MIKRON HSM 400 high speed milling centre. This is a Heidenhain iTNC 530 numerically controlled machine and operates in the range of 60-42000 rpm. A photograph of the machine is shown in the figure 3.1. The static radial runout of spindle-collet-tool system was measured in the clamped state before each cutting trial. The radial runout was estimated from the runout gauge measurements to be 1.6 μm in average, with a standard deviation of 0.76 μm . Considering the focus and usage of Mikron HSM 400 in the presented work, feed is a relatively positional attribute and less systematic errors in the machine will propagate through and hence unlikely affect relative tool pass comparison.



Fig. 3.1 MIKRON HSM 400 high speed milling machine

3.1.2 Hitachi scanning electron microscope (SEM)

The measurement uncertainty normally relates to the instrument used to quantify the output. In this study the measurements are made on nano scale resolution instruments to a well established repeatable output. The Hitachi S-3400N SEM, shown in Fig. 3.2, has a resolution of 4 nm and 3 nm at low voltage and high voltage respectively. An accelerating voltage can be set up to 30 kV. The electron source is tungsten filament cathode. The SEM is capable of functioning with secondary electron (SE) detector as well as back scatter electron (BSE) detector. This SEM was used to capture images of cutting tools, machined surfaces, and chip morphologies in addition to the estimation of tool edge radius, sub surface deformation and deformed chip thickness.

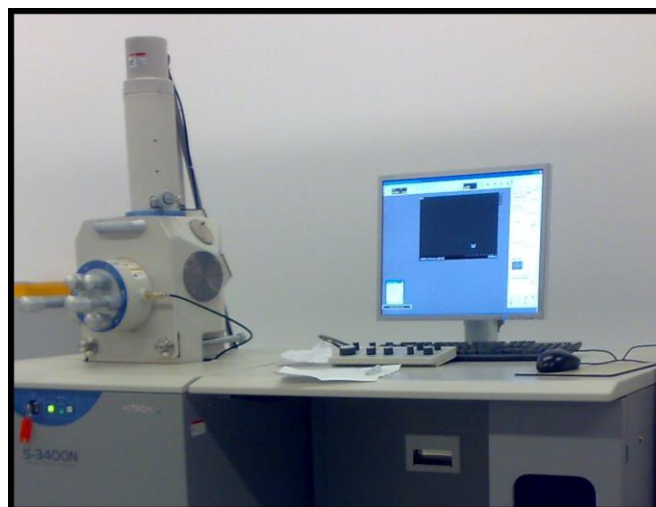


Fig. 3.2 Hitachi S-3400N SEM at the University of Manchester

3.1.3 WYKO[®] NT-1100 white light interferometer

The Wyko NT1100, shown in Fig 3.3, is a white light vertical scanning interferometer used for characterisation of surface texture. It is a three dimensional, non contact, surface profile measurement device. The Wyko's magnification capability ranges from 2.5 to 100 times, with a combination of objective (5.0X, 50X) and field-of-view (0.5X, 1.0X, 2.0X) lenses. The vertical resolution is 1 nm. The three dimensional surface image is attained through the fringes produced by the optical path difference between the reference and reflected beam. The Veeco Vision32[®] software was used to measure the surface roughness and burr width of the machined slots.



Fig. 3.3 Wyko NT1100 at Laser Processing Research Centre (LPRC)

3.1.4 MTS Nano Indenter[®] XP

An MTS Nano Indenter[®] XP as shown in Fig. 3.4 provides an opportunity to record the indenter penetration depth under the applied force throughout the testing cycle, therefore, capable of measuring both the plastic and elastic deformation of the material under test. Displacement resolution is less than 0.02 nm and load resolution is 50 nN (5.1 mg). Berkovich diamond pyramid (tetrahedral) type indenter was used. Maximum indentation depth and positioning accuracy are 2.5 μm and 1.5 μm , respectively. In this technique, indentation is performed for a chosen depth and then removed, the data measured in unloading was used to determine nano hardness, elastic modulus, elastic recovery and sub surface microstructure modification. In particular the location of

indentation point was viewed in a microscope to ensure that the distance from the sample edge as well as spacing between each indent should be about 2.5 times the indenter size to avoid the influence of the deformation.



Fig. 3.4. Nano-indenter XP at the University of Manchester Material Science Centre

3.1.5 Acoustic emission sensing system

A Kistler 5125B121 Piezotron[®] acoustic emission (AE) sensor was used to measure the acoustic signals in this study. The captured signals passed through a Kistler 5125B AE-Piezotron[®] coupler and then recorded to a Nicolet technologies Sigma 30 digital memory oscilloscope. The images of the acoustic emission sensing system are shown in Fig. 3.5.

The AE sensor with built in impedance converter provides a low-impedance voltage signal at the output and allows for measuring acoustic signals over a broad frequency range (100-900 kHz). Being small in size it can be easily mounted with M6 bolt near the source of emission and captures the signal optimally. The AE sensor protected hose is connected directly to the leak-tight terminal in the AE-Piezotron[®] coupler. The coupler processes the high frequency output signals. Gain, filters and integration time constant of the built in RMS converter are designed as plug in modules, which permits, in situ, the best possible adaptation to the particular monitoring function concerned. The gain can be set with a jumper either to 1x (20dB) or 10x (40dB). The high pass and low pass filters cut off frequency are freely selectable between 10 kHz to 1 MHz. The integration time constant of the RMS converter can be selected from 0.12, 1.2 and 12 ms.

Nicolet technologies Sigma 30 is a 4 channel, 200 ksample/sec memory per channel, 5 MHz bandwidth and 12 bit digital memory oscilloscope. It offers signal acquisition, analysis capabilities and connectivity in one portable 10.4 inch touch screen windows 2000 based workstation.



Fig. 3.5 Acoustic emission sensing system

3.2 Measurement methods

The methodologies used to measure cutting edge radius, surface roughness, burr size, and tool wear are discussed below. Moreover, strategy used to evaluate sub surface microstructure modification as well as chip form is also presented.

3.2.1 Tool edge radius measurement

The mechanical micro domain cutting trials were performed with carbide tools. Commercially available tools from Fraisa[®] Ltd and Dixi Polytool[®] Ltd were used. Some of the tools geometries used in these investigations are shown in Fig. 3.6.

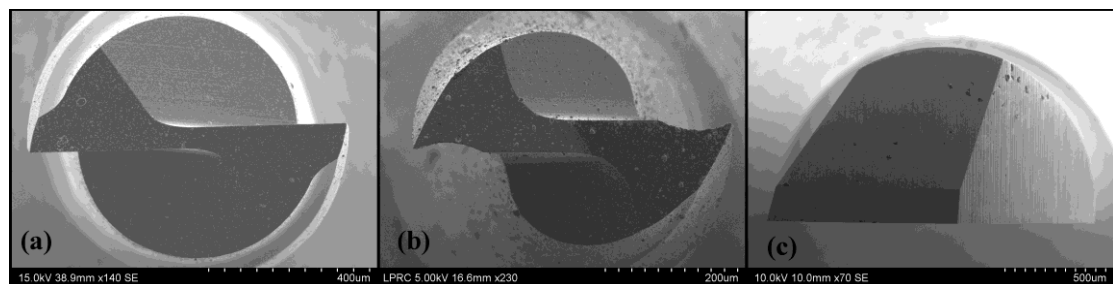


Fig. 3.6 Tool bottom views

(a) Fraisa (800 μm) (b) Dixi (500 μm) (c) Dixi (2mm) in diameters

The tool sharpness influences the material removal mechanisms. As highlighted in literature review, when a tool with a small edge radius is chosen in conjunction with large undeformed chip thickness that would effectively eliminate the edge roundness

effects until tool wear increases and the cutting edge radius of the tool is of the same order of the magnitude as the undeformed chip thickness. The values of tool edge radius employed in this research for new tools ranged from 0.5 μm to 2 μm . The measurement of the tool edge radius was performed by placing best fitted circle to the tool edge radius (intersection of the tool rake face and flank face). An example of the SEM image of tool bottom view which was used to estimate the tool edge radius is shown in Fig 3.7.

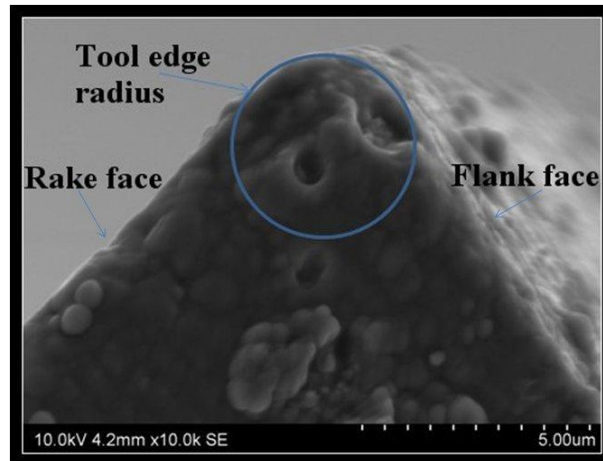


Fig. 3.7 Measurement of tool edge radius

3.2.2 Surface roughness measurement

The surface roughness of the micro milled slots was measured with a Wyko NT11000 optical profiler (white light interferometer). Each slot was sampled at the beginning, middle and end of the slot in the feed direction. Fig 3.8 shows the typical Wyko scan of a portion of the slot. The data obtained from these images was used to calculate average surface roughness (R_a) and then plotted.

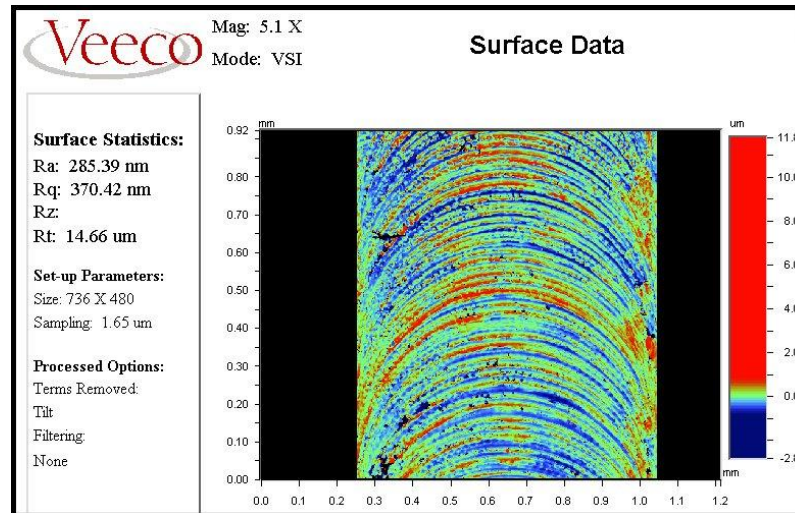


Fig. 3.8 Surface roughness measurement

3.2.3 Burr size measurement

Top burr width in both up and down milling was measured from Wyko scans. The examples of the images used to measure the top burrs width for the two kind of steel are shown in Fig 3.9. When slot milling was used, one side of the slot experienced up-milling and the other side experienced down-milling. It can be seen from the figure that near the edges of the slot (blue profile) there are dull black uneven protrusions. These protrusions are burrs produced during the micro-milling process. The other dull black marks away from the edge of the profile are machining marks (therefore they can be neglected).

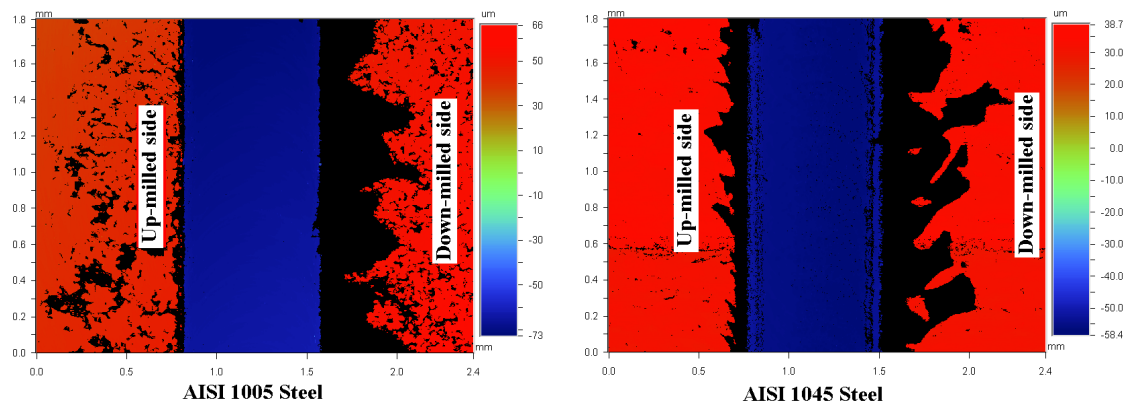


Fig. 3.9 Wyko scans to estimate burr width of ferrous workpieces

Burr root thickness was evaluated from cross sectional images of the slot using back scatter electron (BSE) microscopy. An example of down milled side of a nickel based alloy slot is shown in Fig 3.10.

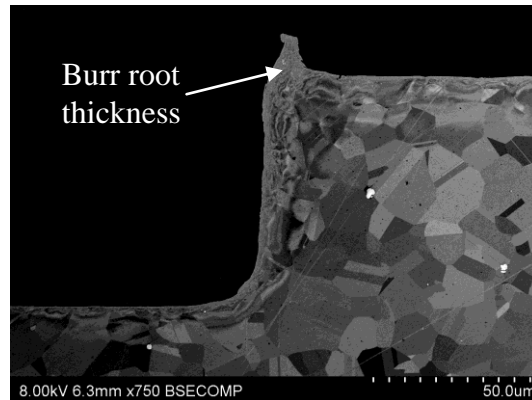


Fig. 3.10 Down milled side burr root thickness measurement

3.2.4 Tool wear measurement

The inspection of micro tool was carried out on an SEM to determine maximum flank wear. Tool wear progression on the flank face was compared and measured from magnified images taken near to the cutting edge of coated and uncoated tools before and after machining. Typical micrographs with such a flank wear on the used tools are shown for bottom cross-sectional images (Fig. 3.11). As wear progresses coatings were abraded from the flank face and tungsten carbide substrate was exposed, depending upon the cutting conditions employed. Additionally, a wear land is also visible on uncoated tool used.

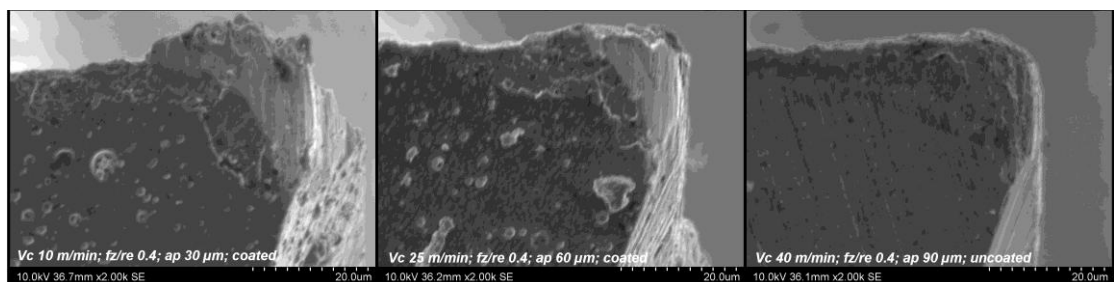


Fig. 3.11 Micrographs showing maximum flank wear

3.2.5 Subsurface microstructure measurement

For subsurface microstructure examination, the micro slots were sectioned and embedded in conductive hot mounted phenolic resin. Considering the very small subsurface deformed zone, all samples were carefully ground and polished on Presi Mechatec 334 with an individual load of 20 N and 10 N, respectively. Final polishing was carried out on a suede cloth with colloidal silica suspension to obtain high quality surface which is prerequisite for back scatter electron microscopy (BSE). All subsurface microstructure assessment was carried out on a Hitachi 3400 scanning electron microscope. BSE images were taken at 10 kV accelerating voltage and 5mm working depth.

In order to evaluate mechanical properties of machined subsurface zone, array of nano-indentation was performed at 0.5 μm indentation depth. An example of nano-indentation marks on down milled side of the investigated ferrous materials is shown in BSE image (Fig 3.12). The depth below the wall surface for the initial point of indentation was specified by positioning the indenter approximately 10 μm away the wall surface to avoid effects of mould material in the measured data. The deformed layer was characterised nano hardness values towards the machined surface.

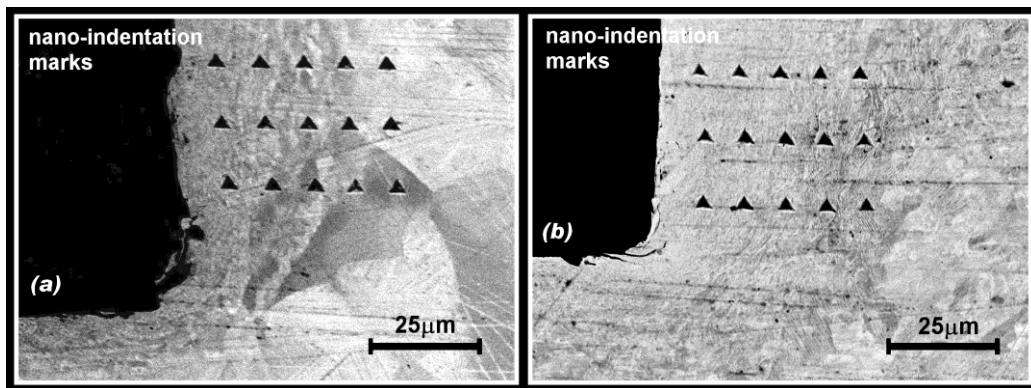


Fig. 3.12 Slot down-milled side (a) AISI 1005 (b) AISI 1045

3.2.6 Micro chips characterisation

Chip form classification based on workpiece materials and process parameters is another area where fundamental information on the dominant cutting mechanism can be obtained. Therefore, micro chips produced were collected and imaged in an optical as

well as scanning electron microscope at each undeformed chip thickness during orthogonal milling experiments. In the case of higher chip load, the chips formed from the shearing of the workpiece are much larger in size, easier to handle and exhibit more strength than the chip produced at the undeformed chip thickness below tool edge radius. The chips collected within lower range were powdery in nature and breaks easily upon contact.

The chips were clamped in clamp mounting with its side profile under observing with magnified lens. Due to fragility of the chip, it was impossible to ensure the orthogonality of the side of the chip. However, necessary care was taken to ensure that the error can be minimised. Then, MetPrep[®] hot and cold mounting materials were used to prepare chip samples moulds. The samples were ground and polished on Presi[®] Mechatec 334 polishing machine. Grinding was carried out with grit sizes of 600 and 1200 for a very short period considering the fragility of the chips. Polishing was done with 9, 6 and 1 μm finishing slurry. Array of nano-indentations were carried out in the area of interest to evaluate the extent of plastic deformation.

3.3 Experimental setup

The cutting tests were conducted in dry conditions on Mikron 400. Fig. 3.13 depicts experimental setups used to perform test on ferrous and Inconel 718 workpieces. Detail description of the setup can be found in the relevant sections of the chapters. In both setups, tools were clamped with constant overhang in order to eliminate potential source of error caused by the deflection and vibrations during the cutting experiments.

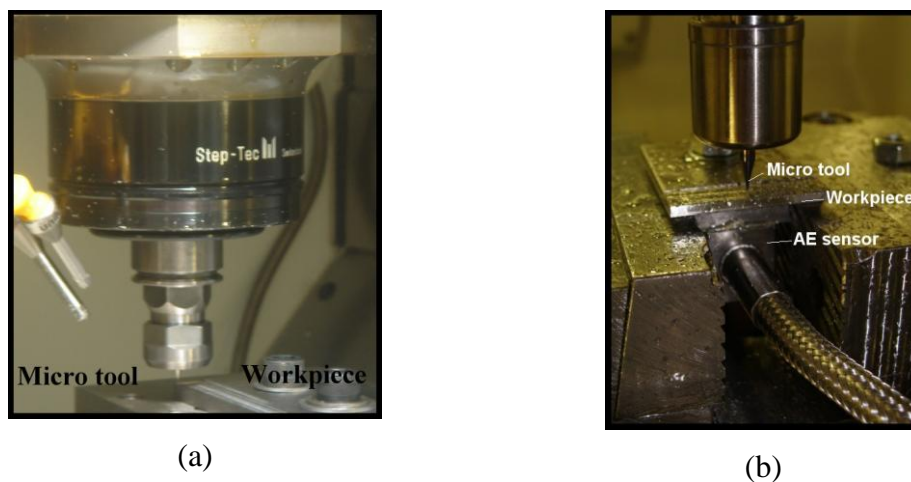


Fig.3.13 Experimental setup for (a) Ferrous workpieces (b) Inconel 718

3.4 Experimental procedure

A standard work procedure was followed as mentioned below to obtain consistent results throughout the experimental work.

- In order to obtain unified results, the workpiece material used came from the same stock. Before experiments, a clean up cut was performed on each workpiece using a fresh tool to minimise subsurface damage and remove residuals of previous operations. Since the machined surfaces would have to be examined under the scanning electron microscope, the maximum dimension of each specimen was limited to 25 mm.
- Prior to each cutting test cutting tools were observed and imaged on the SEM. All tools taken from the single batch and for nearly similar edge radius for each experimental plan in order to reduce variability in the process. The tool was then mounted and brought into contact with the workpiece to define the datum position and then moved to a start position 1mm away from the datum.
- The undeformed chip thickness were spanning across the tool edge radius as well as the workpiece material average grain size of a smaller phase type. Tool diameter was larger than the grain size and radius of cutting edge is smaller than it. This approach was adopted to create micro slots on selected workpiece materials to embrace factors influencing the so called term “size effect”.
- The experimental conditions derived from respective experimental design such as cutting speed, feed and depth of cut were set on the MIKRON 400 HSM.
- Machining centre was run idly for 25 to 30 minutes, while micro-tool was hold in high speed spindle to compensate for thermal elongation of the tool.
- Before commencement of slotting, in order to ensure an axial depth of cut was set accurately, the tool was positioned 15 μm above the probed height of the workpiece. A short pass was taken with the tool while monitoring the AE sensor for signs of contact between the tool and workpiece. Moreover, tool marks were also visualised on the workpiece. This process was repeated, each time incrementally stepping the tool down 5 μm . Once contact height had been established. The surface datum point was recorded and used as a reference

height for depth of cut (a_p) during tests with that particular tool. The process was repeated again after a tool change.

- The AE data acquisition system was turned ON, acoustic emission filtered (AE_{raw}) and root mean square ($AE_{r.m.s}$) signals were captured at regular intervals after full engagement of the tool, for each experimental condition.
- The tool was removed at specific periods of the cutting trial and then cleaned using an ultrasonic cleaner with cleaning solvent before flank face and cutting edge radius were observed and imaged under the SEM. The tool was then mounted back on the machine to continue the machining for the next interval, according to the experimental plan.
- The micro chips produced were also collected and imaged using optical and scanning electron microscopes. The machined surface generated was subsequently characterised with a white light interferometer (Wyko) as well as imaged with the SEM.
- Micro slotting tests were repeated twice, wherever deemed necessary a third test was undertaken so that repeatability of results could be confirmed.

3.5 Acoustic emission signal processing

The AE filtered signal and $AE_{r.m.s}$ were processed using Matlab[®] software to study variations with the changes in process parameters, namely workpiece material, undeformed chip thickness and cutting speed.

A sample of MatLab[®] commands used for analysis of the AE signals is given in Appendix A. Moreover, a brief description of the discrete wavelet transformation is also documented in Appendix B.

Chapter 4

A COMPARATIVE STUDY OF MATERIAL PHASE EFFECTS ON MICRO- MACHINABILITY OF MULTIPHASE MATERIALS

Abstract

In the mechanical micro machining of multiphase materials, the cutting process is undertaken at a length scale where material heterogeneity has to be considered. This has led to increasing interest in optimising the process parameters for micro machining of such materials. In this study the micro-machinability of two steels, a predominantly ferrite material (AISI 1005) and a near balanced ferrite/pearlite microstructure (AISI 1045) was studied. Workpiece sample deformation properties were characterised by nano-indentation testing. Additionally, metallographic grain size evaluation was undertaken for the workpiece microstructures. Surface roughness, workpiece microstructure and burr size for micro machined parts as well as tool wear were examined over a range of feedrates. The results suggest that for micro machined parts, differential elastic recovery between phases leads to higher surface roughness when the surface quality of micro machined multiphase phase material is compared to that of single phase material. On the other hand, for single phase predominantly ferritic materials, reducing burr size and tool wear are major challenges. Thus, the chapter elucidates on material property effects on surface and workpiece edge quality during micro-milling.

Keywords: Micro-milling; Microstructure effect; Size effect

4.1 Introduction

4.1.1 Micro machining

Micro-mechanical machining offers great potential for manufacturing complex micro components [1, 2, 4, 15, 20]. The technology can be described as the process of removing material from a workpiece in the form of chips typically in the micron or sub-micron length scale. For some coarse grained material, this chip formation can take place at a length scale smaller or comparable to the individual grains of a material microstructure [32]. Hence, polycrystalline material must be treated as discrete and heterogeneous at this level [65]. Taking into account the challenges met in micro machining, ultra fine grain, hard and high homogeneous workpiece materials are considered ideal for manufacturing micro components [4, 14, 15]. Simoneau et al suggested that the cutting domain could be moved between macro-, meso- and micro-scale by altering grain sizes of the workpiece material [12]. Thus, it becomes desirable to develop a deeper understanding of the fundamental mechanisms associated with the material microstructure behaviour under different cutting conditions.

The presented work is a continuation of a previous work regarding multiphase material microstructure effect in micro milling [68]. The already published paper focussed on the micro milling of one coarse grained workpiece material AISI 1045 steel. This new paper extends the research work and reports on the micro machinability of single compared to multiphase ferrous workpiece materials. The presented results elucidates on the interaction between cutting parameters and workpiece material properties as driven by microstructure phases.

4.1.2 Material microstructure effect on surface generation in micro machining

The ratio of surface area to volume increases as devices and their features are miniaturized. For this reason, more attention should be given to surface generation and phenomena that affect the surface character. At micro-scale it was reported that the tool-workpiece material interaction strongly influences the machined surface topography [9]. This was evident from Weule et al who reported that variation in material property from one grain to the next influenced the resulting surface finish [15]. This surface roughness varies between the grains of material and is influenced by the tool edge radius, microstructure phases, minimum chip thickness effects [11], crystallographic

orientation [13], material elastic recovery and phase dependent elastic-plastic anisotropy [14]. Furthermore, for single crystal f.c.c. materials, intrinsic plastic behaviour of individual crystals was reported to have more dominant effect on surface roughness compared to with crystallographic cutting direction [13]. Plastic strain mismatch, grain orientation relative to cutting edge and large energy absorption in harder phases cause surface defects on the multiphase microstructure of AISI 1045 steel [16, 17].

Son et al reported the best surface finish occurred at the minimum chip thickness for aluminium, brass and copper workpiece materials and observed that this was associated with the formation of continuous chips [27]. The dominant influence of chip thickness on surface roughness in micromachining was reported in literature [11, 15, 135]. It was suggested the effect of crystallographic orientation on surface roughness could be alleviated by selecting chip load ten times larger than the grain size of the specific material [42]. Moreover, improvement in the surface integrity and quality of micro machined parts can also be achieved through metallurgical and mechanical grain structure modifications [113]. However, this is not always desirable since modifying a material's microstructure changes its properties and can affect functional performance. This case is more critical if micro features are on a large component.

4.1.3 Burrs in micromachining

Burr formation is a critical factor in micromachining since it affects the capability to meet desirable tolerance and geometry definition [15, 19, 20]. Gillespie highlighted that minimization of burr size is most desirable as conventional de-burring process could cause dimensional imperfections and residual stresses in miniature precision parts. Moreover, post-processing for burr removal could often constitute 30% of the cost to produce a part [23]. There are three generally accepted burr formation mechanisms namely; lateral deformation, chip bending and chip tearing. Four basic types of burrs were defined as Poisson, tear, rollover and cut-off burrs [100]. The formation of burrs progress through stages of initiation, initial development, pivoting point, and final development [101].

In terms of burr control Nakayama and Arai [104] proposed that in macro-scale machining the size of the sideward burr could be minimised by decreasing the undeformed chip thickness and reducing shear strain of the chip. It is noted here that in

micromachining, decreasing chip thickness only helps reduce burr size when machining at undeformed chip thickness greater than the tool edge radius. Otherwise ploughing effects would promote relatively larger burr size. Turning the direction of cutting force towards the workpiece and strengthening the workpiece edge was proposed to be useful in this regard [104]. Material properties also influence burr formation. In general, it was suggested that the workpiece materials with a higher ductility produce larger burr size [105].

Burr formation is driven by the size effect, with a larger tool edge radius leading to larger burrs [10, 102, 105]. Cutting modes in slot milling also generates different burr size. Filiz et al reported larger size of burr in down milling as compared to up milling [10]. Fang and Liu suggested that once the workpiece material and other process parameter are specified, the undeformed chip thickness will determine burr height [21]. The enlargement in the tool edge radius which occurs due to tool wear decreases the ratio of undeformed chip thickness to cutting edge radius; this means that effective rake angle becomes more negative. Material ahead of the tool is pushed /compressed and deformed plastically into a burr.

4.1.4 Research motivation

From the reviewed literature, it is clear that, the machinability of micro parts would be favourable if all parts were made from single phase materials with a very fine microstructure and preferably low ductility. However, in practice micro components are manufactured from typical engineering materials that contain multiphase structures.

In building a scientific base for machining such materials it was decided to select two phase materials one dominated by a single phase and the other with an almost balanced volume fraction. Studying the machinability of these materials would enable the elucidation of the effect of phase properties on surface roughness, subsurface microstructure change in the micro machining process.

4.2 Experimental details and evaluations

4.2.1 Material metallographic grain size measurement

The selected workpiece materials were AISI 1005 and 1045 steel alloy. AISI 1005 steel is 99% ferrite content while 1045 steel can be considered as representing balanced volume fractions of ferrite and pearlite. The microstructure of these materials is shown in Fig. 4.1. The grain size of AISI 1005 steel was evaluated according to BS EN ISO643:2003 [136] and found to be on average $67\mu\text{m}$. For AISI 1045 steel the grain size was determined by the linear intercept method. In Fig. 4.1, the white surface is the ferrite phase and its average grain intercept length was $7\mu\text{m}$. The black regions are the pearlite phase with $52\mu\text{m}$ average grain intercept length.

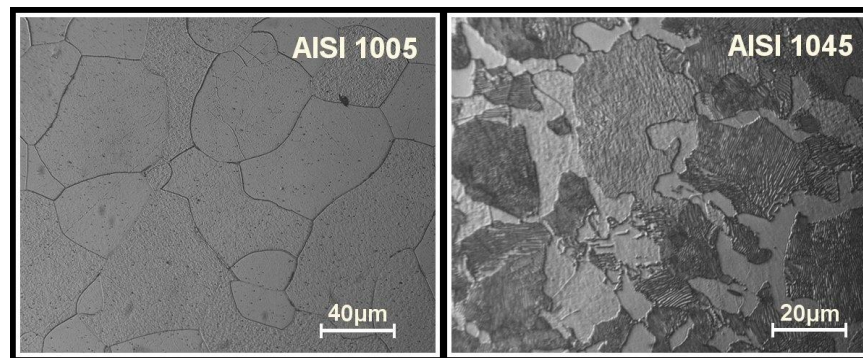


Fig. 4.1 Workpiece microstructure (a) AISI 1005 steel (b) AISI 1045 steel

4.2.2 Material characterisation using instrumented indentation testing

An MTS-XP indentation system was used for material characterisation. Each test was performed ten times on 3 different samples of each workpiece material. Indentation depth was varied from 0.2 to $2\mu\text{m}$. A standard Berkovich indenter was used because it induces plasticity at very low loads. The load and indenter displacement were recorded simultaneously during the entire loading and unloading process. Hence, the process was capable of measuring both the plastic and elastic deformation of the materials under test [137]. Table 4.1 shows the average elastic modulus and nano-hardness data computed from the unloading data and their standard deviation. It is clear that the variability between measurements is very low. However, comparing workpieces, for a single phase material there is low variability compared to the multi-phase AISI 1045 steel. This can be attributed to the different properties of ferrite and pearlite. The data shows that AISI

1045 steel is relatively harder than AISI 1005 steel. The hardness behaviour of a material is normally related to its resistance to plastic deformation. Therefore, it can be expected that AISI 1005 steel, being of lower hardness will plastically deform more.

Table 4.1 Mechanical properties variation as a function of nano-indentation depth

Nano-indentation depth (μm)	AISI 1005 Steel				AISI 1045 Steel			
	Nano-hardness		Elastic Modulus		Nano-hardness		Elastic Modulus	
	Average ($G Pa$)	Standard deviation	Average ($G Pa$)	Standard deviation	Average ($G Pa$)	Standard deviation	Average ($G Pa$)	Standard deviation
0.2	2.65	0.18	231.75	30.9	3.53	0.81	220.8	16.5
0.5	2.43	0.37	233.05	14.3	3.49	0.32	241.5	9.64
1	2.20	0.34	236.36	10.01	2.89	0.40	238.08	17.08
2	2.15	0.24	241.83	17.7	2.66	0.48	244.01	21.21

In scratch testing of polymers and metals, Jardret et al [77] noted that the proportion of the plastic deformation increases with an increase of the Young's modulus to hardness ratio. Using this assumption it can be inferred from Fig. 4.2a that AISI 1005 steel will plastically deform more compared to 1045 steel. On the other hand, Nakayama [78] attributed larger elastic recovery to a high ratio of the hardness to elastic modulus. In order to quantify the elastic recovery of the investigated materials, displacement into the surface was analysed. The percentage of elastic recovery was calculated by taking the difference between maximum indentation depth when fully loaded and residual indentation depth after unloading. The results are shown in Fig. 4.2b. It is evident from the graph that AISI 1045 steel has a higher elastic recovery compared to AISI 1005 steel. The elastic recovery increases with a reduction in indentation depth. This validates the use of hardness to elastic modulus ratio in predicting elastic deformation. Thus it is clear from the nano-indentation testing that pearlite and ferrite have differential deformation patterns and a ferrite structure is expected to show deeper plastic deformation.

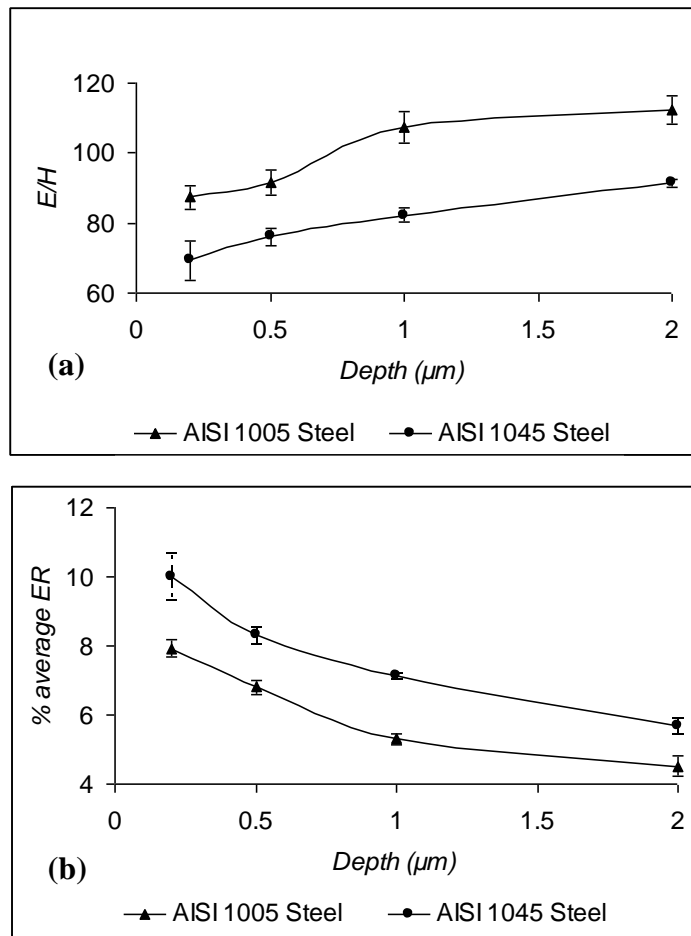


Fig. 4.2 Comparison of (a) elastic modulus/hardness ratio (b) percentage elastic recovery for workpiece specimens

4.2.3 Experimental details and cutting parameters

To study the deformation and machining performance micro milling tests were undertaken. The cutting tools used were flat end mills (Fraisal M5712080) with a diameter of 800 μm . These were manufactured from fine grain tungsten carbide and coated with TiAlN. The cutting edges had a rake angle of 6° and a helix angle of 25° . A tool diameter of 800 μm was selected since this falls within the 1 to 999 μm size range common for micro milling. Additionally, the higher end of the microscale tool diameter range was ideal in order to minimise the chance of tool edge breakage and hence focus on workpiece related machinability aspects. Prior to the cutting tests, each micro-end mill was imaged using a scanning electron microscope (SEM) and the average radii of the cutting edges were estimated from the SEM and found to be in the range of 1 to 2 microns.

The work presented here contributes to a theme of sustainable manufacture where the idea is to investigate the potential for dry or near dry machining. Dry machining can bring environmental and health safety benefits. Environmental regulations are expected to tighten up with regards to the use of machining coolants and lubricants [138]. Moreover, coolant mists and coolant coated chips need appropriate disposal. For these reasons, micro slotting tests were performed dry on a Mikron HSM 400 milling centre. The static radial runout of spindle-collet-tool system was measured in the clamped state before each cutting trial. The radial runout was estimated from the runout gauge measurements to be 1.6 μm in average, with a standard deviation of 0.76 μm .

The cutting parameters used are shown in Table 4.2. The range of maximum undeformed chip thickness (i.e. feed per tooth in slotting) was selected to cover values either side of the tool edge radius. This enabled the study of both negative and positive effective rake angles. Micro-milled slots having a 20 mm length of cut were made at each feedrate. The condition of each tool was observed before machining and re-inspected at stages during the cutting tests. The cutting trials were repeated twice for each experimental run.

Table 4.2 Process parameters

Spindle speed (rpm)	30000
Chip Load ($\mu\text{m}/\text{tooth}$)	0.02, 0.2, 0.5, 1.0, 2.0, 5.0, 10.0, 15.0
Axial depth of cut (μm)	75
Tool Diameter (μm)	800

4.3 Micro milling results and discussions

4.3.1 Surface roughness

The surface topography on the floor of the micro-milled slots, for both workpiece materials, was analysed using a Wyko NT11000 optical profiler (white light interferometer) and Hitachi S-3400 SEM (scanning electron microscope). Surface roughness was measured in twelve different positions across the length of the slot. The Wyko NT1100 surface profiler uses vertical scanning interferometry (VSI) mode at $2.5\times$ magnification, full resolution and $1\times$ scan speed. The area sampled by the Wyko was 2.429 by 1.848 mm, with a picture resolution of 736 by 480, which yielded 3.3 microns/pixel. The resolution in Z axis was 1 nm. The average surface roughness (as well as the scatter in the measured values) was plotted against the corresponding

maximum undeformed chip thickness, as shown in Fig. 4.3. The data shows that the surface roughness is significantly lower than the grain size. This presents the possibility of grain polishing or fracture as an integral part of the mechanics of micro machining for both workpiece materials.

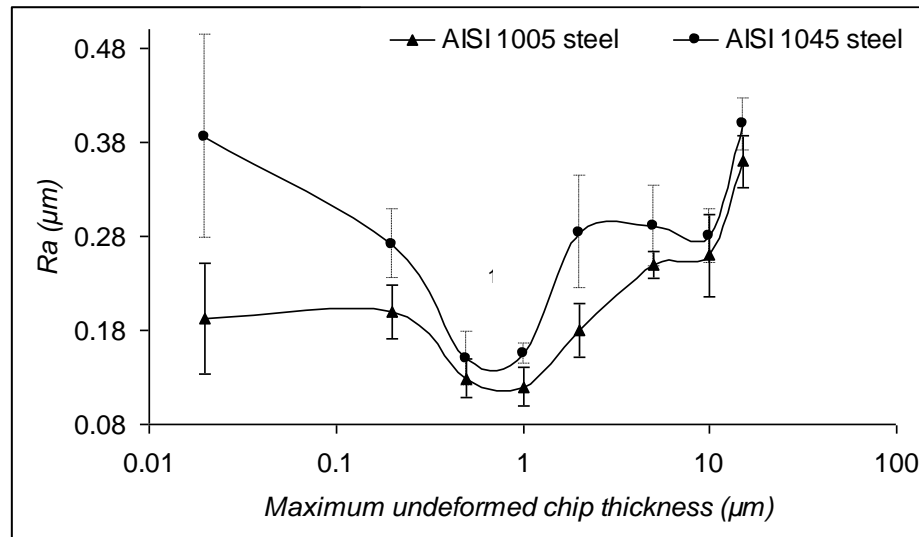


Fig. 4.3 Surface roughness

The overall relationship between the surface roughness and maximum undeformed chip thickness is nonlinear for both workpiece materials. For $0.02 \mu\text{m}/\text{tooth}$ maximum undeformed chip thickness, a substantially high surface roughness and highest scatter was recorded for AISI 1045 steel compared to AISI 1005. This can be attributed to the differences in elastic recovery of ferrite and pearlite as evident by the higher elastic recovery for AISI 1045 in Fig. 4.2. The result suggests that micro machining of a single phase material minimises the differential elastic recovery that would be found in multiphase materials and hence improves surface finish.

In multiphase material the value of minimum chip thickness is lower for a harder phase than a softer phase [11]. This variation in minimum chip thickness causes transition in cutting from one phase to another, affecting surface finish of machined parts. In this respect, the AISI 1045 steel surface topography was examined after machining at $0.02 \mu\text{m}/\text{tooth}$ undeformed chip thickness (about 3% of edge radius). Fig. 4.4(a) shows the image measured from Wyko optical profiler with a $0.32 \mu\text{m}/\text{pixel}$ resolution. Fig 4.4(b) is the 2D surface profile corresponding to a horizontal black line marked in the Fig 4.4(a). First, the dark and light regions correlate well with the average intercept

length of the pearlite and ferrite phases. These were identified from Fig 4.4(a) and then the extracted surface profile for e.g. Fig 4.4(b)) was analysed across those areas. It shows concave and convex forms (differential elastic recovery) on the pearlite and ferrite grains respectively with cutting discontinuity across grain boundaries. This analysis was repeatable at different positions of the machined surface.

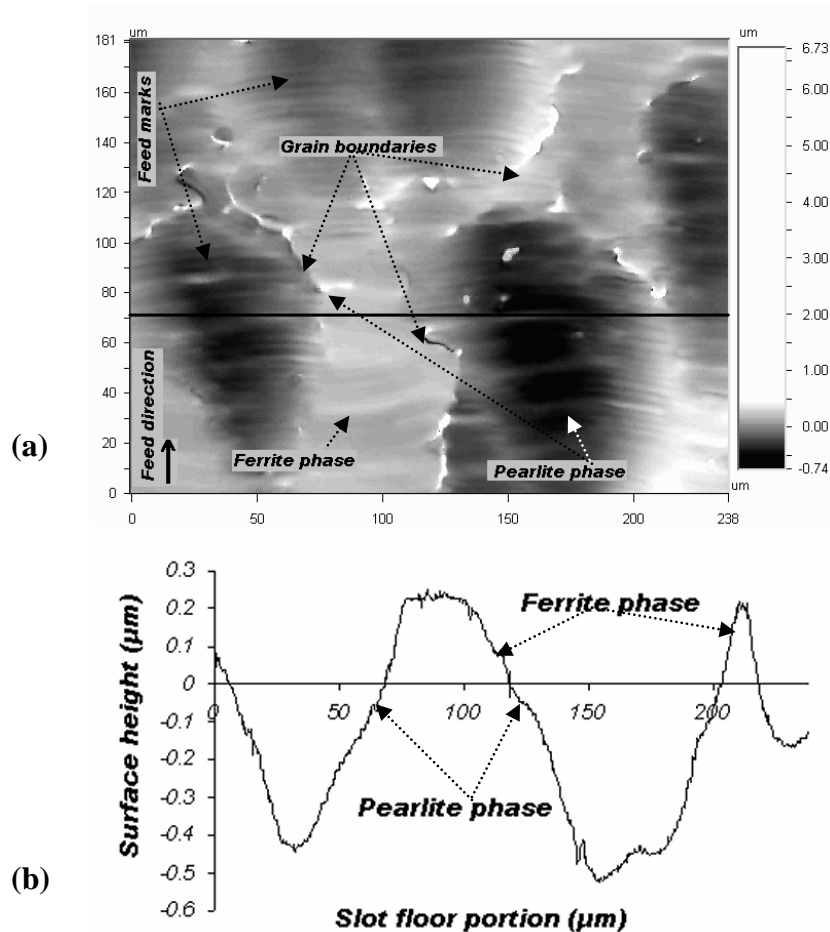


Fig. 4.4 Micro milled slot base for AISI 1045 steel generated at $0.02 \mu\text{m}/\text{tooth}$

When machining at an undeformed chip thickness much smaller than the tool edge radius, the effective rake angle becomes highly negative and material spring-back effects need to be considered. In Fig. 4.3, as undeformed chip thickness is increased and approaches the tool edge radius, the rake angle becomes less negative and the increase in surface roughness due to material spring-back effect is reduced. The best surface finish was achieved at feed per tooth of $1.0 \mu\text{m}/\text{tooth}$ for both workpiece materials. This feed per tooth is comparable to the tool edge radius and located at the lower end of the

tool edge radius values for the tools used. This suggests that in process planning for these workpiece materials, knowledge of the tool edge radius is important.

Again in Fig. 4.3, as the feed per tooth increases beyond the tool edge radius, the difference in surface roughness value, between the two materials, appears more pronounced at $2\ \mu\text{m}/\text{tooth}$ undeformed chip thickness. It is noted that at $2\ \mu\text{m}/\text{tooth}$ undeformed chip thickness, this length scale is shorter than the average width of the ferrite phase. Thus, one possible explanation for surface roughness trends observed could be due to the discontinuity (see Fig. 4.5) in cutting process across the grain boundary and the formation of a comparatively thicker miniature burr on the grain boundary of AISI 1045 steel. Formation of grain boundary burrs was also reported by Volger et al [11]. Moreover, Fig. 4.3 shows that the surface roughness does not significantly increase as the feedrate is increased from 2 to 10 microns as expected. A possible explanation is that at the lower feedrate (2 microns) the formation of burrs at the grain boundaries is more pronounced than at higher feedrates. This has the effect of masking the traditional increase in surface roughness expected when using higher feedrates. However, at higher feedrates the conventional trend of increasing roughness with increasing feedrate as encountered in macro-scale machining also holds for micro cutting for the signal phase ferritic steel.

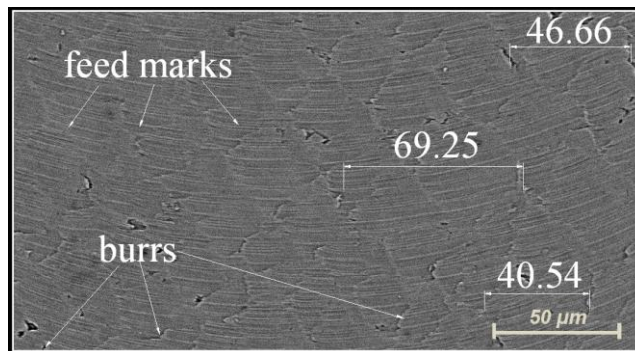


Fig. 4.5 Magnified area of AISI 1045 slot floor machined at $2\ \mu\text{m}/\text{tooth}$

The surface generated was studied at feeds per tooth below minimum chip thickness ($0.02\ \mu\text{m}/\text{tooth}$), within the vicinity of the minimum chip thickness ($0.2\ \mu\text{m}/\text{tooth}$), comparable to ($1\ \mu\text{m}/\text{tooth}$) and above the tool edge radius ($10\ \mu\text{m}/\text{tooth}$). These cases are presented for both materials in Fig. 4.6. The minimum chip thickness has been reported in literature for various workpiece materials [11, 73, 76]. Generally, images for AISI 1005 steel clearly show smoother surface appearance compared to AISI 1045

steel. However, AISI 1005 steel shows a smeared pattern which could be attributable to higher plastic deformation at $0.02 \mu\text{m}/\text{tooth}$. At a feed per tooth of $0.2 \mu\text{m}$ material microstructure effects dominates the surface texture of AISI 1045 workpiece material. Additionally, burr formation can be observed on the image of AISI 1045 steel machined at $1 \mu\text{m}/\text{tooth}$ undeformed chip thickness. Above the tool edge radius feed marks dominate the surface form.

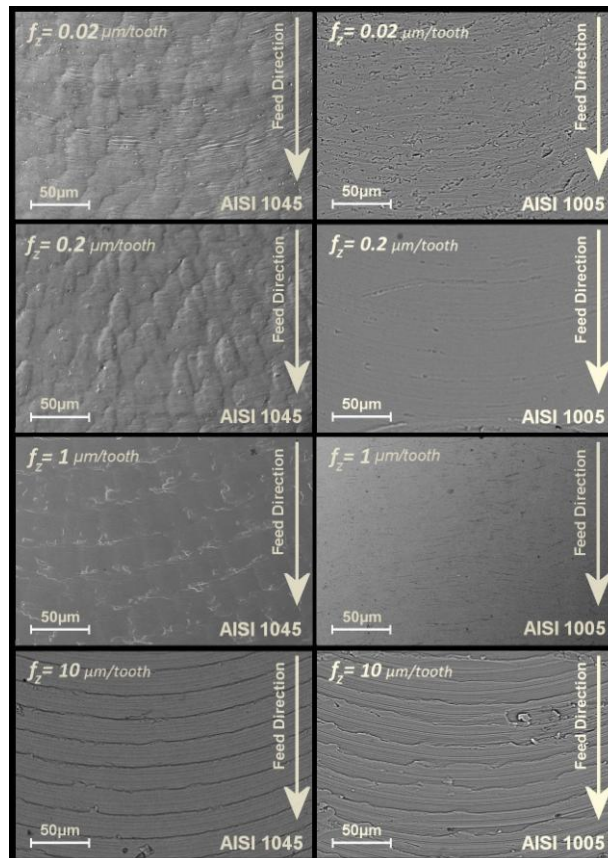


Fig. 4.6 Surface generated at different feedrates

4.3.2 Subsurface microstructure modification

To investigate subsurface deformation and microstructure change, each slot was sectioned and then set in a conductive acrylic hot resin in order to reduce edge rounding during polishing. Scanning electron microscopy and nano hardness testing was performed at the two sides and centre of the slots. Fig. 4.7 shows the material side flow and grain structure for micro machined slots. In AISI 1005 steel, at lowest feedrate the thickness of material being pushed out (extruded) to form a burr is of comparable magnitude to the grain size of the material. For all cases tested AISI 1045 steel demonstrated better edge definition geometry than AISI 1005. Thus, AISI 1005 with a

lower hardness and higher plastic deformation (as discussed before) generates larger burrs compared to AISI 1045.

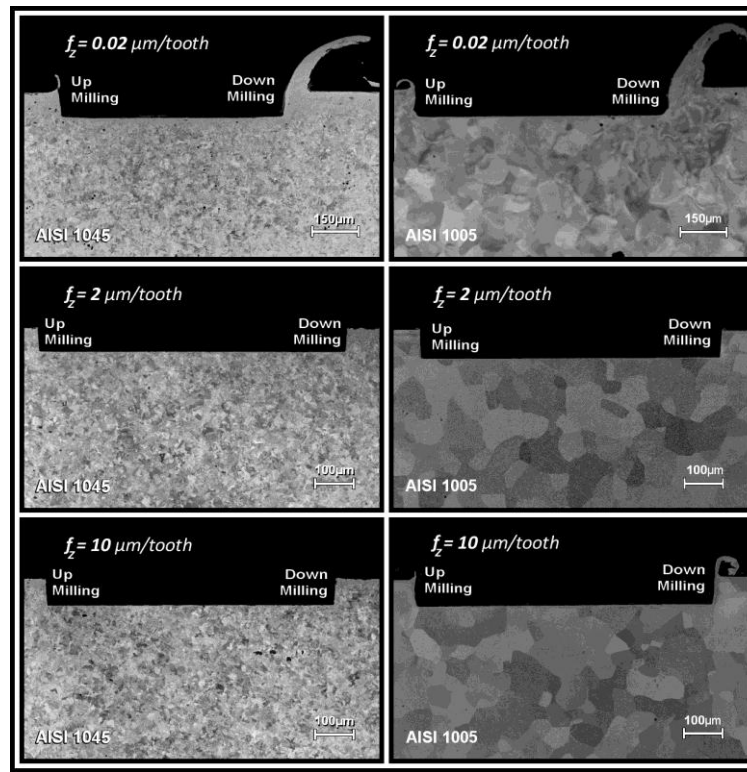


Fig. 4.7 Subsurface micro-structural modification and material side flow

To characterise the machined surface, nano-indentation was performed. An indentation depth of 0.5 μm was selected and a series of tests were carried out at a minimum distance ($\sim 10 \mu\text{m}$) from the edge of the slot to avoid lateral push away of the material. These results are based on repeating measurements with identical process parameters on both workpiece materials. The tests were performed on sectioned pieces taken before the end of second slots. Further measurements revealed similar trends; therefore the results can be seen as quantitatively significant. The nano-hardness and elastic modulus of the modified surface layer at the centre of the slot is shown in Fig. 4.8. Each dot on the graph represents the average value and the bars represent the standard error of the mechanical properties measured from five points on the slot floor. Fig. 4.8(a) shows that AISI 1045 steel exhibit work hardening during the chip formation process when compared to AISI 1005 steel. The AISI 1045 steel produces harder surface than bulk material in the ploughing zone. While, micro machining of AISI 1005 steel induces no noticeable change in hardness for most investigated feed per tooth. The former can be

attributable to higher wear land (will be discussed in section 4.2.4) which contributed to higher tertiary zone temperatures and hence promoting surface modification. It is also worth mentioning here that elastic modulus substantially decreases for both workpieces at the feedrates less than 20% of the tool edge radius (Fig 4.8 (b)).

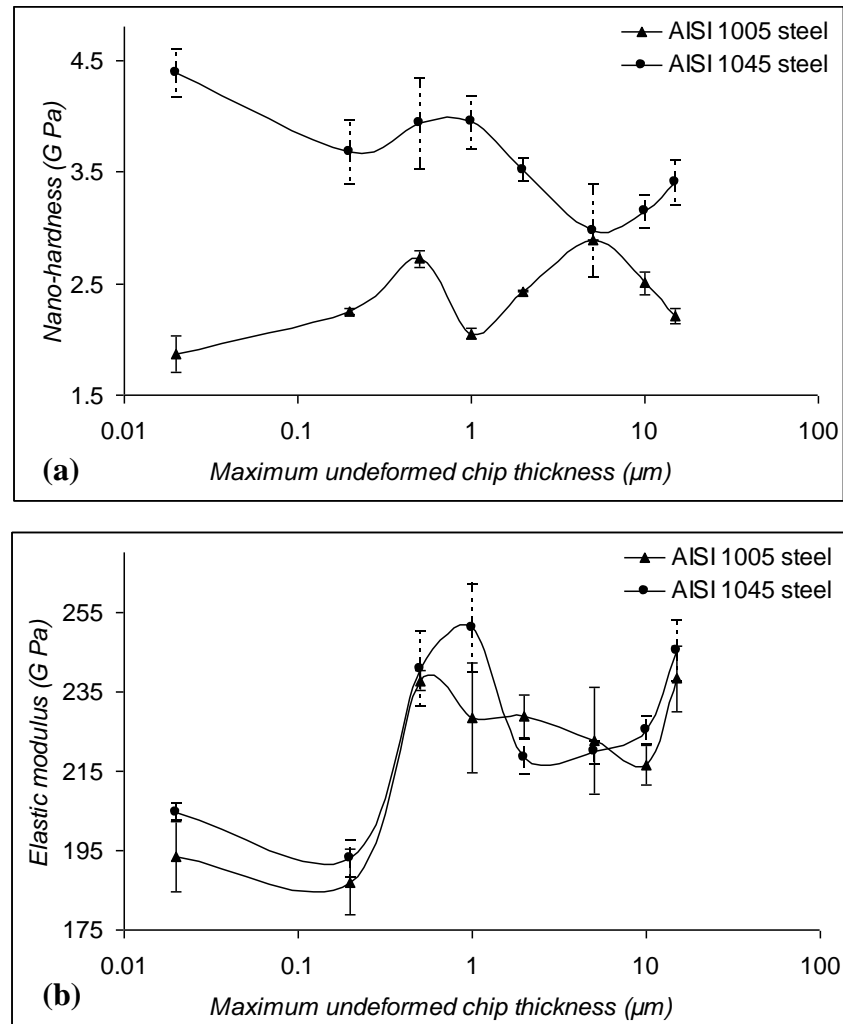


Fig. 4.8 Slot floor subsurface layer properties

(a) Nano-hardness (b) Elastic modulus

Fig. 4.9 shows the nano-indentation marks on the down milling side of the slot for both workpiece materials machined at $0.02 \mu\text{m}/\text{tooth}$. The depth below the wall surface for the initial point of indentation was specified by positioning the indenter approximately $10 \mu\text{m}$ below the wall surface. The indentations then followed an automated process until 15 nano-indentations had been carried out in the form of 3×5 arrays for both sides. The indents were $10 \mu\text{m}$ apart from each other; this provided 3 indents placed parallel at the same distance from the respective wall surface. After performing the

array of indents, BSE images were taken in the indented area to ensure the position of indents for all cases.

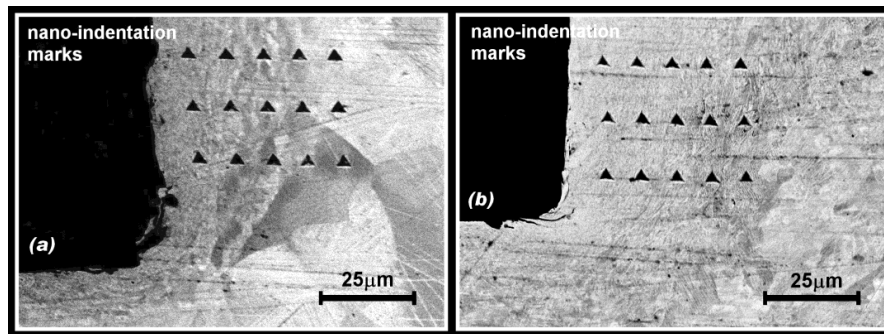
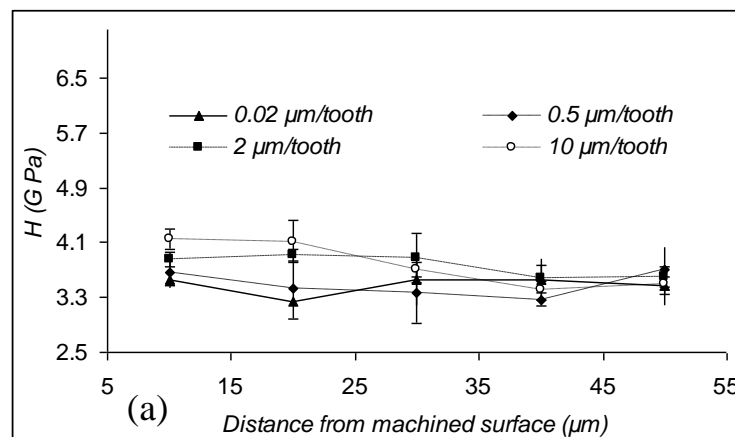


Fig. 4.9 Slot down-milled side (a) AISI 1005 (b) AISI 1045

Figs. 4.10 and 4.11 show in-depth nano-hardness profiles across up-milled and down-milled sides of the slot machined at four different feedrates on AISI 1045 and AISI 1005 steel respectively. The most noticeable increase in hardness was recorded in the subsurface region at the down milling side of the slot wall at the lowest undeformed chip thickness for the both workpiece materials. The results demonstrate that mode of milling imparts differential change in the properties of machined surfaces. When machining below the critical undeformed chip thickness, applying the 0.37 and 0.32 standard deviation from Table 1 to the results after machining in Fig. 4.10 and 4.11 does not mask the distinct trends for the two workpiece materials. Moreover, it is clear from Figure 4.9 that the depth of deformed zone can be in the order of 40 microns. These results imply that the micro machining process modifies the properties of the workpiece material in regions of plastic deformations.



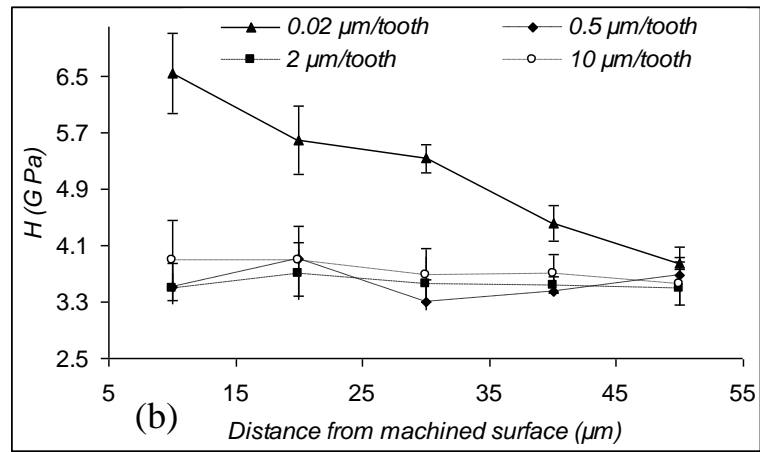


Fig. 4.10 AISI 1045 steel nano-hardness in-depth profiles generated at (a) up-mill side wall (b) down-mill side wall

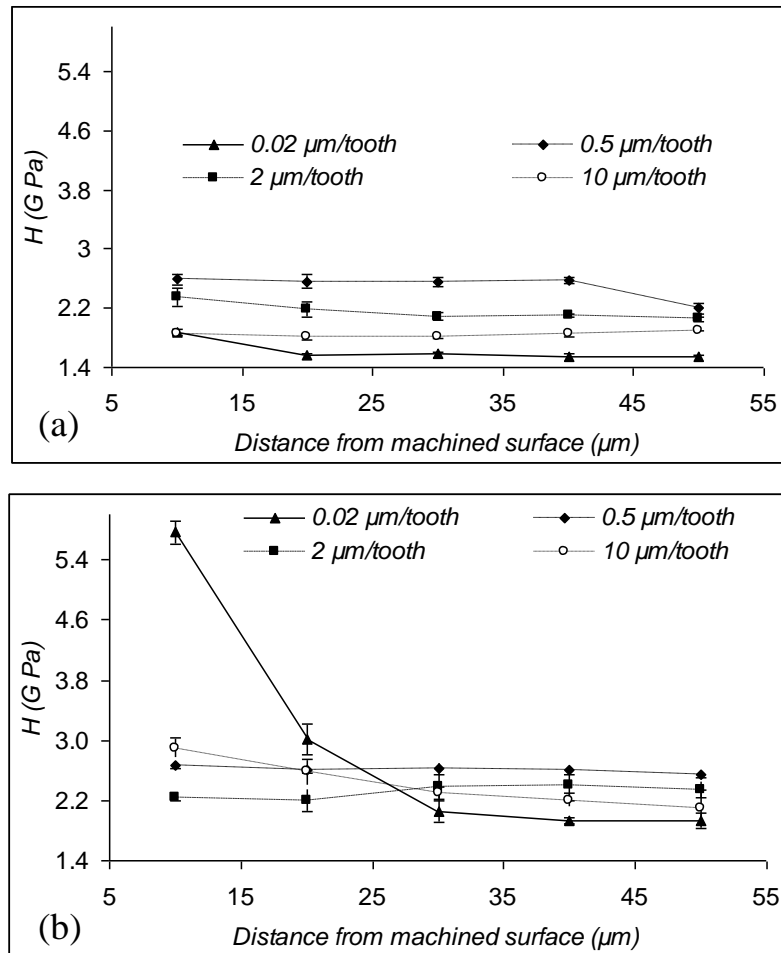


Fig. 4.11 AISI 1005 steel nano-hardness in-depth profiles generated at (a) up-mill side wall (b) down-mill side wall

At lowest undeformed chip thickness, the value of nano-hardness correlates well with the flank wear. The results suggests that a sharp tool (without or with small wear) induced no appreciable change in nano-hardness. While a worn tool results in surface modification and increase in hardness.

4.3.3 Burr formation

There is no common approach in terms of measuring curled 3D burr shape, especially in the micro domain. What emerges from the past literature is that the burr shapes can be qualitatively compared according to the shape [10, 102] or quantitatively measured in terms of burr width [33, 115] and burr height [139]. Both burr height and width do not reflect the fact that the burr could be curled. However, in terms of component functionality, use and assembly burr height and width are relevant measures. In the available techniques, measurement of burr width was chosen to quantify the burrs formed at the top of the slot since this is a parameter that could be more accurately measured by the Wkyo. Focussing the microscope on the apparent top of the burr is difficult with the optical instrument.

The top burr width in both up and down milling was measured from Wyko scans. The variation of the burr width as a function of maximum undeformed chip thickness is shown in Figs. 4.12 and 4.13 for the both workpiece materials. The error bars of the figures were obtained using the standard error calculated from fifteen measurements. Over the entire range of feedrates investigated AISI 1005 steel produced larger burr on the down milling side compared to AISI 1045 steel. This can be attributable to the higher ductility of AISI 1005. This also reveals that the size effect strongly affects the variation in burr width. As chip load decreased for both up and down milling the size of burr increased. At $0.02\ \mu\text{m}$ (less than 5 percent of the tool edge radius) the undeformed chip thickness is lower than the minimum chip thickness for these materials. At this point the slotting operation forces the tool into the material and the burr size is very high on the down milling side. This appears to suggest that this cutting condition forces deformed material to exit from the down milling side.

It was noted that, when the feed per tooth was lower than the tool edge radius, the tool wear (discussed later in section 4.2.4) considerably leads to increased top burr size, especially on the down milling side. Interestingly for the up milling side, the effect of tool wear on burr generation is less dominant at these feedrates. The differences in the

burr size between the two milling modes may be due to the burr formation mechanisms and vibration.

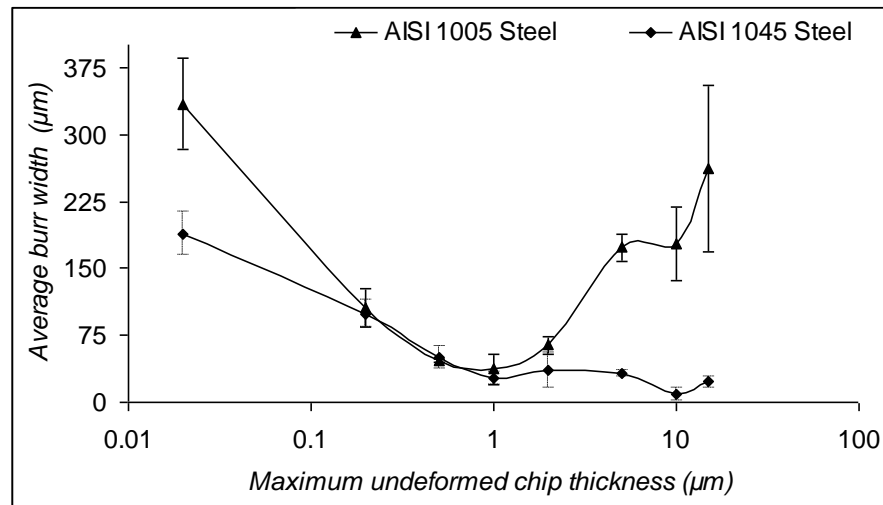


Fig. 4.12 Burr size in down-milling

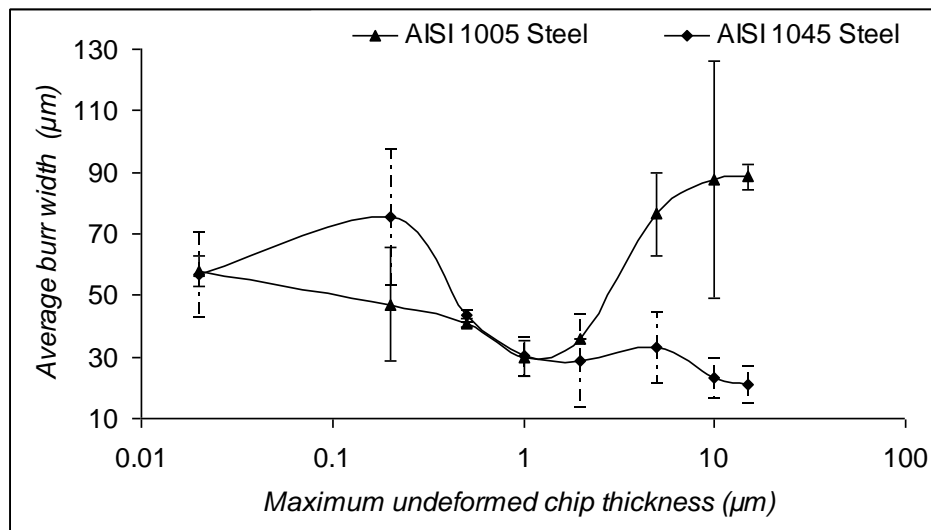


Fig. 4.13 Burr size in up-milling

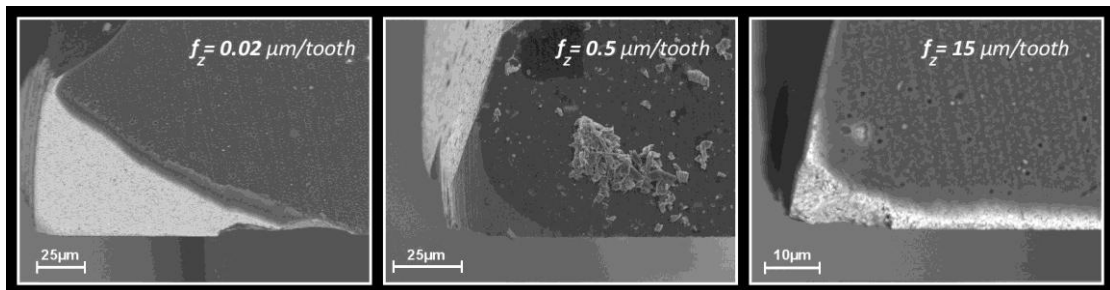
4.3.4 Tool wear

Cutting tool deterioration is a major factor affecting the economics of micro mechanical machining process, the effect of material microstructure on the progression of tool wear can effectively identify economically viable workpiece selection for manufacturing ferrous components. Again in the brief literature review, no unified approach for tracking the condition of micro tools is available. The change in tool diameter [10], edge radius roundness [24] and flank wear measurement from the bottom view of the endmills [33], were the criterion that researches have identified for the evaluation of

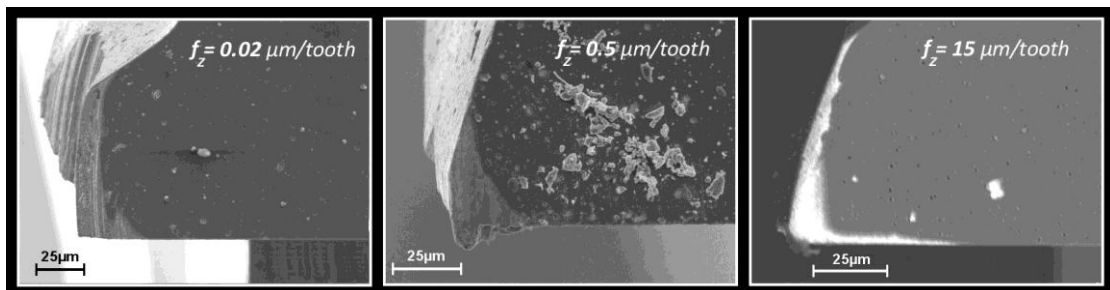
tool wear in micro domain. Moreover, for steels it was evident that trends for flank wear at the bottom cutting edge, edge chipping, cutting edge radius enlargement and percentage tool diameter reduction are positively correlated [140]. It is therefore reasonable to monitor any one of these parameters to assess tool performance in terms of tool life. The tool bottom face is directly in contact with slot floor surface, affecting the surface finish. Therefore, this parameter was adopted in this research.

In contrast to the flat end mills used here, ball nose micro cutters could be considered to increase the cutting edge strength. However, it was noted that in developing technology for ultimately machining inclined slots, ball nose micro tools suffer from push off and deflection and this affects tool life. Thus this study was based on the flat end mills.

Tool wear progression was observed by taking SEM images before and after machining. Some images of the used cutting edges are shown in Fig. 4.14, corresponding to a material removal of 1.2 mm^3 . It is clear from these images that cutting tools used for machining AISI 1045 experienced more uniform and abrasive wear while those used for machining AISI 1005 have flank faces characterised by plastic deformation.



(a) After machining AISI 1045 Steel



(b) After machining AISI 1005 Steel

Fig. 4.14 Material deformation effects on the tool cutting edges

Fig. 4.15 shows a comparison of maximum flank wear land measured on both flutes, from the bottom view of the micro end mill after completion of slots. A relatively higher degree of flank wear was observed when machining the softer AISI 1005 material in line with the higher plastic deformation. For both workpiece materials the reduction in the flank wear as the feedrate increased is consistent with reduced ploughing effects.

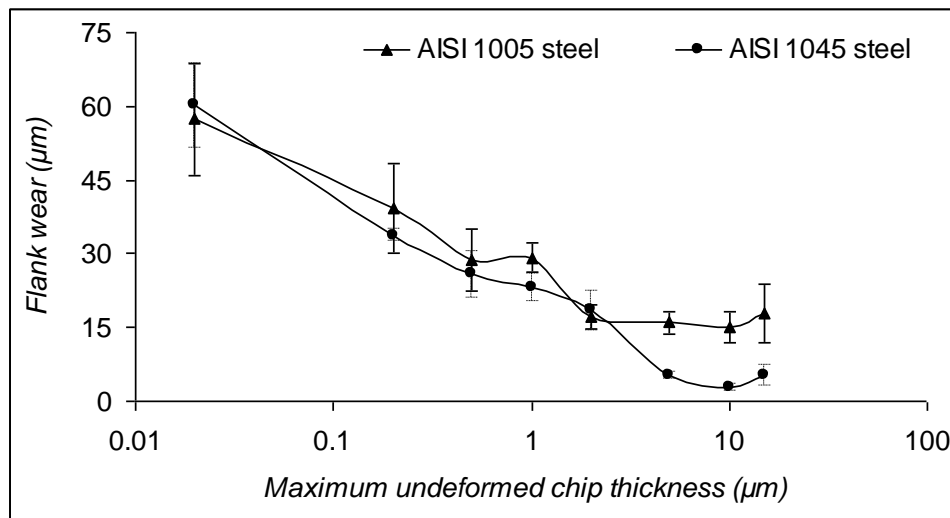


Fig. 4.15 Flank wear comparison

4.4 Conclusions

The work presented in this chapter compared material phase effects, in micro milling over a range of undeformed chip thickness spanning the tool edge radius and grain sizes of two selected workpiece materials. For this range, surface finish, microstructure change, burr formation and tool wear were investigated for the two kinds of steel. Some of the significant findings from this study can be summarized as follows:

- The results show that in terms of surface finish the machinability of AISI 1045 steel compared to AISI 1005 steel is more challenging due to cutting discontinuities and formation of grain boundary burrs.
- The challenge in machining AISI 1005 relates to edge profile definition as driven by burr size growth.

- The best surface finish was obtained at feedrates closer to the tool edge radius for both workpiece materials. This suggests that generation of the best surface finish was more sensitive to tool edge radius than material grain size.
- AISI 1045 steel which was predicted to exhibit a higher elastic recovery also had a higher surface roughness compared to AISI 1005. Thus it is possible that in AISI 1045 alloy steel, differential elastic recovery between the phases compromises surface finish.
- For AISI 1005 alloy steel, higher plastic deformation as predicted by nano indentation tests promotes relatively larger burrs in the down milling mode compared to micro machining of AISI 1045 steel.
- At undeformed chip thickness lower than the tool edge radius, burr size increases with reduced feedrates.
- The micro milling process increases the nano hardness of the workpiece material in the down milling mode. This property modification as driven by milling mode is differential on milled surface profiles.
- The results suggest that nano indentation measurements can be used to provide a qualitative relative assessment of micro machinability for different workpiece materials and hence, reduce the cost and time of technology development.

Chapter 5

IDENTIFICATION OF FACTORS THAT DOMINATES “SIZE EFFECT” IN MICRO MACHINING

Abstract

In micro machining the so called “size effect” is identified as critical in defining process performance. Size effects refers to the phenomenon whereby the reduction of the undeformed chip thickness to levels below the cutting edge radius, or grain size of the workpiece material begins to influence workpiece material deformation mechanisms, chip formation and flow. However, there is no clear agreement on factors that drive this size effect phenomenon. To explore the significance of cutting variables on the size effect, micro milling tests were conducted on Inconel 718 nickel alloy using 500 μm diameter carbide end mill. The experimental design was based on an L9 Taguchi orthogonal array. Fast Fourier transform (FFT) and wavelet transform (WT) were applied to acoustic emission (AE) signals to identify frequency/energy bands and hence size effect specific process mechanism. The dominant cutting parameters for size effect characteristics were determined by analysis of variance (ANOVA). These findings show that despite most literature focussing on chip thickness as the dominant parameter on size effect, the cutting velocity is also a dominant factor. This suggests that manipulating the cutting speed is also an effective strategy in reducing burr thickness, optimising surface finish and in breaking the lower limit of micro machining.

Keywords: Micro milling, Size effect, Inconel 718 alloy, Taguchi methods

5.1 Introduction

5.1.1 Size effect in micromachining

In micro machining the “size effect” modifies the mechanism of material removal compared to conventional (macro-scale) machining [1, 2, 31, 35]. This can arise because the thickness of material to be removed is of the same order of magnitude as the tool edge radius or grain size of the workpiece material. The size effect is typically characterised in machining by a non-linear increase in the energy consumed per unit volume of material removed as the undeformed chip thickness decreases. Experimental observation of this unbounded increase in specific energy in machining of ferrous and non-ferrous materials has been reported. With respect to investigated workpiece materials, difficult to cut materials (Ni, Ti based alloys) have not been reported. Most of the reported research work was undertaken over a limited cutting velocity range and the material thickness removed was in the sub-micron length scale. For a selected cutting speed, the size effect was attributed to tool edge radius effect [43, 44, 58, 141], material microstructure effect i.e. dislocation density/ availability [38, 50], material strengthening effect due to strain, strain rate, strain gradient [10, 40, 41, 46, 48, 142], subsurface plastic deformation [39], and material separation effect [47].

5.1.2 Machinability of nickel alloys

Nickel-based alloys are extensively used in aerospace components because of their high specific strength (strength to weight ratio) which is maintained over a wide temperature range. Approximately, half of the total materials used for a gas turbine engine are nickel alloys [112]. The most widely used nickel alloy, Inconel 718 accounts for as much as 45 per cent of wrought nickel based alloy production and 25 per cent of cast nickel based products [143]. However, nickel based alloys pose a serious machinability challenge to the industry due to their work hardening, high temperature strength, low thermal conductivity and hard abrasive particles [112]. Moreover, a high adhesion tendency with the tool material, leads to galling and welding of chips on the work piece surface and short tool life.

Most recently, Klocke et al [25] presented an assessment of feasibility of micro milling process on single crystal nickel based super-alloy (Rene´ N5). All cutting tests were performed at fixed cutting velocity (50 m/min) and chip load (15 μm / tooth) using 800

μm diameter micro-end mills. In another study, Weinert and Petzoldt [22] demonstrated micro-milling as an alternative production process for NiTi shape memory alloy micro-parts. This was done for a narrow cutting range using 400 μm diameter micro tool. The selected cutting velocity was 33 m/min while chip load was varied from 12 to 20 $\mu\text{m}/\text{tooth}$.

5.1.3 Acoustic Emission (AE) signal in micro milling process

Acoustic emission (AE) refers to the elastic stress waves emitted as a result of the rapid release of strain energy within a material due to rearrangement of its internal structure [124]. In machining, deformation can be considered to be the main AE producing source [144]. This implies that AE from machining processes such as turning, grinding and milling represent the unique characteristics of the mechanics of each process. A milling operation is a discontinuous cutting process with varying chip load performed by multiple cutting teeth. AE associated with this process consists of continuous and transient signals. The continuous AE signals stem from plastic deformation of workpiece material in the primary shear zone, at the chip/tool interface (secondary shear zone) and at the tool flank/workpiece surface interface (tertiary shear zone). While the transient signals are associated with pulse shock loading, such as initiation or breakage of chips or by tool fracture. However, in microscale milling for chip thickness at or below few microns in length, AE generation is attributed to the interaction of the tool edge radius with the micro-structural features of the workpiece material [28].

Uehara and Kanda [119] reported that the amplitude of an AE signal from the cutting tool is reduced during AE transfer from the tool to the workpiece possibly by damping or reflection at the primary interface. As a result, by monitoring the AE signal from the workpiece side, the primary and tertiary deformation zones can be regarded as most accessible sources of AE generation in micro milling. In ultra precision cutting, Carpenter et al demonstrated that the tertiary deformation zone becomes a more significant source of AE due to the increased energy spent on sliding friction between the tool flank face and newly machined surface [120].

In literature it is suggested that, sporadic AE signal collected at the sensor contains many frequencies due to the several AE producing sources being active at the cutting zones [28]. Thus, the frequency of these different frequency bands can be used for identifying the dominant sources of AE in the micro machining process. Fig. 5.1 shows

identified frequency range according to the material removal length scale and signal source mechanisms. It is also clear from Fig. 5.1 that AE signals are better suited to characterising machining at very low length scales typically in the nanometre range as encountered close to the minimum chip thickness in micro machining. Again it can be inferred from Fig 5.1 that decomposing the AE signal into the frequency domain will enable identification of cutting mechanisms such as dislocation mechanics, intergranular micro fracture, cleavage and shearing material machining modes.

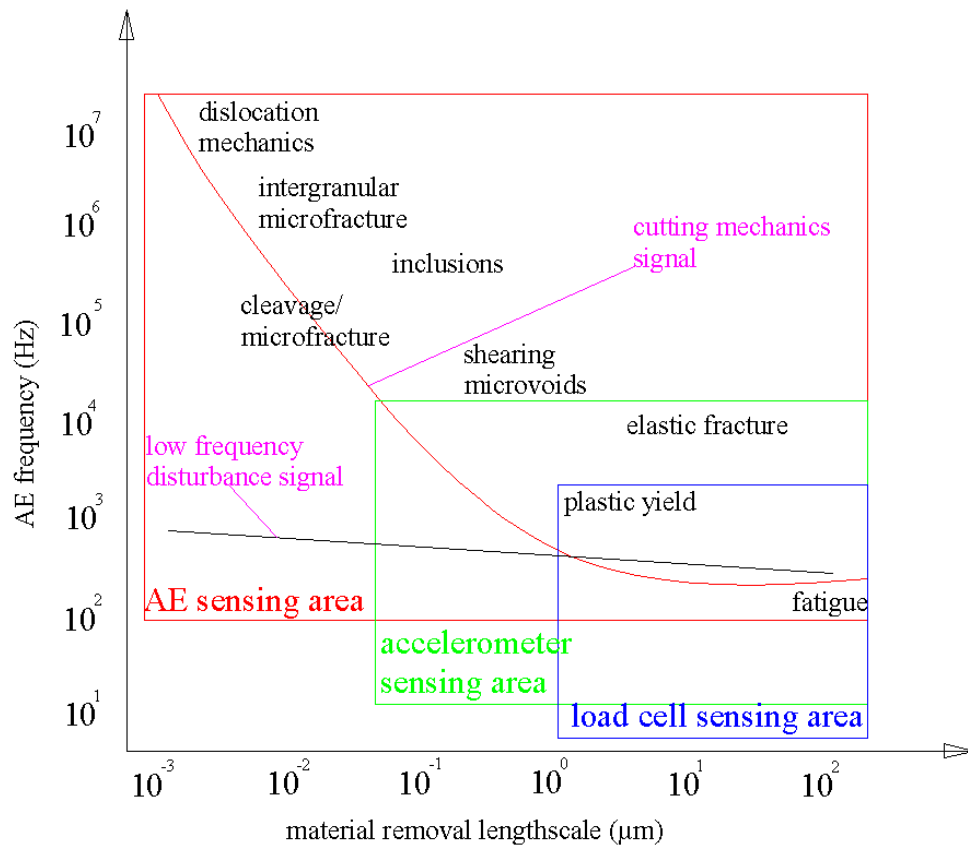


Fig. 5.1 AE signal source mechanisms (adapted from Lee et al [28])

In relation to the cutting zones, it is reported that the primary deformation zone, is the largest AE source and generates in excess of 75% of the total AE signal [121]. Brittle and ductile fracture (as shown in Fig. 5.2) may occur in the deformation of ductile materials that can emit AE from the primary shear zone depending on the type of material being machined and the operating conditions. It is well known that brittle fracture occur in a transgranular (cleavage) manner while ductile fracture takes place in intergranular manner where the grain boundaries are the fracture path within the

material [62]. Most of the metals undergo a transition from transgranular fracture to intergranular fracture when deformation occurs at temperatures greater than 0.5 to 0.7 times that of the melting temperature. Details of these fracture mechanisms are covered elsewhere [123].

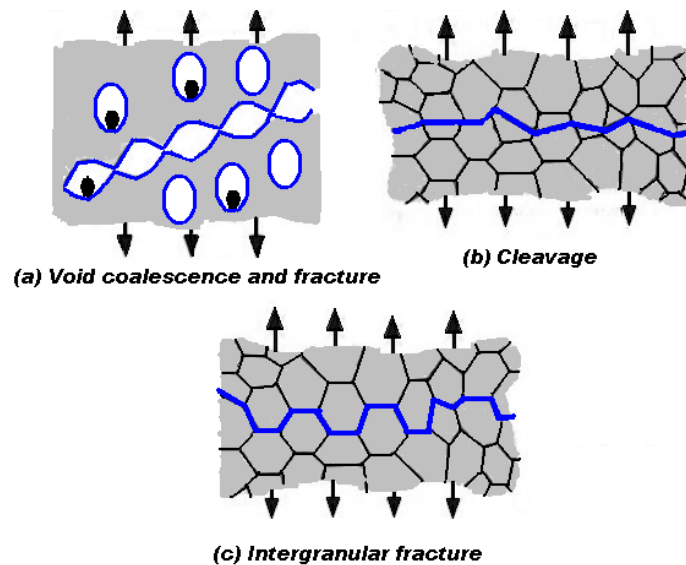


Fig. 5.2 Micro-mechanisms of fracture in metals [123]

In a case of continuous chip formation, Shaw proposed that ductile materials deformed as a result of nucleation, growth and coalescence of microscopic voids (micro crack initiation) that originated at inclusions and from second phase particle separation [122]. However, due to compressive plastic deformation, the micro cracks experience closure and this effectively postpones crack propagation until conditions are reached where plastic deformation does not occur. Barry and Byrne [145] observed a lamellae form as a result of cleavage during the non-overlapping cutting of a low alloy steel of 45.6 HRC with cutting speed of 100 m/min and for a depth of cut slightly greater than the minimum chip thickness during continuous chip formation.

With respect to a saw tooth formation, Komanduri and Schroeder noted thermoplastic instability leading to adiabatic shear in the chip formation process of Inconel 718 which was very similar to the mechanisms reported for titanium as well as hardened AISI 4340 steels, when machining at higher cutting speeds [95]. Furthermore, Barry et al [93] elaborated on this and presented two distinct mechanisms for catastrophic shear failure when machining Ti-6Al-4 V at 80 μm undeformed chip thickness. Under high cutting velocity (180 m/min), material failure was attributed to ductile fracture due to increase

in ductility as a result of thermal softening. However, it was also noted that the upper region of the primary shear zone (segment tip) sheared off due to cleavage. Under low cutting velocity (15 m/min), failure was said to have occurred due to cleavage. Zhou et al argued in favour of the material losing plasticity at high cutting speeds [146]. This observation is also in conformance with stress-strain curves reported for various temperatures for Inconel 718 alloy [95].

5.1.4 Research motivation

Under micro cutting conditions, tool edge radius [43, 44], chip load [39], cutting speed [41] and chip aspect ratio [42] have been reported as some factors which affect the starting point of the nonlinearity in specific cutting energy. Additionally, chip thickness influences increase in surface roughness [11, 15], burr formation [24, 147] and rate of tool wear. The relative contribution and dominance of cutting factors on size effect have recently been experimentally explored for hardened tool steel [148]. However, the application of acoustic emission signals to identify process mechanisms and hence clarify the dominance of cutting variables on the size effect has rarely been reported. Neither is there any related work focussed on nickel alloys. The motivation for this study was to assess the dominant factors in the control of plastic deformation in micro-scale cutting. Understanding the size effect dominant process parameters should enable the manipulation of the minimum chip thickness (e.g. lowering minimum chip thickness) and creating flexibility for generation of optimum conditions for best surface roughness.

5.2 Experimental details

5.2.1 Experimental setup

Micromachining tests were conducted on a wrought Inconel 718 nickel alloy workpiece material that was annealed by heating for one hour at 954 to 982 °C followed by cooling in air. The tests were conducted on a Mikron 400 high speed machining centre. All cutting tests were performed under dry conditions, which provided the opportunity to capture AE signals without coolant noise. Acoustic emission was measured with a Kistler Pieztron[®] acoustic emission sensor (8152B121) and the signal was amplified and filtered using an Kistler AE-Pieztron[®] coupler (5125B). The Inconel 718 workpiece

material, measuring 30 x 35 x 2.2 mm, was mounted on the top of an AISI 1045 steel fixture. The sensor was bolted on to the fixture as close as possible to the cutting zone to minimise the signal loss and achieve good signal to noise ratio. Additionally, the sensor was located at a constant distance from the slot being machined in each trial. Furthermore, to maintain good propagation from the workpiece to the sensor, a film of grease was used as a couplant. Slots of 5 mm in length were machined in each trial to minimize the effect of tool wear on the measured data. Tests were replicated twice to estimate error variance. The static runout of spindle-collect tool system was less than 1 μm .

5.2.2 Workpiece material characterisation

A polished sample of the Inconel 718 was etched with waterless Kalling's reagent and examined under a high resolution Polyvar[®] optical microscope to measure the average grain size. The grains were uni-axed and of 16 micron average diameter. Table 5.1 provides detailed information on chemical composition of the workpiece material. The mechanical properties were measured in terms of nano-hardness to be 3.4 GPa at 0.5 μm indentation depth and elastic modulus was 221GPa. The measurements were taken using an MTS instruments model XP nano-indenter.

Table 5.1 Chemical properties of Inconel 718 alloy in percent

Ni	Cr	Fe	Mo	Nb + Ta	Ti	Al	Other traces
52.5	19	18.5	3	5.13	0.9	0.5	0.47

5.2.3 Micro end mill

Fine grain tungsten carbide tools manufactured by Dixi Polytool Ltd were used. These tools were available coated in TiAlN coating and in uncoated form. The tools were flat end mills, two-fluted, 500 μm in diameter with a 30° helix angle. New tools were used for each run. Scanning electron microscopy (SEM) was used to estimate tool edge radius. The average measured tool edge radii of coated and uncoated micro tools were found to be 2 μm and 1.7 μm with standard deviation of 0.46 μm and 0.53 μm ,

respectively. In addition to cutting variables, the tool coating was selected as a factor because the frictional condition at tool workpiece interface influences the minimum chip thickness and resultant surface quality.

5.2.4 Acoustic emission (AE) measurement

The raw AE signal was bandpass filtered (50 kHz to 1 MHz) and then sent through a preamplifier at a gain 40dB to a data acquisition system. The $AE_{r.m.s}$ data was also acquired, from the band pass-filtered analogue signal with a root mean square (RMS) time constant of 0.12 ms. The filtered and $AE_{r.m.s}$ histories were recorded on a Nicolet technologies Sigma 30 digital memory oscilloscope at a sampling rate of 2 MHz. To retain sufficient amount of information sampling data length of 128,000 and 64,000 points were chosen for cutting velocities of 10, 25 and 40 m/min respectively.

5.2.5 Surface roughness and burr size measurements

A Wyko NT1100 surface profiler, which is a vertical scanning interferometry (VSI) at 10.2 \times magnification, full resolution and 1 \times scan speed was used to measure surface roughness. The area sampled by the Wyko was 607 by 462 μm , with a picture resolution of 736 by 480, which yielded 0.825 $\mu\text{m}/\text{pixel}$. The resolution in Z was 1 nm. Additionally, back scatter electron (BSE) microscope images were used to measure burr root thickness.

5.3 Research methodology

5.3.1 Signal processing technique

In relation to process monitoring approaches, a wide range of signal processing techniques such as fast Fourier transformations (FFT) [69], short time Fourier transformations (STFT) [131] and wavelet transformation (WT) [134] have been reported. These methods were mainly employed in monitoring ultra precision machining. However, these methodologies have rarely been studied especially in micro mechanical machining.

AE signals in micro milling are composed of continuous and spontaneously released transient elastic waves and have highly complex time and frequency characteristics. Due

to the stochastic nature of AE signals, the application of classical methods such as Fourier transform can give precise frequency information in a particular time setup which is very useful in identifying periodic phenomena and gauging their strength [133]. However, results do not adequately describe the transient features in terms of frequency resolution (they do not have the time component that represents when the particular event happened during the micro milling process). Although the STFT can be used to satisfy the problem of representing when a particular phenomenon occurred for such non-stationary signals, it suffers from the fact that the problem of resolution depends on appropriate length of the desired segment of the signal, which is needed for distinguishing the transient features. The main difference between FT and STFT is the window function (FT applied to a small section of the signal at a time). The window width is the key parameter in STFT that determines the spectral resolution and time localisation (a compromise between frequency and time domains is inevitable in choosing a window width).

Wavelet Transformation (WT) was carried out to overcome preset resolution deficiency of the STFT [130]. Essentially, it is a combination of time-frequency domain that makes it more promising approach for analysing highly variable AE patterns as present in the application considered here i.e. it adapts the length of the time window to various frequency bands present in the analysed signal. The high frequency components are evaluated in a short duration window to identify burst and distinct signal changes. Long duration windows are applied to track slow signal changes in low frequency bands.

The main feature of wavelet analysis is to extract information from the original signal by decomposing it into a series of approximations (lower frequency) and Details (higher frequency) distributed over different frequency bandwidths. In this analysis, discrete wavelet transformation (DWT) algorithm of MATLAB[®] wavelet toolbox was used to decompose the signal into five levels. The DWT divides the original AE signal into lower frequency and higher frequency bands. The lower frequency band serves as input signal for the next decomposition level; the information of the higher frequency signal is coded into detail coefficient of the signal. These coefficients represent degree of similarity between wavelet function and signal pattern. The total energy of the considered signal is preserved in this transformation. Therefore, band energy can be computed by integrating square of decomposed signal corresponding to particular frequency band with respect to time [149].

One way to study the effects of the process variables on the AE spectrum is to track signal power changes at different frequencies bandwidths. In 5.4.1 section of the chapter, the application of these signal processing techniques will be presented to identify dominant AE source mechanisms and the cutting state.

5.3.2 Taguchi method

Taguchi's experimental design was employed to find out the dominant contributing factors in size effect [150]. As evident from the reviewed literature, the size effect dominates the cutting mechanism in the ploughing zone. However, it is not clear what parameters significantly influence the extent of marked increase in specific AE energy, surface roughness and burr formation. In this context, the variables chosen for this study were, cutting velocity (V_c), ratio of undeformed chip thickness to cutting edge radius (f_z/r_e), axial depth of cut (a_p) and tool coating. The HSM cutting speeds guideline produced by Schulz and Moriwaki [151] was used to select cutting speed range so as to cover the conventional, transition and high speed regions.

Table 5.2 shows the summary of factors and levels set for the $L_9 (3^4)$ array. The main factors yielded seven degrees of freedom. The interaction effects between the process parameters were not considered here.

Table 5.2 Factors and their levels

Factors	Level 1	Level 2	Level 3
<i>Cutting Velocity (V_c) m/min</i>	10 (Conventional range)	25 (Transition range)	40 (HSM range)
<i>The ratio of undeformed chip thickness (f_z) to cutting edge radius (r_e) (f_z/r_e)</i>	0.4	0.6	0.8
<i>Axial depth of cut (a_p) μm</i>	30	60	90
<i>Tool coating (t_c)</i>	TiAlN	uncoated	-

An $L_9 (3^4)$ OA was constructed using dummy-level or pseudo-level technique. The tool coating factor level 1 (low) was repeated in place of level 3 (high) to the fourth (three-level) column of the array. The effect of the factor assigned to a column created this way will remain uncorrelated with all other factor effects because of the proportional frequencies criterion [150]. In the Taguchi method, repetitions are conducted to access the effect of noise on the outcome. In this study, the aim is to minimise specific AE

energy, surface roughness and burr size. Thus, “smaller the better” was selected as a strategy to determine the factor effect. In addition to “larger the better” was chosen to differentiate cutting parameter effects on different energy bands.

5.4 Results and discussions

Table 5.3 presents the cutting trial and partial data collected against the characteristics of interest on repeated run (output function). For accuracy, all outcomes were measured at two identical locations and averages of those values were used in the analysis. The data shows that size effect indicators (e.g. increases in specific energy, surface roughness or burr root thickness) intensify with decreasing undeformed chip thickness.

Table 5.3 Dummy-level technique on the $L_9 (3^4)$ array and measured outputs

Trial	Column				Specific AE energy ($V^2_{\text{integrated}}/\mu\text{m}^3$) x 10^{-6}		Surface roughness (μm)		Burr root thickness (μm)	
	V_c (m/min)	f_z/r_e	a_p (μm)	(t_c)	<i>obs.1</i>	<i>obs.2</i>	<i>obs.1</i>	<i>obs.2</i>	<i>obs.1</i>	<i>obs.2</i>
<i>t1</i>	10	0.4	30	TiAlN	11	9.1	0.069	0.093	8.6	13.4
<i>t2</i>	10	0.6	60	uncoated	4.0	4.0	0.094	0.091	6.3	3.9
<i>t3</i>	10	0.8	90	TiAlN	1.9	2.5	0.102	0.159	8.2	11.9
<i>t4</i>	25	0.4	60	TiAlN	69	59	0.104	0.078	6.3	9.3
<i>t5</i>	25	0.6	90	TiAlN	17	14	0.104	0.087	5.2	7.3
<i>t6</i>	25	0.8	30	uncoated	32	29	0.121	0.098	7.3	6.5
<i>t7</i>	40	0.4	90	uncoated	530	1600	0.126	0.145	8.3	7.5
<i>t8</i>	40	0.6	30	TiAlN	80	280	0.109	0.100	4.6	5.2
<i>t9</i>	40	0.8	60	TiAlN	67	140	0.167	0.151	3.3	6.0

5.4.1 AE signal spectral analysis

AE signals were collected on each investigated level. Some are shown with their respective $AE_{r.m.s}$ and power spectral density in Figs. 5.3 to 5.5 (all calculations were done using MATLAB®). The comparison between Figs. 3a, 4a and 5a clearly shows that cutting speed and chip load affects the three generated AE signals. The amplitude of the AE signals increases from peaks of 1.5, to 3 and 10V at 10, 25 and 40 m/min and depths of cut of 30, 60 and 90 microns respectively for f_z/r_e of 0.4. The AE signals at higher cutting speeds are consistently higher than lower speeds for both coated and uncoated tools at different undeformed chip thickness. The increase in AE signal with cutting speed has been observed in conventional milling operations [117]. This reflects

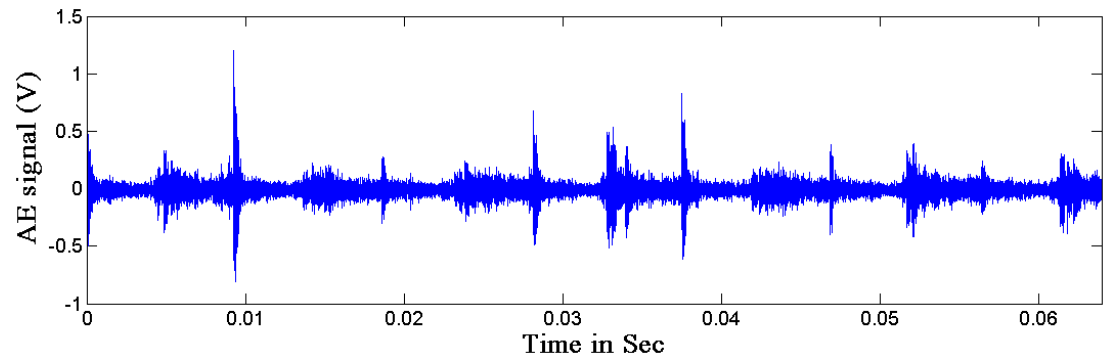
the strong dependence of AE signal on strain rate. Moreover, it also indicates the variations in AE amplitude with each tool rotation, which could be due to the differences in tool edge radius for the two flutes, radial runout, workpiece grain sizes, burr formation, chip detachment and source mechanisms between these conditions.

Typical trend of the $AE_{r.m.s}$ voltage of two flutes cutting during each cycle are shown in Figs. 5.3b, 5.4b and 5.5b. These trends show the high sensitivity of AE signal to the deformation and contact processes taking place during micro milling process. However, AE signatures do not exhibit the one-per-revolution periodicity expected from the kinematics of the process. Initially there is a peak, due to the impact and rubbing action at tool engagement and then the signal falls to a lower level during actual chip formation before the tool disengagement. A higher level of AE activity within the entrance (initial 60° of the tool rotation) and exit (last 30° of the tool rotation) for each cutting flute is seen in most of the cases. This reflects less severe tool-work contact conditions during tool exit (down milling mode) than entry (up milling mode). In general, these peaks can be associated with low cutting and high rubbing actions. However, the cyclic variations with the tool rotation were more distinct as cutting velocity increased.

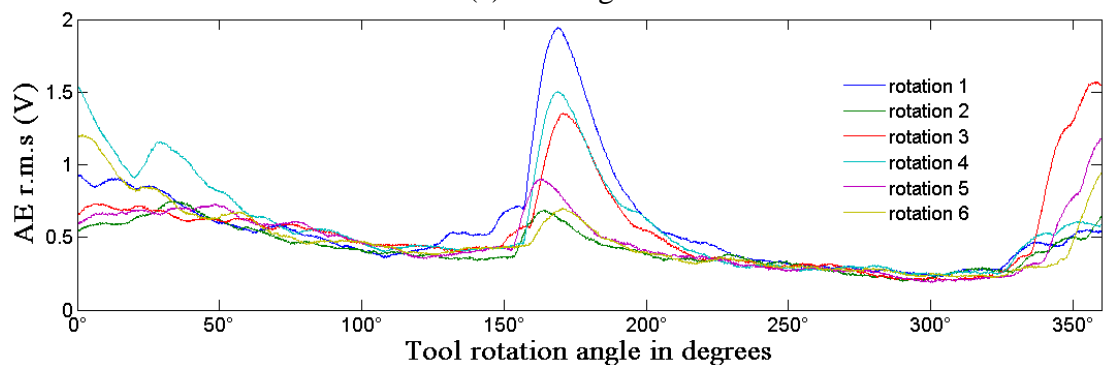
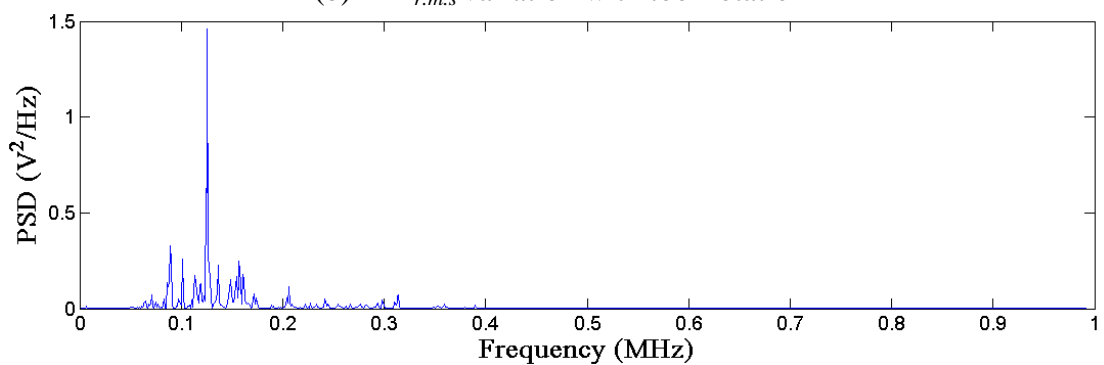
The trend indicates that micro cutting process undergoes two distinct stages in any one of the cycle which is analogues to cyclic force variation. It suggests that up to more than half way stage of the cycle, the tool and workpiece interact elastically, and the elastic strain energy in both work material and cutting edge increase to its maximum. Hence, induced strain rate will decrease due to the build up of elastic strain energy causing reduction in AE activity. In the latter stage of the cycle, due to formation of shear bands, the accumulated elastic strain energy is released. Therefore, sudden increase in induced strain rate will boost up the $AE_{r.m.s}$. Thus, $AE_{r.m.s}$ cyclic characteristics can be attributable to the formation of elastic strain induced shear bands and generation of saw tooth chips.

Figs. 5.3c, 5.4c and 5.5c shows the results of power spectrum density (PSD) of the example cases. In these graphs an increased level of activity approximately corresponding to a frequency of 125 kHz is indicated. Moreover, an increasing trend in the frequency's amplitudes with cutting velocity is visible. Energy concentration has been reported in macro-scale machining, centred around 125 kHz and 150 kHz, and varies with workpiece material and cutting conditions [131]. Moreover, these

frequencies corresponds to cleavage / micro-fracture (refer to Fig. 1). It is interesting to note that the amplitude increases at the higher cutting velocities. This suggests that less plastic flow is generated at higher cutting speed. In other words, the material removal mechanism is shifted from the “ductile mode” to the “brittle mode”.

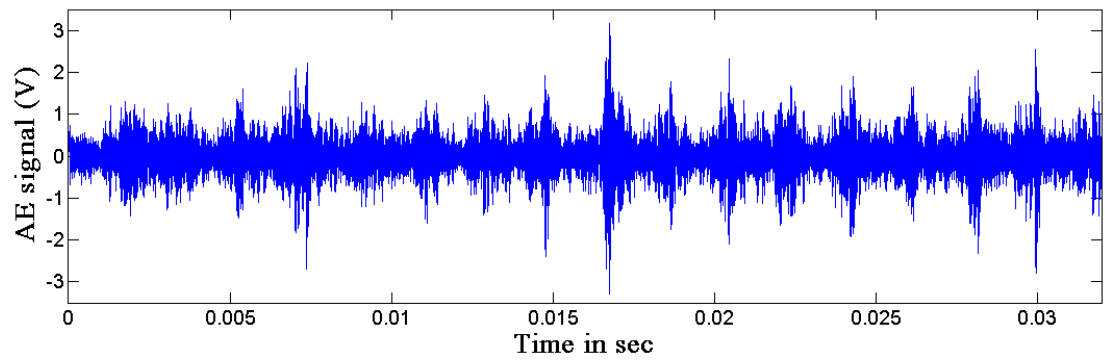


(a) AE signal

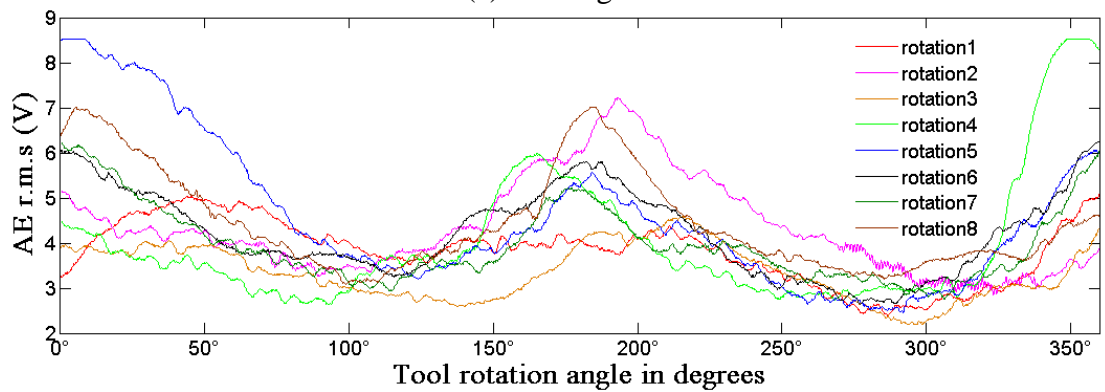
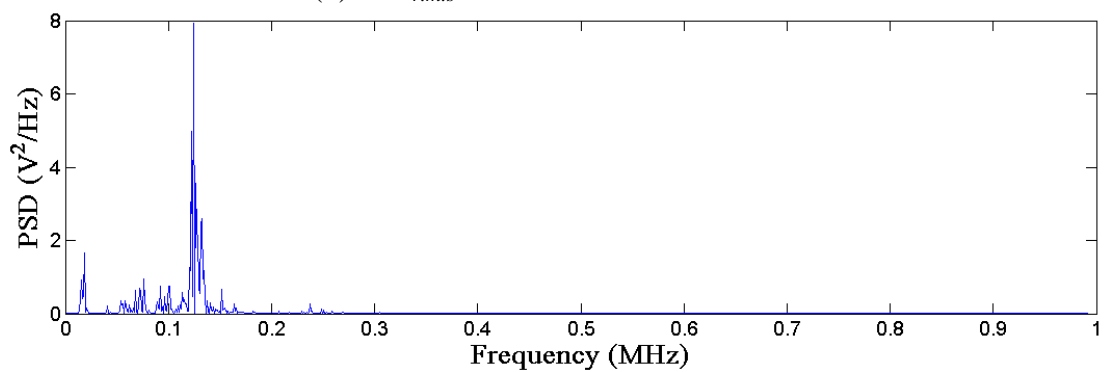
(b) $AE_{r.m.s}$ variation with tool rotation

(c) Power spectral density

Fig. 5.3 AE signal trends at $V_c = 10$ m/min; $f_z/r_e = 0.4$; $a_p = 30\mu\text{m}$; coated.



(a) AE signal

(b) $AE_{r.m.s}$ variation with tool rotation

(c) Power spectral density

Fig. 5.4 AE signal trends at $V_c = 25\text{m/min}$; $f_z/r_e = 0.4$; $a_p = 60\mu\text{m}$; uncoated.

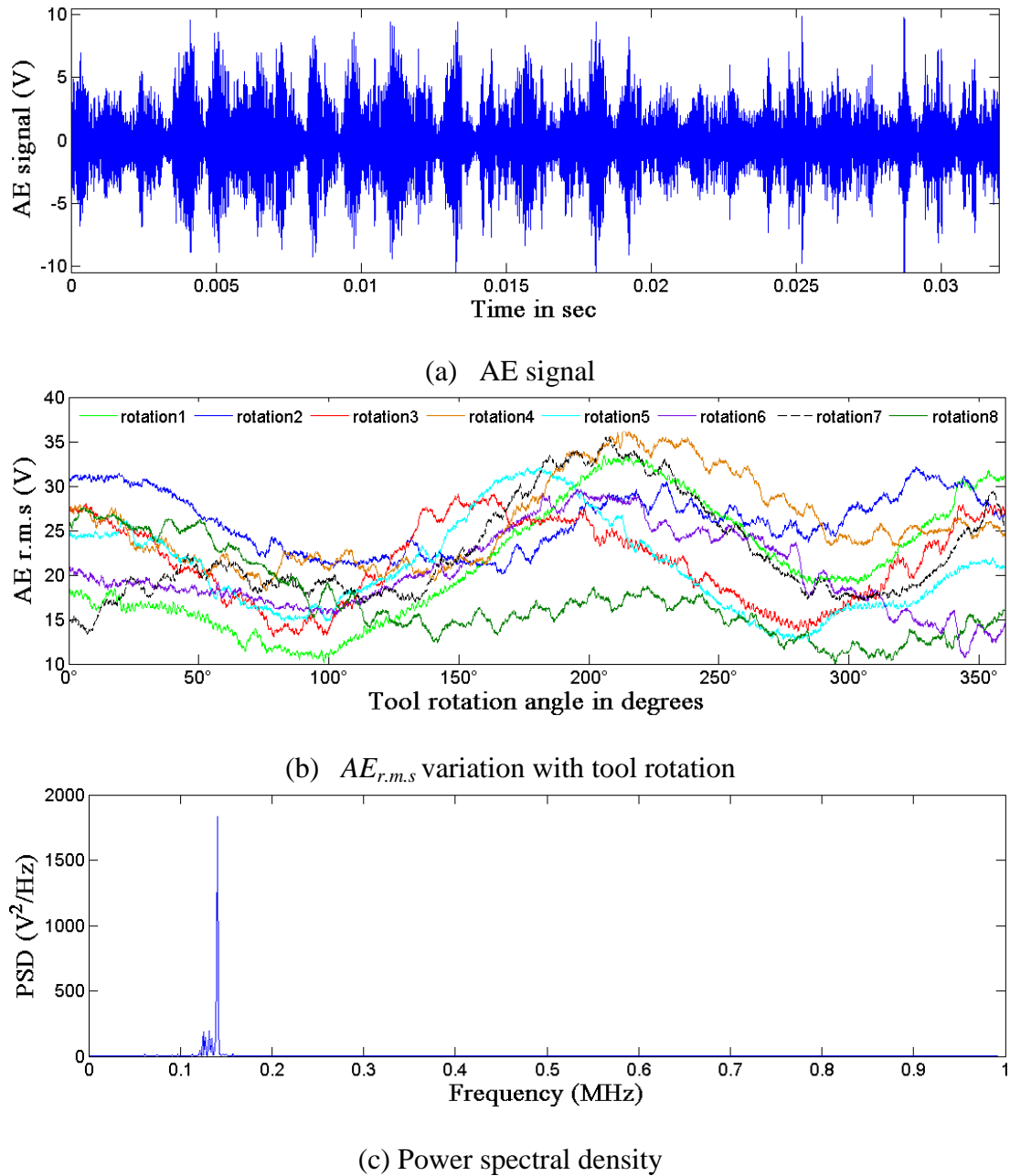
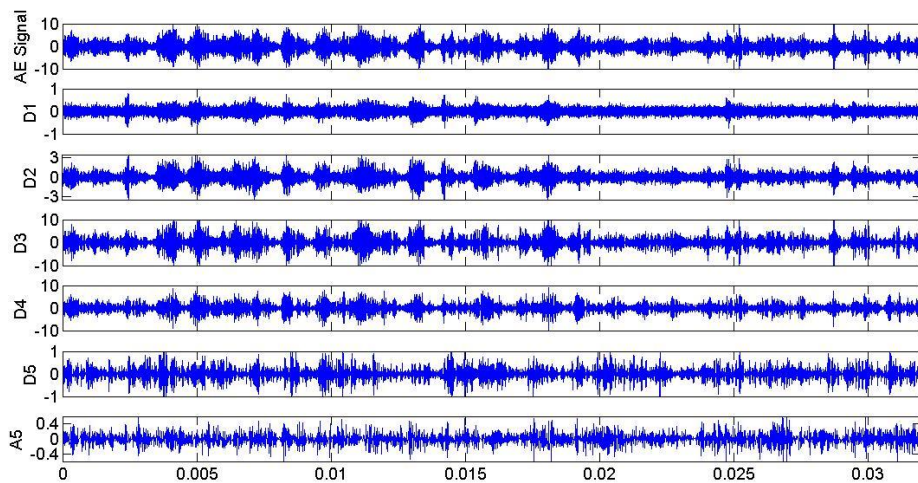


Fig. 5.5 AE signal trends at $V_c = 40$ m/min, $f_z/r_e = 0.4$, $a_p = 90$ μ m, coated

5.4.1.1 Energy analysis

The methodology described in section 5.3.1 was applied to analyse the AE signal obtained in each level of the array. The signals were decomposed to 5 levels with db3 wavelet. According to the wavelet decomposition method, the acquired AE signals (sampled at 2 MHz) were decomposed into the detail signals (D1-D5) and approximation signals (A5). Here, A5 belongs to the frequency bandwidth [0-32.25

kHz], and D1, D2, D3, D4 and D5 correspond to the frequency bandwidths [500-1000 kHz], [250-500 kHz], [125-250 kHz], [62.5-125 kHz], and [32.25-62.5 kHz], respectively. Taking an AE signal measured in trial 9 as an example, as shown in Fig. 5.6, in order to pinpoint the exact location of AE occurrences, wavelet coefficients of each scale of all the signals were reconstructed in the time domain. The signal voltage amplitudes in D3 and D4 (higher magnitudes of 4) are found to be dominant in the total AE spectrum as shown in the figure. Signal energies in other four frequency bands were comparatively small.



abscissa : time (sec), ordinate: amplitude (V)

Fig. 5.6 Wavelet decomposition at $V_c = 40$ m/min, $f_z/r_e = 0.4$, $a_p = 90$ μ m, uncoated

The band energy contribution of all decomposition levels in the respective total energy of each trial was plotted in Fig. 5.7 along with an enlarged view of D1 as energies monitored at this level were very weak. The D1 frequency band trend line indicates that the tendency of intergranular fracture decreases with increasing strain rate. It is also evident from the Fig. 5.7 that about 85 percent of the signal energy is distributed over D3 and D4 energy bands (frequency range is 62.5 kHz to 250 kHz in all investigated cutting trials). The magnitudes of energy contribution in D3 and D5 bandwidths generally have opposing trend with increase in cutting speed. Dominant frequency (measured from power spectral density) borders on upper and lower ends of D3 and D4

bandwidths respectively. Thus the increasing trend in the D3 bandwidth can be attributable to higher cleavage frequency due to increase in cutting speed. Moreover, the proportion of D3 also increase at lowest level of f_z/r_e ratio (trial no. t1, t4 and t7) at each investigated level of cutting velocity and this supports increase in cleavage/ micro fracture frequency as undeformed chip thickness decreases. The contribution of D4 bandwidth remains the same in the investigated cutting range.

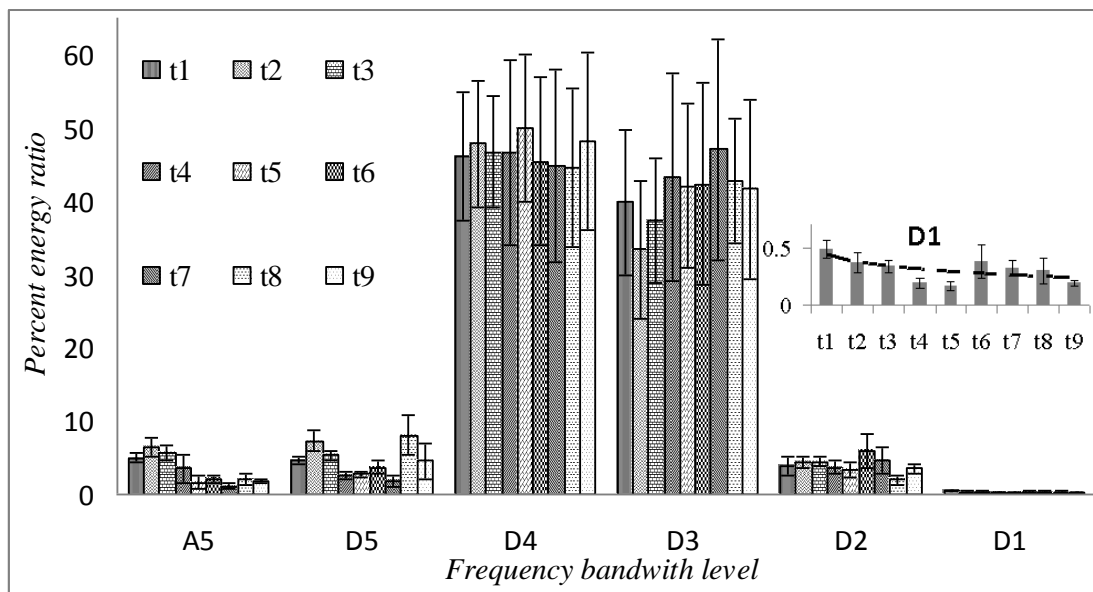


Fig. 5.7 Energy distribution in AE signal

5.4.2 Statistical analysis of factor dominance

Analysis of variance (ANOVA) was conducted to assess the significance of each process parameters on the micro machining process. The largest value of variance (F-ratio) represented the most influential factor on the output function. An F-ratio corresponding to 95 percent confidence level in evaluation of process parameters were considered significant if the measured values is higher than critical values $F_{0.05,1,17} = (4.45)$ and $F_{0.05,2,17} = (3.59)$ for 1 and 2 degree of freedom, respectively. Moreover, the residual due to random variations in the cutting tests, as shown in the tables, can be treated as the amount of variance likely to occur if none of the factors had any effect on the outcome.

5.4.2.1 Specific acoustic emission (AE) energy

Table 5.4 presented the ANOVA for specific cutting energy (which is the integrated voltage of AE filtered per tool rotation signal normalised by the material removed). The contribution ratio of the cutting velocity (25 %) and frictional condition (12 %) were statistically significant factors in these trials which affect the specific AE energy. This reflects the strong influence of strain rate in chip formation and relative velocity of rubbing interfaces on the AE signal generated during micro milling process.

Table 5.4 ANOVA for specific AE energy

<i>Source</i>	<i>Degree of freedom</i>	<i>Sum of square</i>	<i>Mean sum of square</i>	<i>F-ratio</i>	<i>Contribution ratio %</i>	<i>Result interpretation</i>
V_c	2	7.5E-07	3.7E-07	5.93	25	significant
f_z/r_e	2	4.3E-07	2.1E-07	3.41	12	not significant
a_p	2	3.6E-07	1.8E-07	2.84	9	not significant
t_c	1	3.8E-07	3.8E-07	6.00	12	significant
<i>Residual</i>	10	6.3E-07	6.3E-08		42	
<i>Total</i>	17	2.5E-06			100	

5.4.2.2 Surface roughness

Table 5.5 summarises the results of ANOVA on surface roughness. It shows that cutting velocity and ratio of undeformed chip thickness to cutting edge radius have significant effect on the surface roughness, accounting for 29 and 28 % of the total variability. Whereas, depth of cut and tool coating do not present statistical significance as the obtained value is less than the critical value in this case.

Table 5.5 ANOVA for surface finish

<i>Source</i>	<i>Degree of freedom</i>	<i>Sum of square</i>	<i>Mean sum of square</i>	<i>F-ratio</i>	<i>Contribution ratio %</i>	<i>Result interpretation</i>
V_c	2	4.5E-03	2.2E-03	7.31	29	significant
f_z/r_e	2	4.4E-03	2.2E-03	7.19	28	significant
a_p	2	1.6E-03	7.9E-04	2.55	7	not significant
t_c	1	1.6E-05	1.6E-05	0.05		not significant
<i>Residual</i>	10	9.1E+04	9.1E+03		36	
<i>Total</i>	17	6.5E+05			100	

Magnified images of slot floor machined at $f_z/r_e = 0.4$ were taken using non-contact optical profiler Wyko[®] NT 11000 as shown in Fig. 8 (a). While the tool grain size is

around 0.4 microns it is possible that the minor cutting edge on the base of the tool will re-machine the slot floor, thereby refining the surface cusps. Additionally due to the random location of irregular grains on the cutting tool it is possible to generate Ra values lower than the grain size of the cutting tool.

Notch-like marks lined up periodically along the tool rotation which can be seen on the slot floor. These marks are prominent for the higher cutting velocity of 40 m/min. At lower cutting velocity the $AE_{r.m.s}$ variation profiles are generally smooth. The distance between two consecutive notch-like marks for $V_c = 40$ m/min (19.1058 μm measured from extracted 2D profile across the slot as shown in Fig. 5.8 (b)) are also comparable with $AE_{r.m.s}$ cycle arc length (refer to Fig 5.8(b)). This also indicates that $AE_{r.m.s}$ has potential for online monitoring of the micro part surface finish.

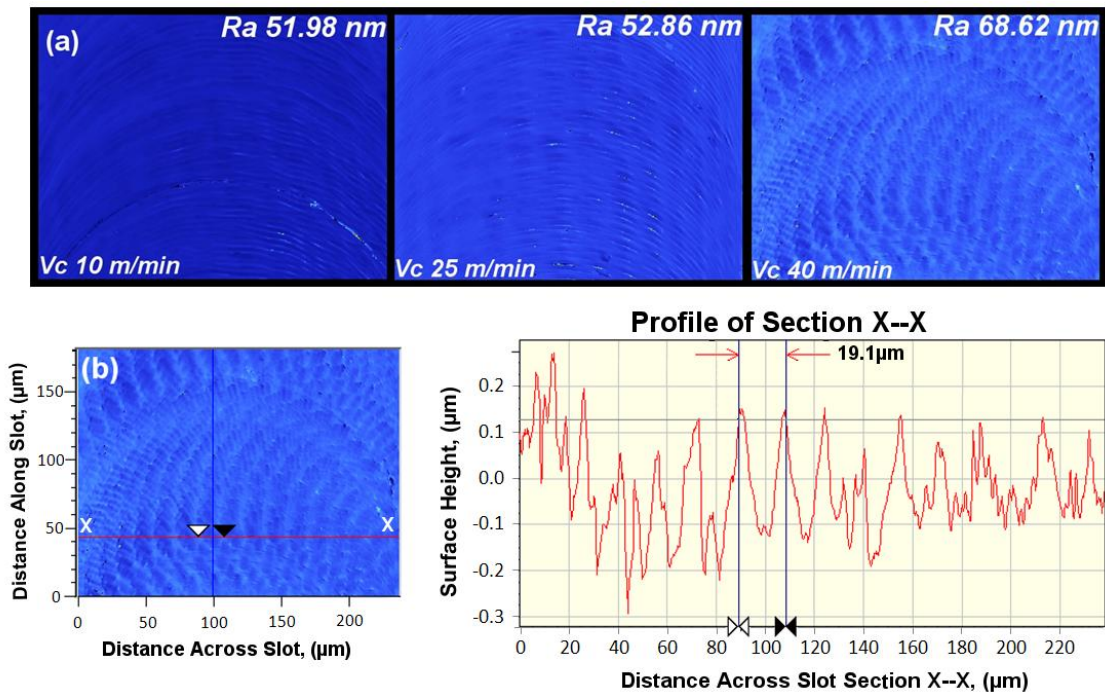


Fig. 5.8 (a) Topographical surface profile maps for $f_z/r_c = 0.4$ at cutting speeds of 10, 25 and 40m/min
(b) Sectional profile across slot width for 40m/min sample.

5.4.2.3 Burr formation

More uniform and relatively larger burrs were observed on the down-milled side of all the slots. The cross sections of the slots were embedded in the resin, polished and viewed under the SEM to measure down-milled side burr root thickness, considering the

worst case scenario. From table 5.6, it can be seen that the cutting velocity and ratio of undeformed chip thickness to cutting edge radius were the most important parameters in controlling the burr root thickness at 17 % and 26 % respectively.

Table 5.6 ANOVA for down-milled burr root thickness

<i>Source</i>	<i>Degree of freedom</i>	<i>Sum of square</i>	<i>Mean sum of square</i>	<i>F-ratio</i>	<i>Contribution ratio %</i>	<i>Result interpretation</i>
V_c	2	2.6E+01	1.3E+01	3.98	17	significant
F_z/r_e	2	3.6E+01	1.8E+01	5.61	26	significant
a_p	2	1.6E+01	8.0E+00	2.47	8	not significant
t_c	1	2.7E+00	2.7E+00	0.82		not significant
<i>Residual</i>	10	3.2E+01	3.2E+00		48	
<i>Total</i>	17	1.1E+02			100	

From the above analysis it can be inferred that cutting velocity and ratio of undeformed chip thickness to cutting edge radius influences process mechanism, burr root size and surface roughness. These factors are good indicators of the size effect in micro machining. At low undeformed chip thickness, due to ploughing effect the tool takes longer to start cutting. Whereas as at high values of feed/tooth the cutting action begins earlier, as a consequence the ploughing effect is reduced.

Fig. 5.9 shows BSE subsurface microstructure images of up-milled and down-milled side root of the same slot at each level of lowest feed/tooth. The nano-hardness in depth profile was taken at 0.5 μm indentation depth. The nano-indentation marks on the edge of the slots have been ignored to avoid the effects of lateral push of workpiece material into the resin. It should be noted that on the up-milled side in the ploughing mode (with subsequent microstructure change) the cut starts with zero undeformed chip thickness regardless of the cutting velocity. Similarly, at down-milled side, the undeformed chip thickness is always zero at exit, there is likely to be subsurface plastic deformation which eventually leads to burr formation. Interestingly, nano-hardness measurements exposed different patterns on both sides of the slots.

A relatively harder and brittle wall surface (Fig. 5.9) was observed at the entrance side (up-milled side). The harder surface also results in thin burrs being formed at the top of the up-milling side. Since the brittle material is being deformed into burrs, it breaks off more easily as compared with more ductile material available on the down milled side.

This explains the results obtained for the down-milled side, where thicker burrs were formed.

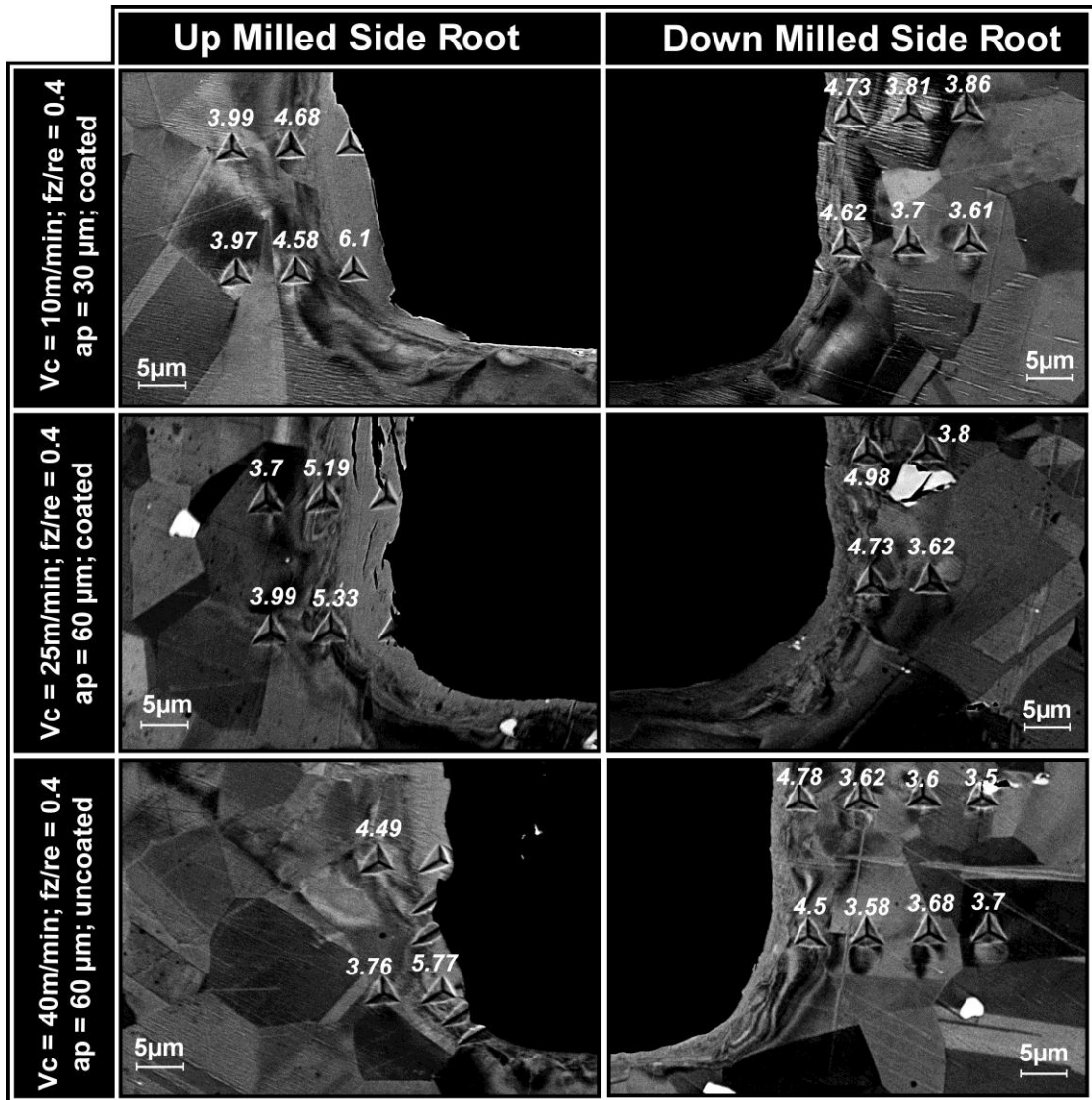


Fig. 5.9 Micro slots root subsurface microstructure and nano hardness (G Pa) variation

5.4.2.4 Energy bands and micro milling mechanism

In order to perform standardised comparison of the AE energy band measured at different cutting conditions, the calculated energy bands were normalised with respect to unit of material removed.

From Table 5.7, it can be recognised that all investigated factors present statistical significance on the D1 energy band (500-1000 kHz). Therefore, higher energy band can

be used to evaluate size effect. The increase in AE high frequency component to decrease in undeformed chip thickness has been observed in ultra precision machining [134]. This reflects the influence of inter-granular micro fracture as well as sliding or rubbing interface (tertiary deformation zone) on the high frequency range AE signal generated during micro machining. These results demonstrated that the lower limit of the feasible process window can be monitored by analysing high frequency energy spectrum.

Table 5.7 ANOVA for D1 energy band

<i>Source</i>	<i>Degree of freedom</i>	<i>Sum of square</i>	<i>Mean sum of square</i>	<i>F-ratio</i>	<i>Contribution ratio %</i>	<i>Result interpretation</i>
V_c	2	3.6E-12	1.8E-12	8.30	26	significant
f_z/r_e	2	2.4E-12	1.2E-12	5.40	16	significant
a_p	2	2.0E-12	9.9E-13	4.53	12	significant
t_c	1	2.2E-12	2.2E-12	10.25	16	significant
<i>Residual</i>	10	2.2E-12	2.2E-13		30	
<i>Total</i>	17	1.2E-11			100	

Table 5.8 shows that the contributions of the all factors were statistically significant at 95 % confidence level for D3. This suggests that low undeformed chip thickness in combination with high cutting speed support segmented formation of chips.

Table 5.8 ANOVA for D3 energy band

<i>Source</i>	<i>Degree of freedom</i>	<i>Sum of square</i>	<i>Mean sum of square</i>	<i>F-ratio</i>	<i>Contribution ratio %</i>	<i>Result interpretation</i>
V_c	2	1.8E-07	8.8E-08	6.60	23	significant
f_z/r_e	2	1.2E-07	5.9E-08	4.44	14	significant
a_p	2	1.0E-07	5.1E-08	3.83	12	significant
t_c	1	1.1E-07	1.1E-07	8.05	15	significant
<i>Residual</i>	10	1.3E-07	1.3E-08		36	
<i>Total</i>	17	6.4E-07			100	

From table 5.9, it can be inferred that cutting velocity was the only factor which encompass statistical and physical significance on the D5 energy band.

Table 5.9 ANOVA for D5 energy band

<i>Source</i>	<i>Degree of freedom</i>	<i>Sum of square</i>	<i>Mean sum of square</i>	<i>F-ratio</i>	<i>Contribution ratio %</i>	<i>Result interpretation</i>
V_c	2	5.7E-10	2.9E-10	6.73	43	significant
f_z/r_e	2	6.3E-11	3.1E-11	0.74		not significant
a_p	2	4.5E-11	2.2E-11	0.53		not significant
t_c	1	3.3E-11	3.3E-11	0.77		not significant
<i>Residual</i>	10	4.2E-10	4.2E-11		57	
<i>Total</i>	17	1.1E-09			100	

5.5 Optimum process parameters and confirmation tests

Signal to noise ratio (SNR) corresponding to each trial for AE specific energy, surface roughness, and burr root thickness was calculated to reveal optimum process parameters. It may be mentioned that SNR analysis takes into consideration the mean value at a given level as well as its repeatability in terms of standard deviation from the mean level. The evaluated optimal micro milling process settings for the selected outcomes are shown in Table 5.10 (additional information not contained in the chapter is given in Appendix C). The optimal condition to obtain best surface finish occurs at 0.6 (f_z/r_e), which can be attributed to the fact that below this threshold value, effects of minimum chip thickness are dominant, while above this level, feed marks assume dominance. This also shows that size effect is promoted when increasing cutting velocity or decreasing f_z/r_e ratio as evident from maximise specific AE energy settings.

In Taguchi analysis, a confirmation test is prerequisite to validate the minimisation or maximisation of the outcomes resulting from the optimisation process. Therefore, three confirmation tests were carried out for each response against the levels of their respective optimal process parameters to ensure repeatability. A summary of the cutting conditions and experimental results are given in Table 5.10. It is apparent from the presented data that the optimal conditions yields best results (better than the initial tests reported in Table 5.2) for their respective objective function. Furthermore, the best process performance in terms of surface roughness and burr formation are not essentially obtained at the same cutting conditions.

Table 5.10 Experimental results at optimal points

Objective function	Optimal process parameters				Experimental results					
	(V_c) (m/min)	(f_z/r_e)	(a_p) (μm)	Tool coating	Ra (μm)		Burr root thickness (μm)		Specific AE energy ($V^2_{\text{integrated}}/\mu\text{m}^3$) $\times 10^{-4}$	
					Ave.	error	Ave.	error	Ave.	error
Minimise surface roughness	25	0.6	30	coated	0.08	0.004	2.45	0.37	1.75	0.85
Minimise burr root thickness	40	0.6	60	uncoated	0.14	0.013	2.23	0.27	1.53	0.28
Maximise specific AE energy	40	0.4	30	uncoated	0.12	0.035	3.27	0.22	3.83	0.92

5.6 Conclusions

- The specific energy, burr root thickness and surface roughness of micro machined parts can be used as relevant measures of the size effect in micro machining.
- The wavelet transformation has a good resolution to extract energy bands related to the deformation mechanisms involved in the micro milling process.
- High frequency bandwidths in the AE signal as well as burr root thickness can be exploited to identify size effect phenomenon.
- More than 50 % of the AE signal was composed of micro-fracture frequency (approximately 125 kHz) in micro machining of inconel 718 at all cutting speeds. Therefore it can be considered as a dominant mechanism of material removal in micro-machining of such materials.
- The analysis of variance showed that the micro milling process is highly sensitive to residual effects. However, at 95 % confidence level, cutting velocity was found to be dominant parameter in for reducing the specific energy or improving surface finish.
- The ratio of feed per tooth to edge radius was the dominant parameter in reducing the burr root thickness.

- Decomposition of the AE signals showed that the cutting velocity is the most significant cutting variable for the intensity of different micro machining mechanism.
- The study suggests that other than the ratio of feed per tooth to tool edge radius, the cutting velocity is another dominant control factor for influencing the size effect or process mechanism. This information is important for optimising the process or for breaking the lower limit of the micro machining process.

Chapter 6

CHIP FORMATION IN MICRO-SCALE MILLING AND CORRELATION WITH ACOUSTIC EMISSION SIGNAL

Abstract

This work investigated the effects of different workpiece materials on chip formation and associated mechanisms in micro cutting. The Wavelet Transformation technique was used to decompose acoustic emission (AE) signals generated from orthogonal micro milling of different workpiece materials. This allowed studying energy levels corresponding to deformation mechanisms. Resulting chip forms were characterised. The results indicated that the computed energies of decomposed frequency bands can be positively correlated with chip morphology. The work provides significant and new knowledge on the utility and importance of AE signals in characterising chip formation in micro machining. Understanding chip formation mechanisms is important in managing the size effect in micro machining.

Keywords: Micro cutting, Acoustic emission, Chip morphology

6.1 Introduction

In macro scale machining, various methods have been used for the prediction of chip form. Examples are variation in cutting force, radiation from chips and acoustic emission (AE) [152]. Among the established techniques, AE monitoring has proven to have an advantage over other techniques as the AE generation is directly originating from plastic deformation or fracture in the cutting process [93, 118, 153].

A mechanism of saw tooth chip formation and discontinuous chip formation were identified by Uehara and Kanda based on AE signal analysis [119]. Dornfeld and co-workers suggested that the application of AE in micro-scale machining is even more useful as the source of AE is linked to material microstructure activities (inter-granular micro fracture, inclusions bursting, voids shearing or micro fracture) [28].

Typically micromachining is defined as a process of material removal that employs one or more geometrically defined cutting edges to produce features less than 999 μm [2]. In a situation where undeformed chip thickness is very low, material microstructure effect comes into play since in one instance grains may be pressed into the workpiece material, under the so called “minimum chip thickness phenomenon” [66], while some might be formed into a chip.

Surprisingly with few exceptions [126, 134], little attention has been paid to the application of AE for detection of chip formation modes in micro machining. In literature, strong experimental evidence of formation of shear bands in micro cutting has been reported [80, 82]. It has also been realised that variation in workpiece material considerably affect the deformation mechanisms in shear zones. In one study, the spacing of the shear fronts appeared greater in face-centered cubic materials as compared to body-centered cubic materials [80]. Simoneau et al suggested that continuous chip formation eventually give way to quasi-shear-extrusion chips as the uncut chip thickness becomes less than the average grain size of the smallest grain type in a medium carbon steel [32]. Material induced vibration was observed in micro cutting of single crystal aluminium where the variations in crystallographic orientation led to variations in cutting force [154]. Surface finish is influenced by the formation of shear bands [155] and cutting under the minimum chip thickness which increases rubbing between the tool and workpiece interface, compromising surface quality [9, 147].

Acoustic emission emanates from rapid release of elastic strain energy within a material under stress which radiates from the source to the surface of the work material [116]. The AE signals are composed of burst and continuous events. Burst AE is a qualitative description of the shorter, rapid rise time and high frequency signals produced by the individual events occurring within the material. Whereas, continuous AE is related to sustained, longer rise time and low frequency events of time-overlapping signals. In machining, both types of emission take place, with continuous AE signals generated

from primary, secondary and tertiary deformation zones and burst type occurring during chip breaking and tool chipping.

According to Shaw, at the micro scale, the chip formation mechanisms in ductile materials are essentially dominated by voids formation, crack propagation and rewelding [122]. When segmented chips are produced, combinations of void shearing and micro fracture activities occur as the chip segment pile up to its maximum thickness and this is then followed by partial or complete fracture. Komanduri and Brown stated four types of serrated chips in machining of metallic materials, namely (a) wavy chips, (b) catastrophic shear chip, (c) segmented chips and (d) discontinuous chips [88].

The literature review above shows that acoustic emission signals have been very important in inferring chip formation mechanisms in macro-scale cutting. However, little work has been undertaken to characterise the micro-scale cutting process. The focus of this work was on studying chip formation in micromachining and its correlation to AE activity. This was illustrated by investigating a range of workpiece materials.

6.2 Research methodology

In previous studies, by exploiting signal processing using various forms of wavelet transformation, aspects of machining were characterised and used for process diagnostics such as defining of machined surfaces form [156], chip form monitoring [157], cutting modes classification [134, 158], micro tool wear [159]. In this chapter, MATLAB[®] discrete wavelet transformation (DWT) algorithm was applied to split an AE signal into a low frequency component called the approximation (A) and high frequency component called the detail (D). The measured Detail acoustic AE energy was decomposed into five different frequency bandwidths with 3db wavelet of D1 [500-1000 kHz], D2 [250-500 kHz], D3 [125-250 kHz], D4 [62.5-125 kHz] and D5 [32.25-62.5 kHz]. The low frequency approximation signal was A5 with a range of 0 to 32.25 kHz.

The decomposition for each of the AE signals gives five D frequency band components which correspond to their source/mechanisms as shown in Fig. 1 [28]. Figure 6.1 aligns D1, D2, and D3 to intergranular micro fracture, inclusions, cleavage/micro fracture, respectively. Whereas, shearing micro voids are shown to occur in D4 and D5

frequencies. On each level, frequency band energy was computed and its relative contribution in the AE signal was obtained to correlate with observed chip forms. The total energy is preserved during this transformation [149]. AE signals were measured and chips were collected at similar interval for each investigated undeformed chip thickness. Thus, as a result chip forms were classified on the basis of the dominant frequency band present in the AE signal for a given workpiece material. Moreover, in order to interpret the material microstructure effect during chip formation, strain hardening severity was also evaluated from longitudinal chip section nano-hardness measurements.

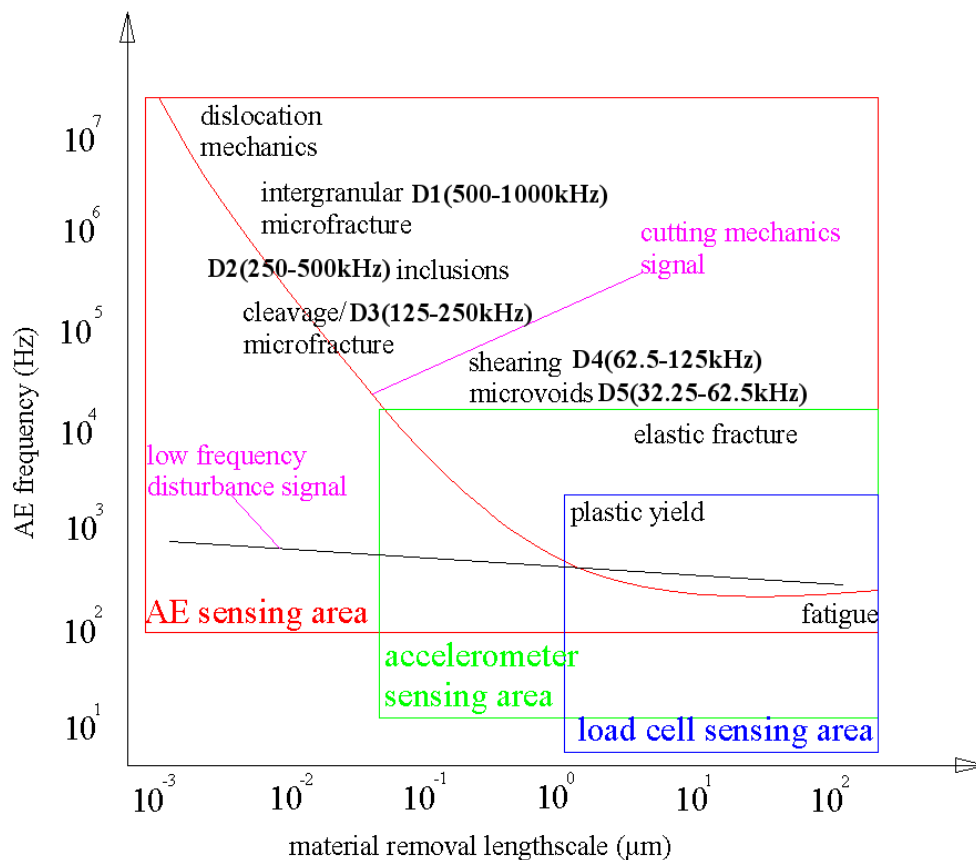


Fig. 6.1 AE source mechanisms (adapted from [28])

6.3 Micro milling experiments

Micro end milling tests were undertaken on a Mikron 400 HSM centre. Fig. 6.2 shows the setup for the experiment. Micro cutting was performed by using commercially available single straight flute uncoated end mills (Dixi-7060). The tool geometry and cutter engagement were selected so as to mimic orthogonal cutting. A single flute tool

with zero helix angle was used in an end milling operation. The height to thickness of the workpiece was controlled so that the bottom of the tool was cutting in free space which enabled only the straight part of the cutting edge to be engaged in orthogonal cutting mode. For each experiment a new cutting edge was used. Since tool edge radius is critical in controlling cutting modes in micromachining. The edge radius was measured for a batch of tools and found to be approximately $0.5 \pm 0.13 \mu\text{m}$. Up-milling was used and hence the chip load increased from zero to a maximum. The maximum undeformed chip thickness was varied from 0.02 to 10 μm in order to capture the characteristics of AE during different stages of the cutting process i.e. rubbing, ploughing and shearing. The lower value of 0.02 μm is 4 % of the tool edge radius and hence expected to fall within the minimum chip thickness regime as reported in literature [11, 27, 54, 76]. All the experiments were conducted in dry conditions. Six different workpiece materials were considered. The details of the cutting condition are shown in Table 6.1.

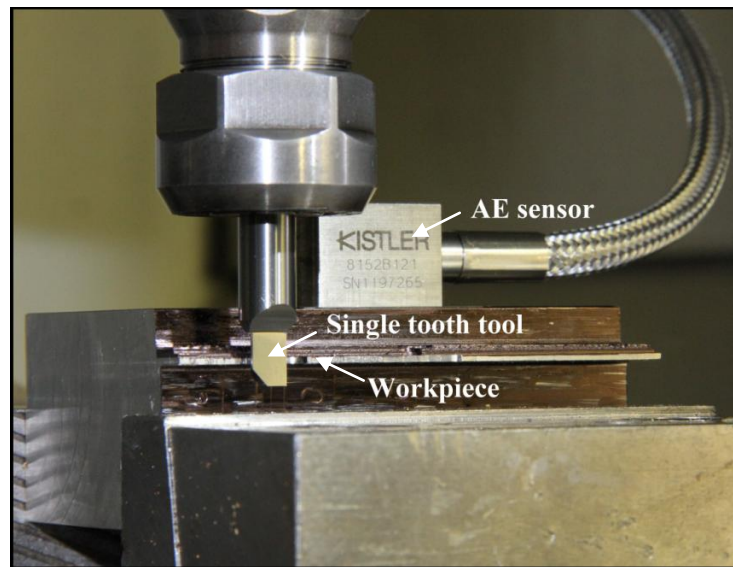


Fig. 6.2 Experimental set up

Table 6.1 Cutting parameters

<i>Tool</i>	Carbide, 1 tooth, 2mm and 6 mm diameter					
<i>Workpiece material</i>	Cu (OFHC)	Al 6082-T6	AISI 1005 steel	AISI 1045 steel	Ti-6Al-4V	Inconel 718
<i>Cutting velocity (m/min)</i>	94.2	94.2	94.2	94.2	50	25
<i>Maximum undeformed chip thickness (μm)</i>	0.02, 0.1, 0.5, 2, 10					
<i>Axial depth of cut (mm)</i>	1					
<i>Radial width of cut</i>	Half of the tool diameter					
<i>Mode of milling</i>	Up-milling under dry condition					

In micro domain machining, the material removal length scale is in the order of workpiece material grain size or tool edge radius, rendering each tool-workpiece combination unique. Keeping this in view, the grain size of different phases present in the workpiece materials was evaluated from optical micrographs shown in Fig. 6.3 and the linear intercept method was employed [136]. Additionally, an MTS nano-indenter[®] was used for the workpiece material characterisation. The average grain size, nano-hardness, elastic modulus measurements at 0.5 μm indentation depth and E/H ratio as a measure of tendency to plastic deformation of the test materials are given in Table 6.2.

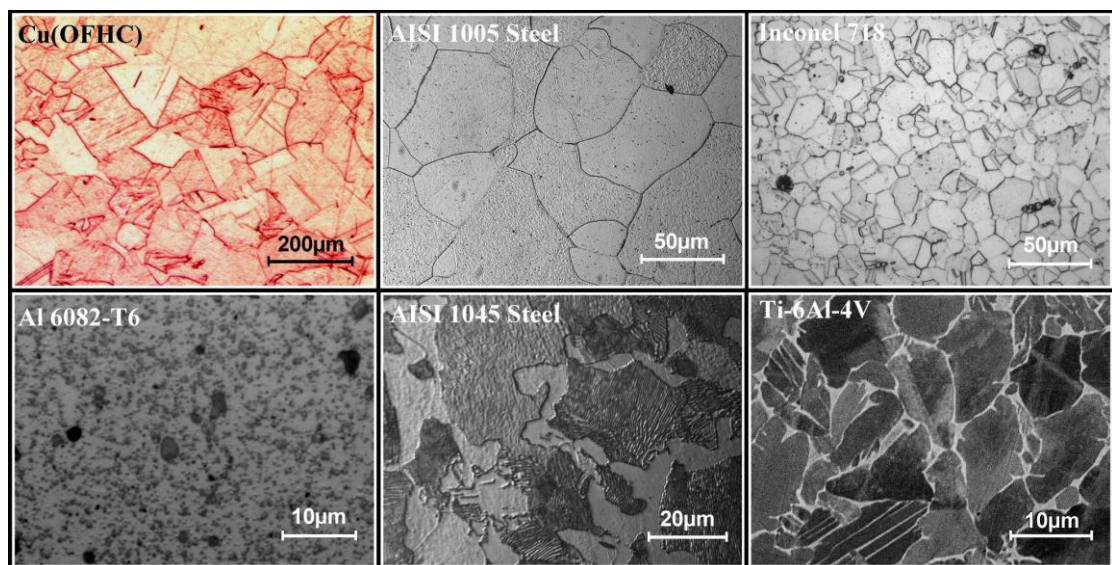


Fig. 6.3 Workpieces microstructure

Table 6.2 Workpiece material characterisation

<i>Workpiece material</i>	Cu (OFHC)	Al 6082-T6	AISI 1005 steel	AISI 1045 steel		Ti-6Al-4V	Inconel 718
<i>Etchant used to reveal microstructure</i>	5g FeCl ₃ , 10g HCl, 90 ml Methanol	Barker's reagent	Nital	Nital		Kroll's reagent	Kallings reagent
<i>Microstructure phases</i>			Ferrite	Pearlite	Ferrite		
<i>Average grain size (μm)</i>	135	-	70	52	7	12	16
<i>Nano-hardness (H in GPa)</i>	1.4	1.2	2.4	3.5		3.8	3.4
<i>Elastic modulus (E in GPa)</i>	127.2	73.5	233.1	241.5		134.0	221.0
<i>E/H ratio</i>	92.8	61.7	97.1	69.0		35.3	65.0
- means micrograph does not reveal grain size							

The E/H ratio of the workpieces display appreciable difference. The preliminary assumption can be made that AISI 1005 steel have a highest tendency to plastic deformation while Ti-6Al-4V fall at the lowest end as indicated in Table 2.

AE signals were sampled at 2MHz sampling rate covering a time span of about 0.64 ms using an AE sensor (Kistler 8152B121). The raw AE signal was pre-processed by an AE coupler (Kistler 5125) using bandpass filtered, 50 kHz to 1 MHz and then sent through a preamplifier at a gain of 20 dB to a data acquisition system. The acquired AE signals were recorded to Nicolet technologies Sigma 30 digital memory oscilloscope.

6.4 Results and discussions

Some of the interesting features of the material dependent chip formation at investigated feedrates are presented and discussed in this section.

6.4.1 Chip morphology

The examination of chip forms and types is an important index to understand metal removal in machining. Moreover, problems with surface finish, workpiece accuracy and tool life can be contributed by changes in the chip formation process.

6.4.1.1 Chip morphology below tool edge radius

At 0.02 $\mu\text{m}/\text{tooth}$, the selected undeformed chip thickness was less than the reported minimum chip thickness for different materials [11, 27, 76], the chips produced were much smaller than would be expected for a swept angle of 90° and radial width of cut (a_e) of 3 mm as shown in Fig. 6.4. At highly negative effective rake angle, it appears likely that the chip formation mechanism was closer to that in grinding. Moreover, the results obtained from previous research advocate a close similarity of grinding and micro machining for highly negative effective rake angle tools [70]. Figure 6.4 also shows a very dark colour for Ti-6Al-4V chips, suggesting that the burnishing effect on the chips. This is promoted by the high reactivity of titanium alloys and the high temperature that occur owing to poor thermal conductivity. The sparking and igniting of chips has already been attributed to high interface temperatures by previous researchers [160]. However, the titanium chips do not appear to be as small as other materials. The

images of titanium chips shown in Figure 6.5 appear to depict an agglomeration of multiple chips through welding. High cutting temperature and material build up could be drivers for the bonding. This supports findings by Barry et al [93] who reported a transition from periodic chips above $20 \mu\text{m}$ feed/tooth to a-periodic saw-tooth chip below this feed and finally continuous type chips when the chip load was in the order of a few microns.

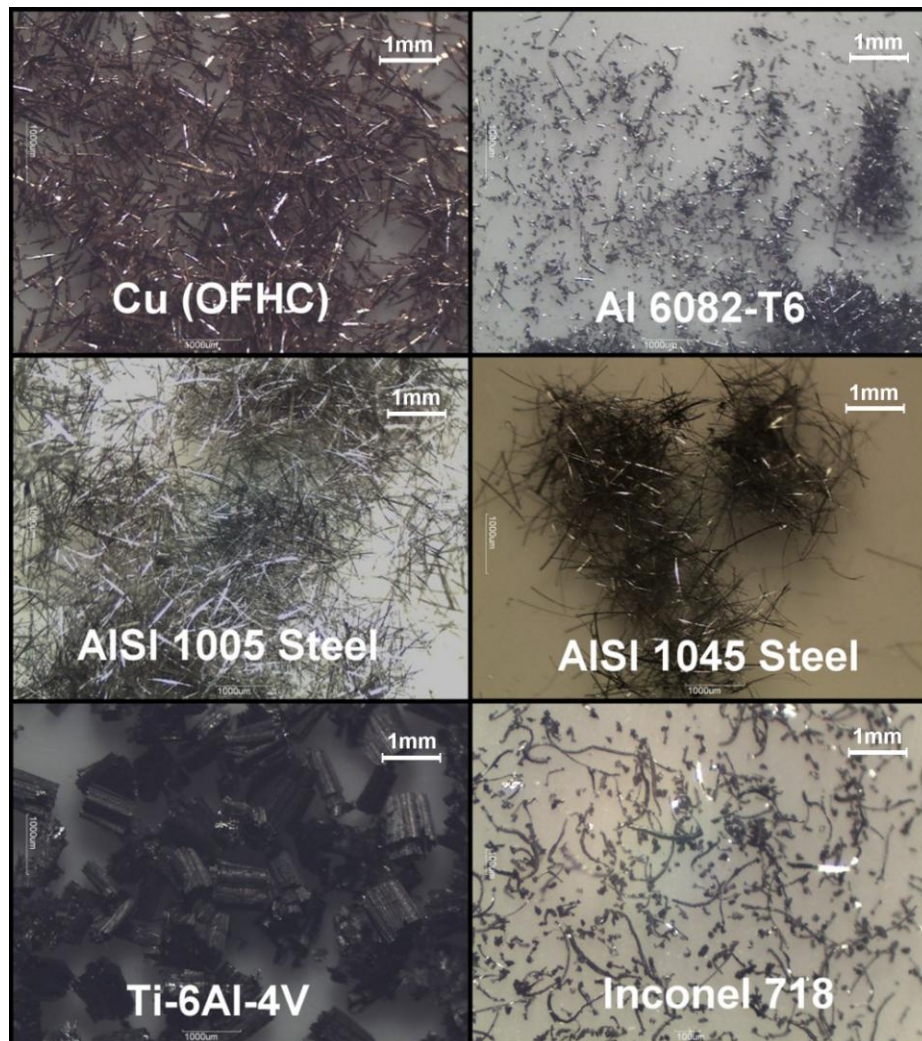


Fig. 6.4 Material dependent chip morphologies at $0.02 \mu\text{m}$ feed/tooth

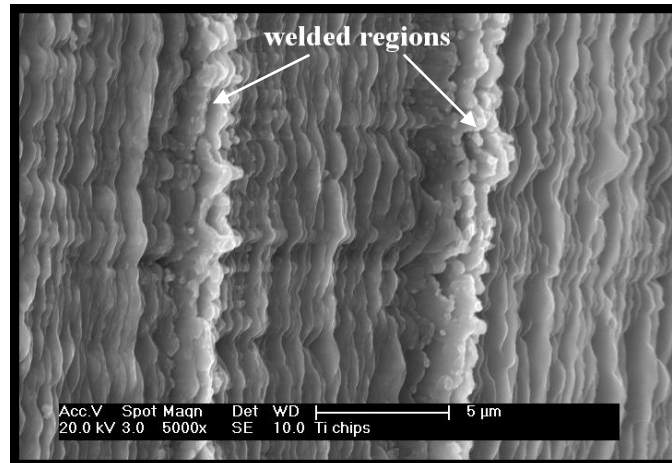


Fig. 6.5 Rewelding of titanium alloy chip at 0.02 μm feed/tooth

Energy dispersive X-ray spectroscopy line scans across the free surface of the titanium alloy chip were carried out on a Philips XL30 FEGSEM. The line scan data were processed to determine the empirical atomic constituents of Titanium (Ti), Aluminium (Al) and Vanadium (V) as shown in Fig 6.6. This revealed heavy presence of nitrogen on the chip. In addition, there was also a sizeable presence of carbon in the chip while the presence of other prospective environment derived reactants like oxygen was found to be negligible. The data show significant transfer of atmospheric nitrogen into the chip. The nitrogen could not originate from the tool since the cutting tool was not coated. The carbon found in the chip could have its source in the tool material, namely tungsten carbide or from carbon dioxide in air, or both. The ratio of the compositions recorded on the chip is closer to the compositions for $\text{TiN}_{0.6}$ to $\text{TiN}_{1.1}$ [161] and hence suggesting the possibility of the reaction occurring. The high temperature typically experienced in machining titanium alloys could be favourable for reactions to occur. Since titanium is reactive and miscible with tool materials, traces of tungsten and cobalt were observed in the chips.

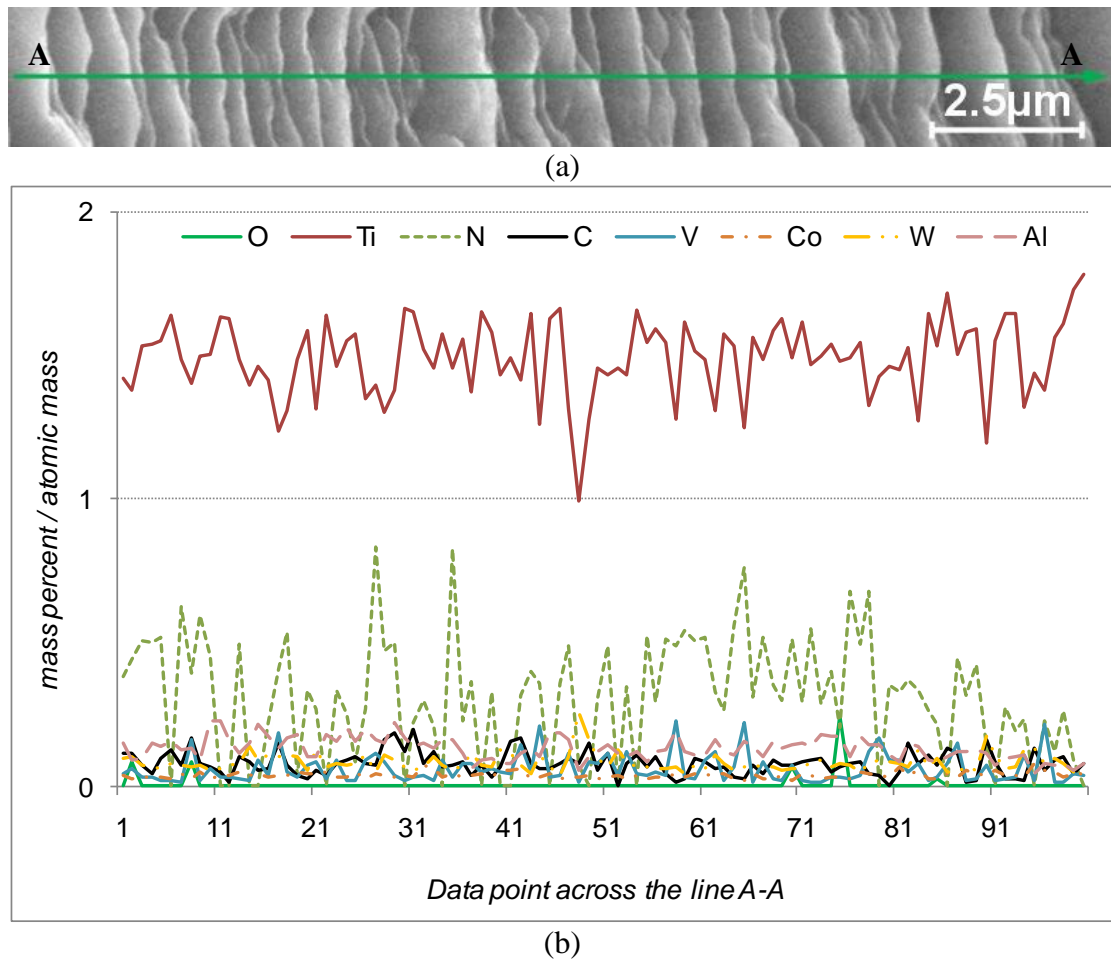


Fig. 6.6 Distribution of elements across line A-A (chip flow direction) on the free surface of Ti-6Al-4V generated at 0.02 μm feed/tooth (a) scanning line A-A on chip (b) Normalised element population

The chips for 0.1 μm/tooth chip load were closer in form to the ones at 0.02 μm/tooth since both are in the vicinity of the minimum chip thickness as reported in literature. For the above reason the chips at 0.1 μm/tooth are not shown in the results.

Fig. 6.7 shows the chips for different material produced at 0.5 μm undeformed chip thickness. The irregular size of the chips provide some evidence that the material will only be cut during the fraction of tool pass when sufficient material is accumulated above the minimum chip thickness.

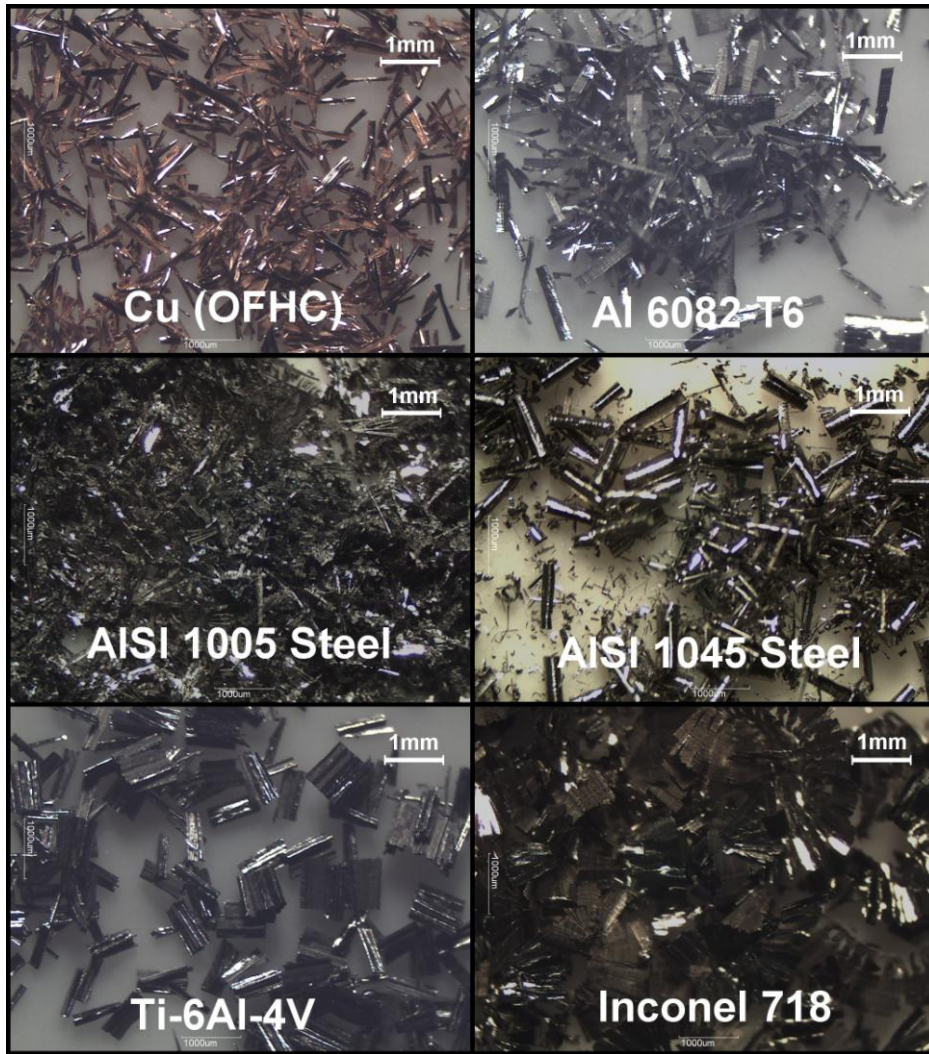


Fig. 6.7 Material dependent chip morphologies at 0.5 μm feed/tooth

The experimental evaluation of the chip size at lower undeformed chip thickness is challenging. The chips collected from machining trials at 0.5 μm undeformed chip thickness ranged dramatically in size and shape. Furthermore, due to chip segmentation it was difficult to determine where each segment originally came from.

To get a crude estimate of the chip size at 0.5 μm chip load, micro chip samples were prepared in MetPrep[®] Di-hard cold mounting resin. The micro chips of copper and AISI 1005 steel workpieces could not accurately be positioned due to a smaller size and hence they were excluded from this analysis. The samples were ground and polished on Presi[®] Mechatec 334 polishing machine. Grinding was carried out with grit sizes of 600 and 1200 for a very short period considering the fragility of the chips. Polishing was done with 9, 6 and 1 μm finishing slurry. The optical images of examined chips are shown in Fig. 6.8. The comparison of these images reveals that titanium produces

thinner chips. The precise quantification of the chip size is affected by the fact that the orientation of the chip is difficult to ascertain.

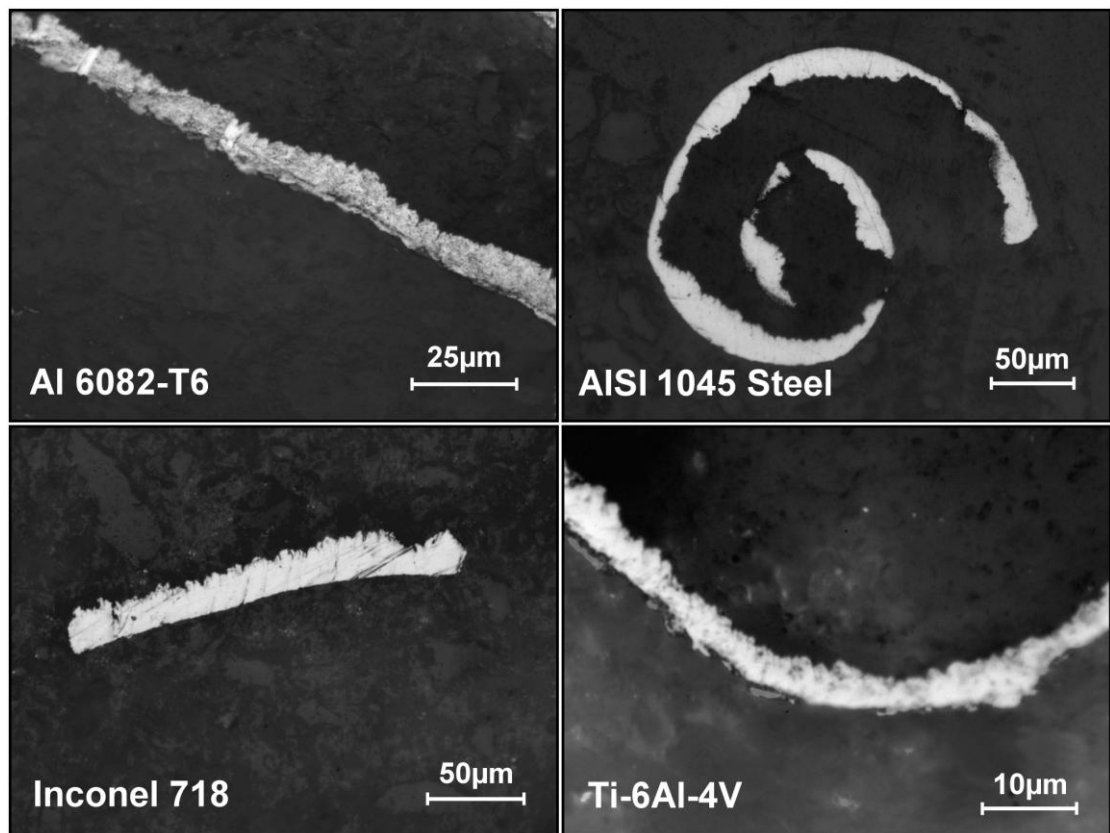


Fig. 6.8 Typical chip side views at 0.5 μm maximum undeformed chip thickness

The chip thickness 10 μm undeformed chip thickness can be estimated from Figure 6.11.

6.4.1.2 Chip morphology above tool edge radius

At higher feedrate 2 and 10 μm/tooth, chip forms were dimensionally similar to what would be usual in shearing dominated process except for discontinuous copper chips as shown in Figs. 6.9 and 6.10 respectively. Cutting parameters, workpiece material, heat flux, contact phenomenon and tool-work frictional characteristics are some of the critical parameters which will determine the chip form.

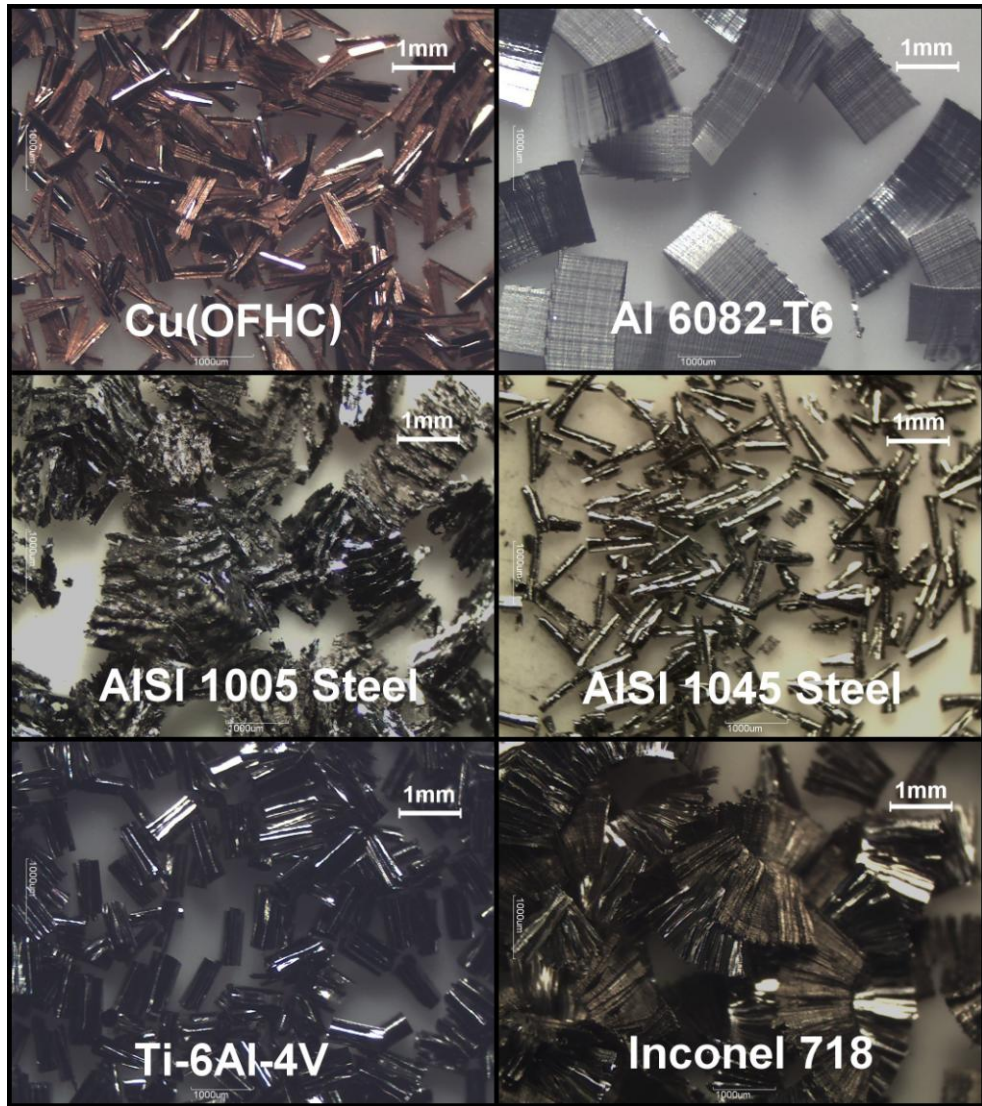


Fig. 6.9 Material dependent chip morphologies at 2 µm feed/tooth

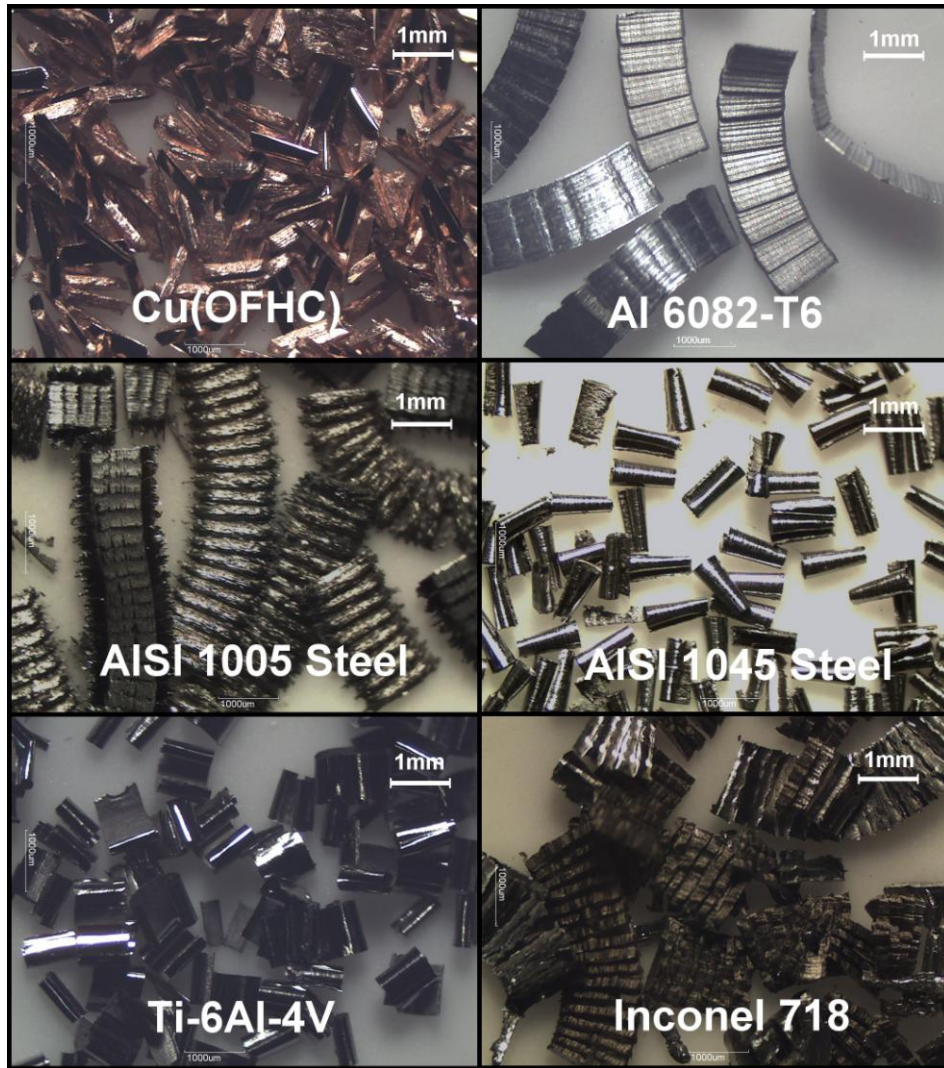


Fig. 6.10 Material dependent chip morphologies at 10 μm feed/tooth

The chip cross sections obtained from orthogonal milling tests at 10 μm maximum undeformed chip thickness were examined. Direct comparison of the deformed chip thickness SEM images (Fig. 6.11) clearly shows that the workpiece material has a significant effect on chip types. The periodic undulations along the periphery of the free surface of the chips can be commonly observed in all micrographs.

In terms of chip types at an undeformed chip thickness much higher than tool edge radius, copper showed discontinuous chips. The aluminium workpiece material exhibited wavy chips with no evidence of shear localisation. The chip thickness variation was quite diverse for ferrous materials at the same cutting speed. The chip thickness of the AISI 1045 steel was found to be more uniform and considerably lower than the maximum segment thickness of AISI 1005 steel. The higher segmentation of AISI 1005 steel was characterised by large strains leading to micro crack formation in

the shear zone and stick-slip friction on the tool face [88]. The comparison of these two types of steel chips suggests that altering the material microstructure phases can significantly reduce chip segmentation. Inconel 718 alloy showed segmented chips at 25 m/min cutting velocity. The deformed chip segment shows close resemblance to the macro-scale machining of the workpiece material alloy at approximately six times higher cutting speed (> 150 m/min) [95]. This suggests that the intensity of elevated temperature in micro domain cutting. The workpiece of titanium alloy yielded shear localised chips at cutting velocity of 50 m/min, in conformance with the earlier research [94].

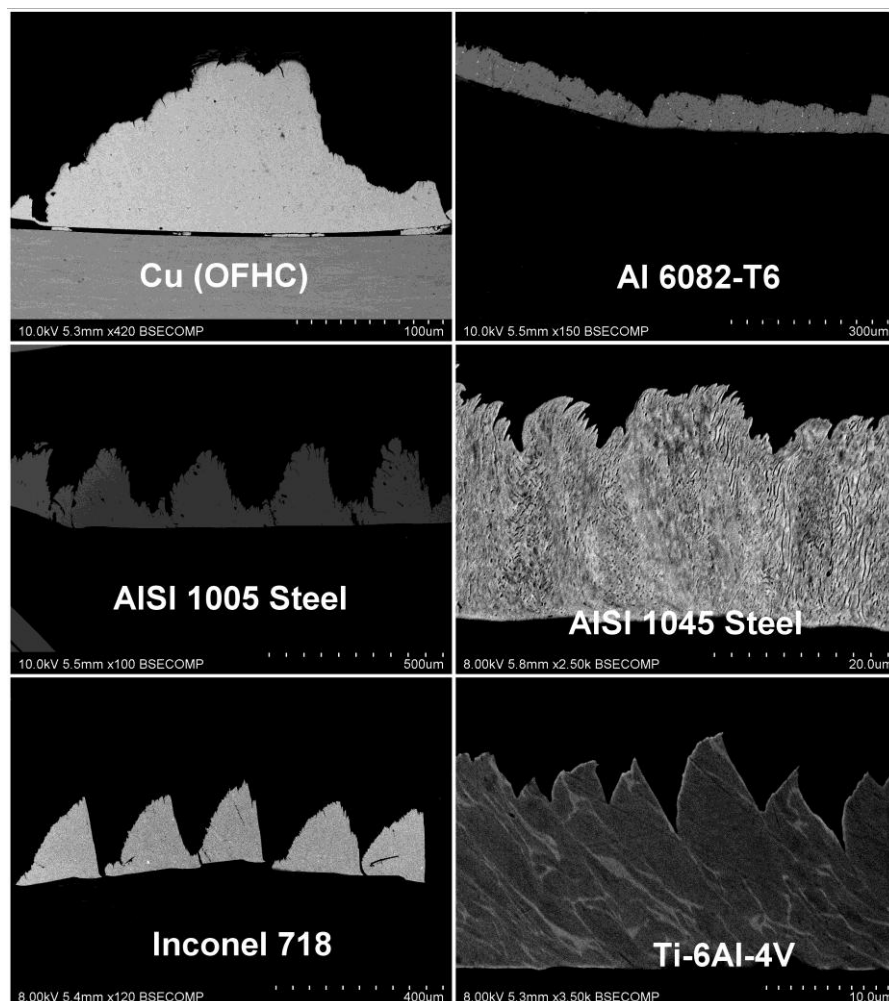


Fig. 6.11 Material dependent chip types at 10 μ m maximum undeformed chip thickness

In order to investigate the presence of high and low plastic deformation zones in the chip section of each workpiece material, nano-hardness measurements were carried out

at 0.5 μm indentation depth as shown in Fig. 6.12. The measured nano-hardness values were greater than the initial hardness of their respective bulk material. The results indicated that copper (OFHC), aluminium alloy (Al6082-T6), single phase steel (AISI 1005 steel) and inconel 718 alloy chip section nano-hardness profiles were more uniform than dual phase steel (AISI 1045 steel) and titanium alloy (Ti-6Al-4V). In the latter cases the inhomogeneous plastic flow inside the chip due to microstructure phases distribution for AISI 1045 steel or formation of very narrow shear localised zones for titanium are likely to be responsible for the variation in nano-hardness. While in former workpiece materials the consistent distribution of nano-hardness indicates a homogenous plastic flow. However, increase in chip segmentation in Inconel 718 followed by AISI 1005 steel and Al6082-T6 shows a compromise between decreases in the strength of the work material due to localised temperature rise and an increased strength as a result of work hardening.

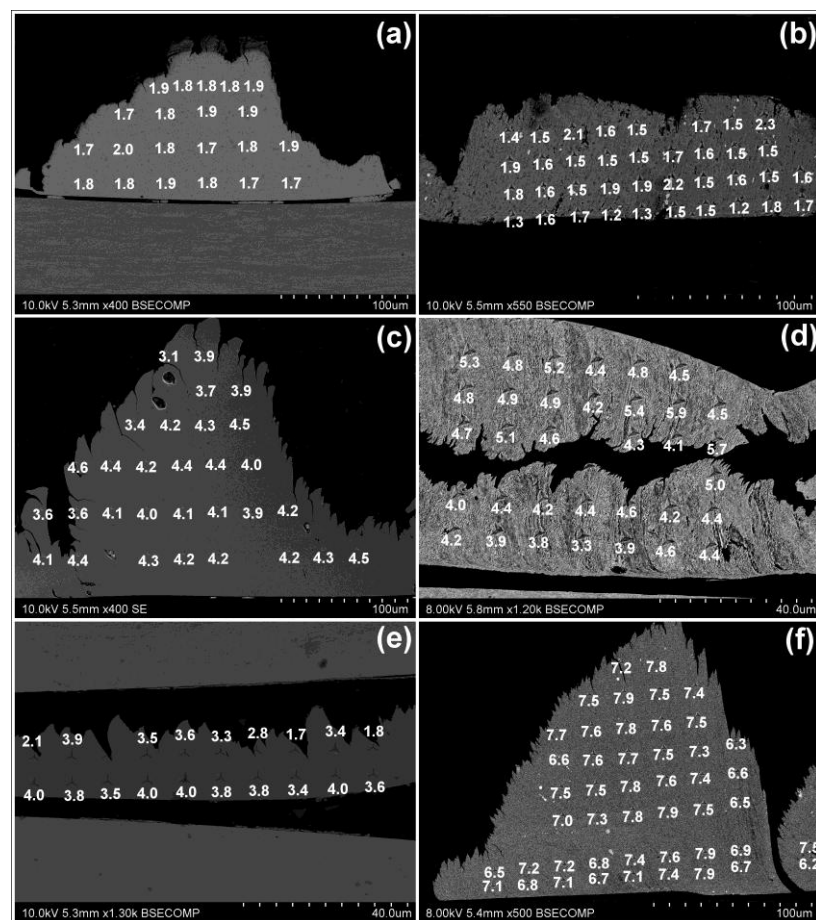


Fig.6.12 Nano hardness (H_{chip} in G Pa) distribution in chip cross section of
 (a) Cu (OFHC) (b) Al 6082-t6 (c) AISI 1005 steel (d) AISI 1045 steel
 (e) Ti-6Al-4V (f) Inconel 718

For further confirmation of the role of workpiece material, the difference in nano-hardness measurements of the chip and initial hardness of the bulk material was normalised by dividing it with the initial hardness of the bulk material, and used as a measure of work hardening severity. Figure 6.13 summarises the influence of workpiece material on the work hardening severity owing to micro machining at $10\ \mu\text{m}$ /tooth undeformed chip thickness. The most worked hardened chips were for Inconel 718 followed by the AISI 1005 steel, AISI 1045 steel, Cu (OFHC), Al6082-T6 and Ti-6Al-4V. This in a way could be a league table of the micro machinability challenge that will be introduced by the size effect. In micro machining if the workpiece material modified surface layers work hardens this means that the selected undeformed chip thickness will be critical as chip thickness smaller than the width of the work hardened zone will be associated with cutting of harder material.

The degree of chip hardening when compared for the two steel types is consistent with the previous research [162] and Table 6.2. However, when comparing all the workpiece materials tested, the measure of tendency to plastic deformation as reported by Nakayama [78] (E/H ratio as shown in Table 6.2) is not robust for all engineering materials for the assessment of their relative machinability.

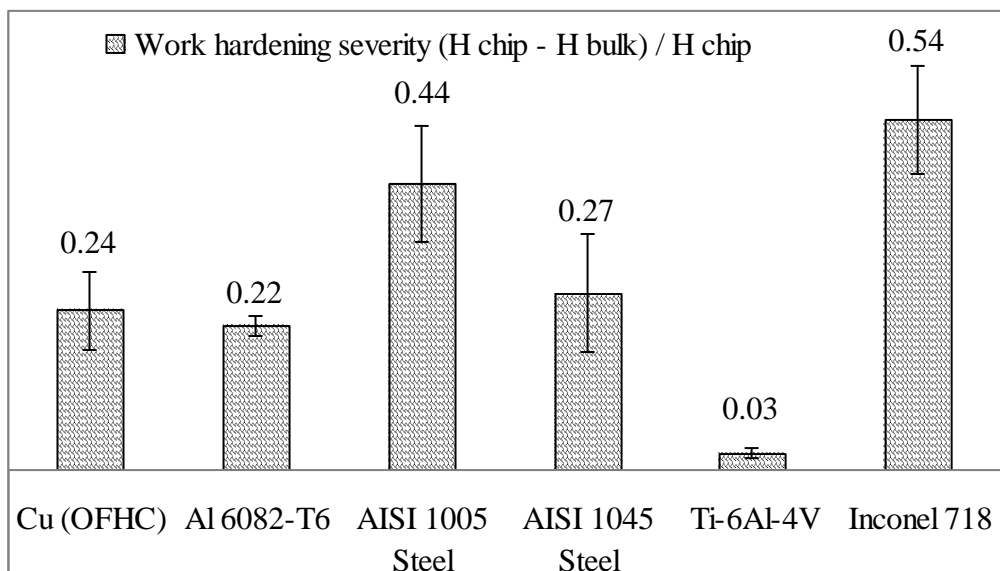


Fig. 6.13 Work hardening severity for different materials

Although there was obvious differences between the chips obtained from the micro cutting of different materials, characterisation of AE signal was made to better identify the cutting mechanisms.

6.4.2 Acoustic emission in micro cutting

These results are based on three to six repeated measurements on all workpiece material with identical process parameters. The error bars shown in the figures were obtained from standard error calculated from the measured data. When error bars are not visible, they are hidden by the marker size on the plot.

6.4.2.1 AE and chip formation

Typical contribution of AE decomposed frequency bands during the micro machining of different workpieces at $10\ \mu\text{m}$ maximum undeformed chip thickness is presented in Fig. 6.14. Up to 85 percent of the AE energy is accounted for by D3 and D4 frequency bands. This supports the results in Figure 6.11 for copper, AISI 1005 steel and Inconel 718 alloy where segmentation was associated with periodic fracture. In contrast, higher contribution of D4 for aluminium and titanium workpieces indicated that fracture does not seem to be a dominant phenomenon. The contribution of both frequency bands was evenly balanced for multi phase AISI 1045 steel. Thus, a direct association between the chip deformation mechanisms of the different workpiece material with their respective decomposed AE energy bands is proposed.

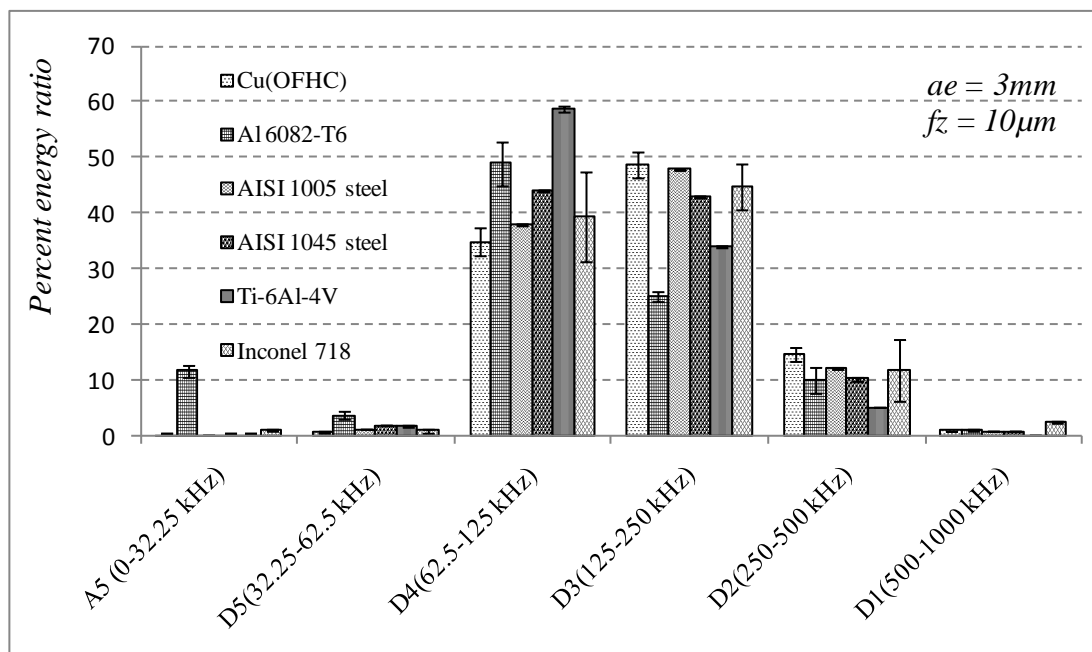
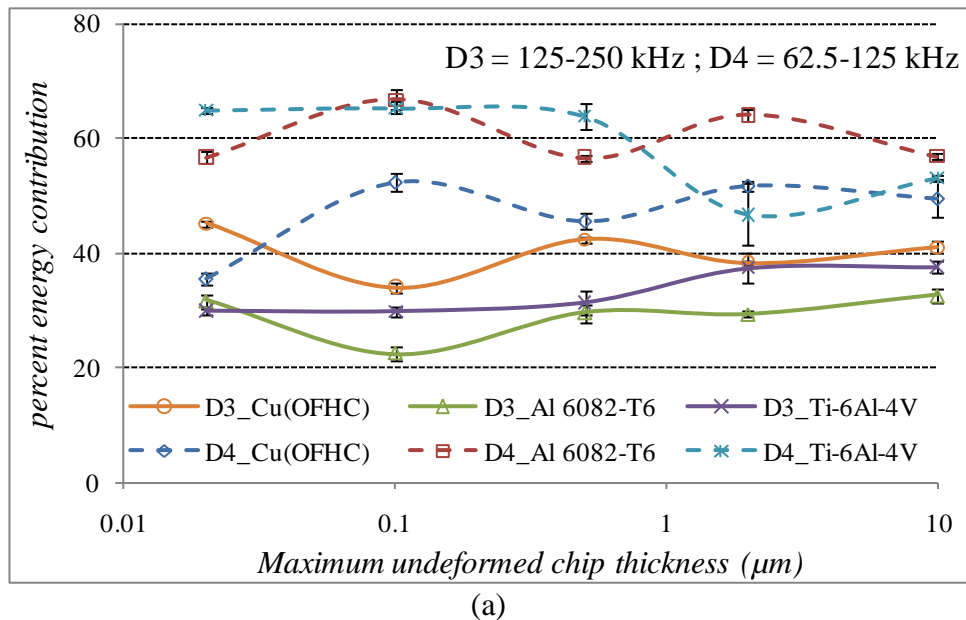
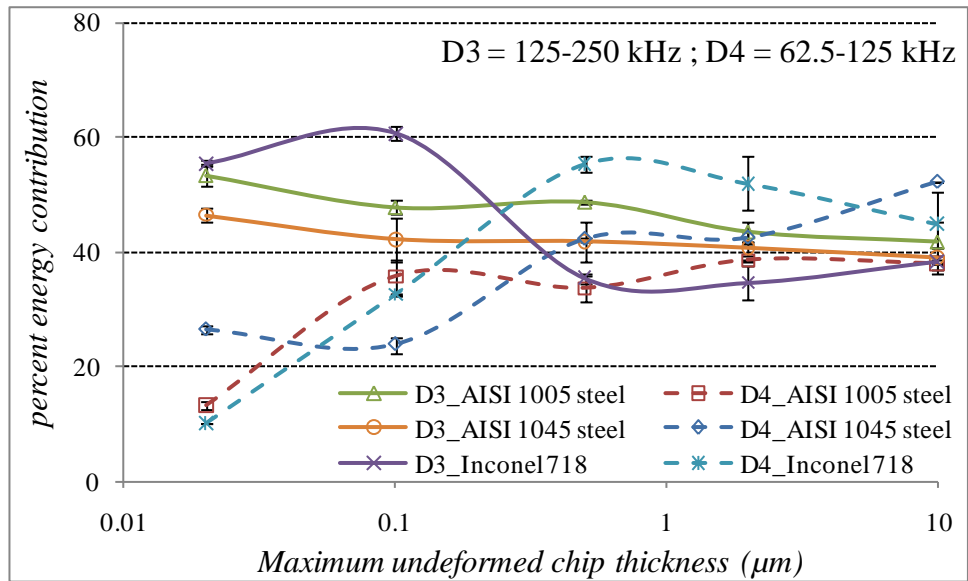


Fig. 6.14 AE Energy distribution for different workpiece material

The energy contribution of D3 and D4 frequency bands in AE signal at 1 mm radial width of cut and feed per tooth ranging from 0.02 to 10 μm are shown in Fig. 6.15. The investigated workpiece materials were divided into two groups. Fig. 6.15 (a) shows the input of D4 and D3 frequency bands in AE signals for copper, aluminium and Ti-6Al-4V workpiece material. The trends suggest that the contribution of D4 frequency band was higher than that of the D3 frequency band for discontinuous, transitional and shear localised chips. However, Fig. 6.15 (b) depicts that the involvement of D4 frequency band in AE signal decreases at low undeformed chip thickness for single and multiphase steel as well as nickel base alloy. This proposes that the proportion of fractures increases at the lower end of the feed range which can be attributable to decrease in fracture toughness at low undeformed chip thickness [163]. Also, Davis et al [164] observed a marked decrease in chip segment spacing with decreasing uncut chip thickness. These results reveal that the materials having a higher work hardening severity were more prone to fracture at micro scale machining conditions. Moreover, it also suggests the benchmarking of these two energy bands can be used to assess the cutting state of a particular workpiece material.





(b)

Fig. 6.15 D3 and D4 frequency bandwidths percent energy contribution at different maximum undeformed chip thickness for (a) Non ferrous materials and titanium alloy
(b) Ferrous materials and nickel alloy

The chips were examined in a back scatter electron (BSE) microscopy mode and results are shown in Fig. 6.16. The comparison of lamellae on the free surface of the chip reveals that the thickness of the sticking region was decreased by lowering the undeformed chip thickness. The pitch is also not constant across the width for all workpiece material indicative of the inhomogeneous strain distribution in the chip. Moreover, sliding interface (by comparing solid line arrow mark with a dotted line arrow for given workpiece) appeared to be increasing with decreasing undeformed chip thickness for copper, AISI 1005 steel and Inconel 718. The increase in the thinner section of the chip caused the lamellae to disintegrate in more work hardened materials at low undeformed chip thickness as can be clearly seen in Fig. 6.16. As already reported by Komanduri and Turkovich [94] for titanium alloys there is intimate contact between the newly formed chip and the tool rake face, therefore sticking would be the dominant phenomenon in the contact region. As a result, chips do not breakup even at the lowest undeformed chip thickness investigated.

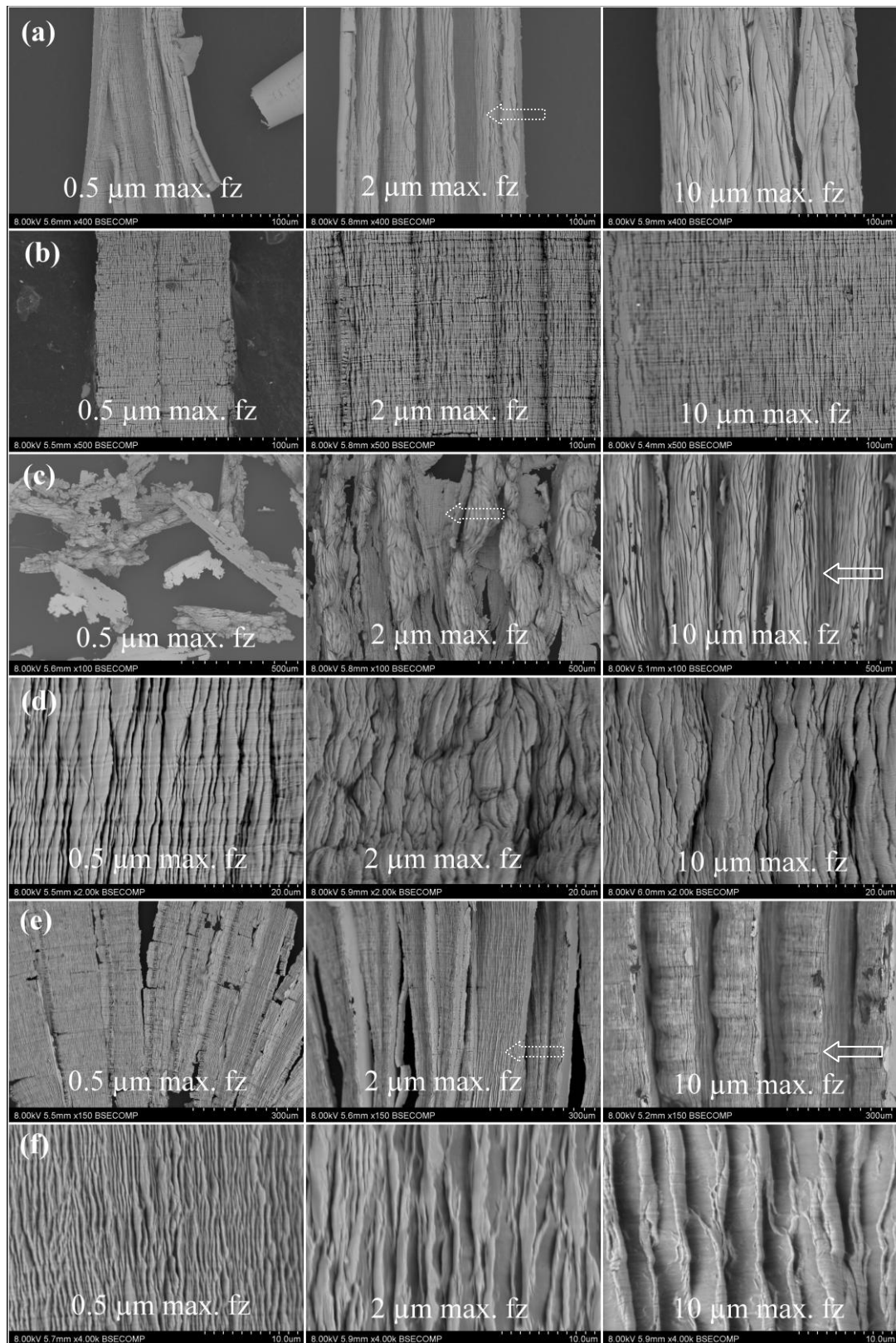


Fig. 6.16 Typical lamellae on the free surface of micro chips produced at different undeformed chip thickness in row (top to bottom) (a) Cu (OFHC) (b) Al 6082-T6 (c) AISI 1005 steel (d) AISI 1045 steel (e) Inconel 718 (f) Ti-6Al-4V

The sticking and sliding region were distinguished from examination of the chip underside contact phenomenon tracks. Fig. 6.17 show the stick slip tracks of Inconel 718 alloy and AISI 1005 steel attributable to their inherent tendency to adhere on the tool rake face. Close examination reveals that pile up stage of the chip segment corresponds to the sticking region and the stage of sudden return of plastic zone towards the tool corresponds to the sliding region. This phenomenon of stick-slip friction on the rake face leading to relaxation oscillations resulting in chip segmentation was similar to AISI 1015 steel as observed by Komanduri and Brown [88]. From these tracks sticking and sliding was quantified for different workpiece materials as shown in Fig. 6.18. The trends showed that sliding contact increases at low undeformed chip thickness. This information is important in defining contact schemes in Finite Element (FE) simulation of the micro machining process.

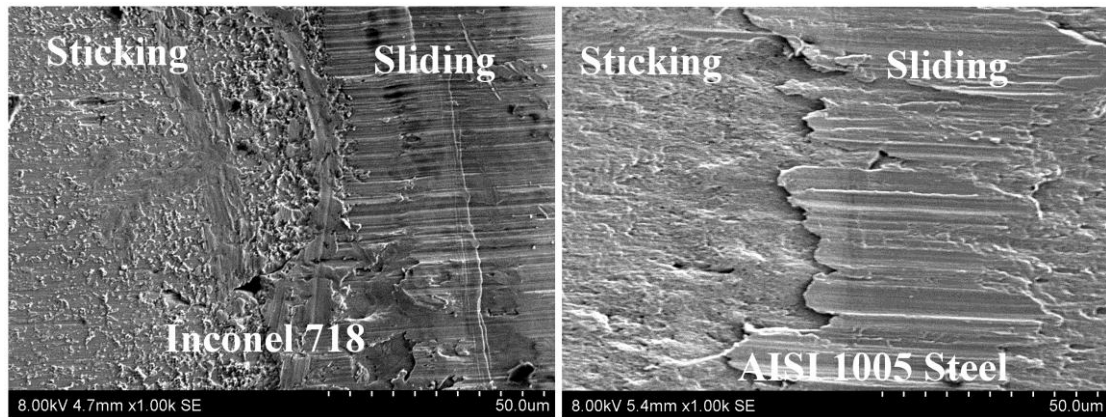


Fig. 6.17 Stick-slip tracks on underside of chip at 10 μm maximum undeformed chip thickness

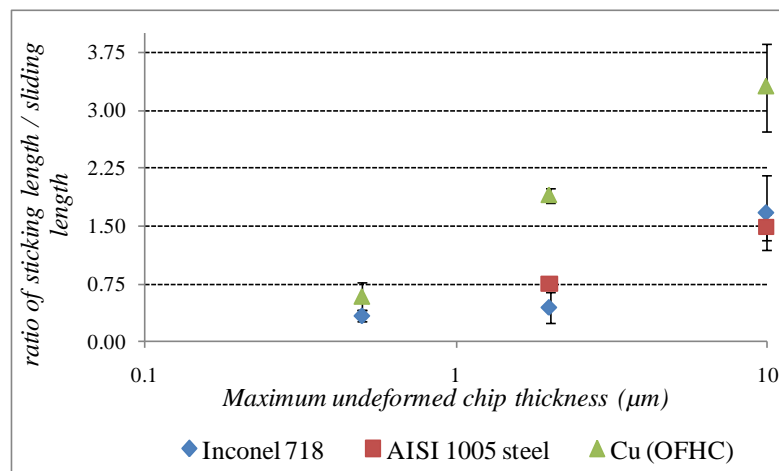


Fig. 6.18 Variation in stick-slip interface at different uncut chip thickness

6.4.2.2 Specific AE energy

Figure 6.19 shows the relationship between specific AE energy (activity) and maximum undeformed chip thickness for a radial width of cut of 1 and 3 μm for all workpiece materials. The illustrated specific AE energy is the integrated voltage of AE filtered signal normalised by the volume of material removed. The value was largest when machining approaches the lowest investigated maximum undeformed chip thickness. The influence of the cutting edge radius becomes significant with decreasing undeformed chip thickness, since a larger portion of the undeformed chip thickness will be machined with a negative effective rake angle. Furthermore, workpiece material shear flow stress increases at low undeformed chip thickness [32]. These trends are in agreement with earlier research by Dornfeld and co-workers [134], who reported that AE root mean square signals could be positively correlated with associated change in energy dissipation in shear zones. The AE signal represent the phenomenon of transient elastic-wave generation due to a rapid release of strain energy caused by a structural alteration in a solid material while specific cutting energy is the shear energy per unit volume. The correlation is reasonable because the two represent the process mechanism and its associated energy. The findings support confirm the relationship available in literature that specific cutting energy increases when the undeformed chip thickness approaches tool edge radius or below [39, 44]. Difference in the magnitude of both curves is attributable to the increase in ratio of undeformed chip thickness to width of cut. However, a more steady and identical state is reached above tool edge radius in which hardly any further increase can be observed for all workpieces in the both cases.

The energy level of AE signal was reported to be dependent on strain rates of shear deformation, yield strength of workpiece material and volume of deformation zone [165]. Similar to the previous research, this research also showed that the AE energy of difficult to machine materials (inconel 718 and single phase steel) falls on the higher end of the spectrum and is dominated by micro-fracture instead of shearing. The effect of materials' microstructure on the specific AE and micro machining process appears to be evident through the mechanism of chip formation. The higher consumption of specific AE energy means that machinability of these materials should be more difficult than expected for removing smaller amounts of material. The results also showed that material having a higher work hardening index were associated with dominant fracture mechanisms for chip formation. This confirms the utility of analysing AE energy bands

to predict the mechanics of the chip formation process for micromachining of different workpiece materials.

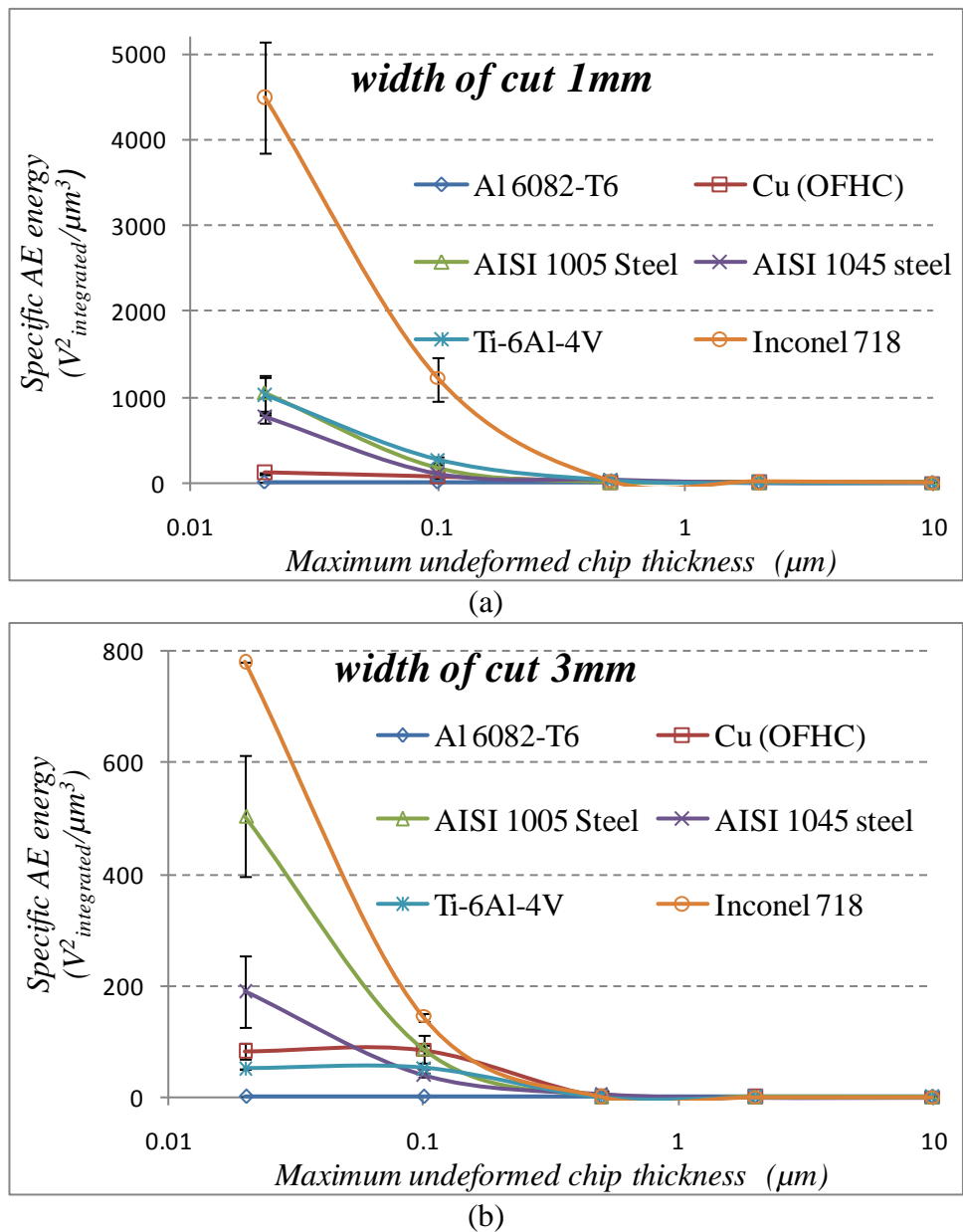


Fig. 6.19 Relationship between specific AE energy and maximum undeformed chip thickness (a) for a 1 mm and (b) 3 mm width of cut

6.5 Conclusions

Study of chip morphologies in combination with signal processing technique revealed the feasibility of acoustic emission as a technique for material dependent chip form detection in micro cutting. On the basis of results obtained the following conclusions were drawn:

- In the micro cutting process, the ratio between unit of material removed and size of tool edge radius controls the resultant chip morphology for specific workpiece materials. Formation of chips through shear mechanism was evident at feed/tooth equal to and above the tool edge radius.
- In most cases, the material microstructure dependent chip cross sections at the upper limit of the investigated range were quite similar to those reported in macro cutting. This suggests that the cutting modes are driven by the size of the tool edge radius in micro mechanical machining.
- Decomposed AE energy bands (using wavelet transformation) can be used to identify micro fracture and shearing micro voids micromachining chip formation mechanisms.
- Specific AE energy (activity) increases as the ratio of the undeformed chip thickness to width of cut increases.
- Stick-slip friction at the tool chip interface has been identified from chips generated in micro machining. The sticking interface of the segment was found to decrease with reduced chip thickness.
- Nano-hardness measurements show that the chip body is at higher hardness compared to the bulk material and hence the extent of plastic deformation permeates the whole chip. This full permeation of plastic deformation is usually not the case in macro scale machining.
- The pearlite phase is reported to be responsible for control of chip segmentation in ferrous materials. However, the results for non ferrous and difficult to cut materials indicate that material microstructure is not the only consideration in chip segmentation. In micromachining intense deformation in a narrow region in

the primary deformation zone and/or formation of stick slip region on tool rake face are factors which assist in shear localisation for titanium alloys. This also influences material pile-up and resistance to deformation and leading to formation of cyclic chip segments for single phase steel, Inconel and copper alloy.

- In microscale machining materials with a higher work hardening severity for the chip were associated with dominant micro fracture chip formation mechanisms.

Chapter 7

ESTIMATION OF MINIMUM CHIP THICKNESS IN MICRO MILLING USING ACOUSTIC EMISSION

Abstract: In micro machining, determination of minimum chip thickness is of paramount importance as features having dimensions below this threshold can not be produced by the process. This study proposes a methodology to determine the value of minimum chip thickness by analysing acoustic emission (AE) signals generated in orthogonal machining experiments conducted in micro milling. Cutting trials were performed on workpiece materials ranging from nonferrous (copper and aluminium), ferrous (single and multiphase steel) to difficult-to-cut (titanium and nickel) alloys. The characteristics of $AE_{r.m.s}$ signals and chip morphology were studied for conditions when the tool was rubbing the workpiece. This provided a foundation to contrast AE signals captured at higher feedrates. This study enabled the identification of threshold conditions for occurrence of minimum chip thickness. The values of minimum chip thickness predicted by this new approach compares reasonably well with published literature.

Keywords: Minimum chip thickness, Acoustic emission, Micro cutting

7.1 Introduction

The minimum chip thickness can be defined as the minimum undeformed chip thickness below which micro machining operations do not produce chips (lower limit of micromachining) [66]. This sets the lower limit of the feasible process window in micro milling operations. When the tool cuts from zero chip thickness to maximum chip thickness, in each cutting pass, elastic deformations are induced on the workpiece until the tool reaches a certain threshold i.e. minimum chip thickness (hereafter, h_{min}). In a situation where undeformed chip thickness starts to exceed the h_{min} the chip begins to form. Material is removed completely in the form of a chip when the undeformed chip thickness is considerably greater than the cutting edge radius of the tool, the actual rake angle of the tool starts taking effect. Fig. 7.1 illustrates the basic concept of micro-scale cutting [166].

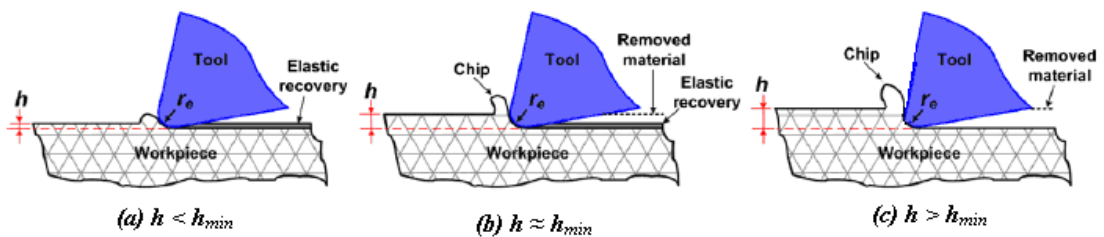


Fig. 7.1 Mechanics of micro-scale cutting (adapted from [166])

The minimum chip thickness is influenced by workpiece deformation. Knowing the material deformation properties is important for selecting suitable machining parameters and for predicting process performance [15]. The thickness of material removed should be chosen to be above the minimum chip thickness threshold to help reduce cutting forces [69], tool wear, surface roughness [11, 15], burr formation [24, 147], and simultaneously improve process stability. It is also scientifically very interesting to quantify the lower limit of the technology and hence identify challenges for pushing process boundaries. This motivated previous researchers to estimate the minimum chip thickness of different tool-workpiece combinations. Table 7.1 presents a summary of research work that covers the determination of minimum chip thickness.

Table 7.1 Previous research on minimum chip thickness effect

<i>Researcher(s)</i>	<i>Workpiece Material</i>	<i>Tool Material</i>	<i>Tool edge radius (r_e)</i>	<i>Estimated h_{min}</i>	<i>Methodology</i>
Ikawa et al [66]	Electroplated copper	Diamond	not specified	10 % of r_e	Using hypothetical atomistic cutting model in face turning
Shimada et al [54]	Copper, Aluminium	Diamond	5-10 nm	5 to 10% of r_e	Molecular Dynamics Simulation
Yuan et al [74]	Electro-polished Al-alloy	Diamond	0.3 μm	33% of r_e	Theoretical analysis
Son et al [27]	Al, Brass, Cu (OFHC)	Diamond	0.5 μm	18 to 24% of r_e	Analytical model
Volger et al [11]	Ferrite			29 to 43% of r_e	Microstructure-level Finite Element Modelling
	Pearlite			14 to 25% of r_e	
Kim et al [75]	Brass	Carbide	3 μm	22 to 25% of r_e	Indirect technique by using cutting force measurement
Liu et al [76]	Al 6082-T6	Carbide	1-4 μm	38 to 40 % of r_e	Analytical slip-line plasticity model
	1040 carbon steel			24 to 35 % of r_e	
Lai et al [53]	Cu (OFCH)	Carbide	2 μm	25% of r_e	Strain gradient plasticity and modified Johnson-cook approach

The reported literature revealed that the estimation of h_{min} is mainly based on numerical predictions. The change in the h_{min} for various work materials was attributed to variation in coefficient of friction between the tool-workpiece material and material behaviour in plastic deformation zones [54, 76]. Taking into account all the results reviewed, h_{min} for machining of different workpiece-tool combination was predicted to occur at undeformed chip thickness of 5 to 43 percent of the tool edge radius. Moreover, the comparison of the results for diamond to those of carbide tools showed that cutting operations can be scaled down (lower minimum chip thickness) when relatively sharp cutting tools are used. From Table 7.1, it can be inferred that the minimum chip thickness has not been defined for hard materials like tool steel or difficult-to-cut materials such as nickel or titanium base alloys.

There has also been research interest in experimental indirect determination characterisation of the mechanics of machining. Atkins and co-workers analysed cutting forces in the initial stages of orthogonal cutting before chip formation is fully established [167]. The fracture toughness information was used to predict the transition between cutting and rubbing [168]. Indirect methodology to estimate h_{min} by Kim et al

[75] was based on cutting force measurement. When the thrust force was higher than the cutting force, rubbing was assumed to be the contact mode otherwise the process would be in the cutting mode. The cutting forces are usually greater than thrust force in the cutting regime. However, the accurate measurement of very small cutting forces is challenging as noise can give a false cutting force signal [1]. Therefore, the experimental determination of h_{min} in micro milling remains an open research challenge.

AE signals have a significant advantage over force sensory systems, as they are independent of the complexity of tool path [169]. Moreover, an ability to detect micro scale deformation mechanisms within a relatively “noisy” micro cutting background [28] makes it more attractive. The AE signals have high sensitivity to tool-workpiece-chip interface activity and deformation in the cutting process. This has encouraged the use of AE signals as a basic tool for cutting mode classification [126, 158], chip form detection [119, 170] and tool condition monitoring. Despite the favourable sensitivity of AE signals to characterising the machining process there are also some challenges. One limitation is the non-transferability of the system from one type of machining operation to another. It is necessary to re-calibrate the AE signal for a different machine tool or process. Margot and co-workers identified problems with the use of AE sensors when the signal traversed a ball bearing (rotary device) [171]. Thus in the application of AE sensors motion and vibration interference has to be considered in the interpretation of signals.

The purpose of this study was to exploit acoustic emission (AE) signal in characterising micro machining mechanisms and hence h_{min} .

7.2 Experimental plan

7.2.1 Micro milling tests

Micro milling tests were conducted for detection of cutting modes. All tests were performed in dry cutting mode. The microstructures of six workpiece materials are shown in Fig. 7.2. Single straight flute uncoated end mills (Dixi-7060) were used in micro milling tests. Tool diameters of 2 mm and 6 mm diameter were selected to minimise tool deflection. The relatively small bending stiffness of the micro tools causes it to deflect easily. Prior to each cutting trial, the tools were examined under a scanning electron microscope (SEM). Fig. 7.3 (a) shows the image of the edge of a

fresh tool along with a magnified base view of the tool. This was used to estimate the cutting edge radius. Fig. 7.3 (b) shows the SEM image of the worn edge. The cutting parameters range is shown in Table 7.2.

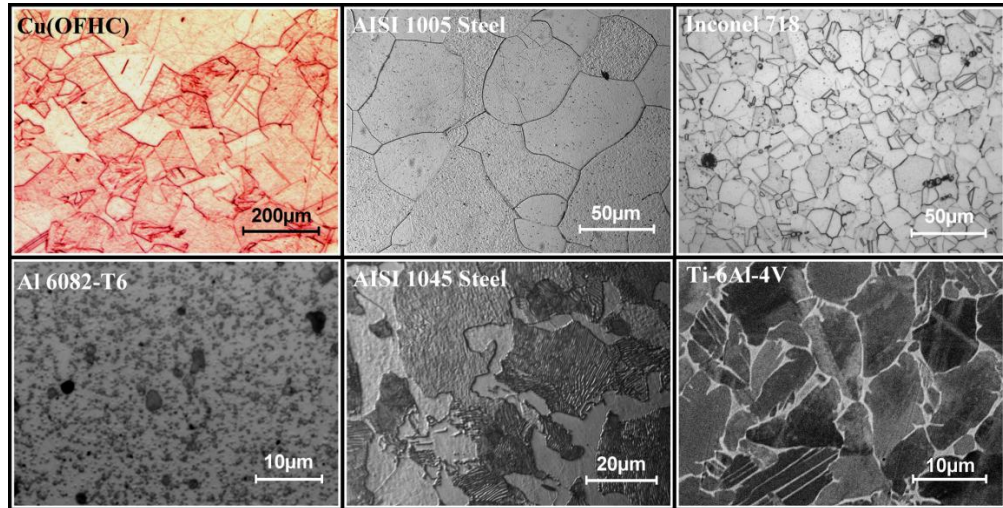
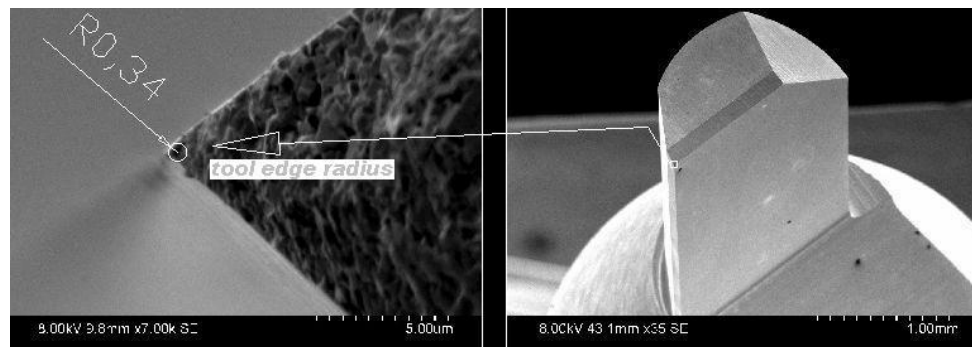
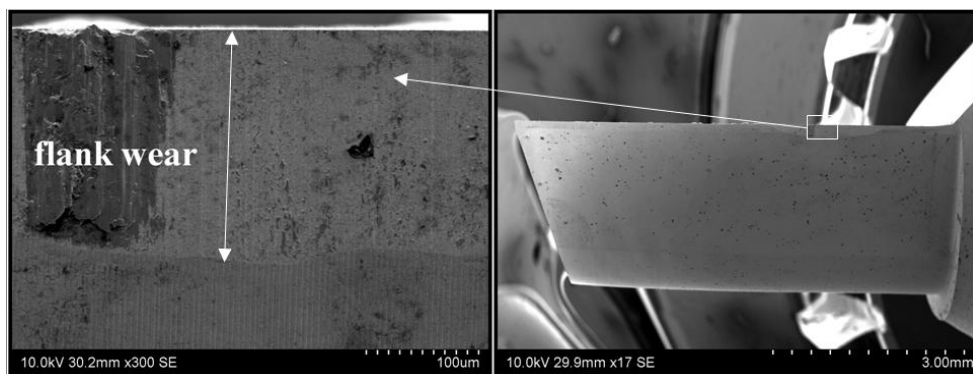


Fig. 7.2 Workpieces microstructures



(a) Tool edge radius measurement for a new tool



(b) Flank wear land for a used tool

Fig. 7.3 Single tooth tool

Table 7.2 Cutting parameters

<i>Workpiece material</i>	Cu (OFHC)	Al 6082-T6	AISI 1005 steel	AISI 1045 steel	Ti-6Al-4V	Inconel 718
<i>Average grain size (μm)</i>	143	-	70	10	12	16
<i>Cutting velocity (m/min)</i>	94.2	94.2	94.2	94.2	50	25
<i>Average tool edge radius and standard deviation (μm)</i>	0.40 \pm 0.11	0.44 \pm 0.20	0.67 \pm 0.42	0.84 \pm 0.52	0.33 \pm 0.07	0.55 \pm 0.12
<i>Maximum undeformed chip thickness (μm)</i>	0.02, 0.5, 2, 10					
<i>Axial depth of cut (mm)</i>	1					
<i>Radial width of cut</i>	Half of the tool diameter (i.e 1 and 3 mm)					
<i>Length of cut (mm)</i>	3 mm for 0.5, 2, 10 μm /tooth 1 mm for 0.02 μm /tooth					
<i>Mode of milling</i>	Up-milling under dry condition					

The experimental setup used on a Mikron 400 HSM centre is shown in Fig. 7.4. A single flute tool with zero helix angle was used in an end milling operation. The tool was engaged with the workpiece in a way to mimic orthogonal cutting. The height to thickness of the work piece was controlled so that the bottom of the tool was cutting in free space which enabled only the straight part of the cutting edge to be engaged. The AE sensor was mounted on the top surface, located at the centre of the Workpiece. The workpiece dimensions were 80 mm long and 70 mm wide.

In up milling mode, the maximum chip thickness occurs at the exit of cut and would theoretically be equal to the feed per tooth since the swept angle was kept constant at 90° . The depth of cut was set at 1 mm. This depth of cut was reported to provide plane strain conditions and reduce the possibility of side spread of material [70]. The axial depth of cut (a_p) and radial width of cut (a_e) were set larger than the average grain sizes of the workpiece material. The cutting process was not localised on one material phase and hence it is difficult to distinguish the effect of material phases on the AE signal. The cutting velocity was kept constant for the 2 mm and 6 mm diameter tool by adjusting the spindle speed. Fresh cutting edges were used for each new test. For 0.5, 2 and 10 μm maximum undeformed chip thicknesses, the length of cut was maintained at 3 mm in each trial to keep the edge radius closer to that measured before machining. At 0.02 μm /tooth, cutting length was limited to 1 mm. For this case which was mainly rubbing the shorter time and the signal was sufficient to characterise the process and avoid excessive wear.

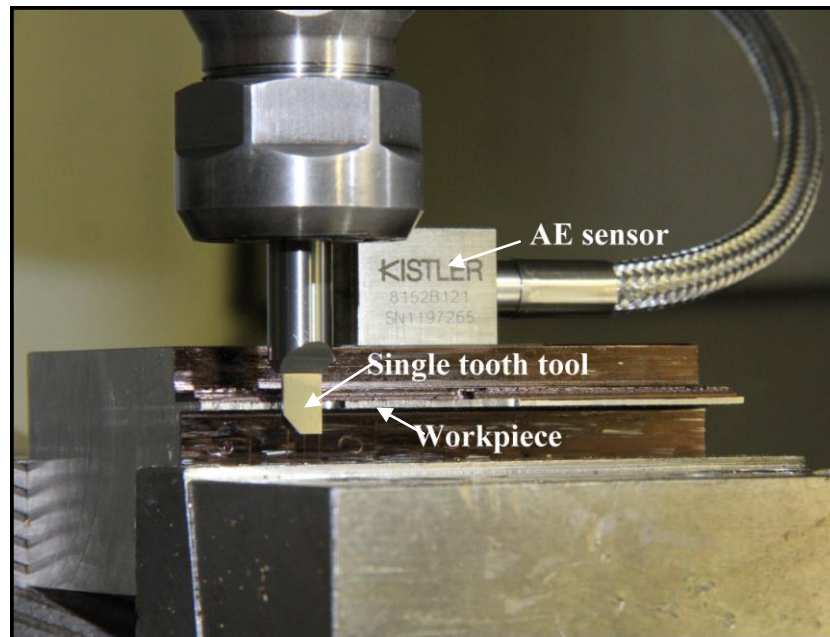


Fig. 7.4 Experimental set up

7.2.2 AE signal acquisition

The AE signal was monitored when the feed per tooth was below ($0.02 \mu\text{m}/\text{tooth}$), comparable ($0.5 \mu\text{m}/\text{tooth}$) and above the tool edge radius (2 and $10 \mu\text{m}/\text{tooth}$). The AE signal was acquired using a Kistler 8152B121 AE sensor as illustrated in Fig. 7.5. The signal was delivered to a Kistler 5125B coupler where it was gain amplified, band pass filtered at 0.5 to 1MHz and output as an AE filtered signal and $AE_{r.m.s}$ signal. These two outputs were recorded through two channels on a Nicolet technologies Sigma 30 digital memory oscilloscope at a sampling rate of 2MHz . The $AE_{r.m.s}$ data were acquired, with a root mean square (r.m.s) time constant of 0.12ms . The integration time constant was carefully selected in order to extract burst events. Jemielniak suggested that the integration time constant should be 10 times shorter than the typical burst duration, which is approximately 2ms [172]. The AE signals were sampled as shown in Table 7.3 for different workpiece materials.

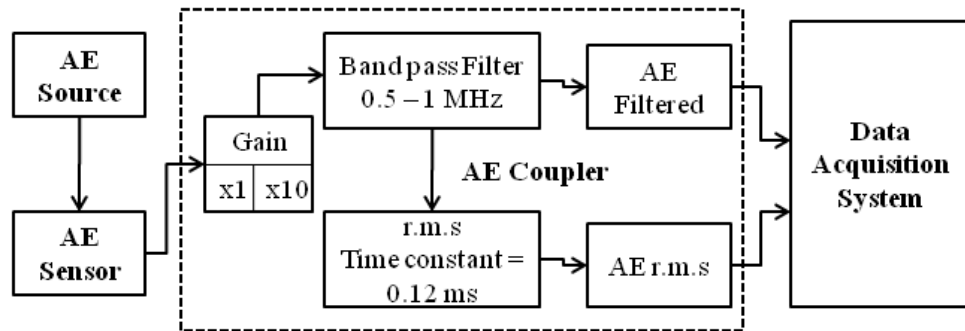


Fig 7.5 Signal measurement chain

Table 7.3 Acoustic emission sampling

Sampling rate	2 MHz					
for workpiece material	Cu (OFHC); Al 6082-T6; AISI 1005 steel; AISI 1045 steel		Ti-6Al-4V		Inconel 718	
for tool diameter	2 mm	6 mm	2 mm	6 mm	2 mm	6 mm
Data length	64000	128000	128000	256000	256000	256000
Data points /rev	8000	24000	15072	45215	30143	90430
Data points / effective cutting period (S_c)	2000	6000	3768	11304	7536	22608
Data points /deg	22.22	66.67	41.87	125.6	83.73	251.2
Total spindle revolutions	8	5.33	8.49	5.66	8.49	2.83
Time span (s)	0.032	0.064	0.064	0.128	0.128	0.128

7.3 Research methodology

The literature reviewed revealed that when a tool starts to cut due to a finite edge radius, tensile stresses exist which give way to crack initiation and propagation [63]. Recently, Subbiah and Melkote showed fracture zones leading to material separation in the chip roots of Al 2024-T3 at 0.67, 1 and 1.33 undeformed chip thicknesses to tool edge ratios [47]. The aim of this study was to use AE signals to characterise the transient events occurring within the primary shear zone which signifies chip initiation.

$AE_{r.m.s}$ signals represent the enveloped curve of both continuous (lower amplitude and low frequency signal generally associated with plastic deformation) and burst (high amplitude and high frequency signal generally associated with fracture) events occurring during the cutting process. During a complete revolution of a single tooth tool, cutting events clearly show the $AE_{r.m.s}$ pattern as presented in the time domain plot. A flowchart of the approach used to extract the $AE_{r.m.s/swept}$ corresponding to the tool

engagement over the swept angle is shown in Fig. 7.6. This is extracted from the time series data $AE_{r.m.s/rev}$. In Figure 7.6, the top row graphs represent the raw $AE_{r.m.s}$ signal data in the time domain. The views in the middle represent the data for subsequent tool engagements corresponding only to the swept angle of cut i.e. 90 degrees. In the final step (bottom image of Figure 7.6) the $AE_{r.m.s}$ signals from the selected tool engagements are referenced to a common origin in time. A method to follow the transition from rubbing to cutting for each cutting pass was developed. This consists of the following steps,

- (i) In order to identify the effective cutting time (t_c) of the flute within each tool revolution, the number of data points for effective cutting period (S_c) was calculated using the Eq. (7.1), where f_s is sampling frequency and N is spindle revolutions per minute.

$$S_c = \frac{f_s \times 60}{N \times 4} \quad (7.1)$$

- (ii) To extract $AE_{r.m.s}$, select a constant lowest non-zero value on the Y-ordinate as the start of tool engagement. This approximates a common signal origin. Then, extract the $AE_{r.m.s}$ for the same interval of S_c in a number of cutting passes “n”. It is assumed that the time required to complete the cutting action does not significantly change for subsequent tool rotations.
- (iii) Display on a common graph and reference point, the extracted $AE_{r.m.s}$ to construct plots that represents the growth of $AE_{r.m.s}$ over the swept angle.

When the tool enters into the workpiece, before initiation of chips, a relatively weak signal can be expected where friction at tool-workpiece interface was reported to be the dominant source of AE [120]. The low signal region (and overlapping parts of the curve) in the $AE_{r.m.s}$ of the initial part of subsequent tool rotations can be considered as a signature for the rubbing. After this point, aperiodic change in $AE_{r.m.s}$ can be attributable to ductile tearing (generate burst component of AE signal) in the shear zone. One apparent question that can be raised is if the interface zone has a built-up edge (BUE) or not. BUE usually occurs over a region on the rake face much higher than the undeformed chip thickness. Therefore, in the initial contact, a sudden increase in $AE_{r.m.s}$ value due to burst type signal can be linked to chip initiation. This was used for defining

the minimum chip thickness threshold. Below this value the micro machining process is not capable of producing features on micro components.

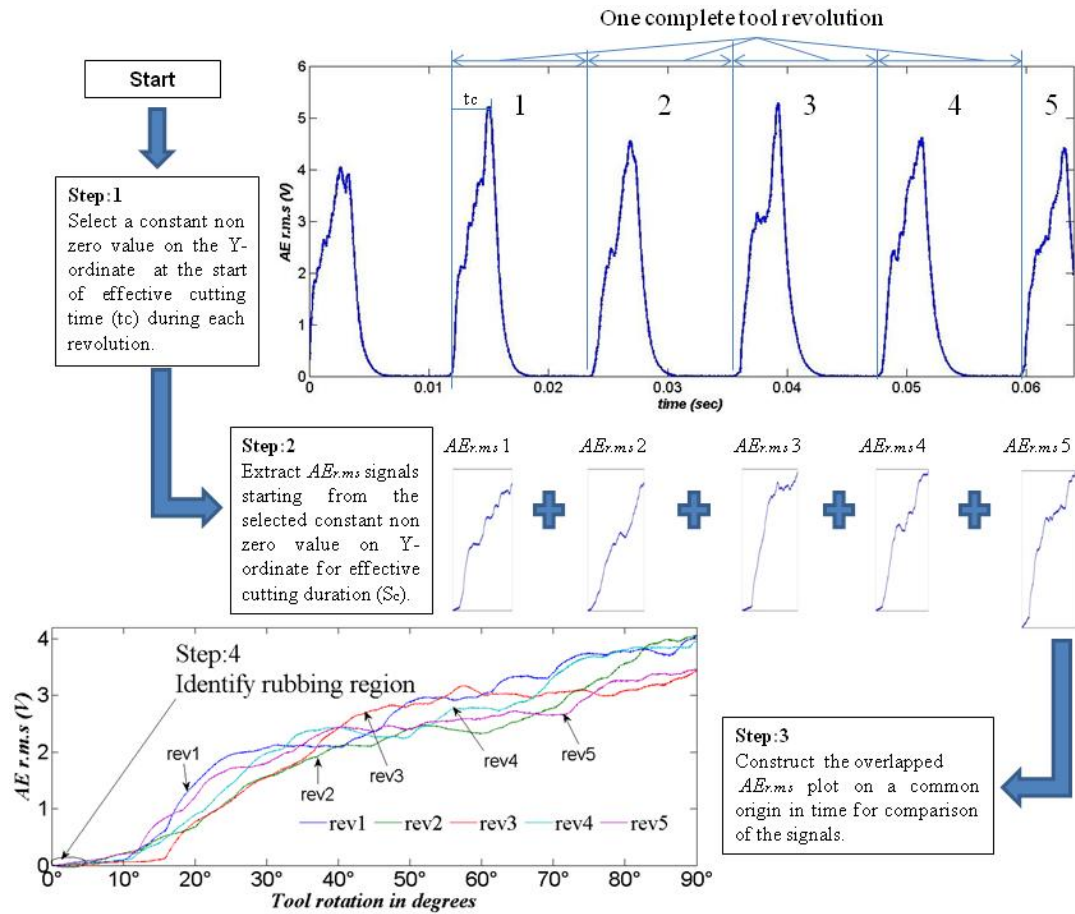


Fig. 7.6 Data handling in extracting AE_{r.m.s} signal characteristics

In a prior study [173], the authors demonstrated the effectiveness of this method to determine the h_{min} of multiphase steel. The presented methodology is now extended to estimate h_{min} encountered in micro-milling of non-ferrous, ferrous and difficult to cut alloys for the cutting conditions in Table 7.2.

7.4 Results and discussions

7.4.1 AE signals in the rubbing dominated region

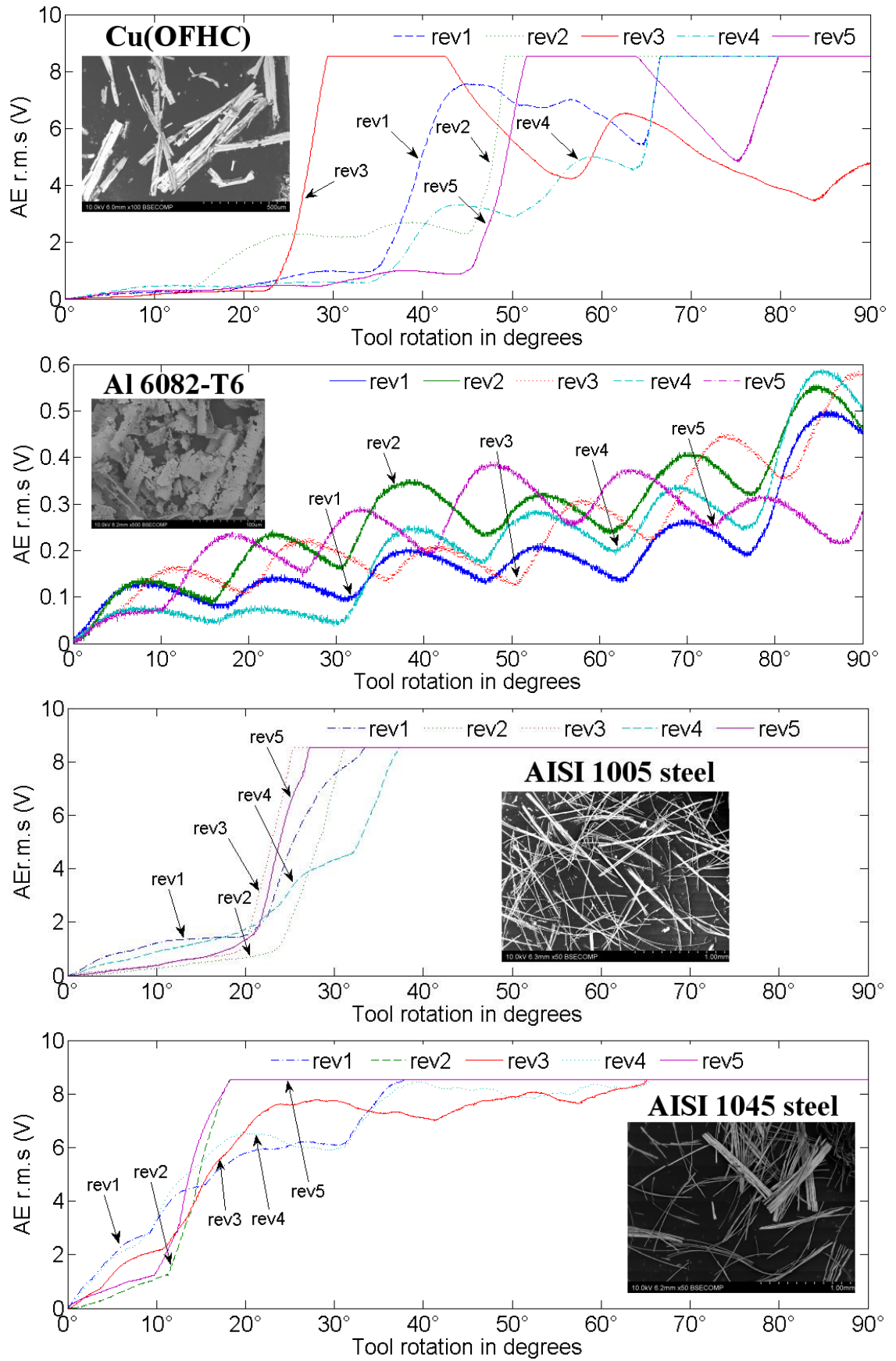
Fig. 7.7 shows the AE_{r.m.s} signals produced when machining at 0.02 μm/tooth maximum undeformed chip thickness for a fresh tool. The workpiece used in the generation of particular signal is mentioned directly on that graph. In these cases, the fraction of feed per tooth to the tool edge radius is much lower than the reported value of minimum chip

thickness for various workpiece materials. Hence, the rubbing mode should take place. At the beginning of tool rotation the signal is weak and characteristic of the rubbing process. However the signal then significantly increases. The subsequent increase of the AE signal after a period of heat generation by friction could coincide with material extrusion mechanisms and is in line with observations made by Liu and Dornfeld [126] in the diamond turning operation. Differences when comparing workpiece materials in the signal attributed to the extrusion duration may be influenced by material tempering due to thermal cycles from the previous tool rotations [174].

For Aluminium and titanium based alloys, considerable low magnitude of $AE_{r.m.s}$ was observed. It is interesting to note that these materials have a relatively low elastic modulus compared to other workpiece materials [170]. The low modulus of elasticity of titanium is a driver for vibration during machining [110]. It is possible that this low modulus of elasticity introduces period contact relief and this affects the build up of $AE_{r.m.s}$ signal. It is also evident that at higher feed the AE magnitudes increase and as expected the cutting process becomes more stable.

The magnitude of $AE_{r.m.s}$ also indicates that the deformation mechanism of the investigated workpiece materials becomes complicated due to the effect of roundness of the tool edge [39, 44]. As the undeformed chip thickness decreases well below the tool edge radius, where an effective negative rake angle is established, this shifts the cutting mechanism to a more energy intense mode.

In machining of mild steel, Komanduri [70] experimentally determined a critical rake angle of -76° beyond which the machining process retards chip formation. The computed effective negative rake angles in these trials were ranging from -70° to -77° . Highly fragmented chips were collected that can be seen from the SEM images embedded in their respective $AE_{r.m.s}$ graphs of different workpiece materials. The sizes of the chips do not correspond to the width of cut. The observed intermittency in the chip form can be linked to relatively large tool edge radius to undeformed formed chip thickness, being lower than minimum chip thickness and therefore resulting in lack of material removal in each cutting pass.



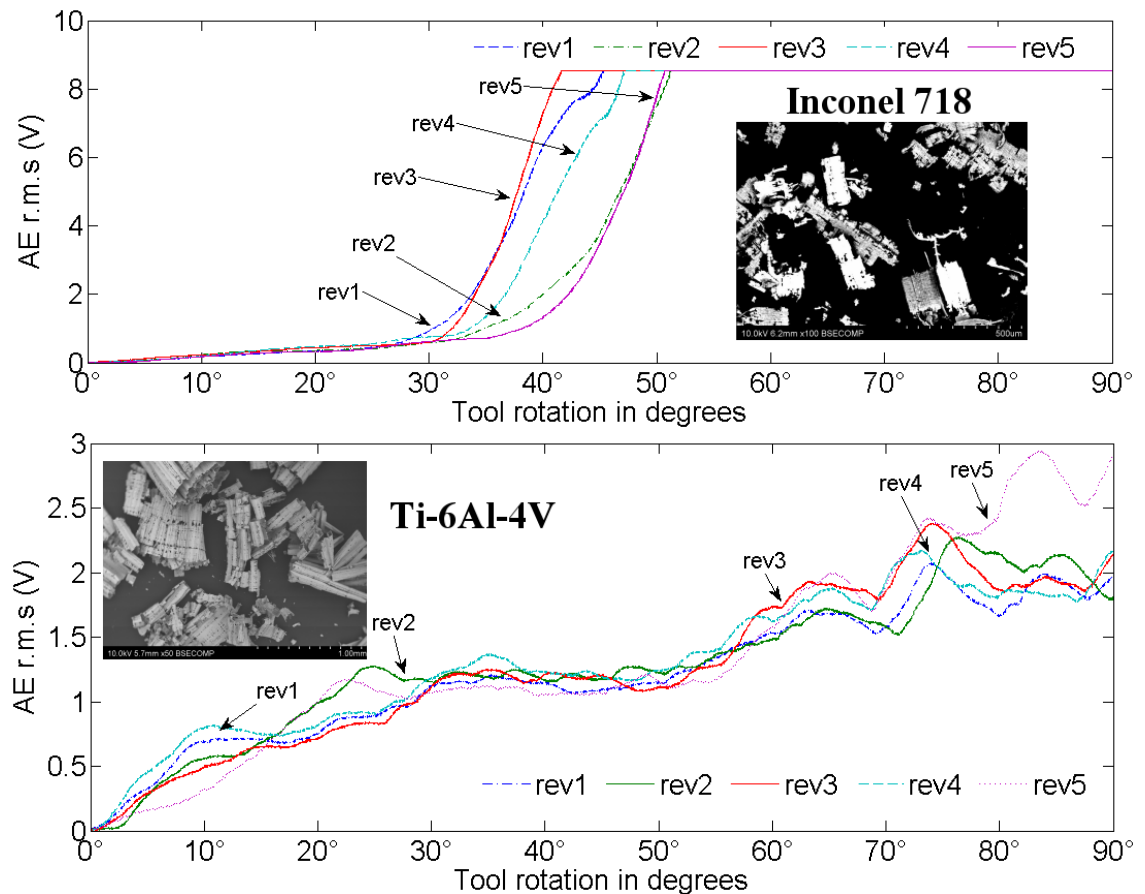
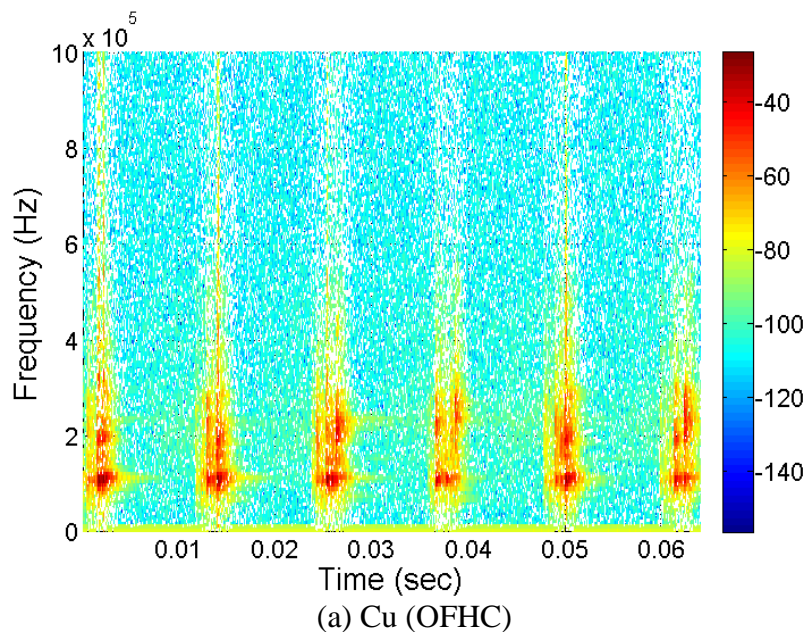
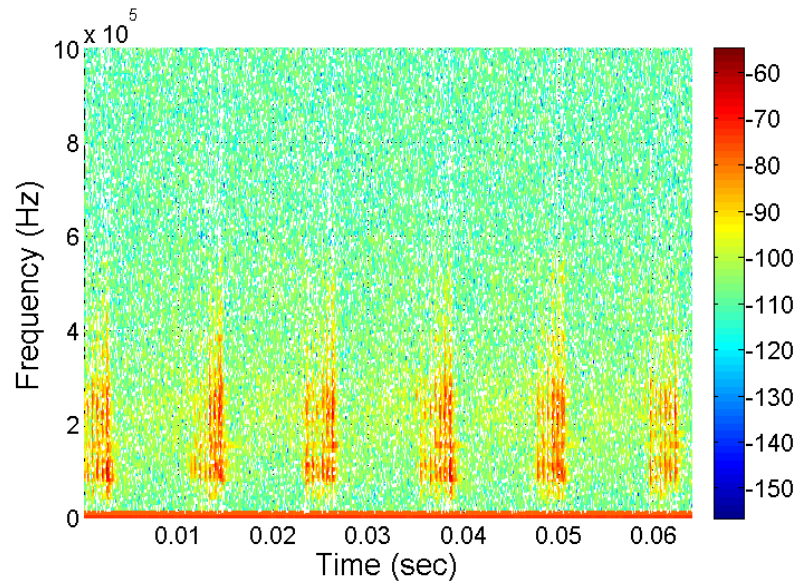


Fig. 7.7 $AE_{r.m.s}$ and chip morphology generated at $0.02 \mu\text{m}/\text{tooth}$

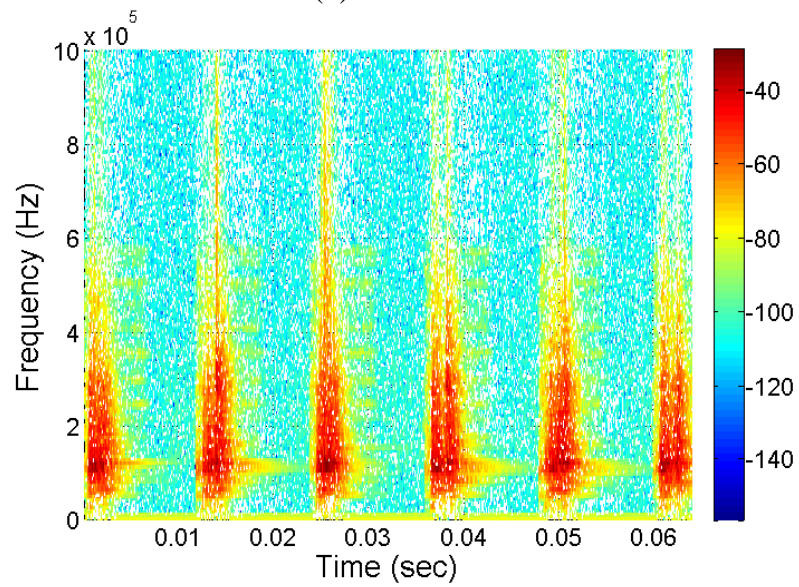
The use of AE spectrogram was shown to be effective for monitoring macro scale milling [131]. In the current chapter, Short-time Fourier transformation (STFT) with a Hamming window (length 256-samples; overlapping-90%) was used to construct a spectrogram of AE signals over a sampling length of 0.064 seconds. Fig. 7.8 contains AE STFT plots of the investigated workpiece materials. This presents variations in the frequency pattern of AE signal with respect to the moments when cutting action takes place. During active tool-workpiece engagement, titanium alloy showed less deviation, whereas noticeable fluctuation in intensity of predominant frequency bands along the number of tool passes was observed in the rest of workpiece materials. The non-stationary periodicity of the frequency bands demonstrate the nonlinear characteristics of actual engagement below h_{min} and hence discontinuity in chip formation process. Since sliding or rubbing effects tend to generate AE signals in the high frequency range [134], the random peaks can also be observed in these spectrograms during each cutting pass for most cases.

The comparison of the spectrograms reveals that predominant frequency bandwidths are very sensitive to the selection of workpiece material. The dominant period of the frequency bands generally increases with tool rotation. When cutting nonferrous materials, (90-115 kHz) and (200-250 kHz) were the major frequency bands that reach significant amplitude. A relatively wider dominant spectrum was occupied by the ferrous materials and titanium based alloy, but energy was mainly concentrated in (90-125 kHz) frequency bands. The mapping of indentified frequency bands to chip formation mechanism was based on the work by Dornfeld and co-workers [28]. The shearing micro voids and cleavage micro fracture were identified as originating source of frequencies of the order 70-250 kHz. An unexpected result from spectrogram analysis is the detection of discrete predominant frequency bands allied with intergranular micro fracture (500-1000 kHz), inclusions bursting (250-500 kHz) and cleavage micro fracture (125-250 kHz) for Inconel 718 alloy (Figure 7.8e). The irregular occurrences of these bands indicate that cutting commenced when the material accumulated from previous passes exceeds the h_{min} . In addition to that short burst of energy in the peak bands was observed beyond the swept angle. The events which were clearly distinguishable from the cutting and/or rubbing phase can be linked to formation of burrs.

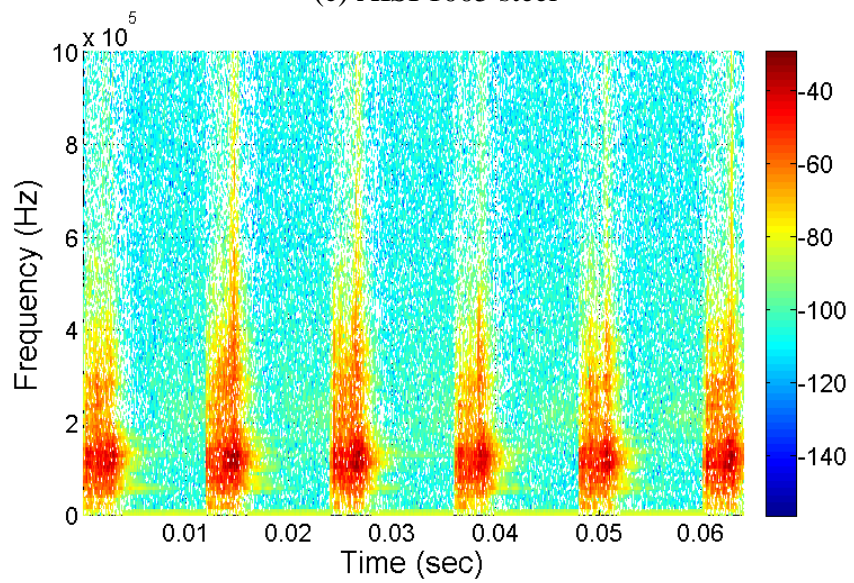




(b) Al 6082-T6



(c) AISI 1005 steel



(d) AISI 1045 steel

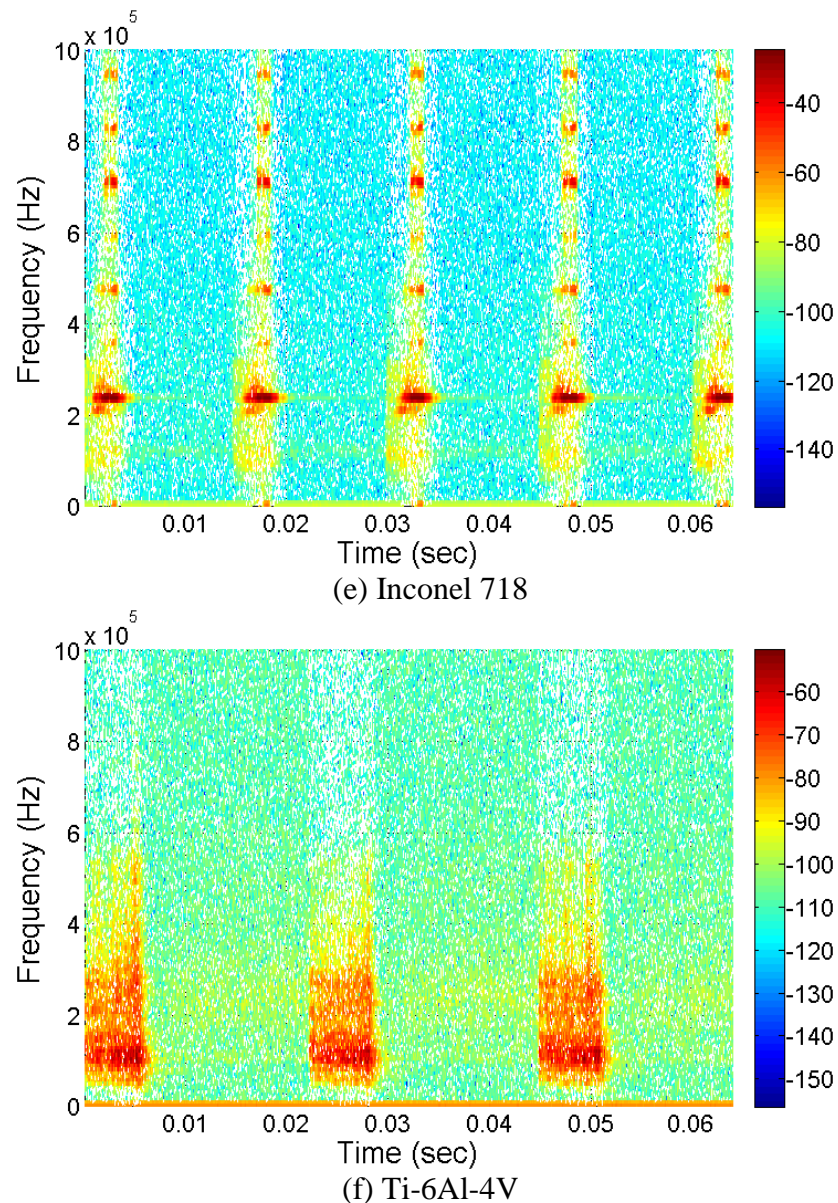


Fig. 7.8 AE STFT plots generated at $0.02 \mu\text{m/tooth}$

Fig. 7.9 shows the variations in the residual stress on the machined surface measured by means of a PROTO-IXRD portable residual stress diffractometer. The size of collimator defining the beam area was 1 mm by 1 mm. The details of the equipment settings are shown in table 7.4. The $\sin^2 \psi$ technique was applied to compute the residual stresses. Residual stresses were measured on machined surfaces at two different locations for each sample. In the case of Inconel 718, tensile stresses were observed. The tensile stress increased with increasing undeformed chip thickness. However, for the rest of the workpieces comparatively higher compressive residual stresses were measured. The compressive residual stresses decreased for higher chip thickness. This provides evidence that material at low undeformed chip thickness is subjected to larger plastic

deformation. The presented analysis and evidence provides a foundation to establish a predictive method for the occurrence of h_{min} by comparing AE signatures at higher undeformed chip thicknesses.

Table 7.4 Proto-IXRD settings

	Cu (OFHC)	Al-6082-t6	AISI 1005 Steel	AISI 1045 Steel	Ti-6Al-4V	Inconel 718
Radiation tube	Mn K α	Cu K α	Cr K α	Cr K α	Cu K α	Mn K α
Filter	-	Ni	-	-	Ni	-
Operating voltage (KV)	20	25	20	20	25	20
Operating current (mA)	4	5	4	4	5	4
Bragg angle(2 θ)	152°	137°	156°	156°	140°	152°
Exposure time (sec)	2	2	1	1	10	1
Number of exposure	20	20	10	10	10	10

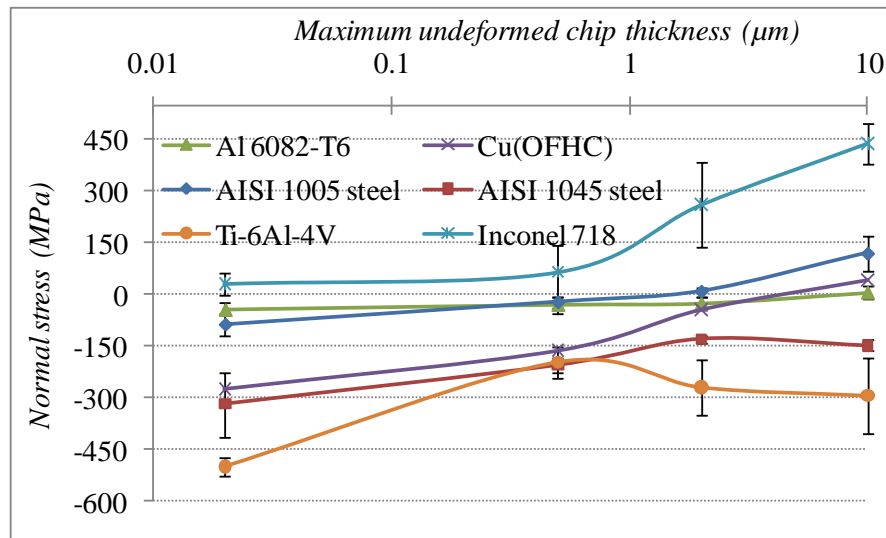


Fig. 7.9 Variations in residual stresses

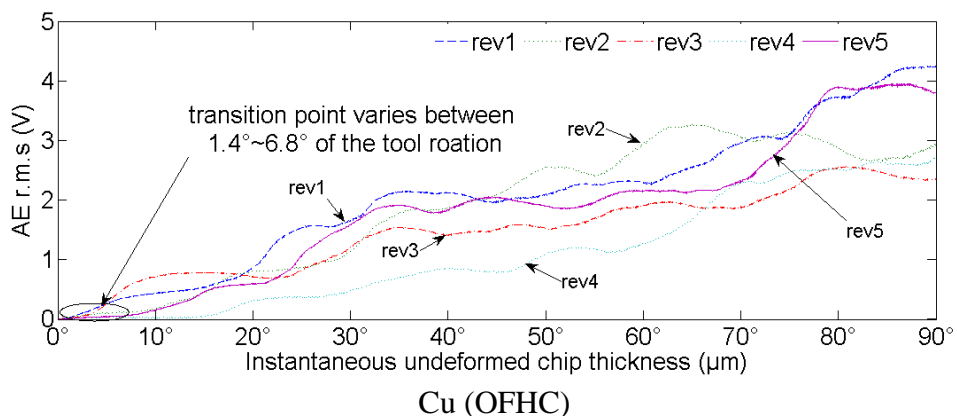
7.4.2 AE signal in shearing dominated region

In prior investigation [173], it was reported that AE signal produced in ploughing dominated zone was influenced by the thermal activation associated with the tool-workpiece interaction in the tertiary deformation zones. Therefore, higher feedrates were chosen to present positive rake angle in the chip formation process. The investigations were carried out when $h/r_e \approx 1, 4$ and 20 i.e $0.5, 2$ and $10 \mu\text{m/tooth}$ respectively. At these undeformed chip thicknesses, chips were undoubtedly formed for the most part of active tool workpiece engagement, which may not be assumed for the first case.

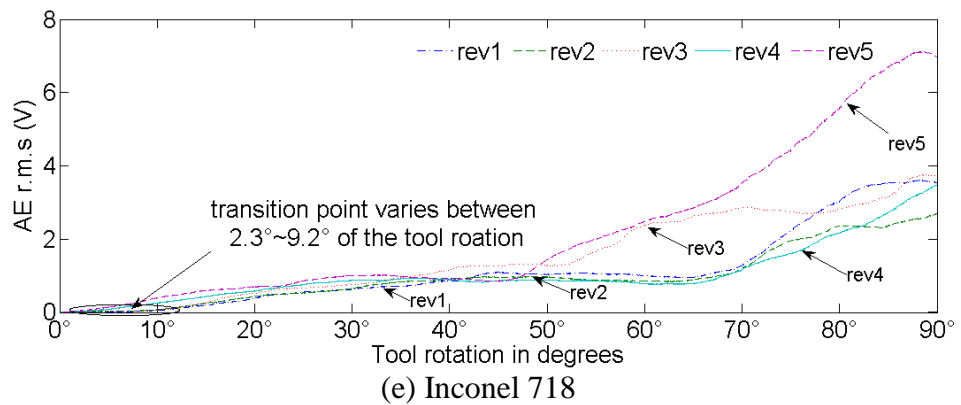
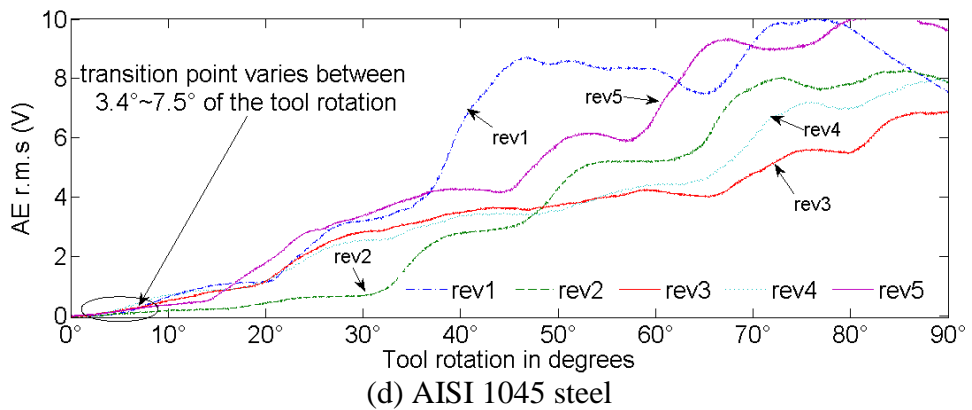
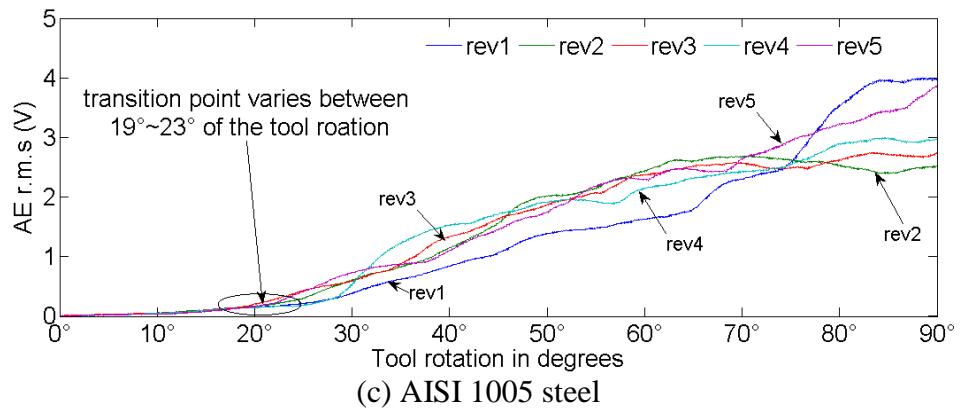
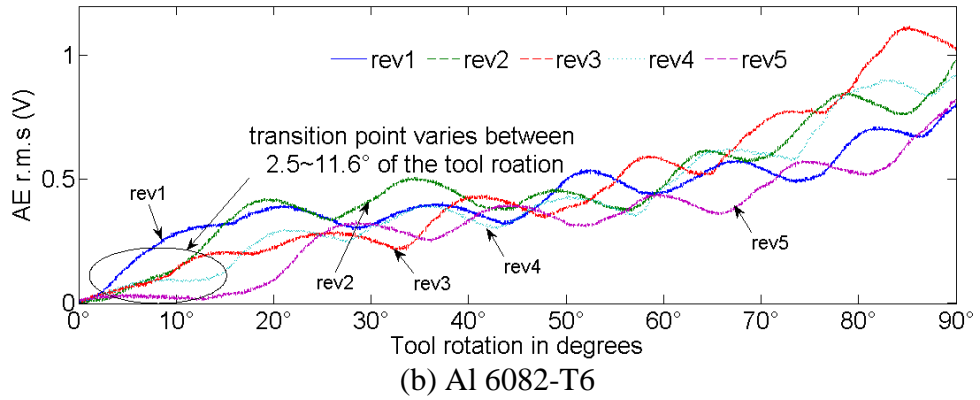
Fig. 7.10 shows the $AE_{r.m.s}$ signatures as a function of tool rotation generated at $0.5 \mu\text{m}/\text{tooth}$ undeformed chip thickness for the investigated workpiece materials. The trends depict lower AE amplitude as compared to $0.02 \mu\text{m}$ feed/tooth (for a prolonged length of cut). This shows that extruding and ploughing mechanisms are reduced at undeformed chip thickness comparable to the tool edge radius.

In subsequent cutting passes, Fig. 7.10 shows that the identified rubbing signature does not coincide with each other. A characteristic variation in the rubbing traces is notable in each experiment at this undeformed chip thickness. The observed phenomenon could be explained from the understanding of minimum chip thickness concept, where material is accumulated from previous noncutting passes until it exceeds the minimum chip thickness value to form a chip [67]. Therefore, the upper limit of rotation angle in the transition range was used to estimate minimum chip thickness.

Once the minimum chip thickness is exceeded, a chip forms and the intensity of $AE_{r.m.s}$ increases. A relatively higher slope can be observed in all cases, increasing with tool rotation angle. It is proposed in literature that the AE energy rate can be evaluated as a square for the $AE_{r.m.s}$ signal [126]. Since the r.m.s signal increases with tool rotation and hence chip thickness the AE energy rate will follow the same trend. The AE signal relates to activity in the three deformation zones. In the cases shown here since the maximum chip thickness is comparable to the tool edge radius then the mechanics of the process concentrates on the flank face. In this case, the $AE_{r.m.s}$ signal picks up the chip formation/deformation, the chip-tool and workpiece-tool contact events.



(a)



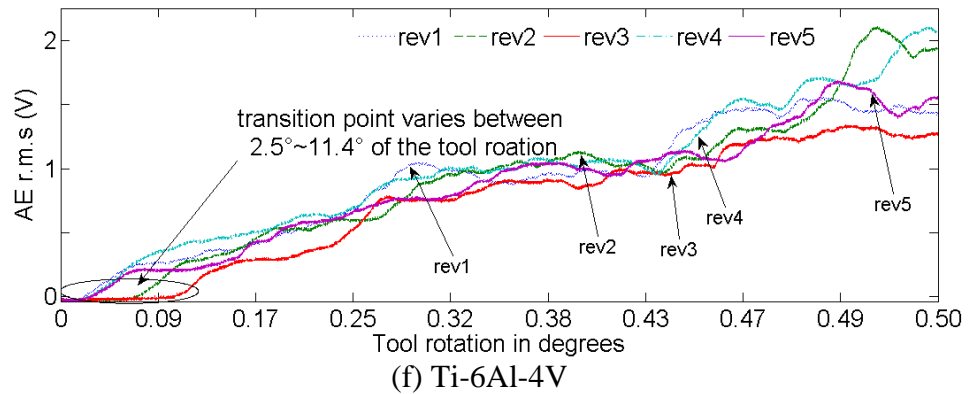


Fig. 7.10 $AE_{r.m.s}$ generated at $0.5 \mu\text{m}/\text{tooth}$

Fig. 7.11 shows the examples of the wall surfaces produced at $0.5 \mu\text{m}/\text{tooth}$. The images were taken with an optical microscope. The cusp features and welded chips on the machined surfaces are marked on the respective images. The variations in the identified $AE_{r.m.s}$ rubbing signature can also be attributed to the interfering of these features with the tool at the beginning of the cut.

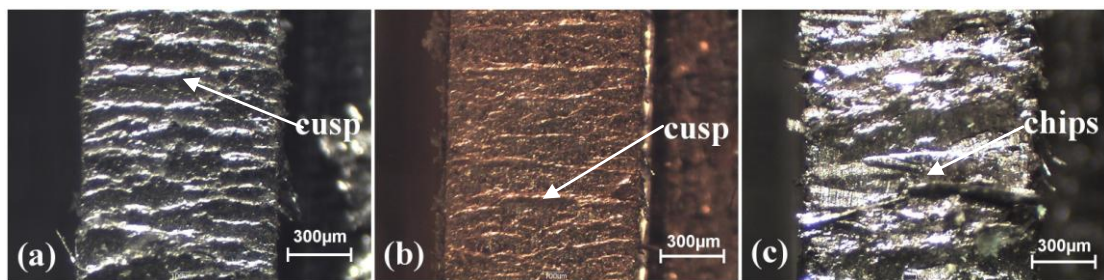
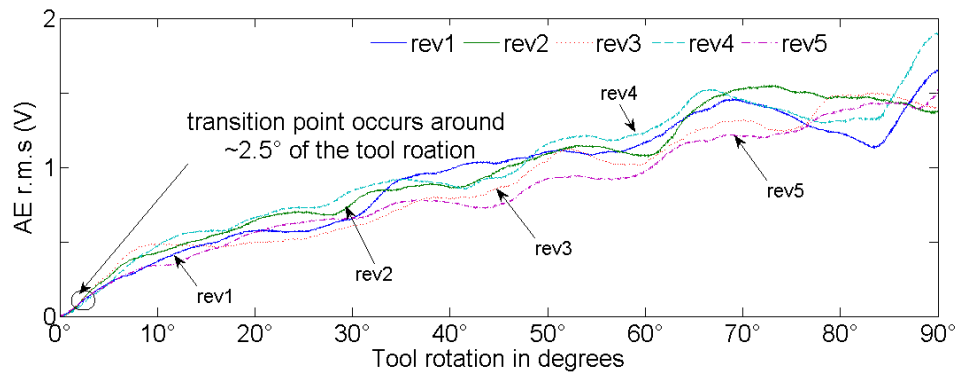


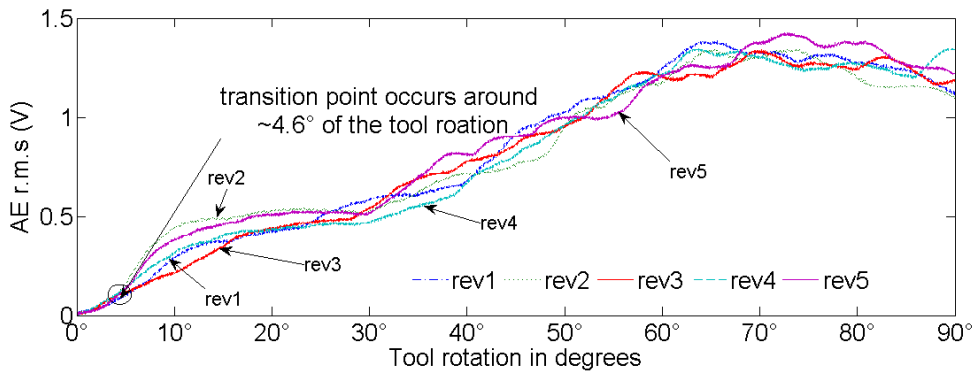
Fig. 7.11 Machined wall surface generated at $0.5 \mu\text{m}/\text{tooth}$ of
(a) Al 6082-T6 (b) Cu (OFHC) (c) Inconel 718

Fig. 7.12 shows the $AE_{r.m.s}$ trends observed at $2 \mu\text{m}$ feed/tooth. The identified rubbing zone relatively decreases and the variation become increasingly less frequent as minimum chip thickness effects relatively reduce at higher feedrates, eventually leading to repeatable values. It also indicates that despite the 4-fold increase in undeformed chip thickness, the AE intensity does not increase in the same distinctive way. In most cases, a slight increase in AE signal was observed. A plausible explanation is that at the lower feed/tooth (comparable or less than tool edge radius) the contribution from the sliding interfaces was more pronounced than at higher feed/tooth (more than tool edge radius). When monitoring the AE signal from workpiece, at the investigated h/r_e ratio, the AE generated from tool actual rake face (secondary shear zone / sliding friction) is not accessible [119]. This has the effect of masking the increase in $AE_{r.m.s}$ expected when

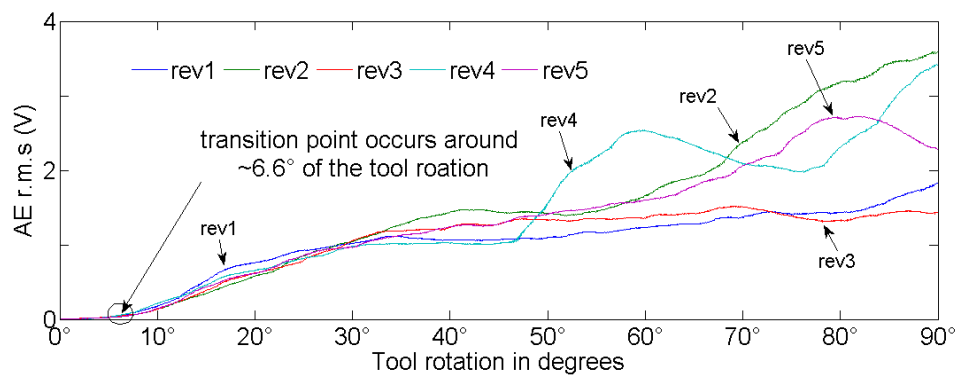
using higher undeformed chip thickness. This also indicates the partial dependence of AE amplitudes on the thickness of the primary deformation zone.



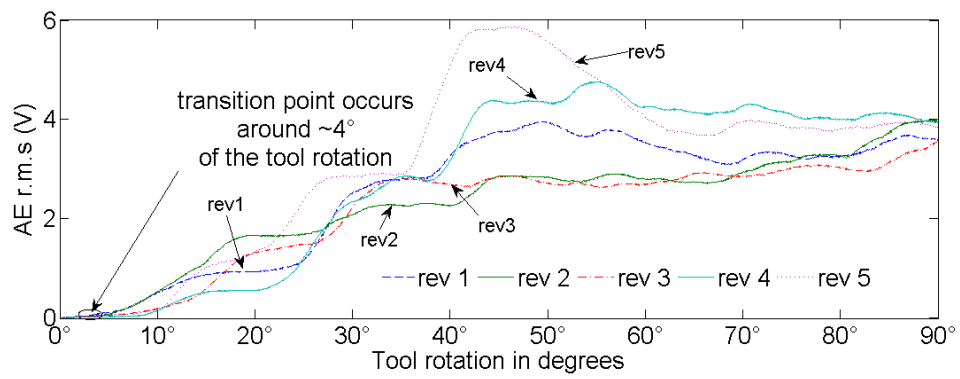
(a) Cu (OFHC)



(b) Al 6082-T6



(c) AISI 1005 steel



(d) AISI 1045 steel

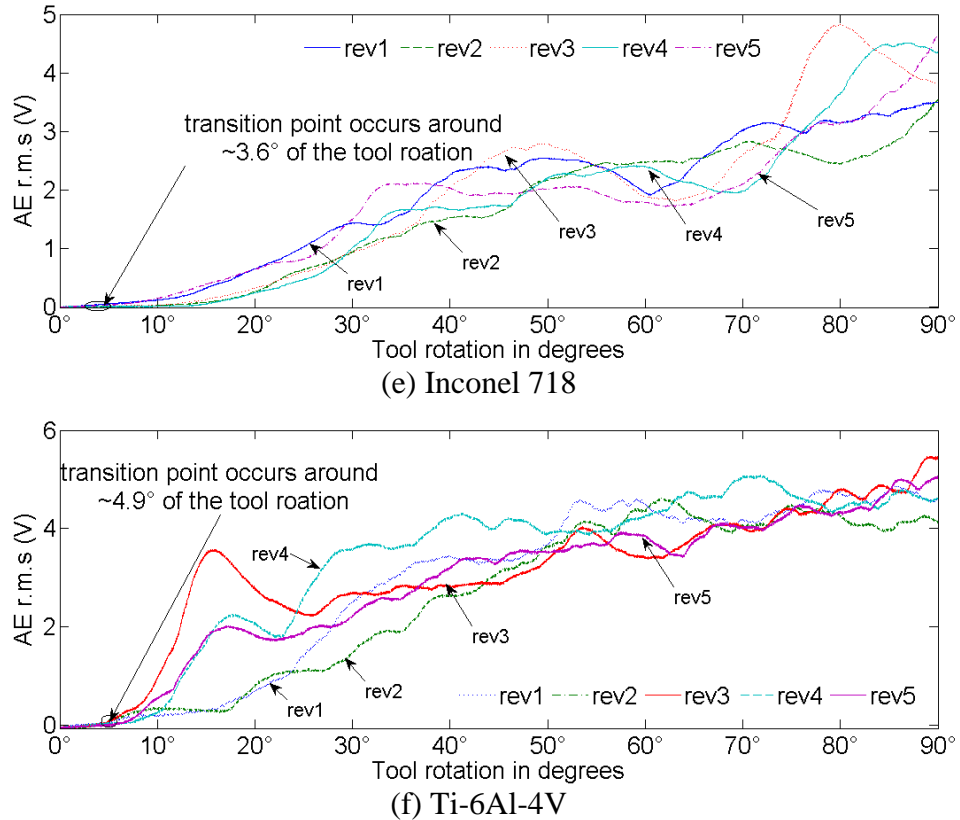


Fig. 7.12 $AE_{r.m.s}$ generated at $2 \mu\text{m}/\text{tooth}$

For examination of chip thickness at $2 \mu\text{m}/\text{tooth}$, the micro chips samples of the investigated workpieces were prepared in MetPrep[®] Di-hard cold mounting resin. The samples were ground and polished on Presi[®] Mechatec 334 polishing machine. Grinding was carried out with grit sizes of 600 and 1200 for very short period considering the fragility of the chips. Polishing was done with 6 and $3 \mu\text{m}$ finishing slurries.

Fig. 7.13 shows typical chip thicknesses formed at $2 \mu\text{m}/\text{tooth}$ maximum undeformed chip thickness. The shear fronts formation are hallmarks of micro chips since this type of chips were discovered during micromachining of crystalline materials [80] as well as amorphous materials [82]. The influences of workpiece microstructure and stick-slip on the rake face can be regarded as critical factors that affect final chip form. The Al-6082-T6 exhibited wavy chips. In sticking regions, the chip thickness was found to be increased appreciably for copper, AISI 1005 steel and Inconel 718. The encounter of ferrite and pearlite structures at an instant of tool rotation was thought to be responsible for variation in the deformed chip thickness for AISI 1045 steel. Ti-6Al-4V revealed an aperiodic saw-tooth chip characterised by the presence of irregular lamellae on the free

surface. This is in agreement with the consensus that with low values of undeformed chip thickness, saw-tooth formation is suppressed and an aperiodic chip forms [93]. From these images, it would be safely concluded that burst component generated in AE signal due to crack initiation and propagation from the free surface of the chip can account for waviness in the $AE_{r.m.s}$ signature per tool rotation.

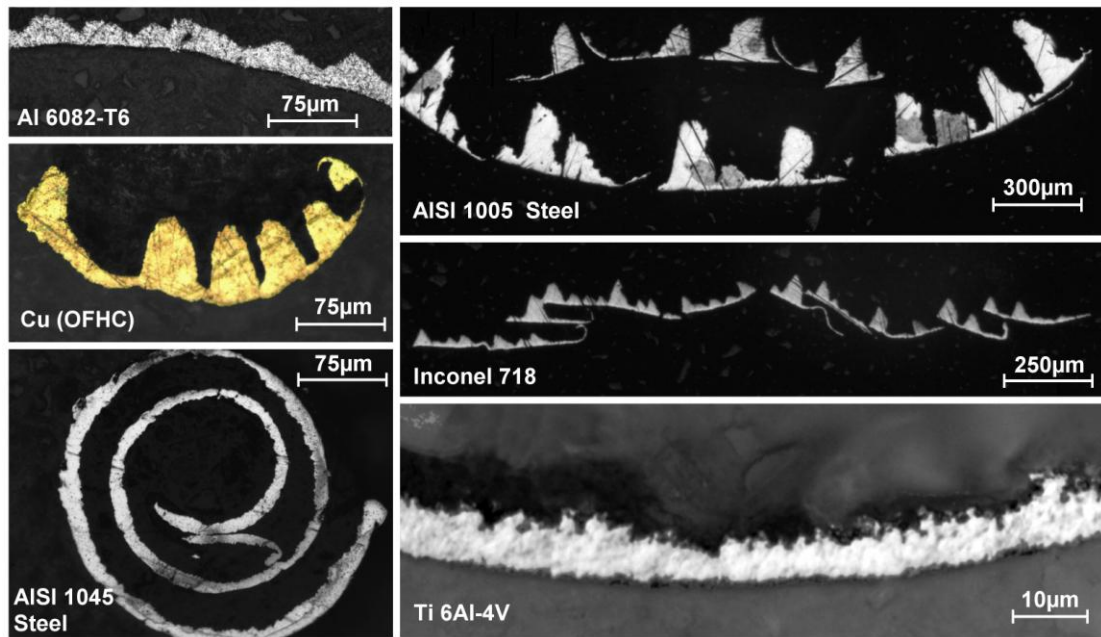
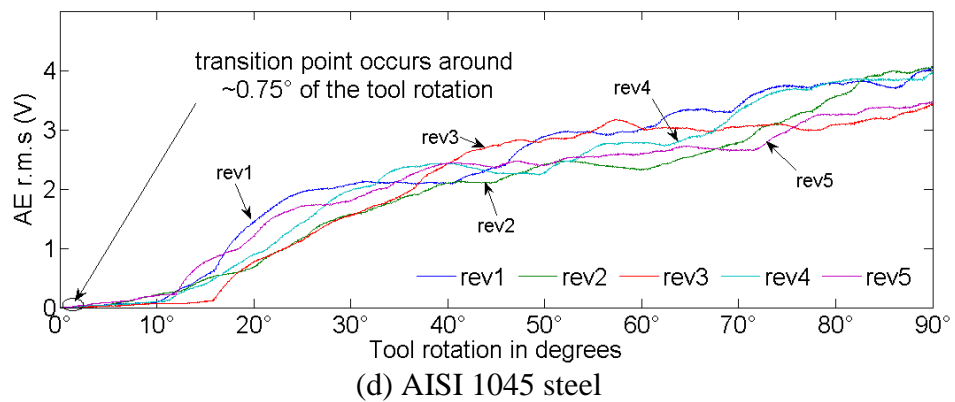
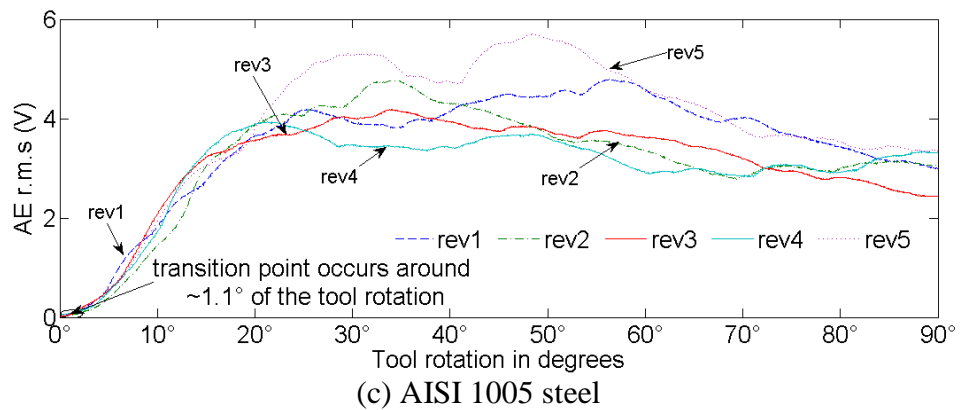
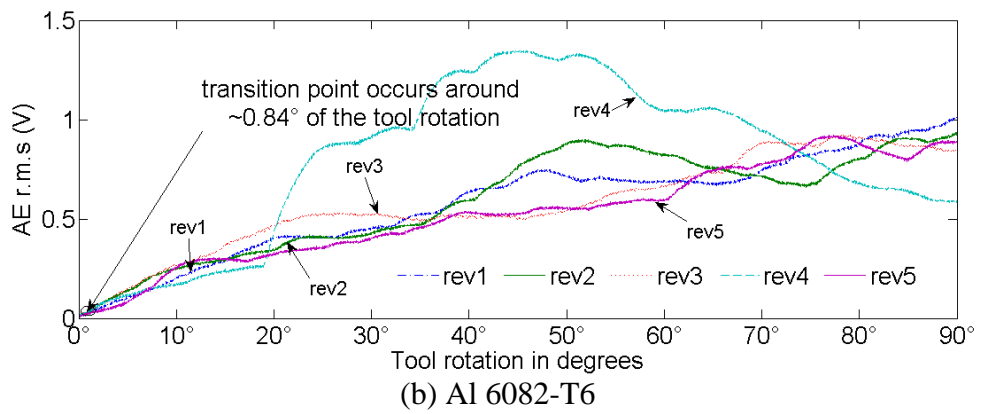
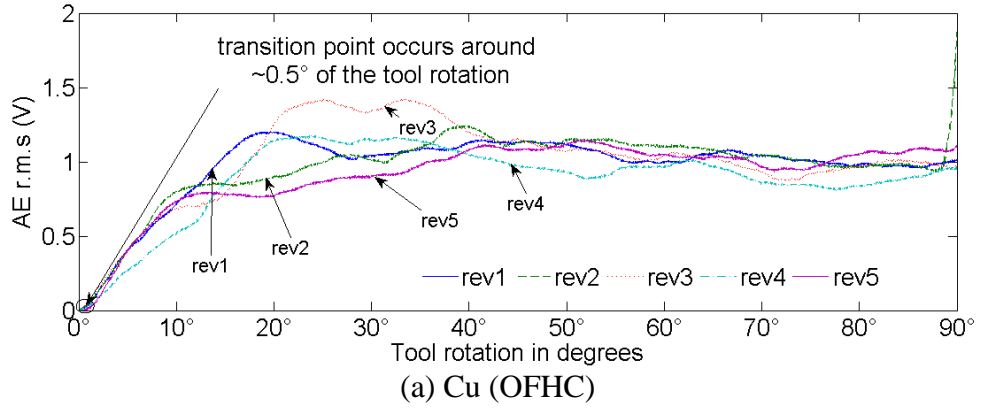


Fig. 7.13 Typical chip thickness variation at 2 μm feed/tooth

Fig. 7.14 shows that $AE_{r.m.s}$ when undeformed chip thickness is much larger than the tool edge radius. The identified rubbing signatures shifted near to the origin of the graphs. It suggests that actual engagement is the same as feed per tooth. Hence, any material engaged with the tooth should be completely removed from the workpiece at higher undeformed chip thickness to tool edge radius ratio. The low $AE_{r.m.s}$ amplitude compared to previous cases indicates that contribution of tool and workpiece interface in the AE generation is continuously decreasing at higher h/r_e ratios. Again, it may be mentioned here the effect of the rake face on AE generation can not be accurately judged in the existing experimental setup.



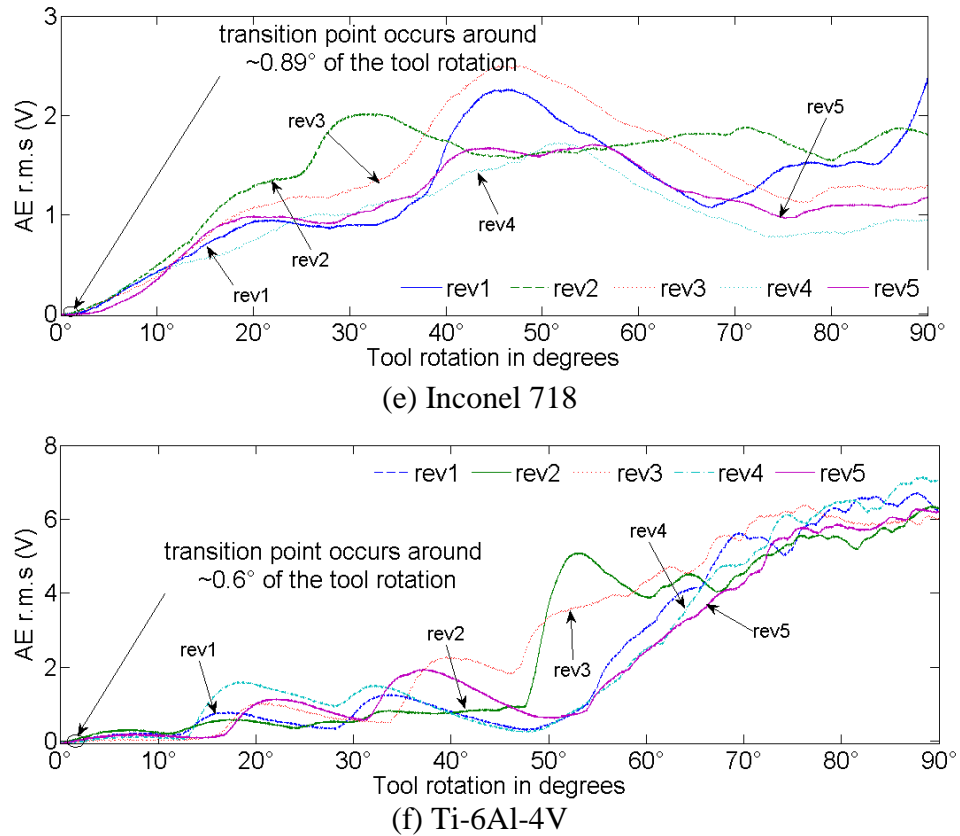


Fig. 7.14 $AE_{r.m.s}$ generated at $10 \mu\text{m}/\text{tooth}$

From the comparison of $AE_{r.m.s}$ trends observed at 0.5, 2, $10 \mu\text{m}$ maximum undeformed chip thickness suggested that once the transition from rubbing to chip formation occurs, the $AE_{r.m.s}$ gradually increases regardless of h/r_e . However, under certain condition, $AE_{r.m.s}$ remains constant after approximately 25° of initial tool-workpiece engagement for copper, AISI 1005 steel and Inconel 718 workpiece materials (Fig. 7.14 (a, c and e)). In contrast, a nearly linear relationship exists between $AE_{r.m.s}$ and tool position angle for Al 6082-T6, AISI 1045 and Ti-6Al-4V workpiece materials as shown in Fig. 7.14 (b, d and f)) at the same chip load of $10 \mu\text{m}/\text{tooth}$.

The chip thickness variations along the tool position angle can possibly address this anomalous relationship between $AE_{r.m.s}$ and chip thickness. Fig. 7.15 shows the typical variation in the deformed chip thickness for two kind of ferrous material and titanium alloys. These chips were mounted in hot resin, polished and photographed under scanning electron microscopy. Fig. 7.15 (a) shows that the thickness of periodic pile up in each chip segment of AISI 1005 steel remains the same after a certain position angle and a crack initiated at free surface propagates partway of chip thickness. However, in

the initial arc of contact shear fronts extended across the thin chip thickness. AE signals are presumably less attenuated and hence increases proportionally during this period. Fig. 7.15 b and c shows gradual increase in chip thickness along the width of cut for AISI 1045 and Ti-6Al-4V, respectively. These are in line with their respective $AE_{r.m.s}$ trends.

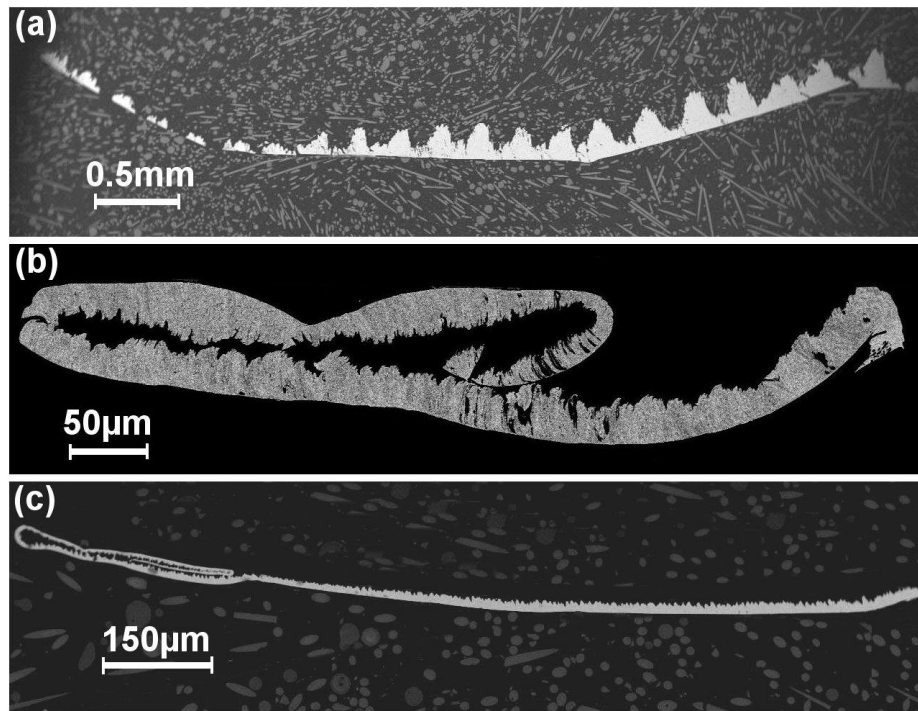


Fig. 7.15 Typical chip thickness variation at 10 μm feed/ tooth in micro milling of (a) AISI 1005 steel (b) AISI 1045 steel (c) Ti-6Al-4V alloy

The exact tool cutting edge position is difficult to ascertain at the beginning of the tool engagement process. However, it is suggested that this in the initial 200 μs of tool contact the signal is lost in the noise [126]. The referencing of the signal as done in this procedure may help isolate the initial beyond zero burnishing period. In order to estimate the possible range of minimum chip thickness for selected workpiece materials, the identified rubbing signature at the certain position of tool rotation (ϕ) in the investigated feeds per tooth (f_z) were put into the eq. (7.2) developed for classical milling process [175]. The undeformed chip thickness (h) varies according to the relationship

$$h = f_z \sin \phi \quad (7.2)$$

The computed range of the results are summarised in Table 7.5. Then the estimated minimum chip thicknesses were compared with the corresponding tool edge radius to access the validity of this approach. The normalised values were in agreement with the minimum chip thickness values available for different workpiece material shown in Table 7.1. Note that the estimated values associated with different undeformed chip thickness were found to be comparable. Thus the resulting relationship indicates that tool edge radius is crucial in defining the threshold value regardless of the undeformed chip thickness.

Table 7.5 Estimated minimum chip thicknesses from AE signals

	Cu (OFHC)	Al 6082-T6	AISI 1005 steel	AISI 1045 steel	Ti-6Al-4V	Inconel 718
Estimated h_m (μm)	0.06 to 0.1	0.1 to 0.16	0.2 to 0.23	0.07 to 0.13	0.08 to 0.1	0.1 to 0.17
h_m/r_e in percentage	11 to 18	23 to 39	31 to 42	20 to 36	19 to 28	18 to 26

7.5 Boundary Conditions for Successful Implementation of this Methodology

In order to obtain the most accurate and reliable results, the following measures were identified as important:

- i. During the course of research it was found that the location of AE sensor and its sensitivity should be optimised to control the strength of AE signal and hence circumvent the loss of useful information.
- ii. After each cutting test, a new cutting edge was used to avoid possible deviation in the measured AE signal due to tool wear. To test this premise, cutting was performed with a worn tool (0.2 mm maximum flank wear) at $0.02 \mu\text{m}/\text{tooth}$ on ferrous workpiece materials. Fig. 7.16 shows the outcome of those trials. Considerably lower magnitude of $AE_{r.m.s}$ signal can be observed as compared to that for a new tool. Hence, by ignoring the cutting edge condition prior to cutting, information inferred from the AE signals can be misleading. Also, the sub-surface images in the Fig. 7.16 demonstrate an obvious correlation of microstructure modification with the corresponding tool wear. The decrease in AE signature as a function of microstructure change was attributed to the increase in damping rate of the tool/ workpiece system [174]. These results show that raw AE signal can be

used to monitor the influence of the micro cutting on the subsurface microstructure of the workpiece.

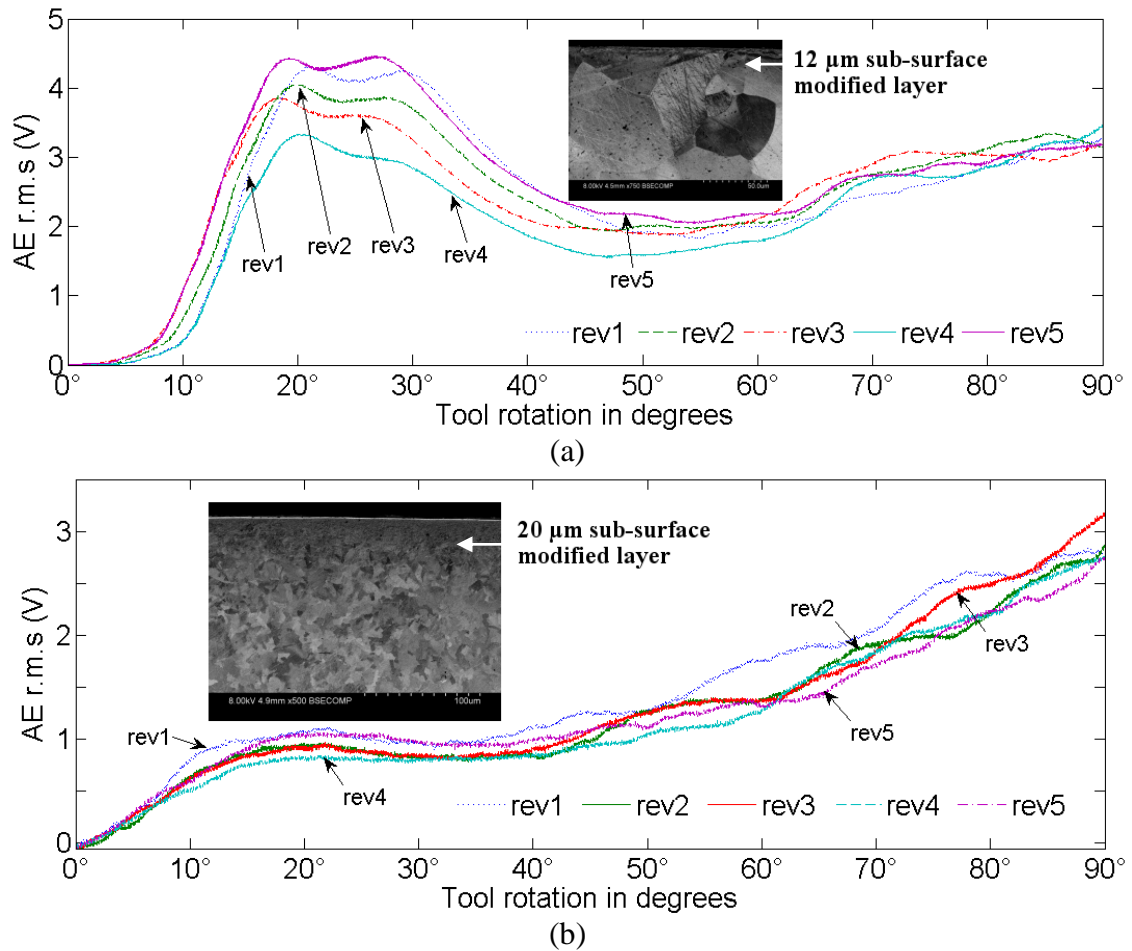


Fig. 7.16 Material microstructure damping effect on $AE_{r.m.s}$ signature at 0.02 μm chip load in micro milling of (a) AISI 1005 steel (b) AISI 1045 steel

- iii. At times entrance or exit conditions of the tool cutting passes produce slight aberrations in the $AE_{r.m.s}$ signals. Fig. 7.17 shows examples of such cases where the variations in $AE_{r.m.s}$ signal can be seen in non-active cutting time for aluminium and copper workpiece materials generated at 10 μm/tooth. The images of aluminium chips welded on the previously machined surface and copper rollover burrs produced at exits of the cut were also inserted in their respective graphs. In Fig. 7.17 (a) dotted circle indicates the interference of chips with the tool edge radius, causing earlier rise in the $AE_{r.m.s}$ signature. Whereas, dotted circles in Fig. 7.17 (b) discern the disturbance of $AE_{r.m.s}$ signal in five successive rotations due to continuous engagement of relatively large burrs with the tool after the active cutting pass. Thus, it is impossible to select a constant Y-ordinate at the start of every engagement.

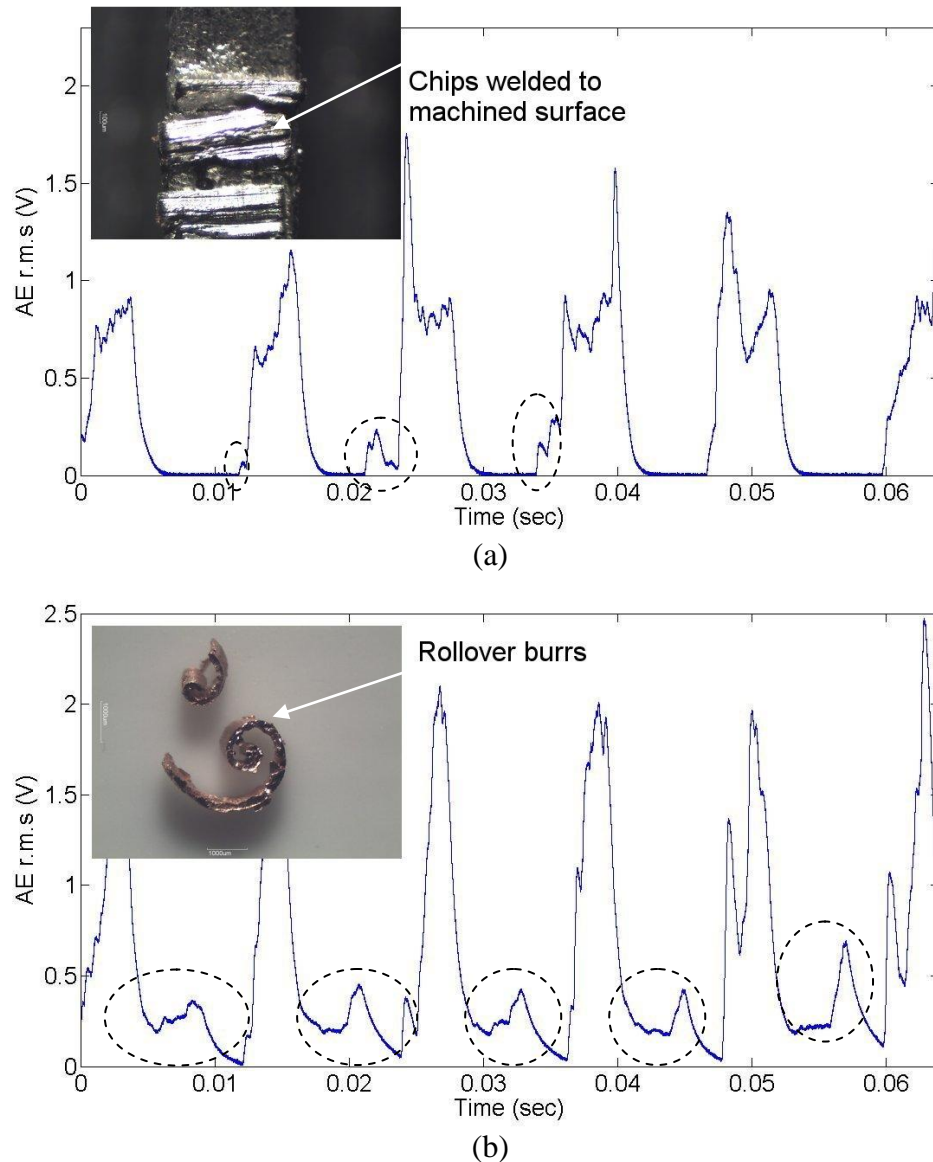


Fig. 7.17 Material microstructure damping effect on $AE_{r.m.s}$ signature at $10\ \mu\text{m}$ chip load in micro milling of (a) Al 6082-T6 (b) Cu (OFHC)

- iv. Always extract the identified $AE_{r.m.s}$ rubbing signature in the successive tool rotation in order to keep time information intact. An undeformed chip thickness to tool edge radius in the order of four was found to be more practical to get consistent values. Thus the repeatability and finer calibration of the results, is enhanced by the use of a feed per tooth that is higher than the tool edge radius.

7.6 Conclusions

The present study proposed an indirect methodology for the estimation of minimum chip thickness in micro milling operation. It is based on acoustic emission emanating in micro machining. The significant findings can be summarised as

- Comparing the AE spectrogram for a tool engaged below the minimum chip thickness and that cutting in a shear dominated zone can help define the signal characteristics that correlate with the onset of minimum chip thickness in milling.
- The value of minimum chip thickness estimated from the identified rubbing AE_{rms} signature during micro milling process falls within the range reported in literature. It should, however, be emphasized that most literature derived the minimum chip thickness from modelling rather than experimental investigations. The potential of using the new approach to improve the accuracy of prediction or calibrate numerical models is an interesting area.
- In general, the implementation of this methodology will be challenging for those materials whose chips have higher tendency to adhere on the machined surface or produce thicker burrs at the exit of the cut.
- Increase in the compressive residual stress on the surface layer was observed with decrease in the undeformed chip thickness.
- AE has potential to provide real-time process monitoring that can shed light on machined subsurface micro-structural change.
- The minimum chip thickness was found to occur at 11 to 18 percent, 18 to 26 percent, 19 to 28 percent, 20 to 36 percent, 31 to 42 percent, and 23 to 39 percent of the tool edge radius, for a Cu (OFHC), Inconel 718, Ti-6Al-4V, AISI 1045 steel, AISI 1005 steel and Al 6082-T6 respectively.
- The results as stated above were tested on a stand alone machine tool in cutting ductile materials. In implementing the minimum chip thickness AE evaluation technique, it is important to identify the susceptibility of the signal to attenuation

and high operational background noise. Signal interference may compromise the ability to relate the resultant AE signature to the chip formation mechanism. The application of the technique in ductile mode cutting is not reported in this chapter.

Chapter 8

CONCLUSIONS AND RECOMMENDATIONS FOR FUTURE RESEARCH

8.1 Conclusions

The fundamental difference between the macro milling and micro milling arises due to the scale of operation. In this respect, the primary focus of the research was to investigate the tool edge radius and workpiece material microstructure size effects in micro milling when cutting was performed with carbide tools. To achieve this, a combination of experimental, statistical and signal processing techniques were employed.

During this course, some interesting and important results were discovered that can be useful in the advancement of knowledge in the field of micro machining. These include:

- Based on the findings on AISI 1005 and AISI 1045 steel, it may be suggested that surface generated with single phase ferritic materials are easier to predict and control as compared to multi-phase material due to combined effects of differential elastic recovery between the phases and micro burr formation at grain boundaries. However, the challenge in machining single phase ferritic material relates to edge profile definition as driven by burr size growth.

- Reflecting on all the results on surface roughness, it can be concluded that for very short machining times, micromachining (of large grained structure) in the ploughing mode (undeformed chip thickness less than tool edge radius) gives best surface finish. Therefore, stringent surface finish requirements can then be met by machining at undeformed chip thickness closer to the edge radius to obtain good surface finish at relatively small burr size provided that frequent tool changeovers are undertaken to mitigate the effects of rapid wear.
- The best surface finish was obtained at feedrates closer to the tool edge radius for both workpiece materials. This suggests that generation of the best surface finish was more sensitive to tool edge radius than material grain size effects. Thus information on tool edge radius should be available to micromachining process planners.
- Increase in the nano-hardness was observed in the vicinity of machined regions. This property modification as driven by milling mode is differential on milled surface profiles.
- In slotting operation the up milled side experienced small burrs as compared to down milled side. The information gained can be utilised in tool path planning for micro machined components. Final passes can be done in up milling mode.
- The specific energy, burr root thickness and surface roughness of micro machined parts can be used as relevant measures of the size effect in micro machining.
- Other than the ratio of feed per tooth to tool edge radius, the cutting velocity is another dominant control factor for influencing the size effect or process mechanism. This information is important for optimising the process or for breaking the lower limit of the micro machining process.
- It was found that manipulating the cutting velocity would be an effective way to manage size effect in the micro domain machining. Micro tools used for finishing operations can be run at high cutting speeds to reduce burr size but ensuring that the tool is changed early before significant tool wear.

However, this also needs to be balanced with compromise in surface roughness.

- Exploiting decomposed AE energy bands enabled identification of dominant chip formation mechanisms in micromachining. The workpiece materials with a higher work hardening severity were associated with dominant micro fracture chip formation mechanisms in the ploughing dominated mode.
- In micro cutting the tool on engagement initially experiences friction and rubbing and this is associated with a relatively weak AE signal this prevails until chip formation sets in which produces a burst in AE signal. Thus overlapping AE signals for subsequent tool engagements enables the identification of minimum chip thickness as the point where the initially weak AE signal experiences a burst and grows significantly.

8.2 Recommendations

The current research opens up new avenues for further research that can be undertaken in light of the conclusions reached here. The identified potential areas are outlined below:

- Wavelet decomposition of the acoustic emission signals has proved to be a useful tool towards systematic analysis of tool workpiece interactions at low undeformed chip thickness and smaller depth of cut. Conclusions and results from this research present a strong case to expand this approach to other difficult to cut materials, advanced composite materials and shape memory alloys to apprehend micro scale deformation mechanisms.
- During the course of present research, Taguchi methodology yielded information about the contribution ratios of main process variables on the selected outcomes. It would thus be logical research to employ suitable arrays to capture the contribution ratios of interaction effects of the factors that influence “size effect” phenomenon.
- Further research may be carried out towards the development of minimum chip thickness maps that can be exploited in selecting cutting speeds and feedrates for high precision components. The effect of frictional conditions

on the minimum chip thickness should also be investigated for a wider range tool coatings and cutting conditions.

- The in-depth profile measurement of residual stresses can be handy to assess the actual fatigue life of the micro components. This aspect can also elucidate the link between service life and different micro structural and mechanical properties of machined subsurface region.

References

- [1] Chae, J., Park, S. S., and Freiheit, T., Investigation of micro-cutting operations, *International Journal of Machine Tools and Manufacture*, 2006, 46 (3-4) 313–332.
- [2] Dornfeld, D., Min, S., and Takeuchi, Y., Recent advances in mechanical micromachining, *CIRP Annals - Manufacturing Technology*, 2006, 55 (2) 745–768.
- [3] Alting, L., Kimura, F., Hansen, H. N., and Bissacco, G., Micro engineering, *CIRP Annals - Manufacturing Technology*, 2003, 52 (2) 635–657.
- [4] Bissacco, G., Hansen, H. N., and De Chiffre, L., Micromilling of hardened tool steel for mould making applications, *Journal of Materials Processing Technology*, 2005, 167 (2-3) 201–207.
- [5] Friedrich, C. R., Micromechanical machining of high aspect ratio prototypes, *Microsystem Technologies*, 2002, 8 343–347.
- [6] McKeown, P. A., The role of precision engineering in manufacturing of the future, *CIRP Annals - Manufacturing Technology*, 1987, 36 (2) 495–501.
- [7] Kang, H.-J., and Ahn, S.-H., Fabrication and characterization of microparts by mechanical micromachining: precision and cost estimation, *Proceedings of the Institution of Mechanical Engineers, Part B: Journal of Engineering Manufacture*, 2007, 221 (2) 231-240.
- [8] Jáuregui, A., Siller, H., Rodríguez, C., and Elías-Zúñiga, A., Evaluation of micromechanical manufacturing processes for microfluidic devices, *The International Journal of Advanced Manufacturing Technology*, 2010, 48 (9) 963-972.
- [9] Bissacco, G., Hansen, H. N., and De Chiffre, L., Size effects on surface generation in micro milling of hardened tool steel, *CIRP Annals - Manufacturing Technology*, 2006, 55 (1) 593–596.
- [10] Filiz, S., Conley, C. M., Wasserman, M. B., and Ozdoganlar, O. B., An experimental investigation of micro-machinability of copper 101 using tungsten carbide micro-endmills, *International Journal of Machine Tools and Manufacture*, 2007, 47 (7-8) 1088–1100.
- [11] Vogler, M. P., DeVor, R. E., and Kapoor, S. G., On the modeling and analysis of machining performance in micro-endmilling, part I: surface generation, *Journal*

- of Manufacturing Science and Engineering, Transactions of the ASME, 2004, 126 (4) 685–694.
- [12] Simoneau, A., Ng, E., and Elbestawi, M. A., The effect of microstructure on chip formation and surface defects in microscale, mesoscale, and macroscale cutting of steel, *CIRP Annals - Manufacturing Technology*, 2006, 55 (1) 97–102.
- [13] Zhou, M., and Ngoi, B. K. A., Effect of tool and workpiece anisotropy on microcutting processes, *Proceedings of the Institution of Mechanical Engineers, Part B: Journal of Engineering Manufacture*, 2001, 215 (1) 13–19.
- [14] Zhou, M., Ngoi, B. K. A., Zhong, Z. W., and Wang, X. J., The effect of material microstructure on microcutting processes, *Materials and Manufacturing Processes*, 2001, 16 (6) 815–828.
- [15] Weule, H., Huntrup, V., and Tritschler, H., Micro-Cutting of steel to meet new requirements in miniaturization, *CIRP Annals - Manufacturing Technology*, 2001, 50 (1) 61–64.
- [16] Simoneau, A., E. Ng, and Elbestaw, M. A., Grain size and orientation effects when microcutting AISI 1045 Steel, *CIRP Annals - Manufacturing Technology* 2007, 56 (1) 57–60.
- [17] Simoneau, A., Ng, E., and Elbestawi, M. A., Surface defects during microcutting, *International Journal of Machine Tools and Manufacture*, 2006, 46 (12-13) 1378–1387.
- [18] Schmidt, J., Spath, D., Elsner, J., Hüntrup, V., and Tritschler, H., Requirements of an industrially applicable microcutting process for steel micro-structures, *Microsystem Technologies*, 2002, 8 (6) 402-408.
- [19] Takács, M., Verö, B., and Mészáros, I., Micromilling of metallic materials, *Journal of Materials Processing Technology*, 2003, 138 (1-3) 152–155.
- [20] Schmidt, J., and Tritschler, H., Micro cutting of steel, *Microsystem Technologies*, 2004, 10 (3) 167–174.
- [21] Fang, F. Z., and Liu, Y. C., On minimum exit-burr in micro cutting, *Journal of Micromechanics and Microengineering*, 2004, 14 984–988.
- [22] Weinert, K., and Petzoldt, V., Machining NiTi micro-parts by micro-milling, *Materials Science and Engineering*, 2008, 481-482 672–675.
- [23] Gillespie, L. K., Deburring precision miniature parts, *Precision Engineering* 1979, 189–198.

- [24] Lee, K., and Dornfeld, D. A., Micro-burr formation and minimization through process control, *Precision Engineering*, 2005, 29 (2) 246–252.
- [25] Klocke, F., Quito, F., K. Arntz, Souza, A. A., and Ader, C., Micro milling of single crystal Nickel-based superalloy Rene N5, 3rd international Conference High performance cutting (HPC) , Dublin, Ireland, June 12-13th, 2008, 1 (561-574)
- [26] Wang, J., Gong, Y., Abba, G., Chen, K., Shi, J., and Cai, G., Surface generation analysis in micro end-milling considering the influences of grain, *Microsystem Technologies*, 2008, 14 (7) 937-942.
- [27] Son, S. M., Lim, H. S., and Ahn, J. H., Effects of the friction coefficient on the minimum cutting thickness in micro cutting, *International Journal of Machine Tools and Manufacture*, 2005, 45 (4-5) 529–535.
- [28] Lee, D. E., Hwang, I., Valente, C. M. O., Oliveira, J. F. G., and Dornfeld, D. A., Precision manufacturing process monitoring with acoustic emission, *International Journal of Machine Tools and Manufacture*, 2006, 46 (2) 176–188.
- [29] Masuzawa, T., State of the art of micromachining, *CIRP Annals - Manufacturing Technology*, 2000, 49 (2) 473–488.
- [30] Masuzawa, T., and Tönshoff, H. K., Three-dimensional micromachining by machine tools, *CIRP Annals - Manufacturing Technology*, 1997, 46 (2) 621–628.
- [31] Liu, X., DeVor, R. E., Kapoor, S. G., and Ehmann, K. F., The mechanics of machining at the microscale: assessment of the current state of the science, *Journal of Manufacturing Science and Engineering, Transactions of the ASME* 2004, 126 (4) 666–678.
- [32] Simoneau, A., Ng, E., and Elbestawi, M. A., Chip formation during microscale cutting of a medium carbon steel, *International Journal of Machine Tools and Manufacture*, 2006, 46 (5) 467–481.
- [33] Aramcharoen, A., Mativenga, P. T., Yang, S., Cooke, K. E., and Teer, D. G., Evaluation and selection of hard coatings for micro milling of hardened tool steel, *International Journal of Machine Tools and Manufacture*, 2008, 48 (14) 1578–1584.
- [34] Dhanorker, A., and Özel, T., Meso/micro scale milling for micro-manufacturing, *International Journal of Mechatronics and Manufacturing Systems* 2008, 1 (1) 23 - 42

- [35] Vollertsen, F., Biermann, D., Hansen, H. N., Jawahir, I. S., and Kuzman, K., Size effects in manufacturing of metallic components, *CIRP Annals - Manufacturing Technology*, 2009, 58 (2) 566-587.
- [36] Miao, J. C., Chen, G. L., Lai, X. M., Li, H. T., and Li, C. F., Review of dynamics issues in micro-end-milling, *The International Journal of Advanced Manufacturing Technology*, 2007, 31 897-904.
- [37] Robinson, G. M., Jackson, M. J., and Whitfield, M. D., A review of machining theory and tool wear with a view to developing micro and nano machining processes, *Journal of material science*, 2007, 6 (4) 2002-2015.
- [38] Backer, W. R., Marshall, E. R., and Shaw, M. C., Size effect in metal cutting, *Transactions of the ASME* 1952, 74 (1) 61-72.
- [39] Nakayama, K., and Tamura, K., Size effect in metal-cutting force, *Journal of Engineering for Industry, Transactions of the ASME*, 1968, 90 119-126.
- [40] Larsen-Basse, J., and Oxley, P. L. B., Effect of strain-rate sensitivity on scale phenomenon in chip formation *Proceedings of 13th International machine tool Design & Research Conference, University of Birmingham*, 1973, 209-216.
- [41] Kopalinsky, E. M., and Oxley, P. L. B., Size effects in metal removal process, *3rd Conference on Mechanical Properties at High Rates of Strain, Oxford*, 1984, 389-396.
- [42] Furukawa, Y., and Moronuki, N., Effect of material properties on ultra precise cutting processes, *CIRP Annals - Manufacturing Technology* 1988, 37 (1) 113-116.
- [43] Lucca, D. A., Rhorer, R. L., and Komanduri, R., Energy dissipation in the ultraprecision machining of copper, *CIRP Annals - Manufacturing Technology*, 1991, 40 (1) 69-72.
- [44] Lucca, D. A., Rhorer, R. L., and Komanduri, R., Effect of tool edge geometry on energy dissipation in ultra precision machining, *CIRP Annals - Manufacturing Technology*, 1993, 42 (1) 83-86.
- [45] Ng, C. K., Melkote, S. N., Rahman, M., and Kumar, A. S., Experimental study of micro- and nano-scale cutting of aluminum 7075-T6, *International Journal of Machine Tools and Manufacture*, 2006, 46 929-936.
- [46] Liu, K., and Melkote, S. N., Material strengthening mechanisms and their contribution to size effect in micro-cutting, *Journal of Manufacturing Science and Engineering, Transactions of the ASME* 2006, 128 (3) 730-738.

- [47] Subbiah, S., and Melkote, S. N., Effect of finite edge radius on ductile fracture ahead of the cutting tool edge in micro-cutting of Al2024-T3, *Materials Science and Engineering: A*, 2008, 474 (1-2) 283–300.
- [48] Wu, J., and Liu, Z., Modeling of flow stress in orthogonal micro-cutting process based on strain gradient plasticity theory, *The International Journal of Advanced Manufacturing Technology*, 46 (1) 143-149.
- [49] Taniguchi, N., 1993 ASPE distinguished lecturer, *Precision Engineering*, 1994, 16 (1) 5-24.
- [50] Shaw, M. C., The size effect in metal cutting, *Sadhana*, 2003, 28 (5) 875–896.
- [51] Fang, N., Slip-line modeling of machining with a rounded-edge tool-part II: analysis of the size effect and the shear strain-rate, *Journal of the Mechanics and Physics of Solids*, 2003, 51 743–762.
- [52] Liu, K., and Melkote, S. N., Finite element analysis of the influence of tool edge radius on the size effect in orthogonal micro-cutting process, *International Journal of Mechanical Sciences*, 2007, 49 650–660.
- [53] Lai, X., Li, H., Li, C., Lin, Z., and Ni, J., Modelling and analysis of micro scale milling considering size effect, micro cutter edge radius and minimum chip thickness, *International Journal of Machine Tools and Manufacture*, 2008, 48 (1) 1-14.
- [54] Shimada, S., Ikawa, N., Tanaka, H., Ohmori, G., Uchikoshi, J., and Yoshinaga, H., Feasibility study on ultimate accuracy in microcutting Using Molecular Dynamics Simulation, *CIRP Annals - Manufacturing Technology*, 1993, 42 (1) 91–94.
- [55] Moriwaki, T., Okuda, K., and Shen, J. G., Study on ultraprecision orthogonal microdiamond cutting of single-crystal copper, *JSME International Journal, Series C*, 1993, 36 (3) 400–406.
- [56] Shaw, M. C., Energy conversion in cutting and grinding, *CIRP Annals - Manufacturing Technology*, 1996, 45 (1) 101-104.
- [57] Albrecht, P., New developments in theory of metal-cutting process -1. Ploughing process in metal cutting, *Journal of Engineering for Industry, Series B, Transactions of the ASME* 1960, 82 (4) 348–358.
- [58] Kim, J. D., and Kim, D. S., On the size effect of micro-cutting force in ultraprecision machining, *JSME International Journal, series C*, 1996, 39 (1) 164–169.

- [59] Lucca, D. A., Seo, Y. W., Rhoer, R. L., and Donaldson, R. R., Aspects of surface generation in orthogonal ultraprecision machining, *CIRP Annals - Manufacturing Technology*, 1994, 43 (1) 43–46.
- [60] Komanduri, R., Chandrasekaran, N., and Raff, L. M., Effect of tool geometry in nanometric cutting: a molecular dynamics simulation approach, *Wear*, 1998, 219 (1) 84–97.
- [61] Inamura, T., Takezawa, N., and Kumaki, Y., Mechanics and energy dissipation in nanoscale cutting, *CIRP Annals - Manufacturing Technology*, 1993, 42 (1) 79-82.
- [62] Astakhov, V. P., *Metal Cutting Mechanics*. 1999: CRC press: Boca Raton, FL.
- [63] Shaw, M. C., *Metal Cutting Principles*. second ed. 2005: oxford university press.
- [64] Atkins, A. G., Modelling metal cutting using modern ductile fracture mechanics: Quantitative explanations for some longstanding problems, *International Journal of Mechanical Sciences*, 2003, 45 373–396.
- [65] Moronuki, N., Liang, Y., and Furukawa, Y., Experiments on the effect of material properties on microcutting processes, *Precision Engineering*, 1994, 16 (2) 124–131.
- [66] Ikawa, N., Shimada, S., and Tanaka, H., Minimum thickness of cut in micromachining, *Nanotechnology*, 1992, 3 6–9.
- [67] Kim, C. J., Bono, M., and Ni, J., Experimental analysis of chip formation in micro-milling, *Transactions of the NAMRI/SME*, 2002, 30 1–8.
- [68] Mian, A. J., Driver, N., and Mativenga, P. T., Micromachining of coarse-grained multi-phase material, *Proceedings of the Institution of Mechanical Engineers, Part B: Journal of Engineering Manufacture*, 2009, 223 (4) 377–385.
- [69] Vogler, M. P., DeVor, R. E., and Kapoor, S. G., On the modeling and analysis of machining performance in micro-endmilling, part II: cutting force prediction, *Journal of Manufacturing Science and Engineering, Transactions of the ASME* 2004, 126 (4) 695–705.
- [70] Komanduri, R., Some aspects of machining with negative rake tools simulating grinding, *International Journal of Machine Tool Design and Research*, 1971, 11 223–233.
- [71] Abdelmoneim, M. E., and Scrutton, R. F., Post-machining plastic recovery and the law of abrasive wear, *Wear*, 1973, 24 1–13.

- [72] L'vov, N. P., Determining the minimum possible chip thickness, *Machine Tool (USSR)*, 1969, 40 45.
- [73] Basuray, P. K., Misra, B. K., and Lal, G. K., Transition from ploughing to cutting during machining with blunt tools, *Wear*, 1977, 43 341–349.
- [74] Yuan, Z. J., Zhou, M., and Dong, S., Effect of diamond tool sharpness on minimum cutting thickness and cutting surface integrity in ultra precision machining, *Journal of Materials Processing Technology*, 1996, 62 327–330.
- [75] Kim, C. J., Mayor, J. R., and Ni, J., A static model of chip formation in microscale milling, *Journal of Manufacturing Science and Engineering, Transactions of the ASME* 2004, 126 (4) 710–718.
- [76] Liu, X., DeVor, R. E., and Kapoor, S. G., An analytical model for the prediction of minimum chip thickness in micromachining, *Journal of Manufacturing Science and Engineering, Transactions of the ASME*, 2006, 128 (2) 474–481.
- [77] Jardret, V., Zahouani, H., Loubet, J. L., and Mathia, T. G., Understanding and quantification of elastic and plastic deformation during a scratch test, *Wear*, 1998, 218 (1) 8–14.
- [78] Nakayama, K., Topics on fundamentals of precision machining, *Machining Science and Technology*, 1997, 1 (2) 251–262.
- [79] Taniyama, H., Eda, H., Zhou, L., Shimizu, J., and Sato, J., Experimental investigation of micro scratching on the two-phase steel: plastic flow mechanisms of the ferrite and cementite phases, *Key Engineering Materials*, 2003, 238-239 15–18.
- [80] Black, J. T., Shear front-lamella structure in large strain plastic deformation Processes, *Journal of Engineering for Industry*, 1972, 94 (2) 307-316.
- [81] Von Turkovich, B. F., and Black, J. T., Micro-machining of copper and aluminum crystals, *Journal of Engineering for Industry*, 1970, 92 (2) 130-134.
- [82] Ueda, K., and Manabe, K., Chip formation mechanism in microcutting of an amorphous metal, *CIRP Annals - Manufacturing Technology*, 1992, 41 (1) 129-132.
- [83] Manjunathaiah, J., and Endres, W. J., A study of apparent negative rake angle and its effect on shear angle during orthogonal cutting with edge-radiused tools, *Transaction of NAMRI/SME XXVIII*, 2000, 197–202.

- [84] Ohbuchi, Y., and Obikawa, T., Finite element modeling of chip formation in the domain of negative rake angle cutting, *Journal of Manufacturing Science and Engineering, Transactions of the ASME* 2003, 125 324–332.
- [85] Moriwaki, T., Sugimura, N., and Luan, S., Combined stress, material flow and heat analysis of orthogonal micromachining of copper, *CIRP Annals - Manufacturing Technology*, 1993, 42 (1) 75-78.
- [86] Astakhov, V. P., Shvets, S. V., and Osman, M. O. M., Chip structure classification based on mechanics of its formation, *Journal of Materials Processing Technology*, 1997, 71 (2) 247-257.
- [87] Moriwaki, T., Horiuchi, A., and Okuda, K., Effect of cutting heat on machining accuracy in ultra-precision diamond turning, *CIRP Annals - Manufacturing Technology*, 1990, 39 (1) 81-84.
- [88] Komanduri, R., and Brown, R. H., On The mechanics of chip segmentation in machining, *Journal of Engineering for Industry*, 1981, 103 (1) 33-51
- [89] Tönshoff, H. K., Arendt, C., and Amor, R. B., Cutting of hardened steel, *CIRP Annals - Manufacturing Technology*, 2000, 49 (2) 547-566.
- [90] Nakayama, K., Arai, M., and Kanda, T., Machining characteristics of hard materials, *CIRP Annals - Manufacturing Technology*, 1988, 37 (1) 89-92.
- [91] Recht, R. F., A dynamic analysis of high speed machining, *Journal of Engineering for Industry*, 1985, 107 309-315.
- [92] Xie, J. Q., Bayoumi, A. E., and Zbib, H. M., A study on shear banding in chip formation of orthogonal machining, *International Journal of Machine Tools and Manufacture*, 1996, 36 (7) 835-847.
- [93] Barry, J., Byrne, G., and Lennon, D., Observations on chip formation and acoustic emission in machining Ti-6Al-4V alloy, *International Journal of Machine Tools and Manufacture*, 2001, 41 (7) 1055–1070.
- [94] Komanduri, R., and Von Turkovich, B. F., New observations on the mechanism of chip formation when machining titanium alloys, *Wear*, 1981, 69 (2) 179-188.
- [95] Komanduri, R., and Schroeder, T. A., On shear instability in machining a nickel-iron base superalloy, *Journal of Engineering for Industry, Transactions of the ASME*, 1986, 108 93–100.
- [96] Min, S., Sangermann, H., Mertens, C., and Dornfeld, D., A study on initial contact detection for precision micro-mold and surface generation of vertical

- side walls in micromachining, *CIRP Annals - Manufacturing Technology*, 2008, 57 (1) 109–112.
- [97] To, S., Lee, W. B., and Chan, C. Y., Ultraprecision diamond turning of aluminium single crystals, *Journal of Materials Processing Technology*, 1997, 63 (1-3) 157–162.
- [98] Liu, X., Devor, R. E., and Kapoor, S. G., Model-based analysis of the surface generation in microendmilling-Part 1: Model development, *Journal of Manufacturing Science and Engineering, Transactions of the ASME* 2007, 129 (2) 453–460.
- [99] Liu, X., Devor, R. E., and Kapoor, S. G., Model-based analysis of the surface generation in microendmilling-Part II: Model development, *Journal of Manufacturing Science and Engineering, Transactions of the ASME* 2007, 129 (2) 461–469.
- [100] Gillespie, L. K., and Blotter, P. T., The formation and properties of machining burrs, *Journal of Manufacturing Science and Engineering, Transactions of the ASME*, 1976, 98 66–74.
- [101] Hashimura, M., Chang, Y. P., and Dornfeld, D., Analysis of burr formation mechanism in orthogonal cutting, *Journal of Manufacturing Science and Engineering, Transactions of the ASME*, 1999, 121 (1) 1-7.
- [102] Lee, K., and Dornfeld, D. A., An experimental study on burr formation in micro milling aluminium and copper, *Transactions of the NAMRI/SME* 2002, 30 255–262.
- [103] Aurich, J. C., Dornfeld, D., Arrazola, P. J., Franke, V., Leitz, L., and Min, S., Burrs-analysis, control and removal, *CIRP Annals - Manufacturing Technology*, 2009, 58 (2) 519-542.
- [104] Nakayama, K., and Arai, M., Burr formation in metal cutting, *CIRP Annals - Manufacturing Technology*, 1987, 36 (1) 33–36.
- [105] Schaller, T., Bohn, L., Mayer, J., and Schubert, K., Microstructure grooves with a width of less than 50 μm cut with ground hard metal micro end mills, *Precision Engineering*, 1999, 23 (4) 229–235.
- [106] Friedrich, C. R., and Kulkarni, V. P., Effect of workpiece springback on micro milling forces, *Microsystem Technologies*, 2004, 10 472–477.

- [107] Vogler, M. P., DeVor, R. E., and Kapoor, S. G., Prediction model for micro-milling of multi-Phase materials, *Journal of Manufacturing Science and Engineering, Transactions of the ASME* 2003, 125 (2) 202–209.
- [108] Trent, E. M., *Metal Cutting*. 1984, second edition London: Butterworth & Co. Ltd.
- [109] Hearn, E. J., *Mechanics of Materials, Volume 1 - An Introduction to the Mechanics of Elastic and Plastic Deformation of Solids and Structural Materials* (3rd Edition). 1997, Elsevier.
- [110] Ezugwu, E. O., and Wang, Z. M., Titanium alloys and their machinability--a review, *Journal of Materials Processing Technology*, 1997, 68 (3) 262-274.
- [111] Choudhury, I. A., and El-Baradie, M. A., Machinability of nickel-base super alloys: a general review, *Journal of Materials Processing Technology*, 1998, 77 (1-3) 278-284.
- [112] Arunachalam, R., and Mannan, M. A., Machinability of nickel-based high temperature alloys, *Machining Science and Technology*, 2000, 4 (1) 127–168.
- [113] Popov, K., Dimov, S., Pham, D. T., Minev, R., and Rosochowski, A., Micro milling: material microstructure effects, *Proceedings of the Institution of Mechanical Engineers, Part B: Journal of Engineering Manufacture*, 2006, 220 (11) 1807–1813.
- [114] Rahman, M., Kumar, A. S., and Prakash, J. R. S., Micro milling of pure copper, *Journal of Materials Processing Technology*, 2001, 116 (1) 39–43.
- [115] Aramcharoen, A., and Mativenga, P. T., Size effect and tool geometry in micromilling of tool steel, *Precision Eng*, 2008,
- [116] Rangwala, S., and Dornfeld, D., A study of acoustic emission generated during orthogonal metal cutting-1: Energy analysis, *International Journal of Mechanical Sciences*, 1991, 33 (6) 471–487.
- [117] Diei, E. N., and Dornfeld, D. A., Acoustic emission from the face milling process - the effects of process variables, *Journal of Engineering for Industry, Transactions of the ASME*, 1987, 109 (2) 92–99.
- [118] Dornfeld, D. A., and Kannatey-Asibu, E., Acoustic emission during orthogonal metal cutting, *International Journal of Mechanical Sciences*, 1980, 22 (5) 285–296.

- [119] Uehara, K., and Kanda, Y., Identification of chip formation mechanism through acoustic emission measurements, *CIRP Annals - Manufacturing Technology*, 1984, 33 (1) 71–74.
- [120] Carpenter, S. H., Heiple, C. R., Armentrout, D. L., Kustas, F. M., and Schwarzberg, J. S., Acoustic emission produced by sliding friction and its relationship to AE from machining, *Journal of Acoustic Emission*, 1992, 10 (3-4) 97–101.
- [121] Saini, D. P., and Park, Y. J., A quantitative model of acoustic emissions in orthogonal cutting operations, *Journal of Materials Processing Technology*, 1996, 58 (4) 343–350.
- [122] Shaw, M. C., A new mechanism of plastic flow, *International Journal of Mechanical Sciences*, 1980, 22 (11) 673–686.
- [123] Anderson, T. L., *Fracture mechanics : fundamentals and applications* Edition 2nd ed. ed: Boca Raton, Fla. ; London : CRC Press, 1995 688.
- [124] Kannatey-Asibu Jr., E., and Dornfeld, D. A., Quantitative relationships for acoustic emission from orthogonal metal cutting, *Journal of Engineering for Industry, Transactions of the ASME*, 1981, 3 (103) 30–340.
- [125] Lan, M.-S., and Dornfeld, D. A., Acoustic emission and machining - process analysis and control, *Materials and Manufacturing Processes*, 1986, 1 (1) 1–21.
- [126] Liu, J. J., and Dornfeld, D. A., Modeling and analysis of acoustic emission in diamond turning, *Journal of Manufacturing Science and Engineering, Transactions of the ASME*, 1996, 118 199–207.
- [127] Liu, M., and Liang, S. Y., Analytical modeling of acoustic emission for monitoring of peripheral milling process, *International Journal of Machine Tools and Manufacture*, 1991, 31 (4) 589–606.
- [128] Childs, T. H. C., Maekawa, K., Obikawa, T., and Yamane, Y., *Metal Machining - Theory and Applications*. (pp: 155). 2000: Elsevier.
- [129] Kamarthi, S. V., Kumara, S. R. T., and Cohen, P. H., Flank wear estimation in turning through wavelet representation of acoustic emission signals *Journal of Manufacturing Science and Engineering, Transactions of the ASME*, 2000, 122 12–19.
- [130] Teti, R., Jemielniak, K., O'Donnell, G., and Dornfeld, D., Advanced monitoring of machining operations, *CIRP Annals - Manufacturing Technology*, 2010, 59 (2) 717-739.

- [131] Sturges, R. H., Monitoring milling processes through AE and tool/part geometry, *Journal of Engineering for Industry, Transactions of the ASME*, 1992, 114 (1) 8–14.
- [132] Rangwala, S., and Dornfeld, D., A study of acoustic emission generated during orthogonal metal cutting--2: Spectral analysis, *International Journal of Mechanical Sciences*, 1991, 33 (6) 489–499.
- [133] Li, C. J., Signal processing in manufacturing monitoring, in *Condition Monitoring and Control for Intelligent Manufacturing*. 2006. p. 245–265.
- [134] Chen, X., Tang, J., and Dornfeld, D., Monitoring and analysis of ultraprecision metal cutting with acoustic emission, *Mechanical engineering congress and exposition, ASME*, 1996, 387–393.
- [135] Li, H., Lai, X., Li, C., Feng, J., and Ni, J., Modelling and experimental analysis of the effects of tool wear, minimum chip thickness and micro tool geometry on the surface roughness in micro-end-milling, *Journal of Micromechanics and Microengineering*, 2008, 18 (2) 1–12.
- [136] British Standard: Steels — Micrographic determination of the apparent grain size, BS EN ISO 643:2003
- [137] Gouldstone, A., Chollacoop, N., Dao, M., Li, J., Minor, A. M., and Shen, Y. L., Indentation across size scales and disciplines: Recent developments in experimentation and modeling, *Acta Materialia*, 2007, 55 (12) 4015–4039.
- [138] Aronson, R. B., Why dry machining?, *Manufacturing Engineering*, 1995, 114 (1) 33–36.
- [139] Park, J. B., Wie, K. H., Park, J. S., and Ahn, S. H., Evaluation of machinability in the micro end milling of printed circuit boards, *Proceedings of the Institution of Mechanical Engineers, Part B: Journal of Engineering Manufacture*, 2009, 223 (11) 1465–1474.
- [140] Aramcharoen, A., and Mativenga, P. T., Tool wear modes in micro/mesoscale milling of hardened die steel, in *CIRP 3rd International conference high performance cutting (HPC)*. 2008. Dublin, Ireland.
- [141] Armarego, E. J. A., and Brown, R. H., On the size effect in metal cutting, *International Journal of Production Research*, 1961, 1 (3) 75–99.
- [142] Joshi, S. S., and Melkote, S. N., An Explanation for the size-effect in machining using strain gradient plasticity, *Journal of Manufacturing Science and Engineering, Transactions of the ASME*, 2004, 126 (4) 679–684.

- [143] Choudhury, I. A., and El-Baradie, M. A., Machining nickel base superalloys: Inconel 718, Proceedings of the Institution of Mechanical Engineers, Part B: Journal of Engineering Manufacture, 1998, 212 (3) 195–206.
- [144] Dornfeld, D., Application of acoustic emission techniques in manufacturing, NDT & E International, 1992, 25 (6) 259–269.
- [145] Barry, J., and Byrne, G., Study on acoustic emission in machining hardened steels Part 2: acoustic emission during continuous chip formation with a non-overlapping cutting arrangement, Proceedings of the Institution of Mechanical Engineers - Part B - Engineering Manufacture, 2001, 215 (11) 1561–1570.
- [146] Zhou, L., Shimizu, J., Muroya, A., and Eda, H., Material removal mechanism beyond plastic wave propagation rate, Precision Engineering, 2003, 27 (2) 109–116.
- [147] Mian, A. J., Driver, N., and Mativenga, P. T., A comparative study of material phase effects on micro-machinability of multiphase materials, The International Journal of Advanced Manufacturing Technology, 2010, 50 (1) 163-173.
- [148] Aramcharoen, A., and Mativenga, P. T., Evaluation of critical parameters in micro machining of hardened tool steel, International Journal of Nanomanufacturing, 2009, 3 (1/2) 100–111.
- [149] Debabrata, P., Detection of change in processes using wavelets, Proceedings of the IEEE-SP International Symposium on Time-Frequency and Time-Scale Analysis, 1994, 174–177.
- [150] N.Logothetis, Managing for total quality from Deming to Taguchi and SPC. 1992: Prentice Hall International (UK) Ltd.
- [151] Schulz, H., and Moriwaki, T., High speed machining, CIRP Annals - Manufacturing Technology, 1992, 41 (2) 637–43.
- [152] Jawahir, I. S., and van Luttervelt, C. A., Recent developments in chip control research and applications, CIRP Annals - Manufacturing Technology, 1993, 42 (2) 659-693.
- [153] Kakade, S., Vijayaraghavan, L., and Krishnamurthy, R., In-process tool wear and chip-form monitoring in face milling operation using acoustic emission, Journal of Materials Processing Technology, 1994, 44 (3-4) 207-214.
- [154] Lee, W. B., Cheung, C. F., and To, S., Materials induced vibration in ultra-precision machining, Journal of Materials Processing Technology, 1999, 89-90 318-325.

- [155] Wang, H., To, S., Chan, C. Y., Cheung, C. F., and Lee, W. B., Elastic strain induced shear bands in the microcutting process, *International Journal of Machine Tools and Manufacture*, 50 (1) 9-18.
- [156] Chen, X., Raja, J., and Simanapalli, S., Multi-scale analysis of engineering surfaces, *International Journal of Machine Tools and Manufacture*, 1995, 35 (2) 231-238.
- [157] Teti, R., Jawahir, I. S., Jemielniak, K., Segreto, T., Chen, S., and Kossakowska, J., Chip form monitoring through advanced processing of cutting force sensor signals, *CIRP Annals - Manufacturing Technology*, 2006, 55 (1) 75-80.
- [158] Griffin, J., and Chen, X., Classification of the acoustic emission signals of rubbing, ploughing and cutting during single grit scratch tests, *International journal of Nanomanufacturing*, 2006, 1 (2) 189-209.
- [159] Tansel, I., Rodriguez, O., Trujillo, M., Paz, E., and Li, W., Micro-end-milling— I. Wear and breakage, *International Journal of Machine Tools and Manufacture*, 1998, 38 (12) 1419–1436.
- [160] Jaffery, S., and Mativenga, P., Assessment of the machinability of Ti-6Al-4V alloy using the wear map approach, *The International Journal of Advanced Manufacturing Technology*, 2009, 40 (7) 687-696.
- [161] Pierson, H. O., *Handbook of Refractory Carbides and Nitrides* Westwood. 1996: NJ:William Andrew Publishing.
- [162] M'Saoubi, R., and Chandrasekaran, H., Role of phase and grain size on chip formation and material work hardening during machining of single and dual phase steels *Ironmaking & Steelmaking*, 2004, 31 (3) 258-264.
- [163] Karpat, Y., Investigation of the effect of cutting tool edge radius on material separation due to ductile fracture in machining, *International Journal of Mechanical Sciences*, 2009, 51 (7) 541-546.
- [164] Davies, M. A., Chou, Y., and Evans, C. J., On chip morphology, tool wear and cutting mechanics in finish hard turning, *CIRP Annals - Manufacturing Technology*, 1996, 45 (1) 77-82.
- [165] Lee, M., Thomas, C. E., and Wildes, D. G., Prospects for in-process diagnosis of metal cutting by monitoring vibration signals, *Journal of Materials Science*, 1987, 22 (11) 3821–3830.
- [166] Aramcharoen, A., and Mativenga, P. T., Size effect and tool geometry in micromilling of tool steel, *Precision Engineering*, 2009, 33 (4) 402–407.

- [167] Rosa, P. A. R., Kolednik, O., Martins, P. A. F., and Atkins, A. G., The transient beginning to machining and the transition to steady-state cutting, *International Journal of Machine Tools and Manufacture*, 2007, 47 (12-13) 1904-1915.
- [168] Atkins, A. G., and Liu, J. H., Toughness and the transition between cutting and rubbing in abrasive contacts, *Wear*, 2007, 262 (1-2) 146-159.
- [169] Marinescu, I., and Axinte, D. A., A critical analysis of effectiveness of acoustic emission signals to detect tool and workpiece malfunctions in milling operations, *International Journal of Machine Tools and Manufacture*, 2008, 48 (10) 1148-1160.
- [170] Mian, A. J., Driver, N., and Mativenga, P. T., Chip formation in microscale milling and correlation with acoustic emission signal, *The International Journal of Advanced Manufacturing Technology*, ,D.O.I (10.1007/s00170-011-3185-x)
- [171] Margot R., Boeira A. M. G, Kuster F., Roelof H., Urlau U., and L., W. W., Monitoring Chip Formation in Machining through Strategical On-line Signal Processing of Acoustic Emission, in *The 38th CIRP International Seminar on Manufacturing Systems 2005*.
- [172] Jemielniak, K., Some aspects of acoustic emission signal pre-processing, *Journal of Materials Processing Technology*, 2001, 109 (3) 242-247.
- [173] Mian, A. J., Driver, N., and Mativenga, P. T., Estimation of minimum chip thickness for multi-phase steel using acoustic emission signals, in *Proceedings of the 36th International MATADOR Conference*. 2010: Manchester, UK. p. 197-200.
- [174] Tönshoff, H. K., Jung, M., Männel, S., and Rietz, W., Using acoustic emission signals for monitoring of production processes, *Ultrasonics*, 2000, 37 (10) 681–686.
- [175] Spiewak, S., An improved model of the chip thickness in milling, *CIRP Annals - Manufacturing Technology*, 1995, 44 (1) 39-42.
- [176] Bruce, A., and Gao, H.-Y., *Applied wavelet analysis with S-plus*. 1996, New York ; London : Springer 338.

Appendix A

Sample MatLab Commands

Text	Description
<pre>filterdata=load('CH1#00001_01h.TXT'); Fs=2000000; Tp=1/Fs; tm=linspace(Tp,0.064,128000); plot(tm,filterdata)</pre>	<p>AE signal variation with respect to time</p>
<pre>Q = fft(filterdata,2048); Pyy = Q.*conj(Q)/2048; f = 2000000/2048*(0:1015); plot(f,Pyy(1:1016)) axis([0 5e+5 0 70]); xlabel('Frequency (MHz)') title('Power spectral density')</pre>	<p>FFT computation</p>
<pre>spectrogram(filterdata,256,250,256,Fs,'yaxis')</pre>	<p>spectrogram analysis</p>
<pre>rms=load('CH2#00001_02h.TXT'); % plot(tm,rms) degree=linspace(0.015,90,6000); rev1 = rms(17890:23890); rev2 = rms(41900:47900); rev3 = rms(66140:72140); rev4 = rms(89891:95890); rev5 = rms(114001:120000); set(0,'DefaultAxesColorOrder',[0 0 0],... 'DefaultAxesLineStyleOrder','- -. -- :') plot(degree,rev1,degree,rev2,degree,rev3,degree,rev4, degree,rev5) legend('rev 1','rev 2','rev 3','rev 4','rev 5',5) plot(degree,rev1,degree,rev2,degree,rev3,degree,rev4, degree,rev5)</pre>	<p>AE_{rms} overlapped plot</p>

```
s=load('CH1#00001_01h.TXT');
l_s=length(s);
[C,L]=wavedec(s,5,'db3');
cA5=appcoef(C,L,'db3',5);
cD5=detcoef(C,L,5);
cD4=detcoef(C,L,4);
cD3=detcoef(C,L,3);
cD2=detcoef(C,L,2);
cD1=detcoef(C,L,1);
A5=wrcoef('a',C,L,'db3',5);
D1=wrcoef('d',C,L,'db3',1);
D2=wrcoef('d',C,L,'db3',2);
D3=wrcoef('d',C,L,'db3',3);
D4=wrcoef('d',C,L,'db3',4);
D5=wrcoef('d',C,L,'db3',5);
Fs=2000000;
Tp=1/Fs;
tm=linspace(Tp,0.032,64000);
d1=D1.*D1;
d2=D2.*D2;
d3=D3.*D3;
d4=D4.*D4;
d5=D5.*D5;
a5=A5.*A5;
energy_d1= trapz(tm,d1);
energy_d2= trapz(tm,d2);
energy_d3= trapz(tm,d3);
energy_d4= trapz(tm,d4);
energy_d5= trapz(tm,d5);
energy_a5= trapz(tm,a5);
Sig=s.*s;
energy = trapz(tm,Sig);

G.Tot=energy_d1+energy_d2+energy_d3+energy_d4
+
energy_d5+energy_a5
```

Energy calculations
using discrete wavelet
transformation algorithm

Appendix B

Wavelet transformation technique

The wavelet transformation provides the time-frequency representation of a signal. This technique is of particular interest where time interval of a particular spectral component occurring at any instant is needed. The main feature of wavelet analysis is that it breaks up the signal into smaller components with high-short and low-long frequency components to extract the exact occurrence of phenomenon from start or finish. A detailed theory of the discrete wavelet transform can be found in [176].

In the presented research, discrete wavelet transformation (DWT) algorithm of MATLAB[®] wavelet toolbox was used to decompose the signal into a series of approximations (A_i) and Details (D_i) frequency bands as shown in Fig. B1. The AE signal was decomposed into five levels ($i = 1, 2 \dots 5$), each corresponding with a certain frequency band. The mapping of these frequency bands to chip formation mechanism was based on the work by Dornfeld and co-workers [28]. Frequency bandwidths D1, D2 and D3 align with intergranular micro fracture, inclusion bursting and cleavage/micro fracture respectively. Whereas D4 and D5 corresponds to shearing micro voids events. The present investigation was motivated by the expectation that AE feature of micro milling can be extracted more accurately by using DWT. This study ultimately provides fundamental understanding of micro deformation mechanisms.

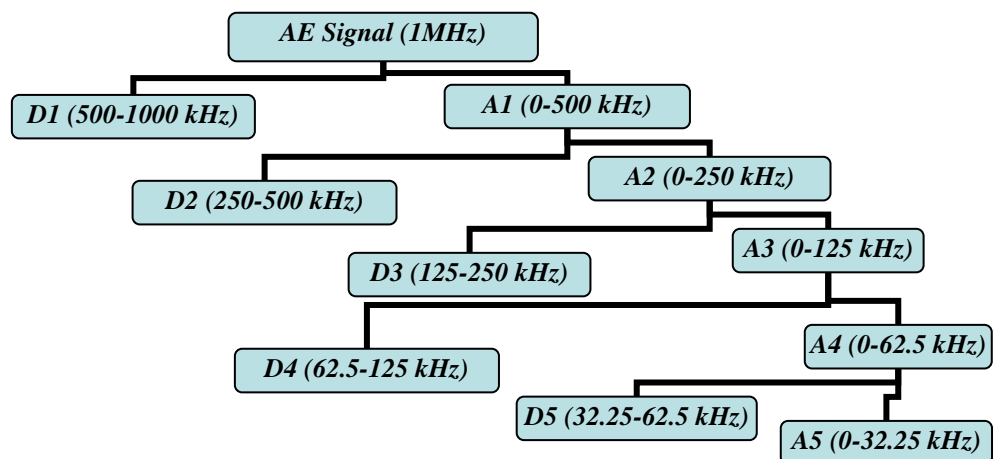


Fig. B1 Wavelet decomposition of a signal

Appendix C

Evaluation of key process variables

The definition of dominant parameters for the size effect is important in developing machinability data. It is the dominant process inputs that can be utilised to manipulate the cutting conditions. Moreover without knowing the dominant process parameters, industry has no knowledge of critical variables to control. This is particularly the case in micro machining of nickel based super alloys where mechanical micro machining is still in the rudimentary phase. Therefore, the present research evaluated key process variables for micro milling of Inconel 718 based on Taguchi analysis.

Taguchi proposed a transformation method to convert replication data into a single value of measure. Signal to noise ratio (SNR) is the transformation that determines the variation in the quality of the output. Three types of SNRs can be used depending on the type of characteristics being present. They include smaller-the-better (SB), nominal-is-best (NB) and larger-the-better (LB). The selection of appropriate SNR depends on the output function that is being evaluated. In this study, the aim is to minimise specific AE energy, surface roughness and burr size. Thus, SB was selected as a strategy to determine the factor effect. In addition to that LB was chosen to differentiate cutting parameter effects on different energy bands. The effect of each cutting parameter on the SNR at various levels can be separated out because the experimental design is orthogonal. The equations for the SNR_{SB} and SNR_{LB} characteristics are

$$SNR_{SB} = -10 \log_{10} \left\{ \frac{1}{n} \sum_i^n y_i^2 \right\} \dots\dots\dots 1$$

$$SNR_{LB} = -10 \log_{10} \left\{ \frac{1}{n} \sum_i^n y_i^{-2} \right\} \dots\dots\dots 2$$

Where n (value of n is 2 in this case) is the number of tests and y_i is the data collected in a trial of an output function.

Fig. C1 shows the factor effects in minimising specific AE energy (which is the integrated voltage of AE filtered per tool rotation signal normalised by the material removed). The optimal micro milling process settings were found to be 10 m/min (V_c), 0.8 (fz/re), 60 μm (a_p) using coated tools.

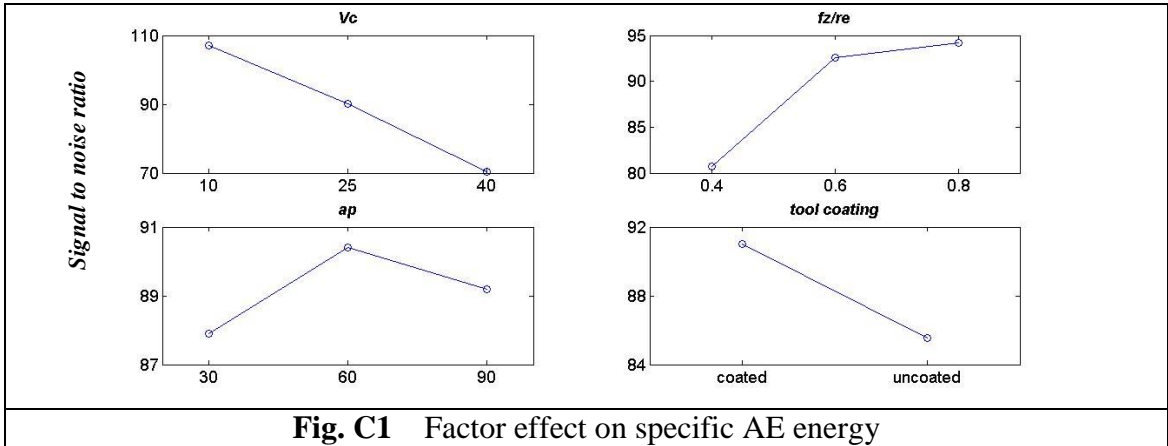


Fig. C1 Factor effect on specific AE energy

The process parameters response on surface roughness is shown in Fig. C2. The SNR plot reveals that the optimal condition to obtain best surface finish occurs at 25 m/min (V_c), 0.6 (fz/re), 30 μm (a_p) using coated tools.

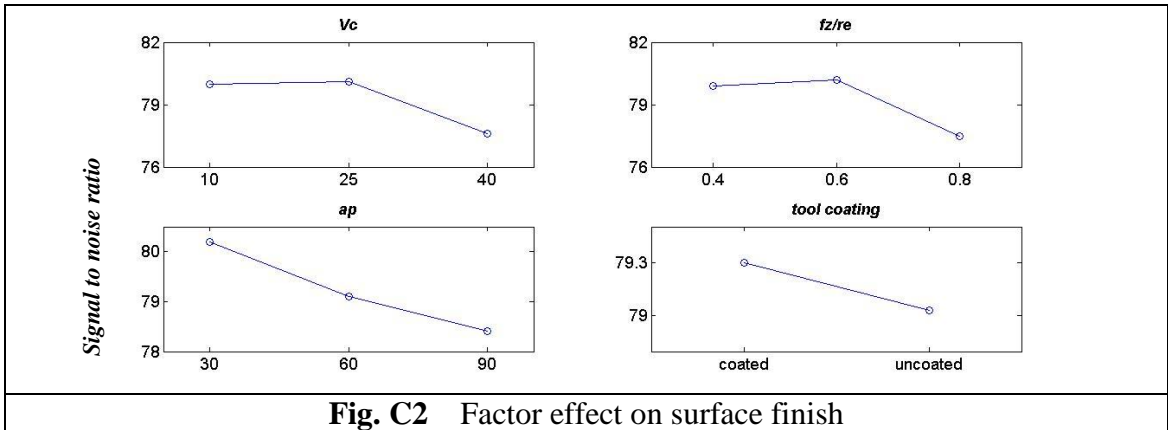
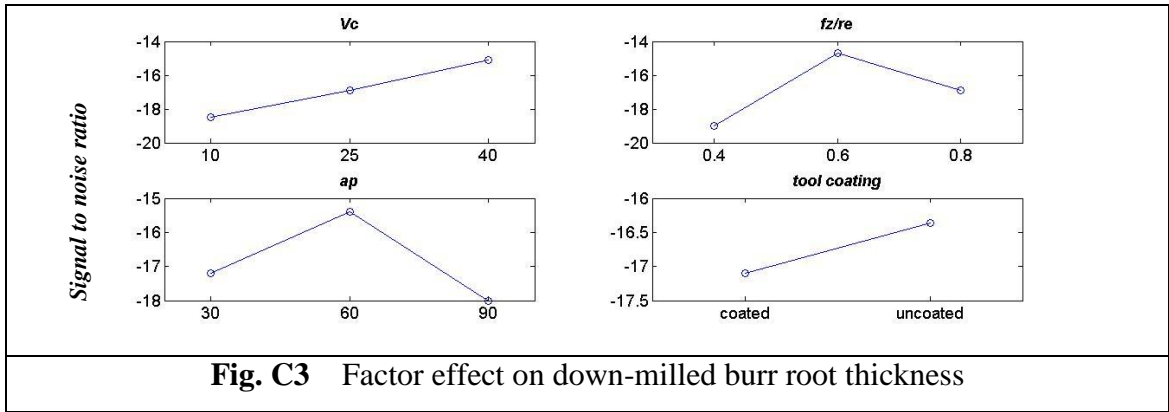


Fig. C2 Factor effect on surface finish

Fig. C3 shows that in order to minimise down-milled burr root thickness the optimum machining parameters should be set at 40 m/min (V_c), 0.6 (f_z/r_e), 60 μm (a_p) using uncoated tools.



In order to perform standardised comparison of the AE energy band measured at different cutting conditions, the calculated energy bands were normalised with respect to unit of material removed. Fig. C4 shows the optimum level at 40 m/min (V_c), 0.4 (f_z/r_e), 30 μm (a_p) using uncoated tools in maximising D1 energy band.

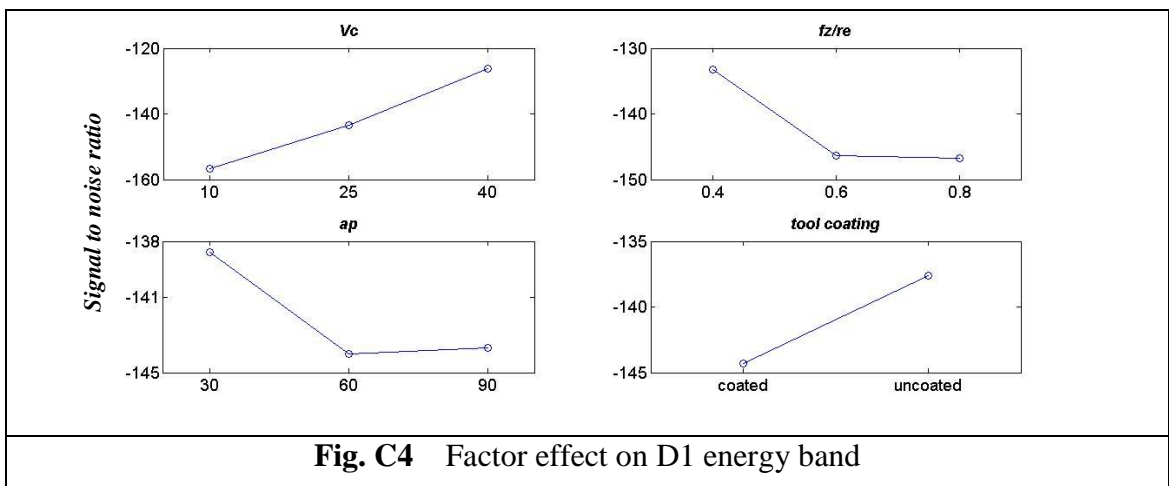
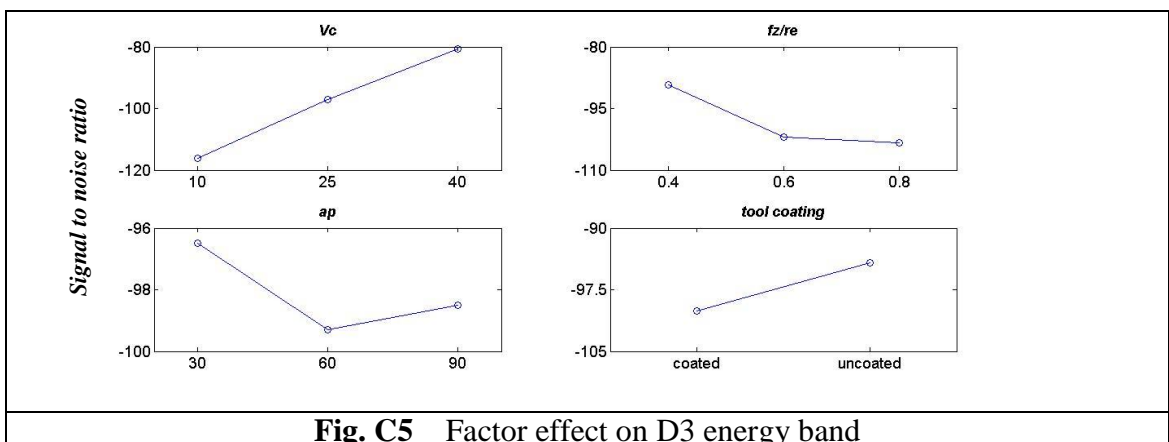


Fig. C5 depicts the optimum level at 40 m/min (V_c), 0.4 (f_z/r_e), 30 μm (a_p) using coated tools in maximising D3 energy band (125-250 kHz).



The optimum level (refer to Fig. C6) in maximising D5 energy band (32.25-62.5 kHz) was at 40 m/min (V_c), 0.4 (f_z/r_e), 30 μm (a_p) using uncoated tools.

